Development of fouling-resistant physically small carbon electrodes for *in vivo* dopamine detection

By

Shaneel Sanjeev Chandra

Master of Science, The University of the South Pacific

A thesis submitted in fulfilment of the requirements for the degree of
Doctor of Philosophy

Department of Chemistry and Biomolecular Sciences

Macquarie University

Sydney, Australia

14 February 2011

Abstract

This thesis reports the development of fouling-resistant physically small carbon electrodes to detect the neurotransmitter dopamine *in vivo*. Dopamine has long been of interest to both chemists and neuroscientists. This is due to its role in modulating many aspects of brain circuitry in a major system of the brain including the extra pyramidal and mesolimbic system, as well as the hypothalamic pituitary axis. In addition, it plays a crucial role in the functioning of the central nervous, cardiovascular, renal and hormonal systems. A loss of dopamine containing neurons or its transmission is also related to a number of illnesses and conditions including Parkinson's disease, schizophrenia, motivational habit, reward mechanisms and the regulation of motor functions and in the function of the central nervous, hormonal and cardiovascular system. In order to detect the neurotransmitter *in vivo*, high sensitivity, chemical selectivity, and fast temporal resolution are among the desirable characteristics in detecting neurotransmitters. In this respect, electrochemical techniques are well suited for the measurement of transient changes in the concentration of a species. Such techniques are concerned with the interplay between electricity and chemistry, namely the measurement of electrical quantities such as current, potential or charge, and their relationship to chemical parameters. Electroanalytical techniques have been widely developed and, more recently, applied to the investigation of neurochemical systems, leading to a better understanding of neurotransmission. This partly stems from the ease of oxidative detection of many neurotransmitters including dopamine. In addition, the development of structurally small electrodes has made *in vivo* detection neurotransmitters possible in biological microenvironments. Moreover, the small dimension of such electrodes permits minimal tissue damage upon implantation and, of equal importance, permits very careful selection of the region of tissue where measurements can be performed. Furthermore, the inherent fast response time of structurally small electrodes makes it feasible to follow biochemical events frequently taking place on a millisecond (ms) time scale (*e.g.* neuronal firing).

Detection of dopamine in a physiological environment with selectivity and sensitivity has been an important topic of electroanalytical research but one that has also experienced great challenges. Direct voltammetric detection of dopamine at naked electrodes requires high selectivity for the neurotransmitter in the presence of interfering ascorbic acid. In addition, electrode passivation by adsorption of species present in the extra-cellular fluid, known as fouling is another obstacle to electrochemical detection of neurotransmitters. To reduce fouling, electrode surfaces can be modified to deter adsorption. Many of these species are hydrophilic. Therefore, common methods employed to achieve this include film incorporation, conversion to a hydrophobic surface such as that *via* hydrogenation, application of a diamond layer among others. Therefore, an overall aim of this study is to develop, characterise and apply physically small carbon electrodes that are fouling-resistant in detecting dopamine *in vivo*. More specifically, this work aimed at

(1) fabricating and characterising physically small *p*-phenylacetate film-coated carbon electrodes;

(2) fabricating and characterising physically small hydrogenated carbon electrodes; and

(3) assembly of a chemical vapour deposition system for hydrogenating bare carbon electrodes and depositing diamond films.

The study begins with Chapter 2 describing the fabrication of physically small conical-tip carbon electrodes by pyrolysis of acetylene on pulled quartz capillaries with a micrometer-sized tip (<2 μm electrode radius and ~3 μm axial length). These electrodes were then modified by electrochemically depositing a *p*-phenylacetate film-layer on the surface. The modified electrodes were subjected to voltammetric characterisation in hexamine ruthenium(III) chloride, dopamine and potassium ferricyanide, respectively, and the results were compared to those at the electrode before modification. Increased limiting currents at the modified electrodes for hexamine ruthenium(III) chloride and dopamine, and decreased currents for potassium ferricyanide were observed, respectively. Characterisation under laboratory conditions showed that the anionic film on the electrode surface was stable over a 40-day period. In detecting

dopamine, the modified electrodes demonstrated a limit of detection of 541 pM and a sensitivity of 16 pA/nM, compared to 543 nM and 19 pA/nM, respectively, at bare carbon electrodes. Moreover, the film-coated electrodes also displayed higher sensitivity and lower limit of detection (0.1 nA/nM and 6 nM respectively) for dopamine over ascorbic acid (0.1 nA/μM and 1.4 μM).

Analytical performance of both film-modified electrodes and bare carbon electrodes was also examined in a synthetic solution consisting of 1.0% (v/v) caproic acid (a lipid), 0.1% (w/v) bovine serum albumin and 0.01% (w/v) cytochrome C (both are protein) and 0.002% (w/v) human fibrinopeptide B (a peptide. The film-coated electrodes displayed a 3-fold increase in sensitivity, while the limit of detection remained about the same. On the other hand, bare carbon electrodes demonstrated evidence of severe surface degradation, with unmeasurable changes to the sensitivity and limit of detection following exposure to the synthetic solution. In detecting dopamine in an anesthetised rat, a greater degradation (62%) of the dopamine oxidation signal after 60 min of monitoring was observed at bare carbon electrodes, compared to 50% at film-coated electrodes. In addition, the film-coated electrodes were observed to offer some resistance to fouling for the first 40 mins of implanting the electrode. This however decreases after 40 min, suggesting possibly more severe fouling. This was attributed to a result of lack of longevity of the *p*-phenylacetate film on the electrode surface. In comparison, bare carbon electrodes demonstrated a steady decline in the oxidation peak signal. This suggested that the *p*-phenylacetate film was successful in retarding fouling for the first 40 min after implanting in the rat brain, by which time the carbon electrode surface had degraded to a greater extent.

In Chapter 3, physically small bare carbon electrodes were subjected to radio frequency plasma hydrogenation. Surface characterisation studies using atomic force microscopy, Raman spectroscopy and X-ray photoelectron spectroscopy were performed to evaluate the success of hydrogenation. The atomic force microscopy revealed the hydrogenated electrodes having smoother surfaces by 3 orders of magnitude compared to bare carbon electrodes. Raman spectroscopy provided information on the nature of carbon bonding at the hydrogenated

electrode to be largely sp^3 while that at bare carbon electrodes was dominated by sp^2 carbon. The X-ray photoelectron spectroscopic measurements showed a reduction in the surface oxygen to carbon ratio. The results from these studies all suggested the successful incorporation of a hydrogenated layer onto the electrodes. Results from voltammetric studies in the hexamine ruthenium(III), dopamine and ferricyanide redox systems were also found to be consistent with a hydrogenated layer. The hydrogenated electrodes were found to achieve a limit of detection of 721 pM and sensitivity of 0.16 pA/nM. The sensitivity of hydrogenated electrodes was found to be lower than that for bare carbon electrodes while limit of detection was higher at hydrogenated electrodes for dopamine. The reduced sensitivity is presumably due to the change in the surface charge of the electrodes (from negative at bare carbon electrodes to largely neutral at hydrogenated electrodes) following hydrogenation. Performance analysis of the hydrogenated electrodes for dopamine detection in the presence of interfering ascorbic acid showed negligible contribution from ascorbic acid towards dopamine detection at the hydrogenated electrodes, while bare carbon electrodes showed distortion of the dopamine oxidation signal. In the presence of a similar synthetic laboratory solution to that prepared in Chapter 2, the sensitivity and limit of detection of hydrogenated electrodes for dopamine were found to suffer only slightly after immersion. Finally, the electrodes were subjected to *in vivo* dopamine detection to evaluate their resistance to fouling. The results showed hydrogenated electrodes only suffered 50% degradation in the oxidation signal of dopamine after 60 min of monitoring. This compared favourably with bare carbon electrodes (62% degradation in signal). Moreover, fouling occurs at a rapid rate for the first 20 min of implanting the electrode in the brain. After this initial rapid fouling rate, the electrode surface appears to equilibrate with the environment, and undergoes a considerably slower rate of degradation. These results compare favourably with those of similar monitoring experiments performed at bare carbon electrodes, which showed consistent fouling of the electrode surface throughout the monitoring period.

Chapter 4 outlines our efforts to assemble a remote plasma chemical vapour deposition system capable of depositing nanodiamond films. Such a system was developed and performance-tested to evaluate its functioning. Briefly, blank quartz substrates were seeded with diamond powder

vi

and later subjected to a stream of methane in excited hydrogen using remote microwave plasma. Five sets of conditions were identified that led to deposition of films of various morphologies. These films were subjected to Raman spectroscopy and scanning electron microscopy. The results showed traces of diamond and sp^2 carbon in all five depositions. Moreover, the nucleation clusters of diamond were of varying sizes in response to the process parameters applied. With careful manipulation of these parameters, namely pressure, duration, and methane concentration, diamond films of defined morphology consistent with the literature have been fabricated.

In Chapter 5, we have concluded the outcomes of this study with a comparative summary of the performance of the electrodes. Both *p*-phenylacetate film film-coated electrodes as well as hydrogenated electrodes demonstrate stable behaviour when applied to *in vivo* dopamine detection. However, the hydrogenated surface is more resistant to fouling as evidenced by the fouling rate. In comparison, film-coated electrodes demonstrate a certain degree of fouling-resistance, after which the performance of the electrode is observed to be severely degraded. In comparison to bare carbon electrodes however, both electrode modifications imparted better fouling-resistance.

Acknowledgements

This thesis is the culmination of the efforts and sacrifices of many. It is the result of the guidance of my supervisors, Dr Danny K Y Wong and Associate Professor James Rabeau. Thank you Danny, for your consistently-high standards when I was happy to have simply met the target, your patience and guidance when the chips were down, and compassion during the moments of hardship in my life. Thank you Jim, for believing in me, never letting me give up, for your encouragement and the enthusiasm that kept me doggedly at the system, that eventually yielded those beautiful diamonds.

To all collaborators who assisted with this multi-disciplinary project: Tony, Simon, Avi, Scott, Phil, Dieter and Paul - thank you for being there when I needed an alternative perspective, or equipment access, and for availing your time as and when required. Sincere thanks to Chris for being the trouble-shooter-on-demand, and advising when needed.

Thank you to all the friends I met in Australia, Eileen, Tom, Ann, Michael, Steve, Anil, Wendy, Sudhir, Keith Tonkin, Tony, Mark, Carlo, and anyone I may have inadvertently missed. To my RMC family - thank you for those wonderful moments we shared together - we will meet again, surely.

To the most important people in my life who made the biggest sacrifices - my loving wife, Kavi, and my parents. This research is realised with your support foremost. You have endured the most but were always there for me. No measure of success can repay the toll it took on all of us.

This thesis is dedicated to my late dad, truly the most intelligent person I ever knew.

Declaration

I hereby declare that this thesis represents my own work and efforts in its entirety, and has not been submitted for a higher degree or otherwise at any other university, or institution.

_____   **14 February, 2011**

      Shaneel Chandra   **Date**

Table of Contents

CHAPTER 1

INTRODUCTION

1.1   Overview

In the mammalian brain, neuronal networks process vast amounts of information received from a subject's environment through the senses. Much of the signalling within the brain uses small molecules called neurotransmitters, as messengers between neurons. During neuronal communication, neurotransmitters are released from the axon end of a neuron, usually followed by uptake of the released neurotransmitter by receptors (*i.e.* the dendrites) on an adjacent neuron. The process of uptake involves interaction between the released neurotransmitters with membrane-bound proteins called transporters, which transfer the extracellular neurotransmitter back into the cell.   The remaining neurotransmitters can diffuse out of the neuronal region and be subsequently metabolised.[1]   The processing in the brain networks eventually manifests as animal behaviour. The brain is a challenging environment for chemical sensing because low concentration of analytes must be detected in the presence of interferences, with yet minimal tissue damage. To conduct meaningful measurements, the properties of the analytical sensor and the general characteristics of the biological system must be understood.

The catecholamines are a group of biogenic monoamine neurotransmitters containing a nucleus of catechol, which is the aromatic portion comprising of a benzene ring with two adjacent hydroxyl groups and an aliphatic side chain of ethylamine or one of its derivatives. The immunomodulatory functions of catecholamines acting as chemical messengers transporting information between cells have been long documented.[2]

Between cells, catecholamines act as chemical messengers that transport information.[3] This has been an area of interest to researchers as is evidenced by many publications in literature aimed at understanding catecholamine and quinone electrochemistry.[4-7]

Among the catecholamines, dopamine has long been of interest to both chemists and neuroscientists. It is one of the most important neurotransmitters and is ubiquitous in the mammalian central nervous system.[8] It modulates many aspects of brain circuitry in a major system of the brain including the extra pyramidal and mesolimbic system, as well as the hypothalamic pituitary axis.[9] It also plays a crucial role in the functioning of the central nervous, cardiovascular, renal and hormonal systems.[10] A loss of dopamine containing neurons or its transmission is also related to a number of illnesses and conditions including Parkinson's disease, schizophrenia, motivational habit, reward mechanisms and the regulation of motor functions and in the function of the central nervous, hormonal and cardiovascular system.[8, 11-12] It is therefore of interest to measure dopamine in the extracellular fluid in animals in order to monitor neurotransmission processes and correlate neurochemistry with behaviour.[12]

1.2   Measurement of dopamine concentrations

The dynamics of the release and uptake of dopamine into brain extracellular space are currently under intense investigation.[13-15] Dopamine is a well-known extra-synaptic messenger that functions *via* volume transmission, escaping from the synaptic cleft to bind to extra-synaptic receptors and transporters. High sensitivity, chemical selectivity, and fast temporal resolution are all desirable characteristics in detecting neurotransmitters *in vivo*. In this regard, electrochemical techniques are well suited for the measurement of transient changes in concentration. Such techniques are concerned with the interplay between electricity and chemistry, namely the measurement of electrical quantities such as current, potential or charge, and their relationship to chemical parameters.[16,17]

Electroanalytical techniques have been widely developed and, more recently, applied to the investigation of neurochemical systems, leading to a better understanding of neurotransmission through the detection of several compounds including acetylcholine, dopamine, norepinephrine, serotonin, γ–aminobutyric acid, and glutamic acid.[18] They provide a platform for the construction of sensors based on the concentration fluctuations of easily oxidised neurotransmitters in the extracellular fluid of the brain.[17] An overview of the development of analytical chemistry demonstrates that electrochemical sensors represent the most rapidly growing class of chemical sensors.[19-20]

1.3   Electrochemical studies of neurotransmitters

Electroanalytical chemistry can be applied to the study of neurochemical systems. The outcomes of such a study are expected to contribute to a better understanding of many aspects of neurotransmission, for example, neural circuitry and neural substrates of compulsive drug use,[21] neurotransmitter (serotonin)-linked gastrointestinal disorders such as irritable bowel syndrome[22] and effects of pollution and drug abuse on vesicular catecholamine release.[13] This feasibility partly stems from the ease of oxidative detection of many neurotransmitters including dopamine, acetylcholine, norepinephrine, serotonin, glutamic acid and γ–aminobutyric acid. In addition, the development of structurally small electrodes has made *in vivo* detection of neurotransmitters possible in biological microenvironments.[1-2, 21] In this respect, the small dimension of such electrodes permits minimal tissue damage upon implantation and, of equal importance, permits very careful selection of the region of tissue where measurements can be performed. Moreover, the inherent fast response time of structurally small electrodes makes it feasible to follow biochemical events frequently taking place on a ms time scale (*e.g.* neuronal firing).

Various electrode materials have been reported for use in constructing structurally small electrodes of different geometries and sizes.[3, 8-10] Common electrode materials, both

modified and otherwise, include metals such as tungsten and aluminium, gold nanoparticle-deposited aluminium, various forms of carbon *e.g.* doped diamond, nanocrystalline diamond, pyrolysed carbon, carbon fibres, and gold nanoparticles deposited on glassy carbon.

Electrochemical methods traditionally have found important applications in sample analysis. The electrode surface itself can be a powerful tool. By controlling the electrode potential, the chemist can use it as a variable free energy source or sink of electrons.[23]

An electrode for use in biological environments should possess several properties: good sensitivity for the target analyte, rapid response time, a stable background response that is unaffected by changes in the surrounding solution environment and resistance to biomolecule adsorption (deactivation and fouling).[24] The miniaturisation of working electrodes offers many of these practical advantages as well as generating some fundamentally new possibilities. While the term "microelectrode" often refers to electrodes with characteristic dimensions less than 20 μm,[25] the question of how small the dimension of an electrode has to be before it is considered an ultramicroelectrode has been discussed but not resolved.[26] Perhaps a non- quantified working definition would be that a microelectrode is an electrode with at least one dimension small enough that its properties such as mass transport regime are a function of size.[27] Such microelectrodes are commonly known to exhibit several advantages over conventional-sized electrodes. These include reduced ohmic drop that would otherwise arise from conventional electrodes in highly resistive solutions. In addition, the greatly reduced double layer capacitance of microelectrodes, associated with their small size and area allows high-speed voltammetric experiments to be performed at microsecond timescale (scan rates higher than 10^6 V/s) allowing probing the kinetics of very fast electron transfer and coupling chemical reactions or the dynamics of processes such as exocytosis.[8-9, 12]

The electrolytic techniques of constant potential amperometry, fast scan cyclic voltammetry (FSCV) and chronoamperometry all offer some degree of selectivity, temporal resolution and sensitivity in the study of neurochemical events. The selectivity provided by FSCV has enabled the measurement of dopamine concentration changes in freely moving animals.[28-29] It has also enabled the recent measurement and correlation of dopamine transients with sexual behaviour, establishing for the first time that dopamine release can be measured *in vivo* during normal behavioural activities.[30]

Microelectrodes also exhibit excellent signal-to-background characteristics compared to their large counterparts. This is due to the enhanced mass transport of electroactive species accruing from radial (nonplanar) diffusion to the edges of the microelectrodes. Such "edge effects" are significant contributors to the overall diffusion current because the rate of mass transport to and from the electrode (and hence the current density) increases with decreasing electrode size.[9] High sensitivity and selectivity that can be achieved with electrode modifications is required because the physiological actions of many analytes such as the neurotransmitter dopamine at receptors occur at concentrations in the range from nanomolar to low-micromolar. Similarly, high selectivity is required because other electroactive species (*e.g.* ascorbic acid and uric acid) are present in the extracellular fluid of the brain at much higher concentrations than dopamine.[12] Furthermore, diffusion and double-layer charging effects makes microelectrodes suitable for biological applications such as *in vivo* detection of dopamine. As mentioned earlier, their small size also allows minimal tissue damage in the exploration of microscopic domains as well as permitting careful selection of the neural area of implementation.[9, 16]

Since their introduction to electroanalytical chemistry about 30 years ago, microelectrodes have led to unprecedented advances in electrochemical science.[26] Much of this has been through the early work of researchers such as Wightman[31] and others.[2, 11, 25, 32-33] Most of the electrodes used in extremely small environments, for example the cytoplasm of living cells require use of electrodes with tip dimensions on the order of a

few micrometres or less. This is especially true for puncturing living cells where the cell membrane needs to seal around the electrode following implantation.[33]

In recent years, attention has been drawn to the fabrication of low cost, disposable carbon film electrodes for mass scale use as electrochemical sensors,[34] particularly as a chemical sensor for changes in catecholamine concentration.[9, 35-36] In particular, carbon fibre microelectrodes have been viewed as advantageous because of their small micrometre tip diameters[37] and high sensitivity to catecholamines. They can be used with a wide variety of electrochemical techniques, including constant potential amperometry and cyclic voltammetry.[2, 12, 36]

In addition to high sensitivities, electrodes for *in vivo* neurotransmitter detection need to be physically small in size and of a geometry that permits minimal damage upon implantation and also very careful selection of the specific tissue sites where measurements can be performed.[38] In the next section, the geometries of physically small electrodes are described.

1.4   Geometries of physically small electrodes

As low concentrations of dopamine are released and rapidly cleared from the extracellular space, the sensing electrodes must be sensitive, and selective and respond quickly.[9] For *in vivo* detection of dopamine, physically small electrodes are advantageous due to their small size and high sensitivity to catecholamines.[39] There are currently no electrodes small enough to measure dopamine concentrations within the approximately 100-nm synapse region of the brain where dopamine is released,[40] but considerable developments are being made in minimising electrode size to approach synapses as closely as possible and also to minimise tissue damage.[38] In addition,

electrochemical methods using ultramicroelectrodes have been proven to be rapid, simple and sensitive in the determination of dopamine.[38]

Electrodes of different materials have been miniaturised in many geometric shapes with the common characteristic that the electrode is significantly smaller than the diffusion layer at the electrode surface for ordinary voltammetric time scales (*e.g.* 1-10 s).[41] According to Koichi,[42] if the characteristic length of a small electrode, such as an ultramicroelectrode, is made infinitesimally small, it tends to adopt the geometry of either a point, a line, or a plane. On this basis, ultramicroelectrodes can generally be classified into a point electrode, a line electrode, and a plane electrode. Each of these three classifications will be further discussed below.

A point electrode resembles a spot with vague geometry at a long distance from the electrode. It adopts a spherical-shaped concentration profile and potential distribution in the solution. As a result, such electrodes easily achieve a steady state and yield a steady-state current. This current is expected to be proportional to the characteristic length (radius) of the electrode. A typical point electrode is a disc electrode inlaid on an insulating plane.

An ultrathin ring electrode shares characteristics of the point electrode and the line electrode. It appears as a point from a position distal from the electrode, but it resembles a curved line upon closer inspection. It exhibits a steady-state current because of the feature of the point electrode. Next, a plane electrode of interest is a microarray electrode, which is composed of point electrodes and line electrodes on a planar insulator. It is versatile in functionality by designing the geometrical arrangement. A mode of mass transport depends on whether elementary electrodes are a point or a line electrode.

1.4.1 Disc-Shaped Point Electrodes

In general, a disc electrode consists of a short cylindrical rod of the electrode material (*e.g.* carbon fibre disc electrodes,[43] carbon paste disc electrode[44] and boron-doped diamond nanodisc electrodes[45]) embedded in a tightly fitting tube of an insulating material (*e.g.* Teflon). Electrical contact is made at the rear end. Disc-shaped nanometre-sized electrodes are often used because they are relatively simple and can attain true steady-state current. Another approach to fabricate nanometre sized disc electrodes is the glass-sealed approach,[39] in which a metal wire is sealed into a glass pipette before it is pulled into a nanometre-sized tip in a laser pipette puller. Finally, the metal tip covered with glass is exposed either by etching away or by micropolishing a small portion of glass insulator. Alternatively, Wong and Xu[38] fabricated ultrasmall carbon disc electrodes constructed by pyrolysing methane gas at a pressure of approximately 900 kPa in pulled quartz capillaries. This was found to be sufficient to form a carbon deposit at the tip of the capillary. Electrical contact to the carbon deposit was accomplished with mercury and a nichrome wire. The electrodes were estimated to exhibit structural diameters of 500–1000 nm with a fabrication success rate of 85%. Favourable stability was also demonstrated by current deterioration of 10% over a period of 5 days.

More recently, disc microelectrode fabrication has been extended to dual-disc electrodes.[39] This is because two micrometre-sized electrodes are very convenient for detection of two electroactive species and for acquirement of dual information in single cells.

1.4.2 Ultrathin Carbon Ring Electrodes

Investigations for nonplanar electrodes are important because it is easier to construct spherical or conical-shaped microelectrodes than disc-shaped microelectrodes, especially those with a very small tip.[46] Very often, ring electrodes are fabricated by applying a

conductor to the walls of an insulating cylindrical support. This is often a glass rod, or for smaller diameter rings, a flame/laser heat drawn glass rod. To fabricate a metal ring, the support can be either painted with organometallic compounds[47] or coated by vapour deposition,[48] sputtering of metal onto a rotating glass rod or pyrolysis of methane.[33] However, the vapour deposition method ensures a uniform metal coating and permits rings of thickness ranging from 10 nm to 5 µm. The coated support is then insulated from solution by sealing into a larger glass tube with resin or collapsing the glass around the rod. The structure is then sectioned and polished to expose the inlaid ring.[38]

1.4.3 Carbon Fibre Line Electrodes

The first carbon fibre microelectrode reported in literature was that fabricated by Ponchon and co-workers in 1979.[11] This procedure involved pulling a glass tube to obtain a diameter of few micrometres. Then the carbon fibre (outside diameter 8 µm, length 20 to 40 mm) was threaded into the capillary, thus enabling the fibre to be pushed a few mm through the capillary. The authors reported that this method minimised the interstitial space between the capillary and the carbon fibre. Then, the capillary was inverted into a mixture of graphite powder and polyester resin to fill 4 - 5 mm of the body with the paste. A contact wire was then pushed as far as possible into the barrel filled with the paste. Immediately before use, the electrodes were cut to a length of 0.5 mm.[11]

A conventional method for fabricating carbon fibre microelectrodes involves initially aspirating a carbon fibre into a glass capillary that is then pulled to the dimensions of the fibre using a vertical puller. The fibre is then sealed in the glass capillary with epoxy and the electrical junction made by back filling the capillary with graphite and inserting a chrome wire for contact. In this method, poor sealing between the fibre/glass interface can often arise from unavoidable bad sealing and leakage of the epoxy. This results in high noise, low sensitivity, short electrode life and sometimes pollution of the solution in which the electrode is immersed. In addition, owing to difficulty in ensuring a successful

back filling procedure with graphite, the fabrication efficiency of the method is low. Finally, with most types of epoxy being organic based, electrode modification or even application in organic solvents can be a challenge.[49]

Carbon fibre electrodes tend to have a relatively larger cylindrical surface area, compared to, for example, that of ultrasmall carbon ring electrodes. They are readily accessible to the diffusing species, giving rise to a larger detection current at carbon fibre electrodes. However, owing to the soft mechanical strength of carbon fibres, penetration into soft tissue or frequent vibrations under a microscope often make it a demanding task to manipulate the electrode into the *in vivo* microenvironment. To overcome this, Zoski and Mirkin reported a fabrication method involving sealing an etched carbon fibre in an insulating cylindrical-shaped glass.[50-51] The deliberately protruding carbon fibre acts as the conducting electrochemical surface, with structural support provided by the glass, thus overcoming tissue-penetration hurdles.

1.4.4 Microelectrode Arrays

As the electrode size decreases, especially that of point electrodes, Faradaic current generated decreases proportionally to the disc radius, leading to a diminishing ohmic potential drop. In fast experiments, such as those involving high-speed chronoamperometry of 60 ms square pulses of 0 – 0.5 V amplitude (versus Ag|AgCl), applied every 250 ms[28] to the working electrode or fast scan cyclic voltammetry of ranging from 300 to 400 mV/s,[52-53] radial diffusion contributes little to the flux of reactant at the electrode. Thus the cell current, which is proportional to the disc area, plummets rapidly as smaller and smaller discs are used. Consequently, it is necessary to use a high-gain current-to-voltage converter, often with two or more stages of amplification, and careful attention must be paid to noise and bandwidth considerations. A direct way of increasing the current to be measured is to use more than one microelectrode, *i.e.*, arrays of *N* sufficiently-separated and non-interacting discs that will

provide N times the current from a single disc.[54] This enables exploitation of the advantages of microelectrodes whilst ensuring large total currents by using microelectrode arrays, where each microelectrode has the same function. If these microelectrodes are sufficiently spaced apart, the array can act as the sum of the individual responses. On the other hand, if they are very close, the array behaves as a macroelectrode with dimensions equal to that of the assembly. Signal-to-noise ratios can be improved by using such arrays, as the noise levels depend on the active area of the electrodes whereas the signal depends on the total area of the diffusion field.[55]

Xiao *et al.*[45] have reported the construction of a random array of boron doped diamond nano-disc electrodes, formed by a simple three-step method. Initially, molybdenum(IV) dioxide nanoparticles were electrodeposited on a boron doped diamond substrate. This was then covered in an insulating polymer film by electropolymerising 4-nitrophenyldiazonium salt. Next, molybdenum dioxide nanoparticles were dissolved from the boron doped diamond surface (removing the polymer layer directly above them only) using dilute hydrochloric acid etching. This resulted in the exposure of nano-discs of boron doped diamond of approximately 20 ± 10 nm in diameter surrounded by a polymer insulating the remainder of the boron doped diamond. This method produced up to 650 ± 25 million boron doped diamond nano-disc electrodes per cm^2. Various random arrays of boron doped diamond nanodisc electrodes were produced using this method with a similar distribution of nano-disc size and number density, confirming that this was a reliable and reproducible method of manufacturing such nanoelectrode arrays. At scan rates ranging from 10 – 1000 mV/s, the array was found to produce peak currents approaching that of the Randles-Ševčík limit for the equivalent geometric electrode area despite the fact that most of the surface was insulated by the polymer as shown by voltammetric and atomic force microscopic results. Comparison between experimental and simulated results of both ordered and random arrays of nano-disc electrodes revealed that the maximum current obtainable at such arrays was that predicted by the Randles-Ševčík equation. The array of boron doped diamond nano-discs also showed a

significantly reduced capacitive background current relative to the bare boron doped diamond electrode, suggesting that such devices may offer improved signal resolution in electroanalytical measurements.

A common challenge to detecting dopamine *in vivo* is electrode fouling. This is the phenomenon where high-molecular weight and hydrophilic species such as proteins, lipids and peptides adsorb to hydrophilic electrode surfaces such as that of bare carbon. A layer of such adsorbates slows electrode kinetics, reduces the active electrode area and causes distortion of the voltammetric signal of dopamine and suppresses the sensitivity of the electrode.[56-57] In many other instances, the signal at a fouled electrode manifests unpredictability and irreproducibility making electroanalysis unreliable.[58]

A detailed comparison of the strategies to resist electrode fouling during dopamine detection *in vivo* is presented in Chapter 2. Notably, some of these include application of an ion-exchange organic film,[59] immobilisation of a hydrogenated layer,[56] and fabrication of diamond electrodes.[60] The scope of the current study is to apply these methods to physically small carbon electrodes for *in vivo* dopamine detection.

1.5 Scope of the present study

Detection of dopamine in a physiological environment with selectivity and sensitivity has been an important topic of electroanalytical research but one that has also experienced great challenges. Direct voltammetric detection of dopamine at naked electrodes requires high selectivity for the neurotransmitter among other electroactive species at carbon and metallic electrodes (such as Au, Pt) in a biological environment such as the brain.

In addition, electrode fouling by adsorption of non-electroactive species is another obstacle to electrochemical detection of neurotransmitters. Therefore, an overall aim of

this study is to develop, characterise and apply physically small carbon electrodes that are fouling-resistant in detecting dopamine *in vivo*. More specifically, this work aims at:

Fabricating and characterising physically small *p*-phenylacetate film-coated carbon electrodes;

Fabricating and characterising physically small hydrogenated carbon electrodes; and,

Assembly of a chemical vapour deposition system for hydrogenating bare carbon electrodes and preparation of a nanodiamond film.

Each of the following chapters is then devoted to the detailed description and discussion of the results obtained in achieving the respective aim. In Chapter 2, the method of developing bare carbon electrodes with a layer of *p*-phenylacetate film is described, while Chapter 3 describes the fabrication and characterisation of hydrogenated electrodes.

In Chapter 4, efforts to assemble a chemical vapour deposition rig and to test its performance are outlined. This chapter includes efforts to use this rig to respectively deposit a layer of diamond and to immobilise a hydrogenated layer on bare carbon electrodes. Chapter 5 provides a thesis summary, conclusions and future directions.

1.6   References

1.   Michael, D. J.; Wightman, R. M., *J. Pharm. Biomed. Anal.* **1999,** *19* (1-2), 33-46.

2.   Venton, B. J.; Troyer, K. P.; Wightman, R. M., *Anal. Chem.* **2002,** *74* (3), 539-546.

3.   Xiao, Y.; Guo, C.; Li, C. M.; Li, Y.; Zhang, J.; Xue, R.; Zhang, S., *Anal. Biochem.* **2007,** *371* (2), 229-237.

4.   Xu, R. D.; Huang, X.; Kramer, K. J.; Hawley, M. D., *Anal. Biochem.* **1995,** *231* (1), 72-81.

5.   Smythies, J.; De Iuliis, A.; Zanatta, L.; Galzigna, L., *Neurotox. Res.* **2002,** *4* (1), 77 - 81.

6.   Hasegawa, T.; Matsuzaki, M.; Takeda, A.; Kikuchi, A.; Furukawa, K.; Shibahara, S.; Itoyama, Y., *J. Neurochem.* **2003,** *87* (2), 470.

7.   Alhasan, R.; Njus, D., *Anal. Biochem.* **2008,** *381* (1), 142-147.

8.   Troyer, K. P.; Heien, M. L. A. V.; Venton, B. J.; Wightman, R. M., *Curr. Opin. Chem. Biol.* **2002,** *6* (5), 696-703.

9.   Wang, J., *Analytical Electrochemistry*. Third Edition ed.; John Wiley & Sons: Hoboken, 2006.

10.   Arya, S. K., Singh, S. P. and Malhotra, B. D., *Electrochemical techniques in biosensors.* John Wiley & Sons, Ltd.: Chichester, 2007; Vol. 1, p 341-378.

11.   Ponchon, J.; Cespuglio, R.; Gonon, F.; Jouvet, M.; Pujol, J., *Anal. Chem.* **1979,** *51*, 1483-1486.

12.   Hermans, A.; Seipel, A. T.; Miller, C. E.; Wightman, R. M., *Langmuir* **2006,** *22* (5), 1964-1969.

13.   Westerink, R. H. S., *Neurotoxicology* **2004,** *25* (3), 461-470.

14.   Sulzer, D.; Edwards, R., *Neuron* **2000,** *28* (1), 1-9.

15.   Suaud-Chagny, M.-F., *Methods* **2004,** *33* (4), 322-329.

16.   McNally, M.; Wong, D. K. Y., *Anal. Chem.* **2001,** *73* (20), 4793-4800.

17.   Xu, G.-R.; Xu, M.-L.; Zhang, J.-M.; Kim, S.; Bae, Z.-U., *Bioelectrochemistry* **2008,** *72* (1), 87-93.

18.   Sun, W.; Yang, M.; Jiao, K., *Anal. Bioanal. Chem.* **2007,** *389*, 1283-1291.

19.   Laschi, S.; Mascini, M., *Med. Eng. Phys.* **2006,** *28* (10), 934-943.

20.   Wang, J., *Electroanal.* **1991,** *3* (4-5), 255-259.

21.   Evans, A. H.; Pavese, N.; Lawrence, A. D.; Tai, Y. F.; Appel, S.; Doder, M.;
       Brooks, D. J.; Lees, A. J.; Piccini, P., *Ann. Neurol.* **2006,** *59* (5), 852-858.

22.   Zhao, H.; Bian, X.; Galligan, J. J.; Swain, G. M., *Diamond Relat. Mater. 19* (2-3),
       182-185.

23.   Murray, R. W.; Ewing, A. G.; Durst, R. A., *Anal. Chem.* **1987,** *59* (5), 379-390.

24.   Park, J.; Show, Y.; Quaiserova, V.; Galligan, J. J.; Fink, G. D.; Swain, G. M., *J.
       Electroanal. Chem.* **2005,** *583* (1), 56-68.

25.   Fleischmann, M.; Pons, S., *Anal. Chem.* **1987,** *59* (24), 1391-1399.

26.   Zoski, C. G., *Electroanal.* **2002,** *14* (15-16), 1041-1051.

27.   Montenegero, M. I.; Querós, M. A.; Daschbach, J. L., *Chemical Applications of
       Electrochemistry at Ultramicroelectrodes*. Kluwer Academic Press: Dordrecht,
       1991; Vol. Vol. 197, p 3-16.

28.   Yavich, L.; Tiihonen, J., *J. Neurosci. Methods* **2000,** *104* (1), 55-63.

29.   Lane, R. F.; Blaha, C. D.; Hari, S. P., *Brain Res. Bull.* **1987,** *19* (1), 19-27.

30.   Robinson, D. L.; Phillips, P. E. M.; Budygin, E. A.; Trafton, B. J.; Garris, P. A.;
       Wightman, R. M., *NeuroReport* **2001,** *12* (11), 2549-2552.

31.   Wightman, R. M., *Anal. Chem.* **1981,** *53* (9), 1125-1134.

32.   Dayton, M. A.; Brown, J. C.; Stutts, K. J.; Wightman, R. M., *Anal. Chem.* **1980,**
       52, 946-950.

33.   Kim, Y.-T.; Scarnulis, D. M.; Ewing, A. G., *Anal. Chem.* **1986,** *58* (8), 1782-
       1786.

34.   Blackstock, J. J.; Rostami, A. A.; Nowak, A. M.; McCreery, R. L.; Freeman, M.
       R.; McDermott, M. T., *Anal. Chem.* **2004,** *76* (9), 2544-2552.

35. Bath, B. D.; Michael, D. J.; Trafton, B. J.; Joseph, J. D.; Runnels, P. L.; Wightman, R. M., *Anal. Chem.* **2000,** *72* (24), 5994-6002.

36. Heien, M. L. A. V.; Phillips, P. E. M.; Stuber, G. D.; Seipel, A. T.; Wightman, M. M., *Analyst* **2003,** *128*, 1413-1419.

37. Roberts, J. G.; Moody, B. P.; McCarty, G. S.; Sombers, L. A., *Langmuir* **2010,** *26* (11), 9116-9122.

38. Wong, D. K. Y.; Xu, L. Y. F., *Anal. Chem.* **1995,** *67* (22), 4086-4090.

39. Gao, N.; Lin, X.; Jia, W.; Zhang, X.; Jin, W., *Talanta* **2007,** *73* (3), 589-593.

40. Zweifel, L. S.; Parker, J. G.; Lobb, C. J.; Rainwater, A.; Wall, V. Z.; Fadok, J. P.; Darvas, M.; Kim, M. J.; Mizumori, S. J. Y.; Paladini, C. A.; Phillips, P. E. M.; Palmiter, R. D., *Proc. Natl. Acad. Sci. U. S. A.* **2009,** *106* (18), 7281-7288.

41. Lee, Y.; Amemiya, S.; Bard, A. J., *Anal. Chem.* **2001,** *73* (10), 2261-2267.

42. Koichi, A., *Electroanal.* **1993,** *5* (8), 627-639.

43. Zachek, M. K.; Hermans, A.; Wightman, R. M.; McCarty, G. S., *J. Electroanal. Chem.* **2008,** *614* (1-2), 113-120.

44. Oni, J.; Westbroek, P.; Nyokong, T., *Electroanal.* **2003,** *15* (10), 847-854.

45. Xiao, L.; Streeter, I.; Wildgoose, G. G.; Compton, R. G., *Sens. Actuators, B* **2008,** *133* (1), 118-127.

46. Bard, A. J.; Faulkner, L. R., *Electrochemical Methods: Fundamentals and Applications*. 2nd Edition ed.; John Wiley & Sons, Inc.: New York, 2001.

47. Hayes, M. A.; Ewing, A. G., *Anal. Chem.* **1992,** *64* (5), 512-516.

48. MacFarlane, D. R.; Wong, D. K. Y., *J. Electroanal. Chem. Interfacial* **1985,** *185* (1), 197-202.

49. Huang, W. H.; Pang, D. W.; Tong, H.; Wang, Z. L.; Cheng, J. K., *Anal. Chem.* **2001,** *73* (5), 1048-1052.

50. Zoski, C. G.; Mirkin, M. V., *Anal. Chem.* **2002,** *74* (9), 1986-1992.

51. Britz, D.; Chandra, S.; Strutwolf, J.; Wong, D. K. Y., *Electrochim. Acta* **2010,** *55* (3), 1272-1277.

52. Zachek, M. K.; Takmakov, P.; Park, J.; Wightman, R. M.; McCarty, G. S., *Biosens. Bioelectron.* **2010,** *25* (5), 1179-1185.

53. Kuhr, W. G.; Wightman, R. M., *Brain Res.* **1986,** *381* (1), 168-171.

54. Strohben, W. E.; Smith, D. E.; Evans, D. H., *Anal. Chem.* **1990,** *62*, 1709-1712.

55. Fungaro, D., A.; Brett, C. M. A., *Anal. Chim. Acta* **1999,** *385*, 257-264.

56. Alwarappan, S.; Butcher, K. S. A.; Wong, D. K. Y., *Sens. Actuators, B* **2007,** *128* (1), 299-305.

57. Downard, A. J.; Roddick, A., D., *Electroanal.* **1997,** *9* (9), 693-698.

58. Downard, A. J.; bin Mohamed, A., *Electroanal.* **1999,** *11* (6), 418-423.

59. Ali, S. R.; Ma, Y.; Parajuli, R. R.; Balogun, Y.; Lai, W. Y. C.; He, H., *Anal. Chem.* **2007,** *79* (6), 2583-2587.

60. Suzuki, A.; Ivandini, T. A.; Yoshimi, K.; Fujishima, A.; Oyama, G.; Nakazato, T.; Hattori, N.; Kitazawa, S.; Einaga, Y., *Anal. Chem.* **2007,** *79* (22), 8608-8615.

CHAPTER 2

DEVELOPMENT, CHARACTERISATION AND EVALUATION OF PHYSICALLY SMALL *p*-PHENYLACETATE-COATED CARBON ELECTRODES

2.1 Electrochemical detection of dopamine

Dopamine is a widely-present neurotransmitter in the central nervous system, where it modulates several aspects of the brain circuitry.[1-2] It also plays a crucial role in the functioning of the central, nervous, cardiovascular, renal and hormonal systems.[3] It is therefore useful to monitor the release of dopamine, particularly as it has been associated with conditions such as Parkinson's and Alzheimer's diseases.[4] Electrochemical detection of dopamine however is affected by the presence of interferents such as serotonin, 3,4-dihydroxyphenylacetic acid (DOPAC), uric acid and ascorbic acid. In the extracellular fluid of the central nervous system, dopamine is present in the concentration range of $0.2 - 2.0$ µM,[5-6] whereas ascorbic acid level is very much higher at $125 - 420$ µM.[7-8] Ascorbic acid is among the most commonly encountered interferents and an electroactive species that coexists with dopamine in the central nervous system. In general, dopamine is oxidised at 400 mV versus saturated calomel electrode,[9-10] while ascorbic acid is oxidised at 500 mV.[10-11] All these make it a challenging task to selectively detect dopamine in the presence of ascorbic acid.

In addition to interferences, another common challenge in electrochemical analysis of dopamine is the phenomenon of fouling. Electrode fouling is the passivation of an electrode surface caused by adsorption of high molecular-weight proteins, lipids and peptides present in biological matrices, resulting in a decreasing transient electrode

response, distorted voltammetric signals and suppressed electrode sensitivity.[12] Considerable research effort has been devoted to addressing electrode fouling problems. Approaches ranging from applying fast scan voltammetry,[13] immobilising a protective organic film on the electrode surface,[14] completely altering the surface termination,[15] fabricating nanocrystalline diamond coated electrodes[16] to doped diamond electrodes have been reported.[17]   Apart from minimising fouling, these methods have also demonstrated other advantages such as greater durability, increased robustness and enhanced sensitivity. More details about each of these approaches are presented below in order to gain an understanding of why their characteristics facilitate such advantages.

2.1.1   Fast Scan Cyclic Voltammetry

Fast scan cyclic voltammetry is the technique of linearly scanning the potential of a stationary working electrode in an unstirred solution.[18] Scanning rates employed can be as high as kilovolts per second.[19-20] At the end of the linear sweep, the direction of the potential scan is reversed, usually stopping at the initial potential.[21]   These voltammetric measurements allow the rapid concentration dynamics of redox-active species to be followed *in situ*. No other method offers this quantitative and qualitative information concerning endogenous substances on a millisecond (ms) time scale. Fast scan cyclic voltammetry is used to detect the analyte and quantify it before severe fouling takes place.[22] In particular, dopamine released after applying short stimulations (< 1 s) can be monitored and fast-scan cyclic voltammetry provides a good method for the evaluation of drug actions on dopamine neurons.[23]   This, with the added high time resolution of the technique, also allows the kinetics of dopamine release to be followed in greater detail.[24] Fast-scan cyclic voltammetry has been particularly useful for monitoring fluctuations of neurotransmitter concentrations both *in vivo* and *in vitro*.[25-26] For example, Bath *et al*.[25] found that increased sensitivity to 2.5 μM dopamine (in NaCl/4-(2-hydroxyethyl)-1-piperazineethanesulfonic acid/$CaCl_2$ buffer adjusted to pH 7.4 with NaOH) can be achieved by faster electrode scanning *in vitro*.

However, fast-scan cyclic voltammetry also suffers from the drawback of background current that exceeds the Faradaic current from redox reactions of dopamine, due to very high potential scan rates. The background is composed of current required to charge the double layer and current arising from redox reactions of surface-attached functional groups. The magnitude of both of these is directly proportional to the potential scan rate, whereas the current arising from a diffusion-controlled electrochemical reaction is proportional to the square root of the potential scan rate.[27] Thus optimum ratios of the Faradaic to background current are not achieved with fast-scan cyclic voltammetry.[28] For example, Hafizi *et al.*[29] employed fast-scan cyclic voltammetry to measure basal extracellular dopamine but they were unable to detect concentrations much below 200 nM. Fast scan cyclic voltammetry also provides only limited chemical resolution. The redox potential (E^o) of a substance is insufficiently unique for molecular identification. In addition, to distinguish between chemical species that are involved in diffusion-controlled one-electron electrolysis processes, their E^os need to differ by at least 0.118 V.[30] In aqueous solution, decomposition of water to hydrogen and oxygen occurs at approximately -0.83V and -1.23 V respectively, giving rise to a less than 2.0 V potential window.[31-32] Therefore, even under optimum conditions, fewer than 15 compounds can be resolved.[33]

To overcome these issues, as well as to detect dopamine in the presence of interferents such as ascorbic acid and uric acid, various means to improve the sensitivity and selectivity of fast-scan cyclic voltammetry have been adopted. An extension of the anodic scan limit from 800 mV to 1400 mV (versus Ag|AgCl) has been reported to result in a dramatic increase in the sensitivity of carbon fibre electrodes to dopamine.[29] These electrodes were found to retain their sensitivity in brain tissue and were capable of measuring dopamine concentrations of 50 nM in the presence of DOPAC or ascorbic acid. Increasing anodic scan limits were accompanied by negative shifts (suggesting less energy-intensive redox process) of the halfwave potential ($E_{½}$) of the oxidation peaks for dopamine. The authors attributed this to adsorption of dopamine at the electrode surface

via its catechol group, which they suggested was the cause of higher peak currents from dopamine oxidation, thus leading to greater sensitivity.

Recently, an analogue method to subtract the background currents that occur during cyclic voltammetry at high scan rates has been reported.[28] This subtraction enables the use of higher gains before the analogue-to-digital conversion. Furthermore, the application of principal component regression to account for background changes permitted fast-scan cyclic voltammetric measurements to be made for longer times. This has enabled the monitoring of dopamine over time windows that previously were accessible only to microdialysis experiments, but with 600-time greater time resolution. With such high time resolution, short-term dopamine fluctuations in dopamine concentrations can also be measured.

The most common approach to selective determination of dopamine in the presence of ascorbic acid and other interferents using fast-scan cyclic voltammetry is to prevent the interfering species from accessing the electrode surface. This has been achieved by many studies and approaches ranging from application of selective layers of organic films that repel the interferents, to methods of enhancing the dopamine signal while suppressing that of others. In the following sections, these methods are discussed with examples from the literature.

2.1.2   Nafion film

In 1984, the use of Nafion as a permselective film coating on small graphite electrodes was reported by Gerhardt and co-workers.[34] As a protective coating onto the electrode, Nafion prevents fouling of the electrode surface by high molecular-weight proteins, peptides and lipids. Moreover, it is an ion-exchange perfluoronated derivative film of Teflon, which is highly permeable to cations but almost impermeable to anions. Notably, ascorbic acid (pKa = 4.2)[10] exists as anionic ascorbate in extracellular fluid under

physiological pH of 7.4. Therefore, a Nafion-coated electrode will respond minimally to ascorbic acid in extracellular fluid. The membrane also strongly rejects passage of anionic metabolites such as DOPAC and 5-hydroxyindoleacetic acid (5-HIAA). In addition, it is also insensitive to natural metabolites such as 3,4-dihydroxyphenylethyleneglycol. Thus, it is highly selective for only cationic species such as the primary neurotransmitters dopamine (pKa = 8.9),[35] norepinephrine (pKa = 8.4),[36] and 5-hydroxytryptamine (pKa$_1$ = 9.97, pKa$_2$ = 10.73),[37] at physiological pH of ~7.4. Kuhr and Wightman[26] have demonstrated the application of Nafion-modified microelectrodes in conjunction with fast scan cyclic voltammetry to the detection of submicromolar concentrations of dopamine on a ms scale *in vivo*, thereby showing that the technique affords rapid analysis and high sensitivity. Since then, a number of studies have emerged on Nafion-modified electrodes.[38-43]

However, Nafion-modified electrodes also exhibit several disadvantages. For example, the response time of the Nafion-coated sensors increases due to a reduced diffusion coefficient value in the film.[44] This can pose a serious disadvantage for *in vivo* detection of neurotransmitters, where dopamine and other neurotransmitter releases often occur on a sub-second time scale. In addition, the use of Nafion for direct voltammetric analysis is complicated by slow equilibration of the film with solution species,[45] which ultimately affects sensitivity to rapid changes in neurotransmitter concentration. Therefore, there is a need for a modification system that can allow for rapid and selective permeation of the ions of interest. Nafion films also have been reported to suffer from lack of longevity, hence electrodes modified with the film tend to have short life spans.[22]

2.1.3   Conducting polymers

Other coatings such as conducting polymers[18,46] including polypyrrole, polythiophene, polyaniline, polyacetylene, and polyindole have also attracted considerable attention. Among these, polypyrrole and its derivatives play a leading role because of their versatile

applicability and the wide variety of molecular species covalently linked to a pyrrole group.[46] In a similar manner to Nafion, such coatings act as a protective layer on the electrode surface and prevent fouling.

Xiao *et al*.[44] performed an electrochemical esterification of polyethylene glycol with a composite layer of self-assembled 11-mercaptoundecanoic acid monolayer on gold surface electrodes. This composite layer was found to exhibit high sensitivity to dopamine while blocking any interference from ascorbic acid. The authors attributed this to the dissociated carboxylate (COO⁻) groups on the composite layer that repelled the anionic ascorbic acid molecules, while attracting the oppositely-charged dopamine molecules towards the electrode for oxidation. A second reason hypothesised in the study was that the composite layer was less organised than the stand-alone 11-mercaptoundecanoic acid layer, thus its defects facilitated the permeation of dopamine. Dopamine oxidation currents at electrodes modified with the composite layer were found to be approximately 60% higher than those on the 11-mercaptoundecanoic acid-immobilised electrode or even the plain gold electrode.

Other polymeric molecules applied to microelectrodes include polycarbazole and poly(carbazole-co-*p*-tolylsulfonyl pyrrole).[47] Unfortunately, considering that immobilisation of such protective layers on an electrode is neither reproducible nor effective,[48] alternative surface modifications are clearly required.

2.1.4   Nanoparticle-Modified Electrodes

Recently, Jia *et al*.[49] modified glassy carbon electrodes with gold nanorods (GN) and gold nanoparticles (GNP) *via* a template technique and then dispersed the nanorods in a saturated sodium citrate solution by ultrasonication to form a gold nanorod and a gold nanoparticle electrode respectively. The electrodes were labelled as GNR/GC and GNP/GC, respectively. For comparison, glassy carbon electrodes were subjected to the

same procedure but in a sodium citrate solution without any gold particles. These were labelled as activated electrodes. Dopamine was then detected at GNR/GC, GNP/GC, activated glassy carbon and bare glassy carbon electrodes and the resulting anodic peak currents were compared. At the GNR/GC electrode, the dopamine anodic peak current was 5 times larger than that at the GNP/GC electrodes, and 26 times larger than that at the bare glassy carbon electrodes. Peak currents similar to that from bare glassy carbon electrodes were obtained at the activated glassy carbon electrodes, indicating that any increase in the peak current was due to the gold nanorods and not activation alone. The study also found that the increase in electrode surface area resulting from the gold nanorod modification was linearly related to the increase in currents. The detection of dopamine in the presence of 1000-fold ascorbic acid was found to be unhindered by the ascorbic acid at GNR/GC electrodes. This selectivity for dopamine over ascorbic acid by GNR/GC electrodes was attributed to electrostatic interactions. At pH 7.4 which is similar to the pH of extracellular fluid, the dopamine molecule is positively charged as a result of its amine group, whereas the hydroxyl next to the carbonyl group of ascorbic acid is negatively charged. As the dispersed gold nanorods are stabilised by citrate ions and thus hold the negative charges, the gold nanorod-modified glassy carbon electrode was electrostatically repelling ascorbic acid and attracting dopamine. Therefore, the oxidation of ascorbic acid is inhibited and the oxidation of dopamine is promoted at the gold nanorod-modified glassy carbon electrode, which improves the selectivity of detection.

2.1.5   **Electrochemically Grafted Aryl Films**

In recent years, many carbon electrodes were modified by an oxidative procedure that generates oxygen functionalities useful for further chemistries.[50] In 1990, Barbier *et al*.[51] argued that electrochemical or chemical oxidation can often damage the carbon surface and oxidation tends to lead to the generation of superficial carboxylic, quinonyl, ketonic or hydroxylic groups that then further react with the substance to be attached. The exact

nature and number of oxygenated functional groups were thus difficult to ascertain and control, and corrosion of the carbon surface was observed, leading to large background currents.　Their study provided an alternative method that was based on the electrochemical reduction of a phenyldiazonium derivative.　This carbon surface modification procedure involved the formation of a diazonium radical that forms a covalent bond to the glassy carbon electrode surface.　The technique was based on the electrochemical reduction of diazonium salts, which leads to very solid and non-corrosive covalent attachment of aryl groups on carbon surfaces.　The versatility of the method is founded on the possibility of grafting a variety of functionalised aryl groups.　This allows the attachment of a wide spectrum of substances.[52]　In 1992, a study by Delamar and co-workers[53] demonstrated that reduction of diazonium salts at glassy carbon surfaces resulted in a strongly attached surface layer.　They attributed this to covalent bond formation between the aryl radical and the carbon surface.[53-54]　One electron reduction of aryl diazonium salts at carbon electrodes leads to grafting of aryl groups to the surface. Acetonitrile is often used as the modification medium.　Reduction of the diazonium salt can be achieved by cyclic voltammetry or controlled potential electrolysis.　The reaction is favoured both by the adsorption of the diazonium prior to its reduction and by the relatively positive potential of the diazonium prior to its reduction.[54]　Many studies have now focused on this technique of using diazonium salts for modifying electrode surfaces for a whole host of applications.[14, 45, 50, 55-57]　For example, Hong and Porter[58] reported the electrochemical reduction of benzenediazonium tetrafluoroborate in acetonitrile containing tetrabutylammonium tetrafluoroborate to incorporate a phenyl layer on glassy carbon electrodes.　The phenyl modifier showed strong hydrophobicity, hence the choice of phenyl layer as a film.　More recently, Pellissier *et al.*[59] reported the modification of glassy carbon electrodes with phenyl-C_n-H_{2n}-COOH moieties by electrochemical reduction of *in situ* generated diazonium salts bearing carboxylic acid groups.　These groups then served as a precursor to grafting of an enzyme layer.

Downard *et al.*[14] have reported the application of a *p*-phenylacetate layer to macro glassy carbon electrodes. Differential pulse voltammetry of 20.0 μM dopamine and 2.0 mM ascorbic acid (separate solutions) at both modified and unmodified electrodes showed almost a six-fold enhancement of dopamine anodic peaks at the modified electrodes, while the magnitude of the anodic current of ascorbic acid remained similar in the differential pulse voltammetry at modified electrodes and the peaks were no longer as well-resolved as those obtained at unmodified electrodes. Notably, Downard *et al.*'s work is limited to demonstration of enhanced detection of dopamine at conventional-sized glassy carbon electrodes *in vitro*.

This chapter will report on our effort in developing small conical-tip carbon electrodes, which were then modified with a *p*-phenylacetate film. The characteristics of the latter were studied in several redox systems including hexamine ruthenium(III) chloride, dopamine and potassium ferricyanide by comparing to those of bare carbon electrodes. Particular attention will be focussed on dopamine detection at *p*-phenylacetate film-coated electrodes *in vitro* in the presence of interfering ascorbic acid and fouling reagents including proteins, peptides, fatty acids and lipids. Finally, results obtained by applying *p*-phenylacetate film-coated electrodes to the detection of dopamine *in vivo* will be presented and discussed.

2.2   Experimental

2.2.1   Reagents

Ultrapure (Milli-Q) water (18.2 MΩ.cm at 25ºC) was used to prepare all solutions. American Chemical Society analytical grade dopamine, citric acid, potassium chloride, potassium ferricyanide, sodium phosphate dibasic heptahydrate, hexanoic acid, human fibrinopeptide B, Cytochrome C, bovine serum albumin and graphite powder were

purchased from Sigma Aldrich. Tetrabutylammonium tetrafluoroborate anthraquinone-2,6-disulfonate (AQDS) and 4-aminophenyl acetic acid were obtained from Aldrich, while sodium fluoroborate was acquired from Fluka. Hydrochloric acid and diethyl ether were obtained from Univar.   Ultra high purity acetylene and nitrogen gases were purchased from BOC Gases, Australia. Hexamineruthenium(III) chloride, was obtained from Stremm Chemicals (Newport, USA). The epoxy used to seal electrodes was Bond VL1 (from Kua Sen Enterprise Company Limited, China). All chemicals and reagents were used without further purification. All redox solutions and supporting electrolytes were prepared daily and purged with nitrogen for 5 min preceding any analysis to remove oxygen.

2.2.2   Instrumentation and apparatus

Quartz capillaries (1-mm outside diameter, 0.5-mm inside diameter and 75-mm length, Sutter Instruments, Novato, CA) were pulled into a fine tapered end using a model P-2000 Sutter Puller (Sutter Instrument Co.).   Electrochemical measurements involving cyclic voltammetry and chronoamperometry were performed with a potentiostat capable of measuring picoamperes of current (eDAQ Pty Ltd., Sydney, Australia). This potentiostat was operated using EChem version 2.1.2 software on a PC *via* an E-corder interface (eDAQ Pty Ltd.)   A single compartment, three-electrode glass cell that accommodates a Ag|AgCl electrode as a reference and a platinum wire as a counter electrode, respectively, was used. All measurements were made at room temperature (25°C), within 3 h of sealing the electrodes.

Measurement of current in the picoamperes range is an extremely sensitive exercise, which requires careful control of the external environment to eliminate any noise interference which can often affect the analysis. This includes mains hum (50-60 Hz interference) from mains-powered equipment.   To prevent this, common grounding between the recording hardware and computer was ensured, by connecting them to the

same grounded power board that was then attached to a three pin (grounded) power socket. Often, it is also important to isolate the analysis setup in a Faraday cage (adopted for all measurements in this study), which was positioned as far as possible from power leads, computers, monitors and other mains-powered equipment.

2.2.3   Fabrication of conical-tip carbon electrodes

The procedure for fabricating physically small conical-tip carbon electrodes was adopted from that reported by McNally and Wong.[60] Briefly, quartz capillaries were pulled down to a fine tip using a laser micropipette puller. Electrodes of variable shapes and sizes were obtained by altering the parameters that control the heating and pulling processes in the micropipette puller. These parameters are heat, filament, velocity, delay and pull. Their effects on the pulled capillaries are discussed below.

1. **Heat** - this specifies the power output of the laser beam applied to the quartz capillary.

2. **Filament** - the filament specifies the scanning pattern of the laser beam. The puller utilised in this study had six scanning patterns (filaments), each of which defines the longitudinal length and the rate of the scan. The length of the region scanned is analogous to the width of a conventional metal heating filament.

3. **Velocity** - this refers to the velocity of the quartz carriage system as the quartz is fastened to the system and begins to pull apart under a constant load. At the same time, the laser beam was turned on to apply heat.

4. **Delay** - the delay parameter controls the time between the heat being turned off, and the subsequent activation of the hard pull (see below). If the delay equals 128, the pull is activated as the heat is turned off. If the setting is greater than 128, the heat is turned off, and the pull is activated after a period which equates to the delay setting – 128 ms. A setting less than 128 means the hard pull is

activated and the heat turns off after a period corresponding to 128 – delay setting ms. A higher delay value allows the quartz to cool for a longer period before the hard pull is executed. This accordingly resulted in decreased taper length and increased tip diameter.

5. **Pull** - this parameter controls the force of the hard pull. The timing of the pull depends upon the delay parameter setting (see Delay section above). In general, the higher the pull, the smaller the pipette tip diameter and the longer the taper.

This study required electrodes of relatively low taper length and high diameter tip. This enables generation of capillaries that formed electrodes of negligible resistance. The low taper length also has the advantage of being physically more robust, and therefore permits the manipulation of the resulting electrode into small environments without damage to the tip. Upon pulling, the capillary was left inside the puller to cool for 1 min before being used further.

In the next step, acetylene gas was thermally pyrolysed to form carbon within and on the shank of pulled capillaries. All components of the pyrolysis assembly involving acetylene were made of stainless steel. No copper-containing component that can form explosive copper acetylide upon contact with acetylene gas was used.

The large end of the pulled capillary was then connected to a rubber tubing (of 50 mm length and 1 mm inside diameter). The inner diameter of the rubber tubing was slightly larger than the outer diameter of the capillary to provide a gas-tight seal between the capillary and the gas supply. This was then placed through a $\frac{1}{16}$"$\times\frac{1}{16}$"$\times\frac{1}{16}$" stainless steel union tee with the bolts intact (SGE Analytical Science). The tee was placed end-to-end with a locally sourced quartz nuclear magnetic resonance (NMR) tube (internal diameter 5 mm). The junction of the union tee and the NMR tube must be as close to a seal as possible to disallow possible contact of any acetylene gas that was not pyrolysed and could possibly make contact with a Bunsen flame used.

The NMR tube was shortened (Macquarie Engineering & Technology Services) to a length of 100 mm, with both ends remaining hollow. The end of the tube joined to the union tee was uniformly sawed to ensure a surface that was free from the perforations that would have otherwise resulted if the tube had been conventionally snapped off. Any such perforations would have contributed to acetylene leakage through the perforations during pyrolysis.

Before commencing pyrolysis, the nitrogen and acetylene gases were passed through the system for 10 min to flush oxygen from the pipes and tubes. McNally and Wong[60] have discussed the effects of manipulating the pyrolysis assembly on the resulting electrode geometry, shank size, electrode nature and sensitivity in extensive detail. Pyrolysis involving a counterflow of nitrogen gas (shown in Figure 2.1) to that of the acetylene would result in conical-tip electrode fabrication.
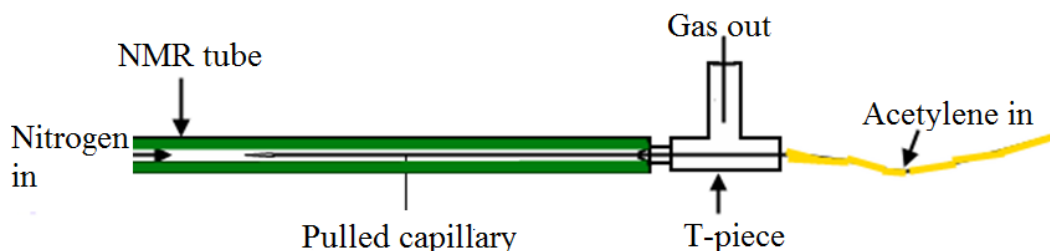
Figure 2.1   Schematic of a large conical-tip electrode pyrolysis assembly.

Using a 60 mL/min counterflow of nitrogen to acetylene gas pressure of 50 kPa, the acetylene gas was blown backward as it effused from the pulled tip of the capillary. Acetylene was then pyrolysed to form carbon at the tip and on the shank of the capillary. These large deposits of pyrolysed carbon on the electrode tip lend a large electrochemical surface area to the electrode. In order to avoid thermal shock to the capillary, which would invariably lead to tip fracture, it was necessary to begin thermally heating the far

end of the NMR tube away from the tip at the start. Next, the flame was slowly moved towards the region of the NMR tube housing the capillary tip. From when the tip was observed to glow to red, the time was monitored to ensure pyrolysis was continued for 3 min. Following pyrolysis, the capillary was left to cool for 20 s before it was carefully removed and its tip rinsed with distilled water to remove any possible remaining solid carbon particles adhering to the tip. This step required a lot of care as the capillary was quite warm after being just removed from the hot assembly.

To accomplish electrical connection, graphite powder was packed in the capillary through the larger open end. Next, a tin-coated copper fuse wire (10 amp) was introduced before the capillary was sealed with epoxy. An electrode fabricated in this manner is presented in Figure 2.2.
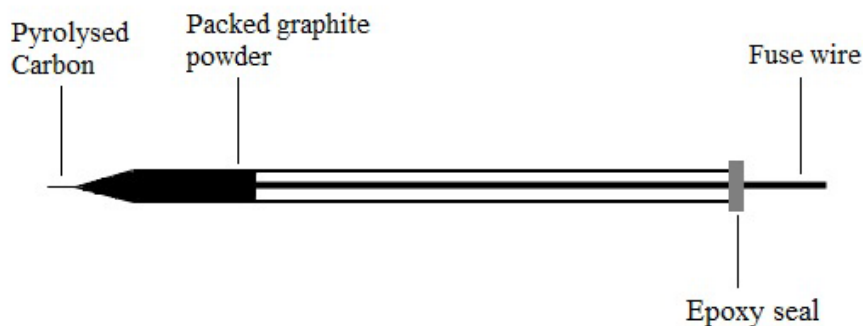
Figure 2.2   Schematic of a completed electrode.

2.2.4   Electrochemical detection

To determine the success of fabrication, cyclic voltammetry of 1.0 mM solutions of hexamine ruthenium(III) chloride [$Ru(NH_3)_6^{3+}$] in 1.0 M KCl as supporting electrolyte was carried out. Further study involving 1.0 mM dopamine in pH 7.4 citrate phosphate buffer, 1.0 mM potassium ferricyanide [$Fe(CN)_6^{3-}$] in 1.0 M KCl and 1.0 mM

anthraquinone-2,6-disulfonate (AQDS) in 0.1 M HClO$_4$ as supporting electrolyte was conducted at electrodes demonstrated to be functioning.

2.2.5   Scanning electron microscopy of electrodes

Scanning electron microscopy permits visual examination of electrode geometry, shape and size. In this study, bare carbon electrodes were examined without gold-coating, using a JEOL - JSM   6480-LA Variable pressure scanning electron microscope, at the Microscopy Unit, Department of Biological Sciences, Macquarie University.

2.2.6   Determination of electrode dimensions and area

Chronoamperometry was employed to determine the electrode dimensions and electroactive area. Briefly, the technique involves ramping a pulse on a resting potential applied to the working electrode in a redox system beyond the oxidation/reduction potential, so as to cause a change in the redox status of the species. In this study, the $Ru(NH_3)_6^{3+/2+}$ redox system was used with its reduction potential determined prior to chronoamperometric experiments by cyclic voltammetry. Based on this, a pulse of -0.60 V was applied for 2.0 s to the electrode at a resting potential of 0.40 V in a solution of 1.0 mM $Ru(NH_3)_6^{3+}$ in 1.0 M KCl. Next, the decaying current was measured as a function of time.

2.2.7   Synthesis of 4-phenylacetic acid diazonium fluoroborate

Before being able to electrodeposit 4-phenylacetic acid diazonium fluoroborate onto the electrode to form *p*-phenylacetate film, the compound must be synthesised. To prepare the 4-phenylacetic acid diazonium fluoroborate, the method of Bourdillon *et al.*[55] was

adopted. In this experiment, 1.51 g of 4-aminophenyl acetic acid (0.01 mol) was solubilised by warming in 3 mL of 12 M HCl and the minimum amount (~2 mL in total) of Milli-Q water. This resulting brown solution was then solubilised by heating on a hotplate for approximately 5 min giving rise a burgundy-red colour. Following this, the mixture was cooled in ice and the light brown hydrochloride precipitated, which occurred between 5 to 10 min. The result was a cake-like formation of the precipitate. Once the precipitate formed, 0.76 g (0.11 mol) of $NaNO_2$, dissolved in the minimum amount of water was added with stirring under a stream of nitrogen. This dissolved the precipitate, after which solid $NaBF_4$ was immediately added (1.47 g, 0.013 mol) and the mixture was stirred for 30 s and cooled rapidly below 0°C in solid carbon dioxide.

The resulting pale yellow precipitate was filtered in a cooled glass frit under a stream of nitrogen, washed with a cooled 5% (w/v) $NaBF_4$ solution to remove traces of acid and then washed with ether and finally stored in a vial. This compound is extremely sensitive to moisture presence, and must be stored in a dessicator containing phosphorus pentoxide as a drying agent.[61-62] In this study, the compound was only retained in the laboratory for 14 days, after which, fresh synthesis was carried out to avoid product decomposition and contamination. The product was characterised using ^{1}HNMR spectroscopy with deuterated dimethyl sulfoxide using a 400 MHz Bruker Avance ^{1}HNMR spectrometer.

2.2.8   Electrochemical deposition of *p*-phenylacetate on physically small carbon electrodes

We have also adopted the procedure reported by Downard *et al.*[14] to electrochemically deposit a *p*-phenylacetate film on physically small carbon electrodes. In this procedure, a 5.0 mM solution of 4-phenylacetic acid diazonium fluoroborate was prepared in 0.1 M Bu_4NBF_4 in acetonitrile. First, cyclic voltammetry of tetrabutylammonium tetrafluoroborate at the carbon electrode in acetonitrile was carried out. Next, the electrodes were subjected to cyclic voltammetry from 200 mV to -1200 mV, 20 - 50

times per electrode to allow for electroreduction of the phenylacetate salt on the electrode surface. Next, the electrodes were sonicated in acetone for 5 min before being removed, dried and stored for analysis.

2.2.9   *In vitro* characterisation of electrodes

In order to investigate the effectiveness of *p*-phenylacetate film-coated electrodes against fouling, cyclic voltammetry of 1.0 mM dopamine in pH 7.4 citrate/phosphate buffer was conducted at the electrodes incubated for a week in a laboratory synthetic solution that mimics extracellular solution. The solution comprised of 1.0% (v/v) caproic acid (a lipid), 0.1% (w/v) bovine serum albumin and 0.01% (w/v) cytochrome C (both are protein) and 0.002% (w/v) human fibrinopeptide B (a peptide).

2.2.10   *In vivo* dopamine detection

Ethics approval for use of rats was obtained from the Animal Ethics Committee, Macquarie University (Animal Research Authority - 2009/053) prior to experimentation. Male Sprague Dawley rats (303 – 330g) were used in the experiments. The animal was mounted on a stereotaxic frame and housed inside a Faraday cage to isolate noise. Next, a concentric bipolar stimulating electrode was implanted into the ventral tegmental area. A 31 g stainless-steel guide infusion cannula was implanted in the left substantia nigra pars compacta, and an Ag|AgCl reference and stainless-steel auxiliary electrode combination was placed in surface contact with contralateral cortical tissue approximately 2.0 mm posterior to bregma. The working electrode was then implanted in the left striatum.

Approximately 5 min following implantation of the recording electrode, a series of 0.5 ms duration cathodic monophasic current pulses (800 µA) was delivered to the

stimulating electrode *via* an optical isolator and programmable pulse generator. Data acquisition was conducted using a potentiostat capable of measuring up to nanoamperes of current (AD Instruments Pty Ltd, NSW, Australia). The potentiostat was operated using Chart version 5.0 software on a PC *via* an E-Corder interface (eDAQ Pty Ltd). A fixed potential of +0.9 V was applied and the dopamine released was monitored by recording the dopamine oxidation peak. The monitoring was continued for 60 min. Peaks were compared at the start and end of the monitoring period to determine the degree of fouling. The current was sampled at 10,000 bits per second. Where needed to distinguish overlapping signals, Gaussian peak fitting was performed. All signals were corrected for the 50 Hz mains cycle contribution. The electrodes were discarded upon conclusion of each *in vivo* experiment.

2.2.11   Data analysis

In this chapter, the statistical significance of all correlation coefficients at the 95% confidence level was tested using Student's t-test. Uncertainties associated with the slope and *y*-intercept of all linear plots, as well as all mean value comparisons were expressed as confidence intervals at the 95% level.

2.3   Results and Discussion

2.3.1   Characterisation of physically small carbon electrodes

Physically small carbon electrodes have been employed for detection of the neurotransmitters dopamine and norepinephrine previously.[15, 63-65] In addition to offering very small tip diameters ranging from 2 - 5 μm,[64, 66] these electrodes being either glass-based[67-68] or those etched from wires of tungsten and platinum,[39, 63] are mechanically strong and allow tissue or cell penetration without peripheral damage.[63] In

this study, electrodes were fabricated by pyrolysing acetylene to form carbon that was deposited at the tip and on the shank of quartz capillaries pulled down to a fine tip. Characterisation was based on the reduction of $Ru(NH_3)_6^{3+}$ to $Ru(NH_3)_6^{2+}$

$$Ru(NH_3)_6^{3+} + e^- \rightarrow Ru(NH_3)_6^{2+}$$
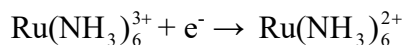
This is an outer-sphere redox system that is sensitive to the electronic structure of the carbon but not to the surface functional group or impurities.[20, 69-71] Figure 2.3 shows a representative cyclic voltammogram obtained at a carbon electrode. The voltammogram was obtained by scanning the potential from +0.2 V to -0.4 V and then reversed to +0.2 V. In this voltammogram, as the potential was scanned from +0.2 V to 0.0 V, $Ru(NH_3)_6^{3+}$ began to diffuse towards the electrode and was reduced. This generated the rapid increase in reduction current between 0.0 V and -0.25 V. At this point, $Ru(NH_3)_6^{3+}$ was diffusing towards the electrode at a maximum rate, giving rise to the current plateau observed between -0.3 V and -0.4 V. Upon switching the scan, the opposite occured. Between -0.4 V and -0.3 V, there was a high concentration of $Ru(NH_3)_6^{2+}$ at the electrode and in the bulk solution. $Ru(NH_3)_6^{2+}$ was then oxidised to $Ru(NH_3)_6^{3+}$, giving rise to the current between -0.25 V and 0.0 V. Between 0.0 V and 0.2 V, there was maximum diffusion of the molecules to the electrode surface, which was evidenced by the current plateau in this region. Two features observed in Figure 2.3 were used as criteria for a functioning electrode. Firstly, a sigmoidal-shaped voltammogram arising from both linear and non-linear diffusion around an electrode with a small surface area, indicating that the electrode is physically small. In addition, the absence of a gap between the forward and reverse scans suggests a well-sealed electrode.[72] As a result, only those electrodes exhibiting the expected response were selected for further characterisation and film coating.
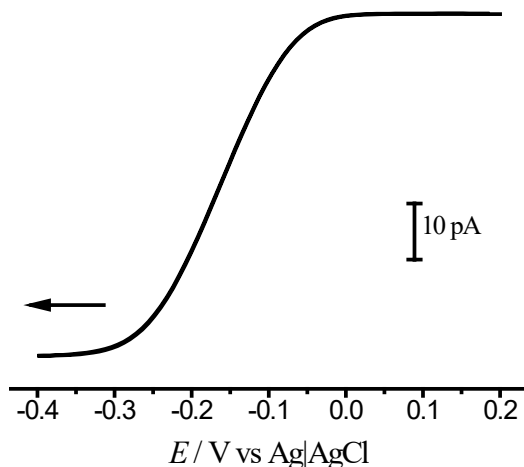
Figure 2.3   Cyclic voltammetry of 1.0 mM $Ru(NH_3)_6^{3+}$ in 1.0 M KCl at a carbon electrode (vs Ag|AgCl). Scan rate: 100 mV/s.

2.3.2   Scanning electron microscopy

Scanning electron microscopy was next used to examine the integrity and to estimate the electrode size. Figure 2.4 depicts a scanning electron micrograph of the side view of a bare carbon electrode. The tapered end of the electrode has a deposition of carbon on it, indicated by the glowing portion at the tip of the structure. Furthermore, there is an absence of gaps on the structure, confirming the integrity of the electrode. The pulled end is also observed to be cone shaped. From the microscopic image, the tip radius for this particular electrode was estimated to be less than 1 μm, and its axial length was estimated to be 3 μm.
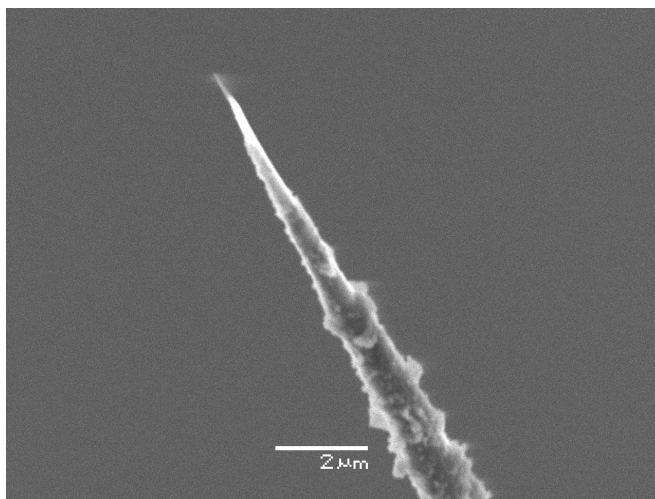
Figure 2.4   Scanning electron micrograph of a physically small bare carbon electrode.

2.3.3   Determination of electrode dimensions

The dimensions (*i.e.* tip diameter and axial length) of electrodes demonstrated to be functioning was next estimated. In this work, we have assumed a cylindrical geometry consisting of a carbon disc at the tip of the electrode and a carbon film on the shank of the electrode, resembling a cylinder. For cylindrical electrode geometry, the Faradaic current of a redox species, *i*, under a constant potential can be expressed as

$$i = \frac{nFADC}{r}[0.5 + \frac{r}{\sqrt{\pi Dt}}] \qquad\qquad \text{Equation (1)}$$

where n denotes the number of electrons transferred, F is the Faraday constant (96,485 C/mol), A is the electrochemical area (cm^2), D is the diffusion coefficient (5.3×10^{-6} cm^2/s),[60] C is the concentration of the redox species (mol/cm^3) and *r* is the radius of the electrode (cm). Therefore, a plot of *i* versus $1/\sqrt{t}$ is expected to yield a straight line with both the slope and the intercept used to estimate A and *r*.[66] Accordingly, chronoamperometry of 1.0 mM Ru(NH$_3$)$_6^{3+}$ was conducted at a carbon electrode in 1.0 M

KCl supporting electrolyte. Based on the cyclic voltammogram shown in Figure 2.3, a resting potential of 0.20 V was selected. In the chronoamperometric experiment, a -0.60 V pulse was applied to the electrode at a resting potential of 0.20 V. The result of the chronoamperometric experiment obtained is shown in Figure 2.5. At 0.20 V, only residual current was observed, suggesting a lack of any redox activity of the $Ru(NH_3)_6^{3+}$ analyte. In the chronoamperomegram, upon the application of the potential pulse, a large current was observed in the vicinity of 0.00 ms as $Ru(NH_3)_6^{3+}$ was diffusing towards the electrode and was immediately reduced at its surface. Then, depletion effects set in and the Faradaic current decayed away as a function of $\sqrt{t}$. The current between 2 and 2.5 ms was selected and substituted into Equation 1 to estimate r and h. Accordingly, the electrode radius was estimated to be 2.1 µm with 0.5 µm standard deviation and an axial length of 3.6 µm with a standard deviation of 0.1 µm (N=14). The radius and axial length estimated using chronoamperometry are of the same magnitude as the electrode size depicted in Figure 2.4.
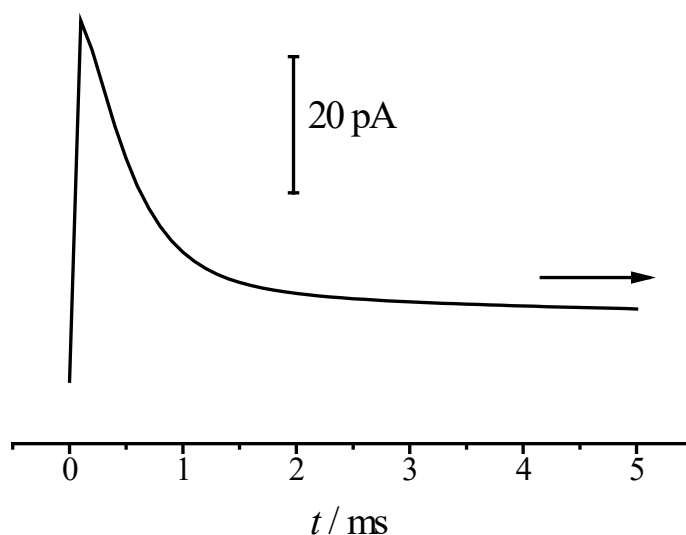
Figure 2.5   Chronoamperomegram of 1.0 mM $Ru(NH_3)_6^{3+}$ in 1.0 M KCl at a carbon electrode (-0.4 V pulse of 500 ms duration).

2.3.4   ¹H nuclear magnetic resonance spectrum of 4-phenylacetic acid diazonium fluoroborate

The compound, 4-phenylacetic acid diazonium fluoroborate is not commercially available, and must therefore be synthesised in the laboratory. To confirm the identity of the product, ^{1}HNMR was used to characterise the compound. A typical ^{1}HNMR spectrum is shown in Figure 2.6. In this spectrum, the major peaks are at 7.4 ppm, 7.7 ppm and further upfield at approximately 3.9 ppm. To aid in the assignment of peaks, the structure of 4-phenylacetic acid diazonium fluoroborate is depicted in Figure 2.7, which shows hydrogen atoms in two different environments attached to the aromatic ring, and the presence of the third type of hydrogen on the methyl group in the acetate portion of the molecule. The two peaks at 7.4 ppm and 7.7 ppm can be attributed to the hydrogen atoms in the aromatic portion of the molecule, while the third peak further upfield at ~ 3.9 ppm is attributed to hydrogen atoms of the methyl group.

In Table 2.1, the major peaks reported by Delamar *et al.*[53] and their assignment are tabulated. The major peaks observed in this study are also tabulated for comparison. These peaks compared well with those reported by Delamar *et al.* and they were therefore assigned accordingly. It is noteworthy though that in ^{1}HNMR spectroscopy, peak locations are a result of the chemical environment of the hydrogen atom in the molecule, and thus it is virtually impossible to get identical peak locations for hydrogen atoms of the same molecule in two different spectrometers, with different acquisition features. The similarity in results thus confirm the identity of the synthesised compound as 4-phenylacetic acid diazonium fluoroborate.
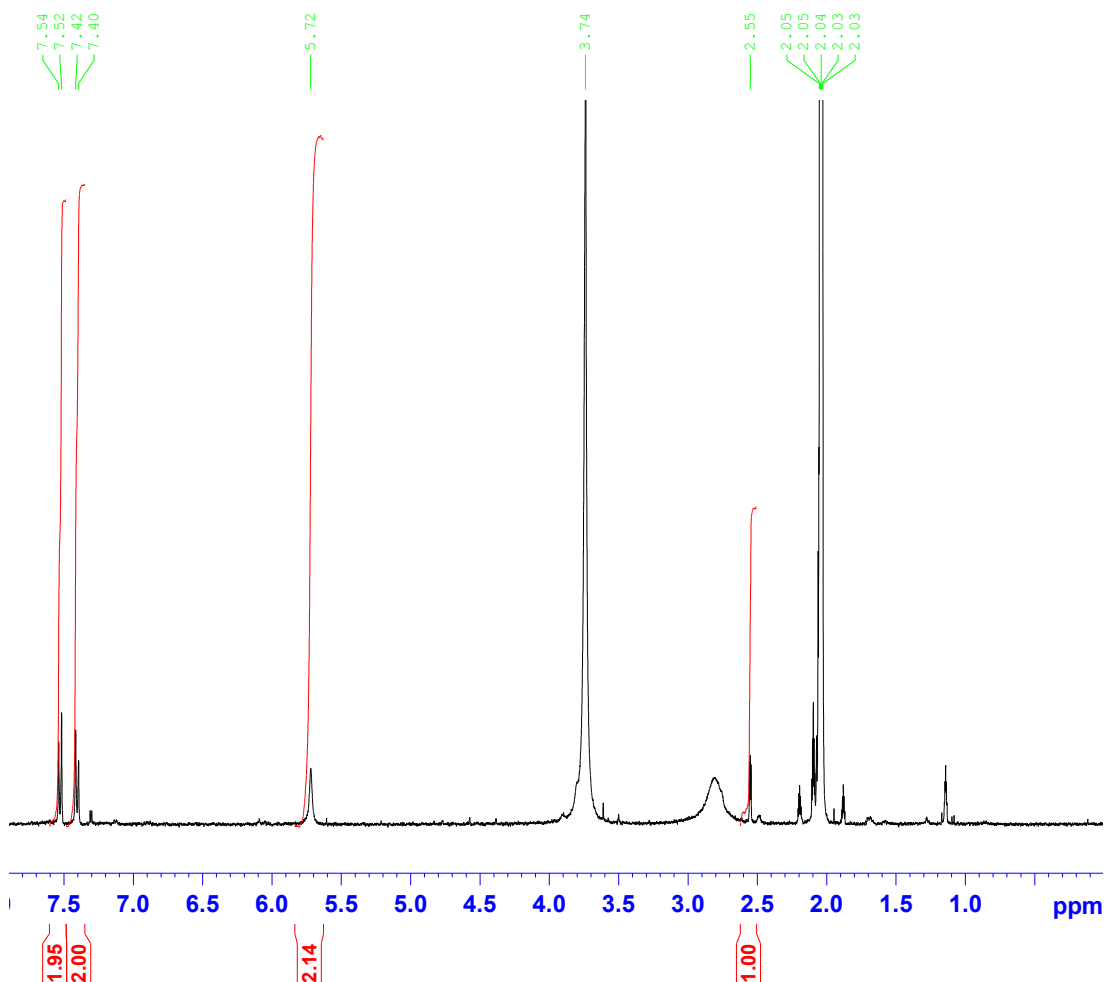
Figure 2.6 ^{1}H Nuclear magnetic resonance spectroscopic analysis of the 4-phenylacetic acid diazonium fluoroborate in acetone.
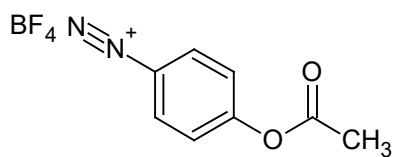
Figure 2.7   Schematic of the 4-phenylacetic acid diazonium fluoroborate molecule.

	Location of peaks reported by Delamar *et al.* [53]	Location of peaks in this study	Peak assignment
1	7.8	7.4	Ar-H, d, 2H
2	8.4	7.7	Ar-H, d, 2H
3	3.9	3.7	CH$_3$, s, 3H

Table 2.1 Hydrogen peak location and interpretation for 4-phenylacetic acid diazonium fluoroborate in deuterated acetone.

2.3.5   Cyclic voltammetry of Bu$_4$NBF$_4$ in acetonitrile

In the next step of our experiment, a *p*-phenylacetate film was electrochemically deposited on physically small carbon electrodes by performing multiple cyclic voltammetry of 0.01 M 4-phenylacetic acid diazonium fluoroborate in 0.1 M Bu$_4$NBF$_4$ in acetonitrile. Figure 2.8A shows the cyclic voltammogram obtained for 0.1 M Bu$_4$NBF$_4$ in acetonitrile at a representative electrode. This is a scan of the supporting electrolyte in which the *p*-phenylacetate compound was dissolved and then used in electrodeposition on bare carbon electrodes. It essentially shows a featureless voltammogram, indicating a lack of oxidation or reduction of any species in the supporting electrolyte. This therefore affirms that there was no contribution from the modifying medium in the electromodification of the electrode. In Figure 2.8B, cyclic voltammetry was repeated using 0.1 M Bu$_4$NBF$_4$ containing 0.01 M 4-phenylacetic acid diazonium fluoroborate in acetonitrile. In this voltammogram, as the potential was scanned between +0.20 V and -1.20 V, a reduction current peak was observed between -0.6 V and -1.2 V. With subsequent scanning of the potential, the magnitude of the reduction current is observed to decrease. This decreasing magnitude of current was attributed to the formation of a
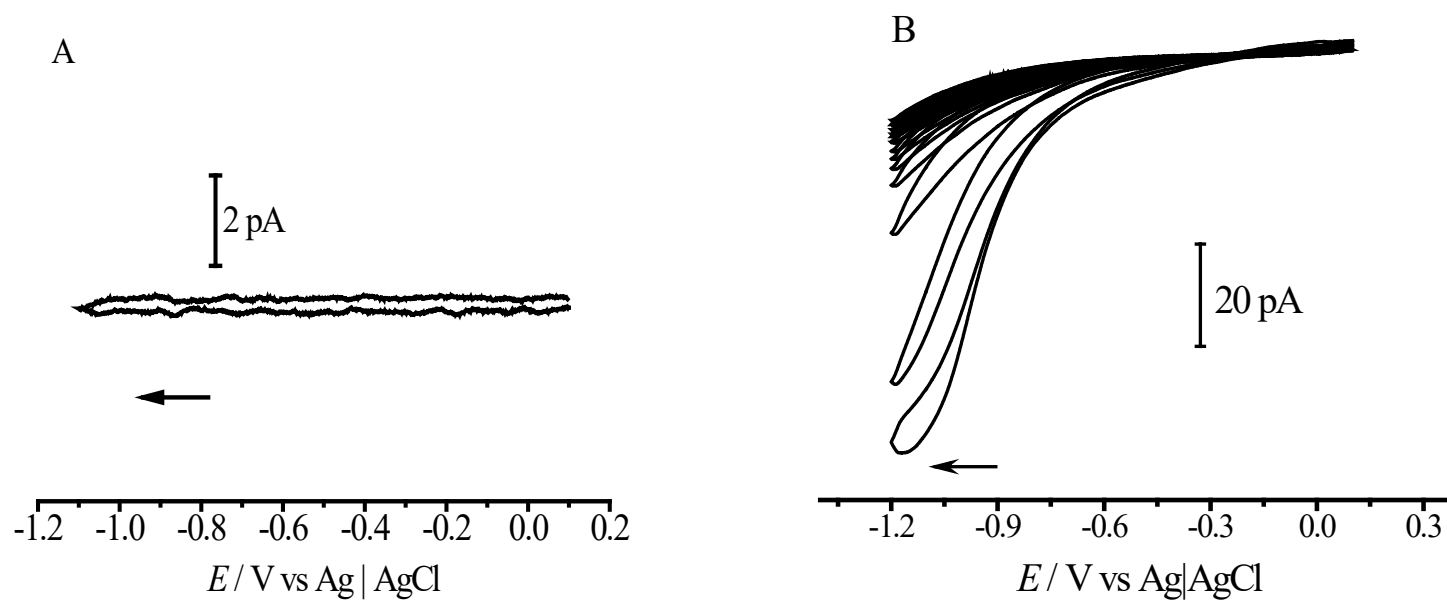
Figure 2.8   Cyclic voltammetry of 0.1 M Bu$_4$NBF$_4$ in acetonitrile (A) and 0.01 M 4-phenylacetic acid diazonium fluoroborate in 0.1 M Bu$_4$NBF$_4$ in acetonitrile (B). Scan rate: 100 mV/s.

coating on the electrode surface, inhibiting further reduction of 4-phenylacetic acid diazonium fluoroborate at the electrode surface.[73] Owing to considerable heterogeneity between bare carbon electrodes in terms of electroactive area, electrode dimensions and shape of the tapered end, between 20 – 50 scans were generally required for the electrodes used in this experiment.

2.3.6   Voltammetry of redox systems

At least three major phenomena affect electron transfer reactivity and these vary in importance for different redox systems and solution conditions. First, many systems are susceptible to surface cleanliness.[74] Therefore, observed electron transfer rates are strongly dependant on surface history. Secondly, the microstructure of the carbon film on the electrode plays an important role on most redox systems. For example, basal plane of highly oriented pyrolytic graphite tends to exhibit slower electron transfer than glassy carbon. Third, some redox systems are sensitive to the presence of surface oxides which act as catalysts for electron transfer.[74] In order to examine the microstructure of the electrodes before and after film-modification, 4 different redox markers, (1) $Ru(NH_3)_6^{3+/2+}$, (2) $Fe(CN)_6^{3-/4-}$, (3) dopamine and (4) anthraquinone-2,6-disulfonate were used as probes to study the characteristics of bare carbon and *p*-phenylacetate modified electrodes. The results of these are discussed in the following.

2.3.6.1   Voltammetry of hexamine ruthenium(III) chloride

For comparison, cyclic voltammetry of 1.0 mM $Ru(NH_3)_6^{3+}$ in 1.0 M KCl supporting electrolyte was conducted at *p*-phenylacetate film-coated carbon electrodes. Figure 2.9 shows the voltammograms obtained before and after a *p*-phenylacetate film was immobilised on an electrode.
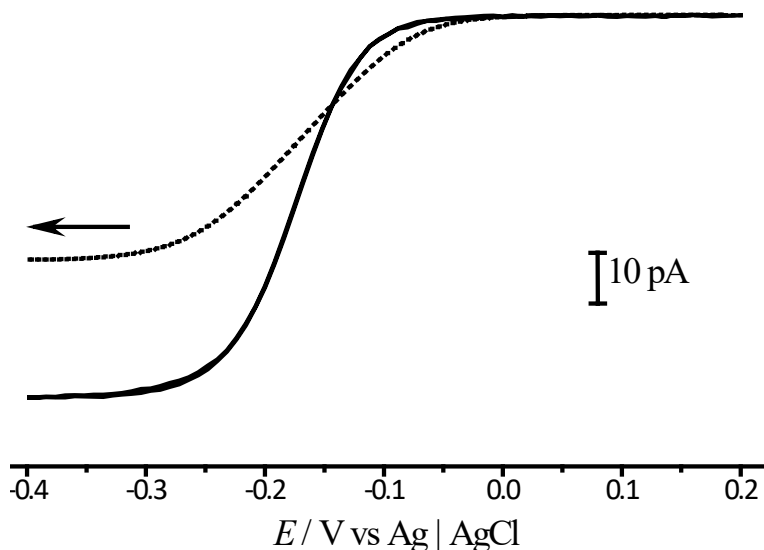
Figure 2.9   Cyclic voltammetry of 1.0 mM $Ru(NH_3)_6^{3+}$ in 1.0 M KCl supporting electrolyte before (dashed line) and after (solid line) application of *p*-phenylacetate. Scan rate: 100 mV/s.

The sigmoidal-shaped voltametric signal corresponds to current limited by the rate of diffusion of analyte molecules to the electrode surface.[18, 21] Therefore, the sigmoidal voltammogram for $Ru(NH_3)_6^{3+}$ obtained before and after the carbon electrode was coated with a *p*-phenylacetate film indicates that microelectrode features were maintained at the electrode post-modification. A 54% (with a standard deviation of 7%) increase in the limiting current for the reduction of $Ru(NH_3)_6^{3+}$ was observed at the film-coated electrode, compared to the bare carbon electrode (N = 6). The incorporated slightly anionic film was expected to attract the cationic redox marker towards the electrode for reduction, giving rise to a larger limiting current.

Roberts *et al.*,[75] have previously described the structure of graphitic carbon at the surface of electrodes being a mixture of sp^3 and sp^2 carbon atoms, with surface termination at edge planes comprising of a mixture of hydrogen, hydroxyl and carbonyl molecules as depicted in Figure 2.10.
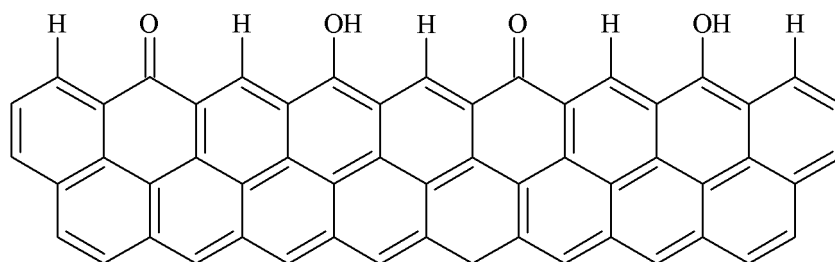
Figure 2.10   The graphitic surface of a bare carbon electrode.

Following modification of the electrode surface by *p*-phenylacetate molecules, the *p*-phenylacetate layer would most likely attach to the sp^2-hybridised carbon atoms on the electrode surface due to electrostatic attraction.[60, 76] This is depicted in Figure 2.11.
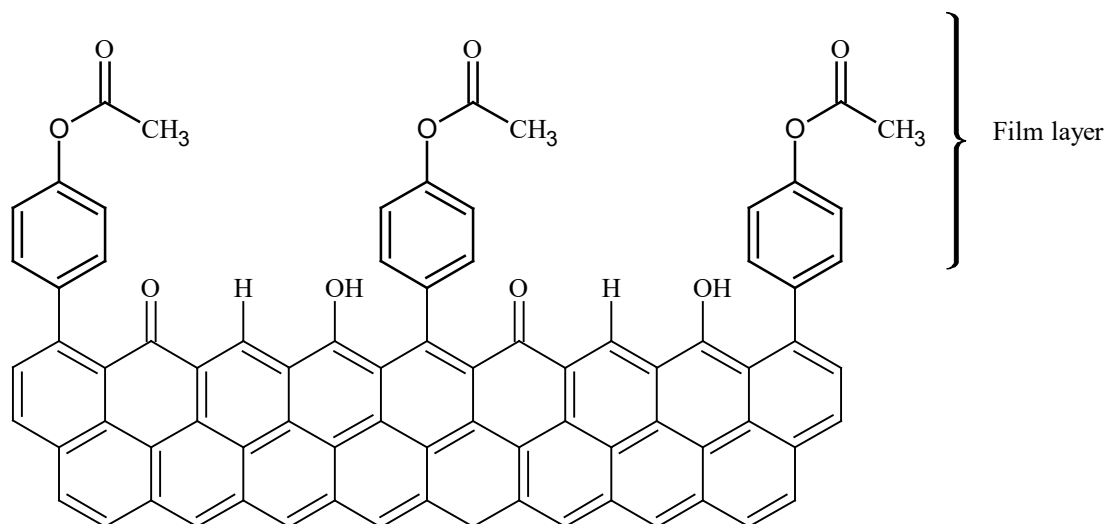
Figure 2.11   Graphitic carbon surface at edge planes modified with *p*-phenylacetate (labelled).

As proposed in Figure 2.11, the incorporation of a *p*-phenylacetate layer containing carbonyl groups and ether linkages, in addition to the hydroxyl and carbonyl functional groups already present would impart a strong negative-charge on the electrode surface. Therefore, following film-application, the modified electrode surface would exert increased electrostatic attraction towards the cationic $Ru(NH_3)_6^{3+}$, thus leading to greater diffusion and current, as is observed in Figure 2.9.

Based on a cyclic voltammogram, a measure of the reversibility of a reaction is the waveslope. A waveslope value of 59/*n* mV/decade, where n is the number of electrons exchanged, represents a reversible reaction at the electrode surface.[77] The rate of such a reaction is limited by the rate at which diffusion of ions occurs at the electrode surface.[21] Another important parameter, the halfwave potential, $E_{\frac{1}{2}}$ denotes the potential for the midpoint between the limiting and the residual currents. Both the waveslope and $E_{\frac{1}{2}}$ can be determined from the limiting current, and current at other potential in a cyclic voltammogram. For a reversible reaction, the equation relating the current and potential can be expressed as:[18, 78]

$$E = E_{\frac{1}{2}} + \frac{0.059}{n} \log_{10} (\frac{i_{\lim iting} - i}{i})$$ Equation (2)

A plot of *E* versus the log term of Equation 2, which yields a linear relationship with the intercept corresponds to the $E_{\frac{1}{2}}$ and slope equating the waveslope. As shown in Figure 2.9, following modification, the cyclic voltammogram of $Ru(NH_3)_6^{3+}$ exhibits negligible change in the waveslope. A slight shift in the $E_{\frac{1}{2}}$ from -166 mV to -173 mV is also observed. The values obtained are summarised in Table 2.2, and these results will be further discussed on page 54.

Redox System		Waveslope / mV/decade	N	Halfwave potential / mV	N
$Ru(NH_3)_6^{3+}$	Before film	68 ± 11	6	-166 ± 13	6
	After film	71 ± 4	6	-173 ± 8	6
Dopamine	Before film	124 ± 7	6	258 ± 25	6
	After film	104 ± 14	6	252 ± 12	6
$Fe(CN)_6^{3-}$	Before film	224 ± 49	6	107 ± 49	6
	After film	279 ± 76	6	102 ± 78	6

Table 2.2   Waveslope and halfwave potential data for electrodes in redox systems before and after film application.

The $E_{½}$ for a redox reaction is reported to be variable, largely dependent on the type of carbon surface, such as for polished glassy carbon (-190 mV), hydrogenated glass carbon (-175 mV) and highly oriented pyrolytic graphite (-150 mV).[60]

2.3.6.2   Voltammetry of dopamine

Dopamine is the analyte of interest in this study. Hence hence cyclic voltammetry of dopamine at bare carbon electrodes and *p*-phenylacetate modified carbon electrodes was conducted in pH 7.4 citrate/phosphate buffer as supporting electrolyte. The results obtained are depicted in Figure 2.12. In these voltammograms, there was an approximately 71% (with 3% standard deviation) increase in the limiting oxidation current of dopamine at the *p*-phenylacetate film coated electrode, compared to the corresponding bare carbon electrode. As the film is anionic, dopamine molecules were electrostatically attracted to the oppositely-charged film and this accentuate the diffusion of the molecules to the modified electrode surface. This in turn is expected to yield increased oxidation currents for dopamine at modified electrodes.

For dopamine oxidation, the waveslope was found to be 124 ± 7 mV/decade and 104 ± 14 mV/decade before and after the electrode was modified with a phenylacetate film, respectively. On the other hand, there was only a marginal -6.0 mV shift in the $E_{\frac{1}{2}}$ values before and after film application.
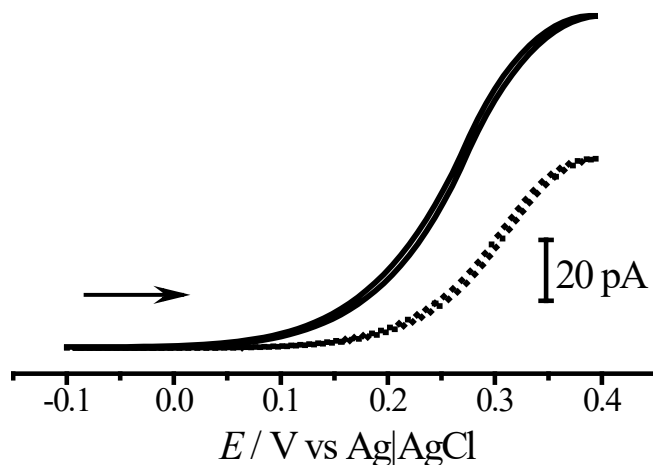
Figure 2.12   Cyclic voltammetry of 1.0 mM dopamine in pH 7.4 citrate/phosphate buffer before (dashed line) and after (solid line) application of film. Scan rate: 100 mV/s.

2.3.6.3   Voltammetry of potassium ferricyanide

The $Fe(CN)_6^{3-}$ redox system was previously reported to be unresponsive to carbon surface treatment procedures such as electrode polishing.[79] Alwarappan *et al.* have however demonstrated that surface alteration procedures such as hydrogenation of carbonyl functionalities at graphitic edge plane sites does cause slowing of electron transfer kinetics.[22] These findings are also supported by others who have shown that, unless surface activation is performed at glassy carbon electrodes, electron transfer rates for the reduction of $Fe(CN)_6^{3-}$ to $Fe(CN)_6^{4-}$ is slow. Holloway *et al.*[71] have proposed that this reduction process is facilitated at edge plane sites, containing carboxyl or quinonyl

functional groups, on carbon electrode surfaces *via* ligand substitution between the $Fe(CN)_6^{3-}$ and the functionalities. In this experiment, we compared the response of the electrodes to $Fe(CN)_6^{3-}$ before and after film application to elucidate any possible effects of the modification. Furthermore, the anionic $Fe(CN)_6^{3-}$ molecule permits the study involving negatively-charged redox marker, compared to the $Ru(NH_3)_6^{3+}$ and dopamine redox systems.

The $Fe(CN)_6^{3-}$ redox reaction depends on oxygen-bearing moieties at the electrode surface.[71] Chen *et al.*[80] have quantified this observation and have reported that a decrease of 1.5% of this ratio causes reduction in reaction kinetics for the $Fe^{3+/2+}$ by $1 - 2$ orders of magnitude. In addition, $Fe(CN)_6^{3-}$ is anionic, particularly at low pH. Liu *et al.*[73] have reported that anionic 4-aminobenzioc acid film-coated glassy carbon electrodes would block any interactions between $Fe(CN)_6^{3-}$ molecules and the modified electrode, while favouring the interaction with cationic $Ru(NH_3)_6^{3+}$. This was evidenced by strong and sharp reduction peaks in the cyclic voltammogram of $Ru(NH_3)_6^{3+}$ reduction and a featureless voltammogram for reduction of $Fe(CN)_6^{3-}$.

Figure 2.13 shows the voltammetric signal of 1.0 mM $Fe(CN)_6^{3-}$ in 1.0 M KCl at a small carbon electrode, before and after being coated with a *p*-phenylacetate film. In comparison with bare carbon electrodes, a 4% decrease in the limiting current was observed for $Fe(CN)_6^{3-}$ at the film-coated surface relative to a bare carbon electrode. This can be attributed to electrostatic interactions between the electrodes surface and the $Fe(CN)_6^{3-}$ molecule. As was shown in Figures 2.10 and 2.11, the bare carbon electrode surface, with occurrences of hydrogen can be considered less negative than *p*-phenylacetate-coated electrodes. An anionic species such as $Fe(CN)_6^{3-}$ is therefore expected to experience more repulsion from the modified surface than it did from the unmodified surface. With increased electrostatic repulsion, diffusion of $Fe(CN)_6^{3-}$ towards the electrode would be reduced which would translate to a reduction in current, consistent with the results depicted in Figure 2.13.
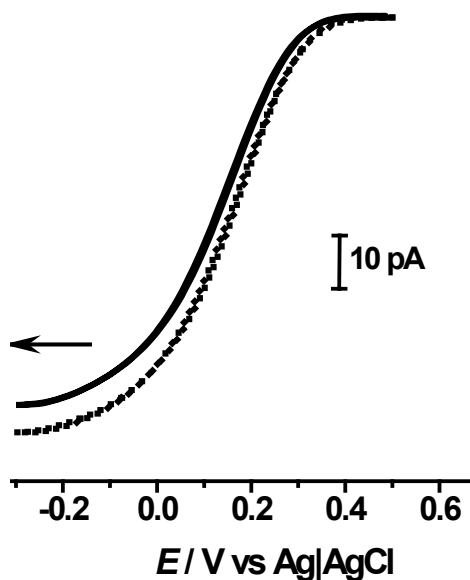
Figure 2.13   Cyclic voltammetry of 1.0 mM $Fe(CN)_6^{3-}$ in 1.0 M KCl before (dashed line) and after (solid line) application of film. Scan rate: 100 mV/s.

For the $Fe(CN)_6^{3-}$ system, the waveslope increased from 224 mV/decade to 279 mV/decade following film application. This demonstrates that for the species, reduction is quasi-reversible and altering the electrode surface characteristics, although demonstrating a 24% increase in waveslope, does not improve reversibility. The $E_{\frac{1}{2}}$ also remained relatively unchanged, from 107 mV to 102 mV. Ji *et al.*[81] have suggested that the involvement of surface carboxylate groups, which would normally be deprotonated in aqueous solution, would repel the anionic $Fe(CN)_6^{3-}$ molecules. This would lead to decreased concentration of $Fe(CN)_6^{3-}$ around the electrode surface and thereby a decreased apparent electron transfer rate. Each *p*-phenylacetate molecule contains one carboxylic group, and the incorporation of a layer of the electronegative oxygen-rich compound appears to cause decreased transfer kinetics in $Fe(CN)_6^{3-}$ after film incorporation. This observation appears to be consistent with this hypothesis.

2.3.6.4   Voltammetry of anthraquinone-2,6-disulfonate

The reduction of anthraquinone-2,6-disulfonate (AQDS) is often used to probe the presence of edge and basal planes on the electrode surface.[82-83] According to Kneten and McCreery, AQDS adsorption requires sufficient surface defect density such as those in graphitic edge regions as opposed to the ordered basal planes.[84] Surface carbon-oxygen functionalities play an important role in promoting strong dipole-dipole and ion-dipole interactions with polar and ionic molecules such as AQDS.[85]

Figure 2.14 shows the cyclic voltammogram of 1.0 mM AQDS in 0.1 M $HClO_4$ prior to film-coating. The electrodes displayed an absence of a voltammetric peak, suggesting an absence of edge effects and presence of basal planes instead on the electrodes.

6 pA

E / V vs Ag|AgCl
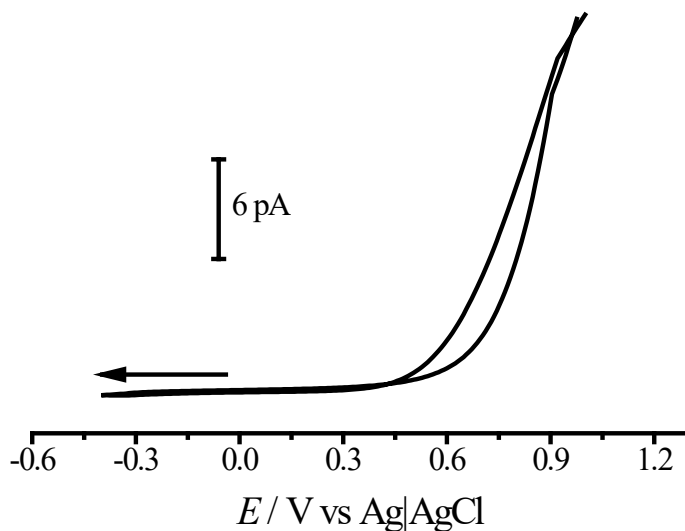
Figure 2.14   Cyclic voltammetry of 1.0 mM anthaquinone-2,6-disulfonate (AQDS) in 0.1 M $HClO_4$ supporting electrolyte. Scan rate: 100 mV/s.

These findings are consistent with previous work in our laboratory, where electrodes fabricated through a similar carbon pyrolysis procedure displayed a lack of voltammetric signal for AQDS.[22, 83] It suggests that the carbon electrodes fabricated in the study have

predominantly basal planes on the surface, which inhibits any adsorption of AQDS and possibly any adsorbed AQDS does not undergo electron transfer to basal plane as has been suggested previously.[83] Owing to a lack of a peak confirming the absence of edge planes, no further characterisation was performed using AQDS.

2.3.7   Waveslope and halfwave potential

Depending on the dimensions of the electrodes and their relative sizes to the diffusion layer in solution, either planar or radial diffusion may result. As discussed by Wang,[18] a dimensionless parameter, Dt/r_o^2 can be used to evaluate the diffusion pattern. In the equation, Dt represents the electrolysis time, while r_o is the smallest dimension of the electrode. A $Dt/r_o^2 > 1$ value indicates the diffusion layer is thicker than the electrode size. Therefore, as the current approaches steady state, a sigmoidal-shaped voltammogram is observed. In contrast, the smaller values of Dt/r_o^2 at conventionally large electrodes result in planar diffusion, which is denoted by peak-shaped voltammograms. This distinction can be extended to the reversibility of a redox reaction. In theory, a reversible redox reaction at a large electrode (where $Dt/r_o^2 < 1$), will yield a peak separation (between oxidation and reduction, denoted as ΔE_p) of $59/n$ mV. For a small electrode with sigmoidal voltammogram, such estimation is not as straightforward, as the voltammogram has a sigmoidal shape without discrete peaks. Thus the waveslope is used to determine reaction reversibility. Table 2.2 summarised the results of the waveslope and $E_{\frac{1}{2}}$ measurements at the electrodes before and after film modification for each redox system.

In carbon films, the basal plane is the exposed hexagonal layer parallel to the graphite layer, whereas the edge plane is where the surface is cut perpendicular to the graphite layer.[81] Edge planes typically show faster electron transfer kinetics than the basal plane for a range of redox couples. This means for some redox couples, an electrode that consists entirely of edge planes can show a nearly reversible voltammogram.

Conversely, an electrode that consists mainly of basal planes can show electrochemically irreversible behaviour with the kinetics, and the rate of the kinetics depends on the amount of edge plane defects in many instances.[70, 86] On this premise, as the dopamine and $Fe(CN)_6^{3-}$ molecules displayed irreversible behaviour at the bare carbon electrodes, it can be assumed that the electrodes in this study consist mainly of basal planes on the surface. Furthermore, the results show that there is very little alteration done to the planes on the surface *via* film deposition. With the exception of $Ru(NH_3)_6^{3+}$, all other redox systems display quasi- to irreversible kinetics. The relative insensitivity of $Ru(NH_3)_6^{3+}$ to electrode surface type[81] is likely to be responsible for the near-reversible kinetics displayed for the redox couple at the bare electrode, and the reversible kinetics displayed after film incorporation. Indeed, a 68 mV waveslope value obtained in this study is in exact agreement with that found earlier[81] for electrodes with known basal planes. The behaviour of the AQDS system at the electrodes also thus affirms that most reactions would be subjected to kinetic over diffusion control. This is important when considering the slow electron transfer rates for $Fe(CN)_6^{3-}$ at the electrodes before and after film incorporation. These results are consistent with the findings of McCreery and co-workers[69] who have suggested that the $Fe(CN)_6^{3-}$ system is very sensitive to surface structures which greatly influence its transfer kinetics. The supposition that electrodes in this study consist of mainly basal planes fits in well with this explanation. Other researchers have previously discussed the complicated nature of results for the reduction of $Fe(CN)_6^{3-}$ towards carbon surfaces.[87-88] One is the higher heterogeneous electron-transfer rate constants for glassy carbon over highly oriented pyrolytic graphite, especially with laser activation or ultraclean polishing of the glassy carbon surface. Moreover, it has also been suggested that activation of highly oriented pyrolytic graphite may not even be related to oxides *per se*, but rather to lattice damage accompanying the film formation. While our electrodes are neither glassy carbon nor highly oriented pyrolytic graphite in the strictest sense, these previous studies highlight the variety of responses different forms of carbon films have towards $Fe(CN)_6^{3-}$.

The $E_{\frac{1}{2}}$ was observed to decrease by approximately 6 mV for all redox systems. Based on this common shift in the value thus, it appears to be quite possibly a result of an altered electrode surface.

2.3.8   Response to ascorbic acid following film incorporation

Previously, *p*-phenylacetate coated macroelectrodes demonstrated suppression in the oxidation signal of ascorbic acid and a corresponding increase in that for dopamine.[14] Thus it was of interest to compare the oxidation response of ascorbic acid at the *p*-phenylacetate film-coated small carbon electrodes to that of dopamine. Figure 2.15 shows the response obtained at small carbon electrodes before and after being coated with the *p*-phenylacetate film. These voltammograms show a 35% reduction in oxidation signal (N = 5) at the film-coated electrode compared to the bare carbon electrode. In order to compare electrodes with varying surface area, all responses were normalised by electrode surface area. Table 2.3 shows the normalised ascorbic acid oxidation signal.
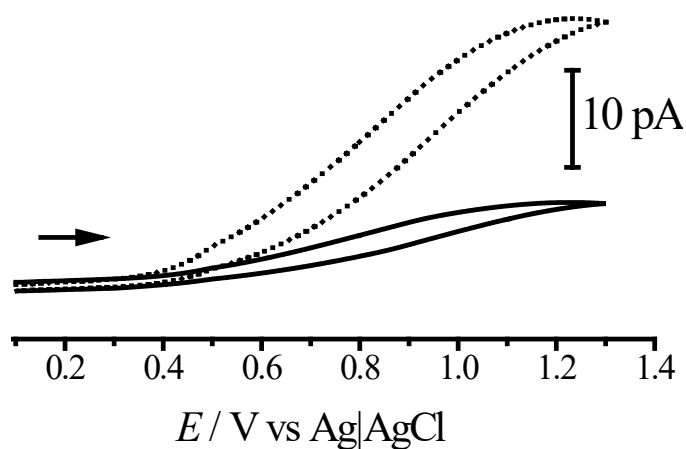
Figure 2.15   Comparison of cyclic voltammetry of 1.0 mM ascorbic acid in pH 7.4 citrate/phosphate buffer before (dashed line) and after (solid line) film application. Scan rate: 100 mV/s.

Notably, there is a 35% decrease in ascorbic acid oxidation current following film incorporation on the carbon electrodes. This loss in oxidation signal is attributable to the electrostatic interactions between the electrode surface and ascorbic acid as discussed previously.[14]

Electrode	Area-normalised percentage decrease in ascorbic acid oxidation current after film-modification / %
1	30.4
2	39.1
3	36.9
4	33.1
5	38.9

Table 2.3   Variation in area-normalised ascorbic acid oxidation signal at electrodes before and after film incorporation.

Figure 2.16 shows a simplified representation of the applied film on the electrode surface. The ether linkage, as well as the carbonyl group augments the pre-existing carbonyl groups from the graphitic sp^2 carbon, thereby increasing the magnitude of negative charge on the electrode surface. With ascorbic acid having a pKa of 4.2 as stated previously in Section 2.1.2, it will be similarly expected to be prevalent as anionic ascorbate at pH 7.4, thus experiencing repulsion from the oxygen-rich ether and carbonyl groups present in the *p*-phenylacetate film coating on the electrode.

Modified electrode   Bare carbon electrode
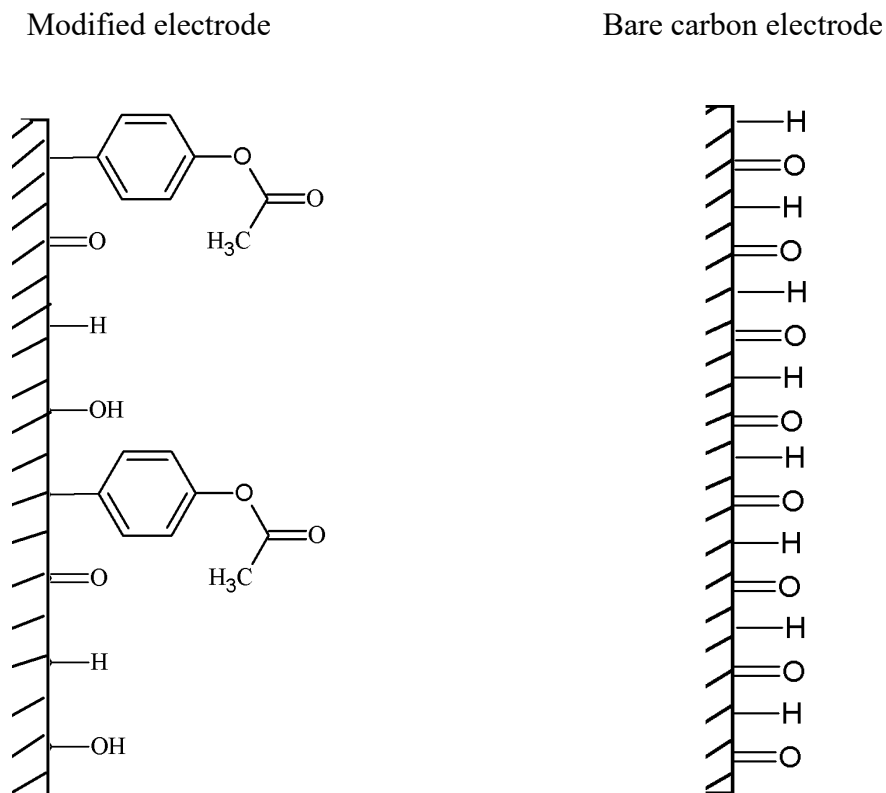
Figure 2.16   Surface termination comparison at a film-coated electrode and bare carbon electrode.

2.3.9   Stability of *p*-phenylacetate film

To determine stability, four electrodes were stored in glass beakers under laboratory conditions (1 atm pressure, 25°C temperature), where their responses to dopamine were determined over a period of 40 days. Two sample cyclic voltammograms from the same electrode, derived 1-day and 40-days after film incorporation, are presented in Figure 2.17.
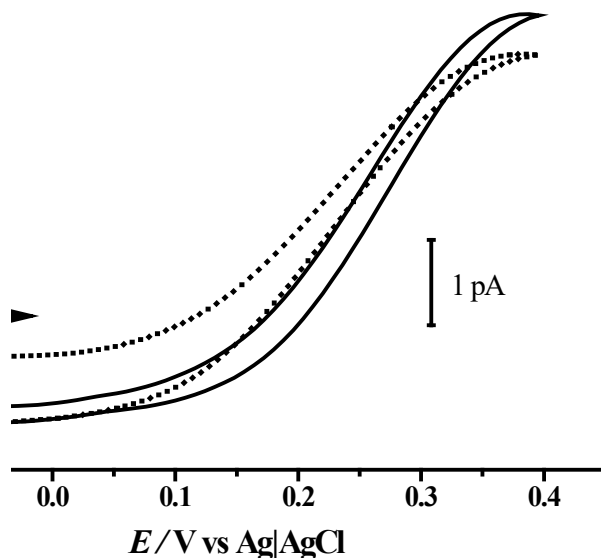
Figure 2.17   Comparison of cyclic voltammetry of 1.0 mM dopamine in pH 7.4 citrate/phosphate buffer on the day of film incorporation (dashed line) and after 40 days after film incorporation (solid line) at a *p*-phenylacetate film-coated electrode. Scan rate: 100 mV/s.

After the 40-day period, the electrodes displayed approximately 11 % decrease in their response to dopamine (N = 4).   In addition, there was no deterioration of the voltammogram character, which was observed to remain sigmoidal in the same period. In comparison, bare carbon small electrodes displayed over approximately 90% loss in signal after the same period as shown in Figure 2.18. This demonstrates the stability of the film-coated electrode surface.
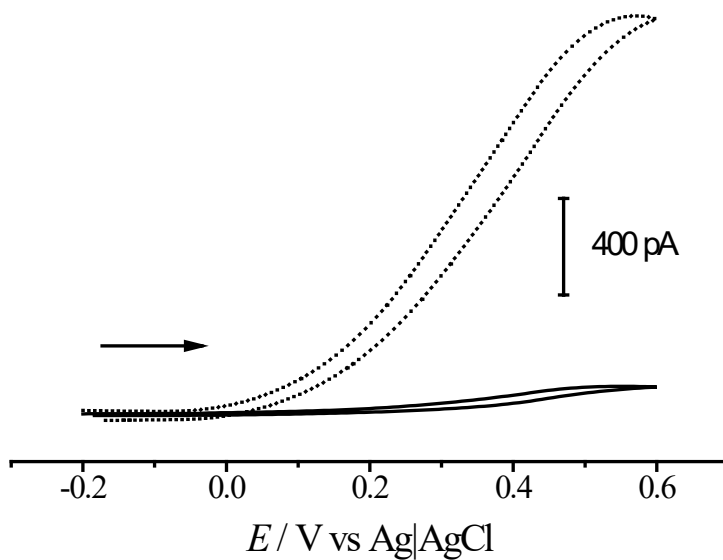
Figure 2.18   Comparison of cyclic voltammetry of 1.0 mM dopamine in pH 7.4 citrate/phosphate buffer on the day of fabrication (dashed line) and 40 days after fabrication (solid line) at a bare carbon electrode. Scan rate: 100 mV/s.

2.3.10   Analytical performance of *p*-phenylacetate film-coated electrodes

Dopamine calibration experiments at both bare carbon and *p*-phenylacetate film-coated electrodes were performed. In the following, the limit of detection is defined as the concentration corresponding to the sum of the mean blank signal, and three times the standard deviation of the blank signal. Similarly, the sensitivity of the electrodes towards dopamine oxidation is estimated from the slope of the linear current versus concentration calibration plot of dopamine. A comparison of these two parameters gives an insight into the relative performance of the electrode sensor in its dopamine detection application. Figure 2.19 shows the calibrations plots obtained at a *p*-phenylacetate film-coated carbon electrode and a bare carbon electrode for comparison.
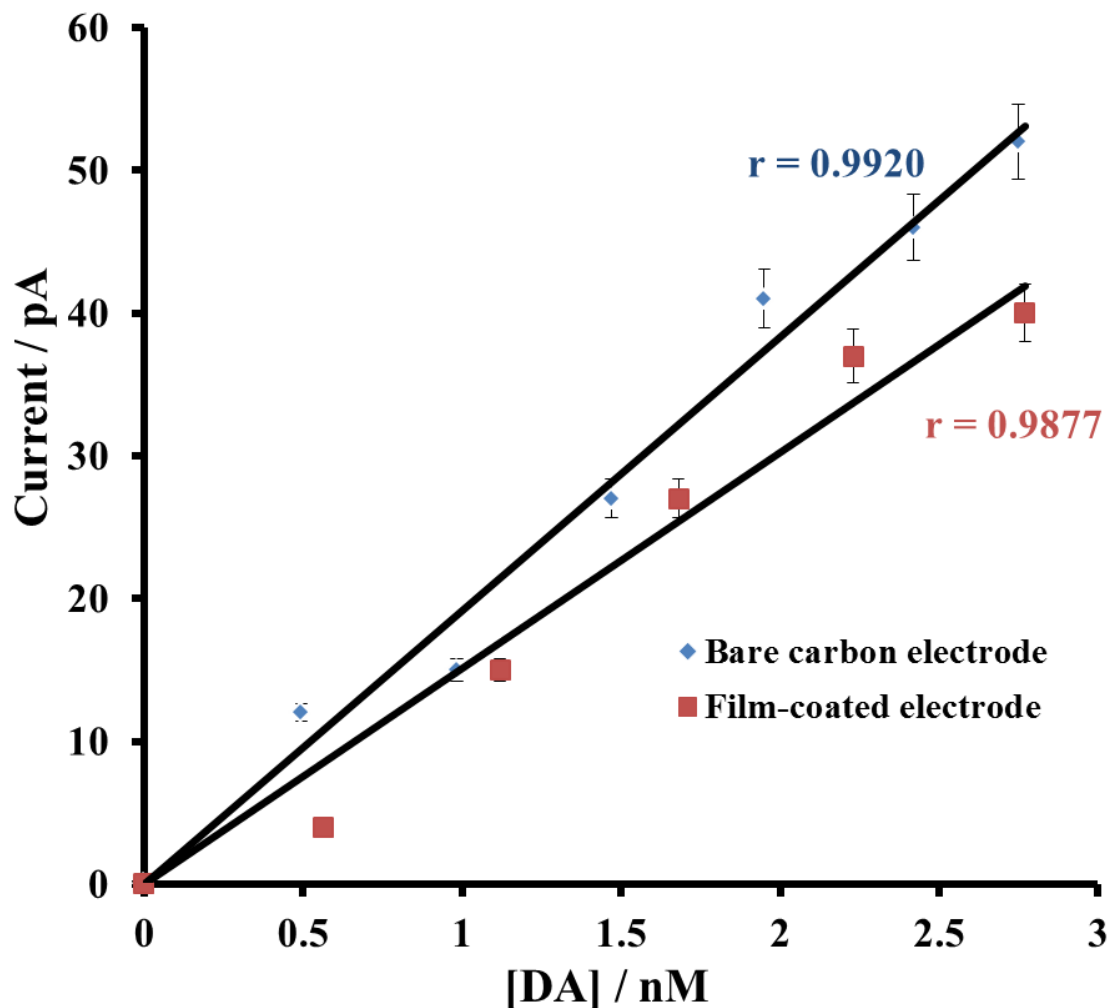
Figure 2.19   Calibration plots for limiting current versus dopamine concentration in pH 7.4 citrate/phosphate buffer solution at film-coated and bare carbon electrodes.

For the calibration plot of dopamine at *p*-phenylacetate coated electrodes, we obtained a correlation coefficient of 0.9877 (N = 7). The correlation coefficient, sample number, limit of detection and sensitivity values for the plots in Figure 2.19 are summarised in Table 2.4. The linear relationship for dopamine detection at these film-coated electrodes can be expressed as

$$\text{Current} / \text{pA} = 16 \pm 0.0031 \text{ pA/nM} \times [\text{dopamine}] / \text{nM} + 9 \pm 4 \text{ pA}.$$

For film-coated electrodes, the limit of detection and sensitivity, were determined to be 541 pM and 16 pA/nM respectively. A relatively high baseline, subsequently subtracted, was also initially observed at the calibration, suggesting possibly high capacitance at the electrode. This is entirely expected based on previous findings of the incorporation of a film, particularly organic having enhanced the capacitance of otherwise pure graphitic carbon electrode surfaces.[89-90] It is supposed that the high degree of activity and response stability result from the fact that the non-polar, relatively oxygen-free surface is less prone to the adsorption of polar impurities that tend to adsorb on and foul sp^2 carbon electrodes.[91] While the film-coated electrodes are enriched with oxygen at the edge plane sites, it appears that for *p*-phenylacetate film, the kinetics of the reaction are controlled by the charge on the film to a large extent. This is evidenced by the slight increases in current for the anionic $Fe(CN)_6^{3-}$ species, which is suspected to overshadow any responses $Fe(CN)_6^{3-}$ may otherwise have to a basal surface.[92]

The calibration for the bare carbon electrodes is expressed as

$$\text{Current} / \text{pA} = 19 \pm 0.071 \text{ pA/nM} \times [\text{dopamine}] / \text{M} + 10 \pm 8.0 \text{ pA}.$$

As shown in Table 2.4, the sensitivity and limit of detection for dopamine at bare carbon electrodes were obtained as 19 pA/nM and 543 pM respectively. Thus the values for sensitivities and limit of detection at *p*-phenylacetate film-coated electrodes and bare carbon electrodes are not significantly dissimilar. However, it is useful to be able to also quantify the response of the electrode to dopamine in the presence of interfering ascorbic acid. Accordingly, in the next experiment, we determined the limit of detection and sensitivity of the electrode to dopamine in the presence of 200 µM ascorbic acid and 0.1% (w/v) bovine serum albumin. The bovine serum albumin was deliberately added to

mimic a chemical environment containing a protein species.[6, 8, 10] Figure 2.20 shows the calibrations obtained for dopamine. The linear relationship can be expressed as

$$\text{Current} / \text{nA} = 0.1 \pm 0.03 \text{ nA/nM} \times [\text{dopamine}] / \text{nM} + 3.8 \pm 0.30 \text{ nA}$$

A linear response up to 20 nM was obtained. In addition, the sensitivity and limit of detection were estimated to be 0.1 nA/nM and 6 nM, respectively.

Figure 2.20   Calibration plot of limiting current versus dopamine concentration in a solution of 0.1% bovine serum albumin+ 200 μM ascorbic acid at a *p*-phenylacetate-coated electrode.

To be able to quantify the sensitivity and limit of detection of the film-coated electrodes to ascorbic acid, a similar calibration plot was obtained for ascorbic acid oxidation in the presence of 0.1% (w/v) bovine serum albumin. The ascorbic acid concentrations employed in this experiment were set at a higher range as initial calibration experiments demonstrated that the electrodes did not detect any ascorbic acid in the nM range. Figure 2.21 shows the plot obtained. The relationship for the plot can be expressed as

$$\text{Current} / \text{nA} = 0.1 \pm 0.002 \text{ nA/}\mu\text{M} \times [\text{dopamine}] / \mu\text{M} + 0.8 \pm 0.4 \text{ nA}$$

which has a linear response up to 20 nM. In addition, the sensitivity and limit of detection were estimated to be 0.1 nA/µM and 1.4 µM respectively. The results demonstrate the film-coated electrodes exhibited lower detection limits and higher sensitivities for dopamine over ascorbic acid. The detection limits are also comparable to those reported for modified sensors in detecting dopamine, for example, 90 nM for *p*-phenylacetate film-coated glassy carbon macroelectrodes;[14] 0.1 µM for electropolymerised carbazole-coated carbon fibre microelectrodes;[93] 5 nM for carbon fibre microelectrodes modified by Nafion and single-walled carbon nanotubes.[35]

In a pH 7.4 citrate/phosphate buffer solution, ascorbic acid molecules tend to exist as dissociated ascorbate anions.[34, 94] The regions of negative charge on the electrode surface would thus exert repulsion towards the ascorbate anions, thereby limiting any attraction the ascorbate would have towards the electrode. This leads to a significantly reduced flux of ascorbate ions compared to previously at the same, unmodified surface. The reduced flux translates into reduced oxidation, in turn leading to a reduced oxidation signal in the voltammogram.

Figure 2.21   Calibration plots of limiting current versus ascorbic acid concentration in a solution of 0.1% (w/v) bovine serum albumin at a *p*-phenylacetate-coated electrode.

Notably, surface modification, as has been represented schematically in Figure 2.12 for film-modified electrodes, is the product of a more complex range of factors. As such, it is not suggested that there is addition of the *p*-phenylacetate to each sp^3-hybridised carbon atom on the electrode surface. Indeed, it is possible that there are unmodified carbon-hydrogen bonds that remain unaffected by the modification process. It would be at these neutral sites on the electrode surface that some ascorbate adsorption will occur, leading to oxidation of some of the species from the bulk solution.

2.3.11   Electrode performance following *in vitro* exposure

A sensor that is susceptible to fouling often suffers from distortion of the voltammetric signal suppression of the electrode sensitivity. As a result, it is useful to evaluate and compare the sensitivity and limit of detection before and after exposure to fouling species. Accordingly, in this experiment, electrodes were calibrated to determine these two parameters at each electrode. These were then compared after incubating the same electrodes in a solution comprising of proteins, lipids and peptides. A solution of this composition was intended to mimic the extracellular fluid in the brain. The species utilised in the composition of the synthetic laboratory solution were selected based on their solubility in an alkaline (pH 7.4) aqueous solution. To mimic the protein, peptide and lipid composition of the extracellular fluid, the solution was prepared to achieve the following: 1.0% (v/v) caproic acid (lipid), 0.1% (w/v) bovine serum albumin and 0.01% (w/v) cytochrome C (both are protein) and 0.002% (w/v) human fibrinopeptide B (peptide).

The electrodes were immersed in this solution continuously for 7 days. Next, the electrodes were again subjected to calibration experiments based on oxidation of dopamine, and the sensitivity and limit of detection were evaluated to assess any changes following exposure to the synthetic laboratory solution.   Figure 2.22 shows the calibration obtained at film-coated electrodes before and after immersion in the synthetic laboratory solution.

The calibration information for dopamine at film-coated electrodes prior to incubation in the synthetic laboratory solution has already been presented in Section 2.3.10. The limit of detection previously was obtained as 541 pM, while sensitivity was determined to be 16 pA/nM, which are favourable compared to 90 nM and 0.041 A/M achieved at *p*-phenylacetate film-coated conventional sized glassy carbon electrodes.[14]   Plot B in Figure 2.22 shows the calibration obtained for dopamine following immersion of the

film-coated electrodes in the synthetic laboratory solution. The equation for the calibration is expressed as

$$\text{Current / pA} = 50 \pm 0.04 \text{ pA/nM} \times \text{[dopamine] / nM} - 6.40 \pm 25.2 \text{ pA}$$
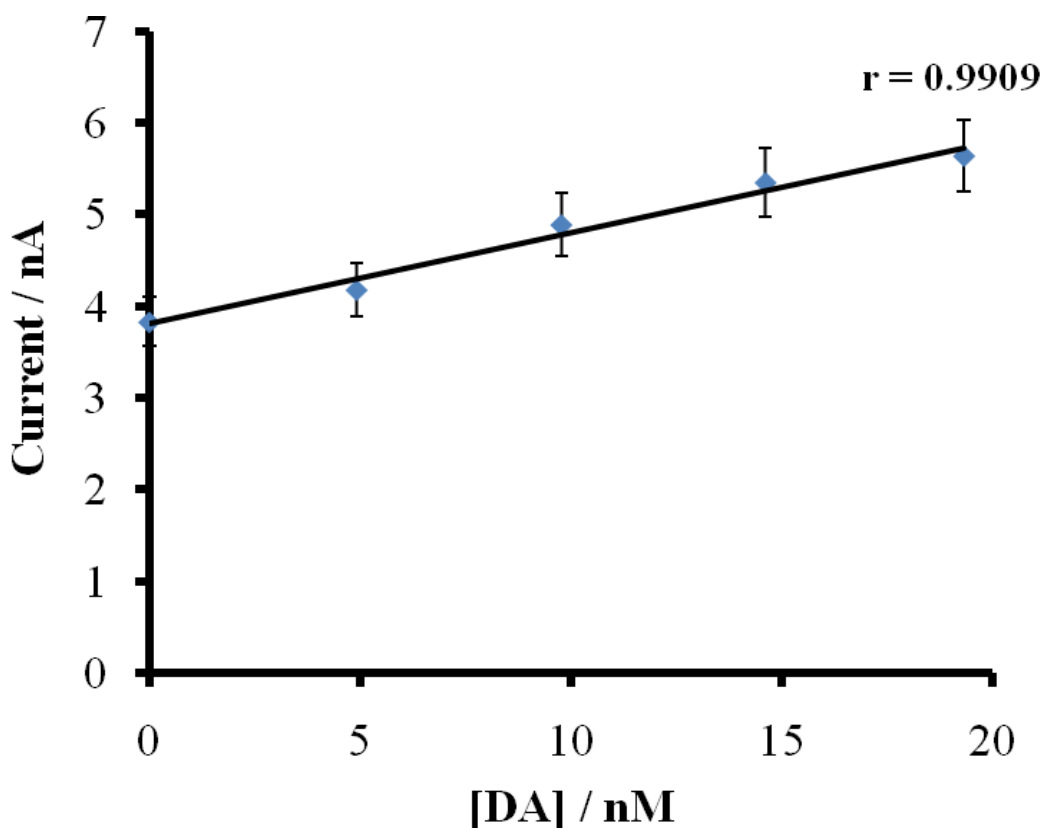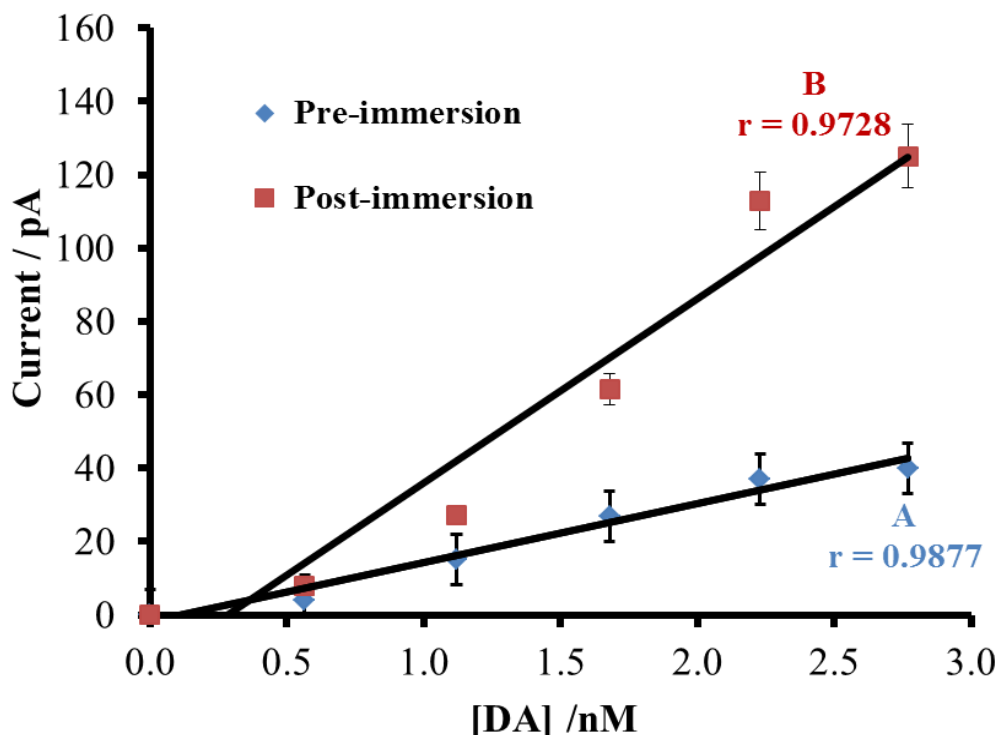

Figure 2.22   Calibration plots of limiting current versus dopamine concentration in a solution of 0.1% (w/v) bovine serum albumin + 1.0% (v/v) caproic acid + 0.002% (w/v) human fibrinopeptide B + 0.01% (w/v) cytochrome C in pH 7.4 citrate/phosphate buffer: before immersion (A) and after immersion (B) at *p*-phenylacetate film-coated electrodes.

The sensitivity of the technique was determined to be 50 pA/nM and detection limit obtained to be 385 pM. Compared to the same parameters before immersion in the synthetic laboratory solution, sensitivity was observed to increase from 16 to 50 pA/nM, while there was a decrease in the limit of detection from 541 pM to 385 pM. The

decrease in limit of detection at the film-coated electrodes is not significant (at 95% confidence intervals). The increase in the observed sensitivity of the electrode to dopamine following exposure to the laboratory synthetic solution may be attributed to artificially-enhanced signals, possibly arising from larger, non-Faradaic currents as a result of some adsorbed hydrophilic molecules from the laboratory synthetic solution at the electrode surface. In comparison to Figure 2.22, Figure 2.23 depicts the calibration plot of dopamine at bare carbon electrodes before and after immersion in synthetic laboratory solution. The calibration plot for bare carbon electrodes prior to has been presented in Section 2.3.10, where an examination of the slope of the plot provided a sensitivity of 19 pA/nM, and the limit of detection at 543 pM. Upon immersion in the laboratory synthetic solution, the subsequent calibration for dopamine yields a plot whose correlation coefficient was statistically insignificant. Moreover, the limit of detection and sensitivity could not be determined. We attribute this to extreme surface degradation leading to almost nil sensitivity to dopamine.

Therefore, in comparison to the film-coated electrodes, the bare carbon electrodes displayed considerable changes to the sensitivity and limit of detection. As seen in Table 2.4, compared to the film-coated electrodes, the bare carbon electrodes are observed to be undergoing more changes to the sensitivity and limit of detection. There is clearly a high degree of loss of sensitivity and a surge in the limit of detection. On the other hand, the film-coated electrodes tend to display relative stability in the two parameters, therefore affirming that the film coated surface does not undergo fouling to the extent observed at bare carbon electrodes.

2.3.12 *In vivo* **dopamine detection at** *p*-**phenylacetate film-coated electrodes**

In vivo application of the *p*-phenylacetate film-coated electrodes to dopamine detection is a powerful means to evaluate the effectiveness of film-coated electrodes in resisting fouling. In this experiment, electrodes were implanted in the left striatum of a rat brain.
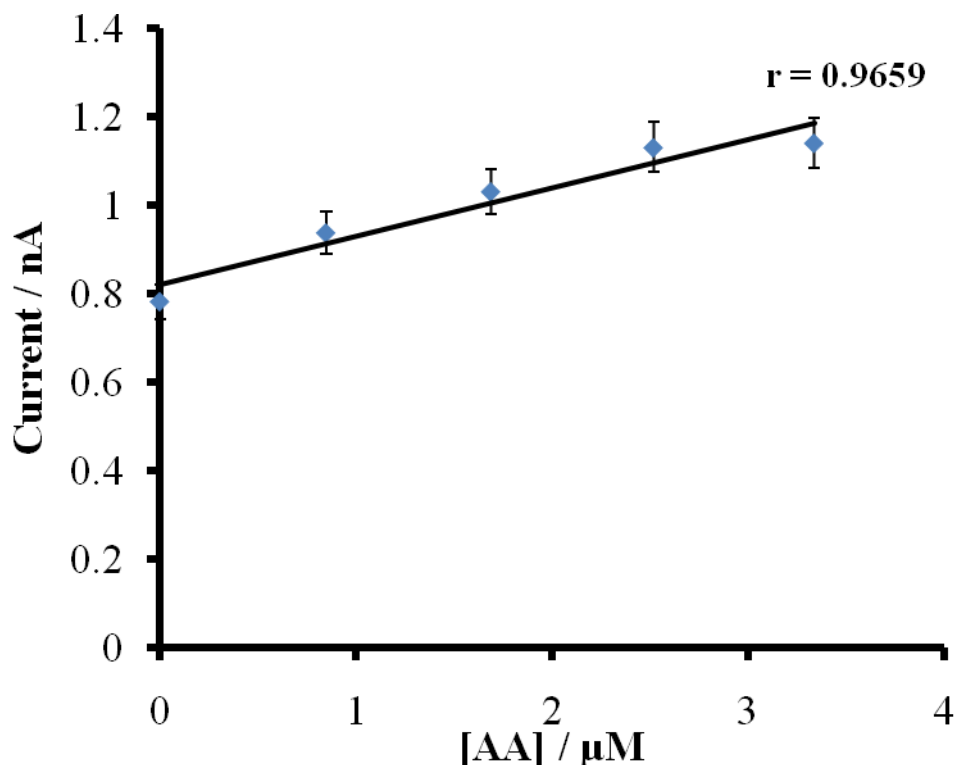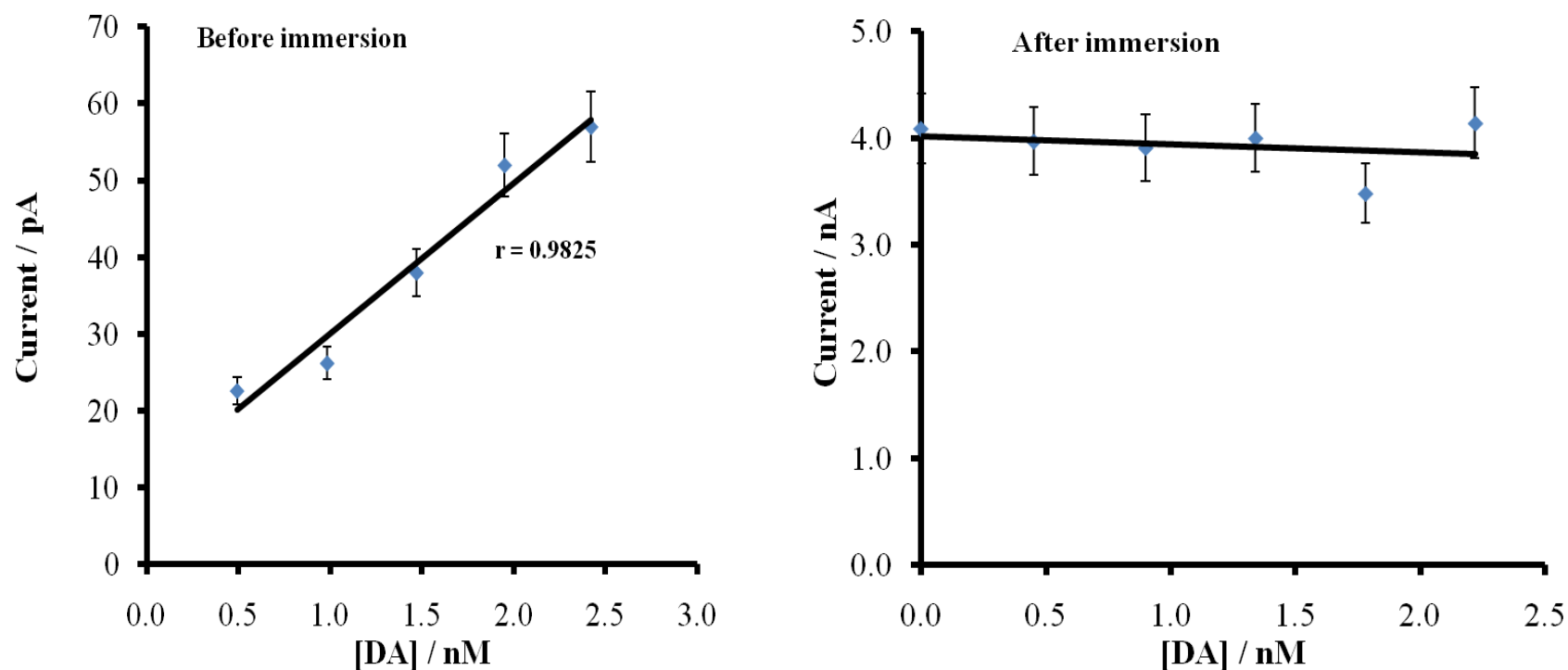
Figure 2.23   Calibration plots of limiting current versus dopamine concentration in a solution of 0.1% (w/v) bovine serum albumin + 1.0% (v/v) caproic acid + 0.002% (w/v) human fibrinopeptide B + 0.01% (w/v) cytochrome C in pH 7.4 citrate/phosphate buffer: before immersion (A) and after immersion (B) at bare carbon electrodes.

Figure	Calibration Plot Type	N	Correlation coefficient	Limit of Detection / pM	Sensitivity
2.19	Dopamine calibration at *p*-phenylacetate film-coated electrode	7	0.9877	541	16 pA/nM
2.19	Dopamine calibration at bare carbon electrode	6	0.9927	543	19 pA/nM
2.20	Dopamine calibration in the presence of 0.1% bovine serum albumin + 200 µM ascorbic acid at *p*-phenylacetate film-coated electrode	5	0.9909	6,000	0.1 nA/nM
2.21	Ascorbic acid calibration in the presence of 0.1% bovine serum albumin at *p*-phenylacetate film-coated electrode	5	0.9659	1,400,000	0.1 nA/µM
2.22	Dopamine calibration at *p*-phenylacetate film-coated electrode prior to incubation in synthetic laboratory solution	7	0.9877	541	16 pA/nM
2.22	Dopamine calibration at *p*-phenylacetate film-coated electrode after incubation in synthetic laboratory solution	7	0.9728	385	50 pA/nM
2.23	Dopamine calibration at bare carbon electrode prior to incubation in synthetic laboratory solution	7	0.9927	543	19 pA/nM

Table 2.4   Summary of limit of detection and sensitivity data at film-coated and bare carbon electrodes.

Due to the abundance of dopamine vesicles in the region, the striatum is an excellent region to perform *in vivo* experiments at our electrodes.[2, 29, 52, 95] Others have previously reported measuring dopamine in abundance in this region with successful results using a range of working electrodes such as graphite paste electrode,[52] carbon fibre electrodes,[96] carbon paste electrodes,[8] and more recently, cylindrical carbon fibre arrays.[97] The stimulation of the ventral tegmental area, particularly using electrical stimulation is also well documented by researchers in literature.[23, 98-99]

Electrode fouling is among factors responsible for distortion of the dopamine oxidation signal.[22, 57] Monitoring the decay in the oxidation signal between the time of implanting the electrode in the striatum and a defined period later can yield useful information on the signal quality, and changes to electrode performance. In our experiment, a series of 0.5 ms duration, 800 µA cathodic, monophasic current pulses was delivered to the stimulating electrode *via* an optical isolator and programmable pulse generator. The dopamine oxidation signals arising in response to the stimulation were recorded at the start of stimulations and every 15 min subsequent to implantation for up to 60 min. The first stimulation was commenced within 1 min of implanting the electrode in the striatum. In the brain, upon appropriate stimulation such as an action potential,[100] dopamine is released at the synaptic cleft between two neurons.[25] As it reaches the implanted working electrode in the striatum, oxidation of dopamine results in a current oxidation peak. The extent of fouling at an electrode surface can be evidenced by decay in this oxidation peak feature height. With increasing adsorption of large molecular-weight hydrophilic species on the electrode surface, less dopamine oxidation occurs at the surface, leading to a decline in the oxidation peak feature height.

Examples of responses obtained after a series of electrical stimulations are shown in Figure 2.24. Figure 2.24A depicts an example of the stimulation pulse signals delivered to the stimulating electrode at the start of the experiment, which results in dopamine peaks presented in Figure 2.24B. To be able to deconvolute the cluster of peaks and to

obtain meaningful information therein, the peaks in Figure 2.24B were integrated using the Gaussian function. The results of this fitting are shown in Figure 2.24C, with the sum of fitted peaks (in green) represented in black (a convention adopted throughout this thesis). Here, negligible current was flowing in the absence of any stimulus from 0.00 s to approximately 0.26 s. Upon stimulation, dopamine stored in vesicles near cell membranes was released and diffused towards the electrode. A rise in current was observed as oxidation of the neurotransmitter occurred. However, the oxidation current quickly decreased as the concentration of dopamine was reduced through processes such as diffusion away from the synapse, interaction with cell receptors or uptake by membrane-bound proteins referred to as transporters.[101] The stimulation was repeated every 15 min (data not shown). The corresponding responses obtained after applying electrical stimulations at 60 min are depicted in Figure 2.24D, and the fitted results in Figure 2.24E. Comparison of the dopamine oxidation current obtained after the first series of stimulations to that obtained after 60 min clearly shows a transient decrease in peak current.

Figure 2.25A shows a plot of the percentage of oxidation current remained against time over which detection of dopamine was monitored at different *p*-phenylacetate film-coated electrodes implanted in the rat brain. Notably, owing to limitations of animal ethics requirement, only 4 electrodes, implanted in two different rats were used in this study. This partly explains the fluctuations of results observed in the figure. Nonetheless, for oxidation current signals after the first series of stimulations, we assume negligible fouling took place between the time the electrode was implanted and measurement of dopamine. Accordingly, the current measured was assigned 100%. The currents generally decrease slightly from 100% to 60-75% in the first 40 min. Over the next 20 mins, the current continued to decline to less than 50%, and even more severe fouling was observed at the end of the experiment. We attribute this to the less stable nature of the film. From the results depicted in Figure 2.25A, the *p*-phenylacetate film appears to
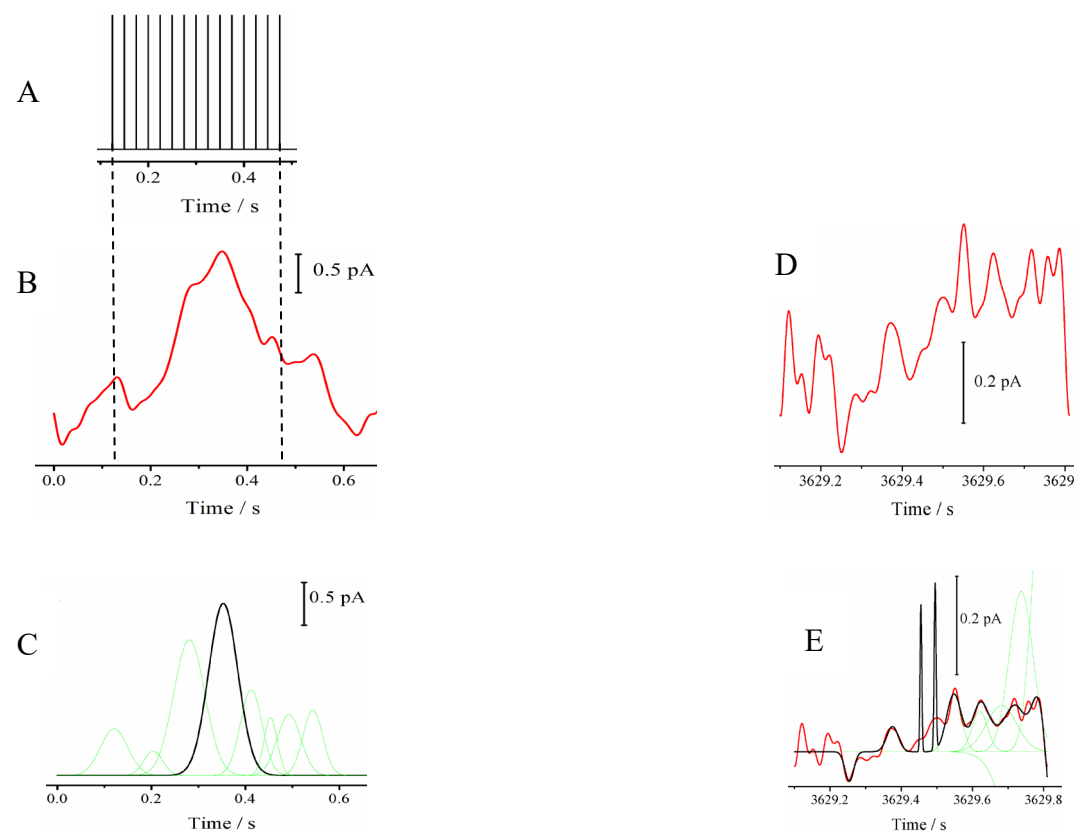
Figure 2.24   Electrical stimulation signals (A) corresponding with dopamine oxidation signal in the rat striatum at film-modified electrodes at the start of the experiment; unfitted (B) and Gaussian-fitted (C). Dopamine oxidation signals, unfitted (D) and fitted (E) after 60 min of monitoring are presented for comparison.
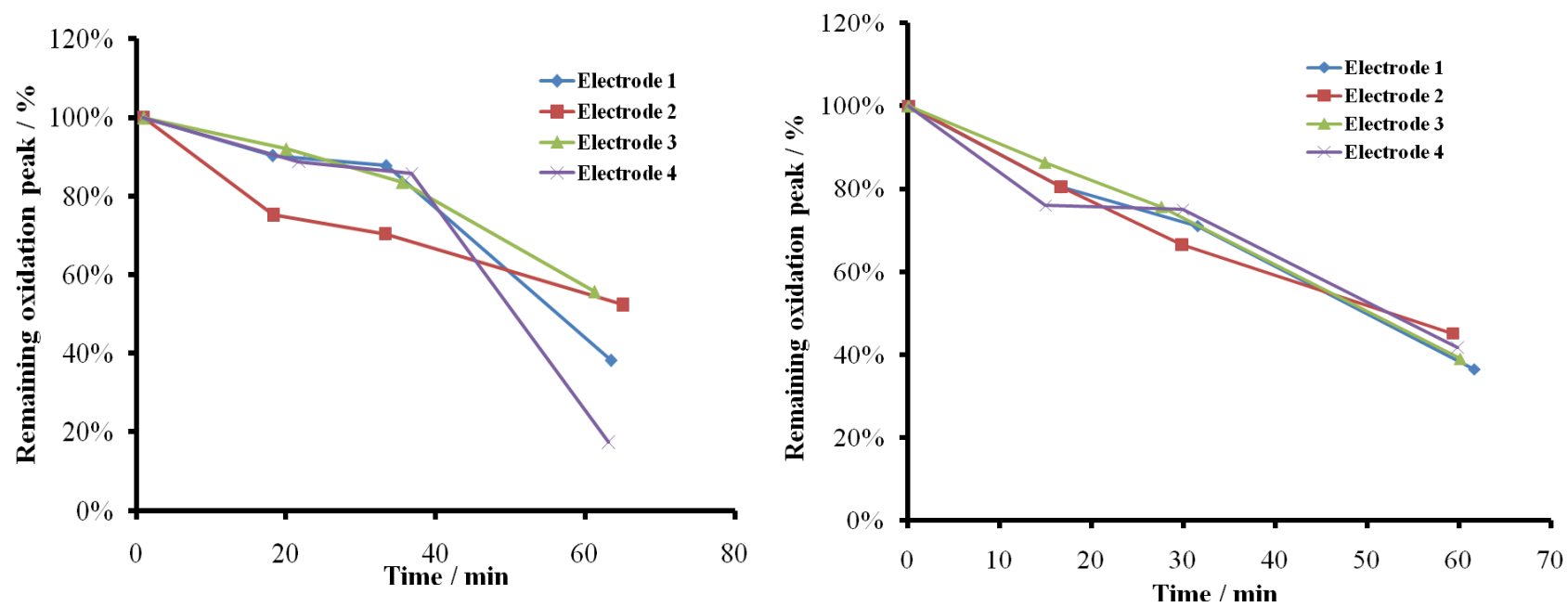
Figure 2.25   Rate of electrode fouling at *p*-phenylacetate film-coated carbon electrodes (A) and at bare carbon electrodes (B).

be manifesting similar behaviour, where the film effectiveness is reduced after ~40 min until the end of monitoring.

In addition, the film-coated electrodes also display variability in resisting fouling. For the first 40 min, the responses of all 3 of the 4 electrodes are similar. However, towards the end of the experiment, 3 electrodes display final current peak feature heights ranging from ~19% to 56%. This is possibly a consequence of lack of reproducibility of film between the electrode surfaces, as has been discussed for similar films (Section 2.1.3). Finally, the rate of fouling, based on a linear plot of the averaged current decay results depicted in Figure 2.25A (data not shown) was determined to be 0.9361 %/min.

In comparison, in Figure 2.25B, constant degradation in oxidation signal was observed at bare carbon electrodes throughout the experiment, suggesting that the severe fouling was occurring at the bare carbon surface without any impedance. This appears to be due to the absence of any protective cover on the electrodes, which results in increasing degree of adsorption of hydrophilic molecules, thus consistently retarding the oxidation of dopamine. Moreover, the average rate of electrode surface fouling, indicated by the current decay was determined to be 0.9612 %/min. Compared to the *p*-phenylacetate film-coated electrodes, thus the bare carbon electrodes exhibit a greater rate of current decay.

A comparison of the fitted peaks in Figure 2.24 C and Figure 2.24E reveals a reduction of $50 \pm 11\%$ (N = 4) in peak height after 60 min. In comparison, the dopamine oxidation signals at bare carbon electrodes at the start of the experiment and towards the end, 60 min later are depicted in Figure 2.26. Similar to Figure 2.25, Figure 2.26A depicts the dopamine oxidation current at the start of the experiment, and the fitted data therein are presented in Figure 2.26B. A comparison between these peaks and those after 60 min is also shown as original peak (Figure 2.26C) and after fitting (Figure 2.26D). A comparison between the fitted peak heights in Figure 2.26B and Figure 2.26D reveals a
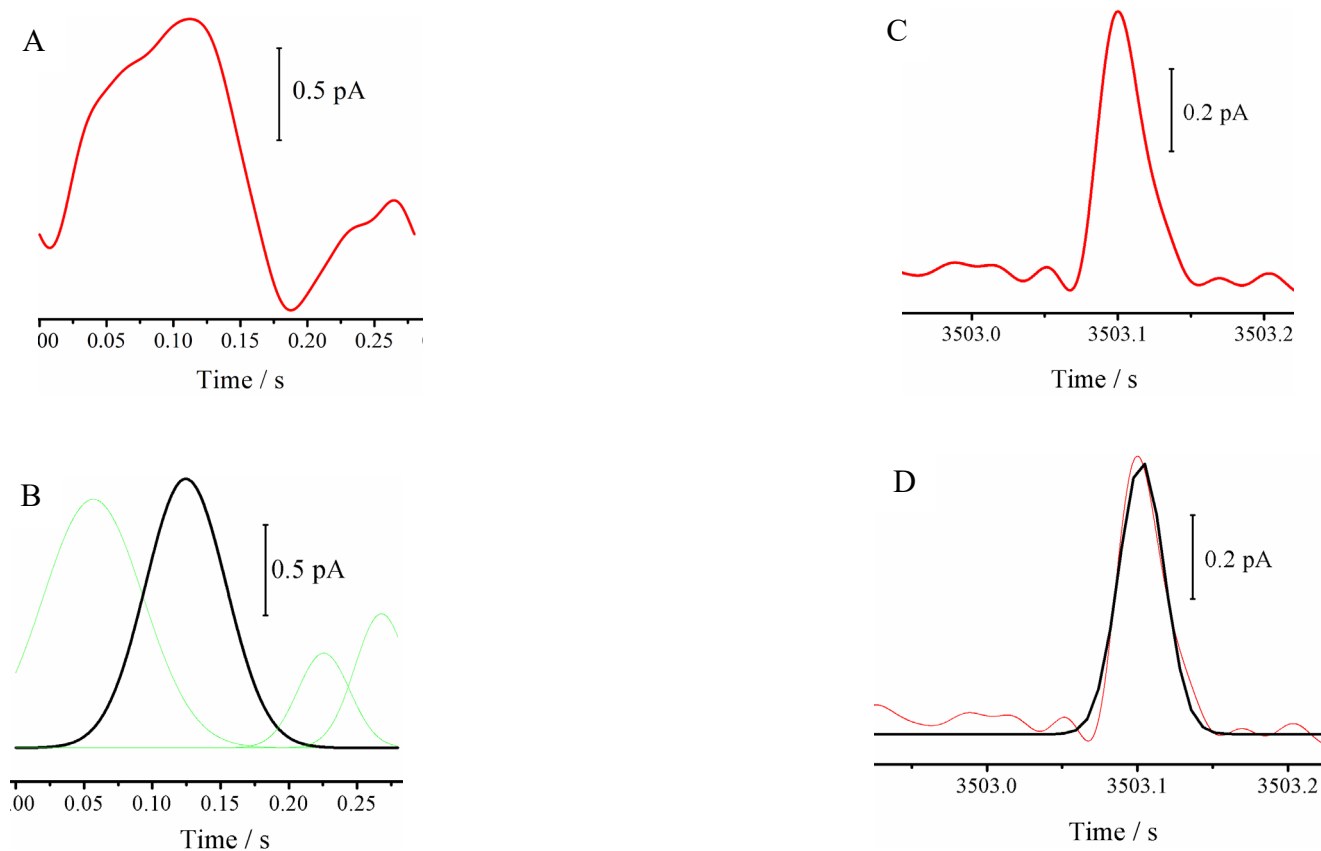
Figure 2.26   Dopamine oxidation signal in the rat striatum at bare carbon electrodes at the start of the experiment (A) and after 60 min (C). Peaks (B) and (D) denote the fitted current signals at the start and after 60 min of monitoring, respectively.

$62 \pm 9\%$ (N = 4) reduction in peak heights at the bare carbon electrodes. The error component in the measurement is the standard deviation of the four measurements. Furthermore, the difference in signal decay of the *in vivo* evoked dopamine at both *p*-phenylacetate film-coated electrodes and bare carbon electrodes was significant at the 95% confidence level. This confirms that the film-coating on the electrodes is effective in resisting fouling at the electrode surface whereas the bare carbon electrode suffers from electrode surface degradation.

2.4   Concluding remarks

Bare carbon electrodes with radii smaller than 5 μm were fabricated and subjected to electrodeposition of a *p*-phenylacetate layer. Comparison of the electrochemical responses of redox systems at these modified electrodes displayed behaviour consistent with that expected of an anionic film. The electrodes were also electrochemically identified to display an excess of basal over edge planes at the surface, which represents typically slower reaction kinetics for electrochemically-active species.

Furthermore, they show a clear suppression of the ascorbic acid oxidation signal by 35%, which suggests its applicability to *in vivo* dopamine detection without contributions to the signal from ascorbic acid. The film coated electrodes are relatively stable with less than 10% decrease in limiting currents for dopamine following storage of the electrodes in the laboratory environment for 40 days.

The film coated electrodes demonstrate similarity in performance to bare carbon electrodes (541 pM and 543 pM limits of detection, respectively, and 16 pA/nM and 19 pA/nM sensitivity respectively). Thus, the modified electrodes demonstrate up to 2-orders of magnitude improvement and lower detection limit than has been found previously for similarly coated, conventional-sized glassy carbon electrodes. In the final

characterisation of the electrodes, data from sensitivity and limit of detection studies for the film coated electrodes indicate that exposure to an *in vitro* synthetic brain environment does not significantly affect the performance of electrodes. This ultimately suggests the modified electrodes display a certain degree of resistance to fouling, and suitability for *in vivo* applications. On the other hand, the bare carbon electrode performance was observed to be severely degraded following exposure to the laboratory synthetic solution.

The results from *in vivo* experiments are consistent with the characterisation results from *in vitro* experiments. Electrodes modified with *p*-phenylacetate film were observed to withstand fouling to a larger extent than bare carbon electrodes. The oxidation signal for dopamine was observed to decay by 50% at the modified electrodes, which compares favourably to the 63% signal degradation at bare carbon electrodes.

The results of these experiments affirm that *p*-phenylacetate film modification is a successful strategy in reducing electrode fouling when applied *in vivo* for dopamine detection. In addition, the film coated electrode was observed to offer some resistance to fouling for the first 40 mins of implanting the electrode. This however decreases after this period, suggesting more severe fouling, possibly. We believe this is occurring as a result of lack of resilience of the *p*-phenylacetate film on the electrode surface. However, the performance of the film-coated electrodes was better than that for bare carbon electrodes which demonstrated a steady decline in the oxidation peak signal. The rate of signal decay, which is an indicator of the extent of electrode surface fouling was greater at bare carbon electrodes (0.9612 %/min), compared to 0.9361 %/min at the *p*-phenylacetate film-coated electrodes. These findings suggest that the film is successful in retarding fouling to a greater extent than unmodified, bare carbon electrodes.

2.5   References

1.   Chandra, S.; Wong, D. K. Y., Electrochemical detection of neurotransmitters at structurally small electrodes. In *Nanostructured Materials for Electrochemical Biosensors*, Umasankar, Y.; Kumar, S. A.; Chen, S.-M., Eds. Nova Science Publishers: New York, 2009; pp 317-337.

2.   Njagi, J.; Chernov, M. M.; Leiter, J. C.; Andreescu, S., *Anal. Chem.* **2010,** *82* (3), 989-996.

3.   Arya, S. K., Singh, S. P. and Malhotra, B. D., *Electrochemical techniques in biosensors.* John Wiley & Sons, Ltd.: Chichester, 2007; Vol. 1, p 341-378.

4.   Vickrey, T. L.; Condron, B.; Venton, B. J., *Anal. Chem.* **2009,** *81* (22), 9306-9313.

5.   Schenk, J. O.; Miller, E.; Rice, M. E.; Adams, R. N., *Brain Res.* **1983,** *277* (1), 1-8.

6.   Lane, R. F.; Blaha, C. D.; Hari, S. P., *Brain Res. Bull.* **1987,** *19* (1), 19-27.

7.   Miele, M.; Fillenz, M., *J. Neurosci. Methods* **1996,** *70* (1), 15-19.

8.   Brazell, M. P.; Marsden, C. A., *Brain Res.* **1982,** *249* (1), 167-172.

9.   Sun, W.; Yang, M.; Jiao, K., *Anal. Bioanal. Chem.* **2007,** *389*, 1283-1291.

10.   Xu, G.-R.; Xu, M.-L.; Zhang, J.-M.; Kim, S.; Bae, Z.-U., *Bioelectrochemistry* **2008,** *72* (1), 87-93.

11.   Ambrosi, A.; Morrin, A.; Smyth, M. R.; Killard, A. J., *Anal. Chim. Acta* **2008,** *609* (1), 37-43.

12.   Park, J.; Quaiserova-Mocko, V.; Patel, B. A.; Novotny, M.; Liu, A.; Bian, X.; Galligan, J. J.; Swain, G. M., *Analyst* **2008,** *133* (1), 17-24.

13.   Robinson, D. L.; Venton, B. J.; Heien, M. L. A. V.; Wightman, R. M., *Clinical Chemistry (Washington, DC, United States)* **2003,** *49* (10), 1763-1773.

14.   Downard, A. J.; Roddick, A. D.; Bond, A. M., *Anal. Chim. Acta* **1995,** *317* (1-3), 303-310.

15.   Suzuki, A.; Ivandini, T. A.; Yoshimi, K.; Fujishima, A.; Oyama, G.; Nakazato, T.; Hattori, N.; Kitazawa, S.; Einaga, Y., *Anal. Chem.* **2007,** *79* (22), 8608-8615.

16.   Hiramatsu, M.; Lau, C. H.; Bennett, A.; Foord, J. S., *Thin Solid Films* **2002,** *407* (1-2), 18-25.

17.   Achatz, P.; Garrido, J. A.; Williams, O. A.; Bruno, P.; Gruen , D. M.; Kromka, A.; Steinmüller, D.; Stutzmann, M., *Phys. Status Solidi A* **2007,** *204* (9), 2874-2880.

18.   Wang, J., *Analytical Electrochemistry*. Third Edition ed.; John Wiley & Sons: Hoboken, 2006.

19.   Schrock, D. S.; Wipf, D. O.; Baur, J. E., *Anal. Chem.* **2007,** *79* (13), 4931-4941.

20.   Wipf, D. O.; Kristensen, E. W.; Deakin, M. R.; Wightman, R. M., *Anal. Chem.* **1988,** *60* (4), 306-310.

21.   Monk, P., *Fundamentals of Electroanalytical Chemistry*. John Wiley & Sons Ltd: Kent, 2001; p 361.

22.   Alwarappan, S.; Butcher, K. S. A.; Wong, D. K. Y., *Sens. Actuators, B* **2007,** *128* (1), 299-305.

23.   Zweifel, L. S.; Parker, J. G.; Lobb, C. J.; Rainwater, A.; Wall, V. Z.; Fadok, J. P.; Darvas, M.; Kim, M. J.; Mizumori, S. J. Y.; Paladini, C. A.; Phillips, P. E. M.; Palmiter, R. D., *Proc. Natl. Acad. Sci. U. S. A.* **2009,** *106* (18), 7281-7288.

24.   Stamford, J. A.; Kruk, Z. L.; Millar, J., *Brain Res.* **1986,** *381* (2), 351-355.

25.   Bath, B. D.; Michael, D. J.; Trafton, B. J.; Joseph, J. D.; Runnels, P. L.; Wightman, R. M., *Anal. Chem.* **2000,** *72* (24), 5994-6002.

26.   Kuhr, W. G.; Wightman, R. M., *Brain Res.* **1986,** *381* (1), 168-171.

27.   Barsan, M. M.; Pinto, E. M.; Florescu, M.; Brett, C. M. A., *Anal. Chim. Acta* **2009,** *635* (1), 71-78.

28.   Hermans, A.; Keithley, R. B.; Kita, J. M.; Sombers, L. A.; Wightman, R. M., *Anal. Chem.* **2008,** *80* (11), 4040-4048.

29.   Hafizi, S.; Kruk, Z. L.; Stamford, J. A., *J. Neurosci. Methods* **1990,** *33* (1), 41-49.

30.   Kissinger, P. T.; Heineman, W. R., *Laboratory Techniques in Electroanalytical Chemistry*. 2nd ed.; Marcel Dekker Inc.: New York, 1984.

31.   Aylward, G.; Findlay, T., *SI Chemical Data*. 6th ed.; John Wiley & Sons Australia Ltd: Milton, 2008.

32.   Zumdahl, S., S; Zundahl, S. A., *Chemistry*. 6th ed.; Houghton Mifflin Company: Boston, 2003.

33.   Heien, M. L. A. V.; Johnson, M. A.; Wightman, R. M., *Anal. Chem.* **2004,** *76* (19), 5697-5704.

34.   Gerhardt, G. A.; Oke, A. F.; Nagy, G.; Moghaddam, B.; Adams, R. N., *Brain Res.* **1984,** *290* (2), 390-395.

35.   Jeong, H.; Jeon, S., *Sensors* **2008,** *8* (11), 6924-6935.

36.   Long, W. J.; Brooks, A. E., Analysis of Polar Compounds Using 100% Aqueous Mobile Phases with Agilent ZORBAX Eclipse Plus Phenyl-Hexyl and Other ZORBAX Phenyl Columns. Inc., A. T., Ed. Agilent Technologies Inc: 2009.

37.   Pratuangdejkul, J.; Nosoongnoen, W.; Guérin, G.-A.; Loric, S.; Conti, M.; Launay, J.-M.; Manivet, P., *Chem. Phys. Lett.* **2006,** *420* (4-6), 538-544.

38.   Wiedemann, D. J.; Kawagoe, K. T.; Kennedy, R. T.; Ciolkowski, E. L.; Wightman, R. M., *Anal. Chem.* **1991,** *63*, 2965-2970.

39.   Selvaraju, T.; Ramaraj, R., *J. Electroanal. Chem.* **2005,** *585* (2), 290-300.

40.   Wiedemann, D. J.; Basse-Tomusk, A.; Wilson, R. L.; Rebec, G. V.; Wightman, R. M., *J. Neurosci. Methods* **1990,** *35* (1), 9-18.

41.   Santos, R. M.; Lourenço, C. F.; Piedade, A. P.; Andrews, R.; Pomerleau, F.; Huettl, P.; Gerhardt, G. A.; Laranjinha, J.; Barbosa, R. M., *Biosens. Bioelectron.* **2008,** *24* (4), 704-709.

42.   Xiang-Qin, L.; Guang-Feng, K.; Ying, C., *Chin. J. Anal. Chem.* **2008,** *36* (2), 157-161.

43.   Evans, A. H.; Pavese, N.; Lawrence, A. D.; Tai, Y. F.; Appel, S.; Doder, M.; Brooks, D. J.; Lees, A. J.; Piccini, P., *Ann. Neurol.* **2006,** *59* (5), 852-858.

44.   Xiao, Y.; Guo, C.; Li, C. M.; Li, Y.; Zhang, J.; Xue, R.; Zhang, S., *Anal. Biochem.* **2007,** *371* (2), 229-237.

45.   Downard, A. J.; Roddick, A. D., *Electroanal.* **1995,** *7* (4), 376-378.

46.   Cosnier, S., Immobilization of biomolecules by electropolymerized films. In *Handbook of Biosensors and Biochips*, Marks, R. S., Cullen, D.C., Karube, I. Lowe, C.R. and Weetall, H.H., Ed. John Wiley & Sons Ltd.: Chichester, 2007; Vol. 1, pp 237-249.

47.   Ates, M.; Castillo, J.; Sezai Sarac, A.; Schuhmann, W., *Microchim. Acta* **2008,** *160* (1), 247-251.

48.   Shin, D.; Tryk, D. A.; Fujishima, A.; Merkoçi, A.; Wang, J., *Electroanal.* **2005,** *17* (4), 305-311.

49.   Jia, Z.; Liu, J.; Shen, Y., *Electrochem. Commun.* **2007,** *9* (12), 2739-2743.

50.   Saby, C.; Ortiz, B.; Champagne, G. Y.; Belanger, D., *Langmuir* **1997,** *13* (25), 6805-6813.

51.   Barbier, B.; Pinson, J.; Desarmot, G.; Sanchez, M., *J. Electrochem. Soc.* **1990,** *137* (6), 1757-1764.

52.   Blaha, C. D.; Lane, R. F., *Brain. Res. Bull.* **1983,** *10* (6), 861-864.

53.   Delamar, M.; Hitmi, R.; Pinson, J.; Saveant, J. M., *J. Am. Chem. Soc.* **1992,** *114* (14), 5883-5884.

54.   Downard, A. J., *Electroanal.* **2000,** *12* (14), 1085-1096.

55.   Bourdillon, C.; Delamar, M.; Demaille, C.; Hitmi, R.; Moiroux, J.; Pinson, J., *J. Electroanal. Chem.* **1992,** *336* (1-2), 113-123.

56.   Downard, A. J.; bin Mohamed, A., *Electroanal.* **1999,** *11* (6), 418-423.

57.   Downard, A. J.; Roddick, A., D., *Electroanal.* **1997,** *9* (9), 693-698.

58.   Hong, H.-G.; Porter, M. D., *J. Electroanal. Chem.* **2005,** *578* (1), 113-119.

59.   Pellissier, M.; Barrière, F.; Downard, A. J.; Leech, D., *Electrochem. Commun.* **2008,** *10* (6), 835-838.

60.   McNally, M.; Wong, D. K. Y., *Anal. Chem.* **2001,** *73* (20), 4793-4800.

61.   Makarova, L. G.; Polovyanyuk, I. V., *Russ. Chem. Bull.* **1967,** *16* (12), 2618-2620.

62.   Ullrich, R.; Grewer, T., *Thermochim. Acta* **1993,** *225* (2), 201-211.

63.   Park, J.; Show, Y.; Quaiserova, V.; Galligan, J. J.; Fink, G. D.; Swain, G. M., *J. Electroanal. Chem.* **2005,** *583* (1), 56-68.

64.   Park, J.; Quaiserova-Mocko, V.; Peckova, K.; Galligan, J. J.; Fink, G. D.; Swain, G. M., *Diamond Relat. Mater.* **2006,** *15* (4-8), 761-772.

65.   Park, J.; Galligan, J. J.; Fink, G. D.; Swain, G. M., *Anal. Chem.* **2006,** *78* (19), 6756-6764.

66.   Britz, D.; Chandra, S.; Strutwolf, J.; Wong, D. K. Y., *Electrochim. Acta* **2010,** *55* (3), 1272-1277.

67.   Wallingford, R. A.; Ewing, A. G., *Anal. Chem.* **1989,** *61* (2), 98-100.

68.   Wong, D. K. Y.; Xu, L. Y. F., *Anal. Chem.* **1995,** *67* (22), 4086-4090.

69.   Cline, K. K.; McDermott, M. T.; McCreery, R. L., *J. Phys. Chem.* **1994,** *98* (20), 5314-5319.

70.   Davies, T. J.; Moore, R. R.; Banks, C. E.; Compton, R. G., *J. Electroanal. Chem.* **2004,** *574* (1), 123-152.

71.   Holloway, A.; Wildgoose, G.; Compton, R.; Shao, L.; Green, M., *J. Solid State Electrochem.* **2008,** *12* (10), 1337-1348.

72.   Zoski, C. G., *Electroanal.* **2002,** *14* (15-16), 1041-1051.

73.   Liu, J.; Cheng, L.; Liu, B.; Dong, S., *Langmuir* **2000,** *16* (19), 7471-7476.

74.   Chen, P.; Fryling, M. A.; McCreery, R. L., *Anal. Chem.* **1995,** *67* (18), 3115-3122.

75.   Roberts, J. G.; Moody, B. P.; McCarty, G. S.; Sombers, L. A., *Langmuir* **2010,** *26* (11), 9116-9122.

76.   Brooksby, P. A.; Downard, A. J., *Langmuir* **2004,** *20* (12), 5038-5045.

77.   Petrosyan, V. A.; Rafikov, F. M., *Russ. Chem. Bull.* **1980,** *29* (9), 1429-1431.

78.   Harris, D. C., *Quantitative Chemical Analysis* 4ed.; W.H. Freeman and Company: New York, 1995.

79.   Engstrom, R. C.; Strasser, V. A., *Anal. Chem.* **1984,** *56* (2), 136-141.

80.   Chen, P.; McCreery, R. L., *Anal. Chem.* **1996,** *68* (22), 3958-3965.

81.   Ji, X.; Banks, C. E.; Crossley, A.; Compton, R. G., *ChemPhysChem* **2006,** *7* (6), 1337-1344.

82.   McDermott, M. T.; Kneten, K.; McCreery, R. L., *J. Phys. Chem.* **1992,** *96* (7), 3124-3130.

83.   Alwarappan, S. Development, Characterization and Applications of Physically Small Carbon Electrodes as Biosensors. Macquarie University, Sydney, 2007.

84.   Kneten, K. R.; McCreery, R. L., *Anal. Chem.* **1992,** *64* (21), 2518-2524.

85.   Chen, Q.; Swain, G. M., *Langmuir* **1998,** *14* (24), 7017-7026.

86.   Davies, T. J.; Hyde, M. E.; Compton, R. G., *Angew. Chem.* **2005,** *44* (32), 5121-5126.

87.   Rooney, M. B.; Coomber, D. C.; Bond, A. M., *Anal. Chem.* **2000,** *72* (15), 3486-3491.

88.   McDermott, C. A.; Kneten, K. R.; McCreery, R. L., *J. Electrochem. Soc.* **1993,** *140* (9), 2593-2599.

89.   Faye, A.; Dione, G.; Dieng, M.; Aaron, J.; Cachet, H.; Cachet, C., *J. Appl. Electrochem.* **2010,** *40* (11), 1925-1931.

90.   Zheng, L.; Wang, Y.; Wang, X.; Wang, X.; An, H.; Yi, L., *J. Mater. Sci.* **2010,** *45* (22), 6030-6037.

91.   Xu, J.; Chen, Q.; Swain, G. M., *Anal. Chem.* **1998,** *70* (15), 3146-3154.

92.   Choi, S.; Seo, B.; Kim, J., *Bull. Korean Chem. Soc.* **2010,** *31* (1), 104-111.

93.   Ates, M.; Sarac, A.; Turhan, C.; Ayaz, N., *Fibers Polym.* **2009,** *10* (1), 46-52.

94.   Hočevar, S. B.; Wang, J.; Prakash, D. R.; Musameh, M.; Ogorevc, B., *Electroanal.* **2005,** *17* (5-6), 417-422.

95.   Njagi, J.; Chernov, M. M.; Leiter, J. C.; Andreescu, S., *Anal. Chem. 82* (3), 989-996.

96.   Buda, M.; Gonon, F.; Cespuglio, R.; Jouvet, M.; François, J., *Eur. J. Pharmacol.* **1981,** *73* (1), 61-68.

97.   Zachek, M. K.; Takmakov, P.; Park, J.; Wightman, R. M.; McCarty, G. S., *Biosens. Bioelectron.* **2010,** *25* (5), 1179-1185.

98.   Clark, J. J.; Sandberg, S. G.; Wanat, M. J.; Gan, J. O.; Horne, E. A.; Hart, A. S.; Akers, C. A.; Parker, J. G.; Willuhn, I.; Martinez, V.; Evans, S. B.; Stella, N.; Phillips, P. E. M., *Nat Meth* **2010,** *7* (2), 126-129.

99.   Sombers, L. A.; Beyene, M.; Carelli, R. M.; Mark Wightman, R., *J. Neurosci.* **2009,** *29* (6), 1735-1742.

100. Dreyer, J. K.; Herrik, K. F.; Berg, R. W.; Hounsgaard, J. D., *J. Neurosci.* **2010,** *30* (42), 14273-14283.

101. Michael, D. J.; Wightman, R. M., *J. Pharm. Biomed. Anal.* **1999,** *19* (1-2), 33-46.

CHAPTER 3

DEVELOPMENT, CHARACTERISATION AND APPLICATIONS OF PHYSICALLY SMALL, HYDROGENATED CARBON ELECTRODES

3.1 Introduction

This chapter describes the development of physically small, hydrogenated carbon electrodes for *in vivo* detection of dopamine. As mentioned in Section 2.1, detection of dopamine *in vivo* is affected by fouling, very often caused by adsorption of hydrophilic high molecular-weight proteins, peptides and lipids present in the physiological medium at a bare carbon electrode. Therefore, one possible strategy for minimising fouling is to use a hydrophobic surface to repel the hydrophilic substances. This chapter reports the hydrogenation of physically small carbon electrodes fabricated by pyrolysis of acetylene to produce electrodes with a hydrophobic surface for detection of dopamine *in vivo*. This is followed by characterisation studies of these electrodes to determine the effectiveness of hydrogenation against fouling and to facilitate comparisons of the modified surface to that of bare carbon electrodes. We will also report the performance of hydrogenated electrodes in detecting dopamine *in vitro*. Finally, the chapter concludes with *in vivo* dopamine detection at hydrogenated electrodes.

Carbon based electrodes are often used in electroanalytical chemistry. This is largely due to the properties of carbon including chemical inertness, broad potential range, low

background current, rich surface chemistry, low cost, ease of pretreatment and impermeability to gases and liquids.[1-2] Carbon based electrodes are thus increasingly being applied to determinations such as detection of pharmaceutical drugs in blood plasma[3] and serum,[4] detection of biological molecules including protein[5] and neurotransmitters.[6-8] In particular, neurotransmitter detection has been of interest to researchers because much of the signalling in the mammalian brain uses neurotransmitters as messengers between neurons. The processing in the brain networks eventually manifests as animal behaviour. The brain is a challenging environment for chemical sensing because analytes of interest are often present at low concentrations in the presence of many interferents. Equally importantly, detection must be conducted with minimal tissue damage.

3.1.1   Challenges to *in vivo* dopamine detection

The challenges to *in vivo* dopamine detection at bare carbon electrodes have been introduced in Section 1.4.4, and some of the strategies to overcome fouling fouling have been discussed in Section 2.1. We have then attempted to protect physically small electrodes by coating them with *p*-phenylacetate film, as reported in Chapter 2. In addition to these strategies, a common approach to resist electrode fouling *in vivo* is to make the electrode surface hydrophobic. This is because most of the high molecular-weight species in the brain such as proteins, peptides and lipids are hydrophilic. At a bare carbon electrode, the surface comprises of a mixture of sp^3 and sp^2 carbon atoms attached to hydroxyl and carbonyl molecules at the surface.[9] Due to these oxygen-containing functional groups, the bare carbon surface is a polar and hydrophilic surface,[10] on which other hydrophilic molecules adsorb readily.

One material that exhibits hydrophobicity is diamond film. This is due to diamond films being composed of closely adjoining, well-faceted micro-crystallites that are hydrogen terminated.[11] The incorporation of hydrogen in the diamond films leads to sp^3 C—H

bonds as reported in the literature.[10, 12]   On such a surface, molecular termination of the bonds is dominated by hydrogen that induces hydrophobic surface properties and a negative electron affinity due to the formation of high density C—H dipoles at the surface.[13]   Previously, diamond films following hydrogenation of a natural diamond substrate using molecular hydrogen have been confirmed through experiments such as sessile drop method. In this method, the angle of a drop of water on the surface is used to determine the extent of hydrophobicity of a surface.[14]   Hydrophobic surfaces display higher contact angles between the drop and the surface than hydrophilic surfaces. Values ranging from 65 to 91 degrees[2, 14-15] have been attributed to hydrophobic surfaces, while for hydrophilic surfaces, the contact angle can be as low as 42 degrees.[14]

Another form of diamond reported to exhibit similar hydrophobicity is boron-doped diamond.[16]   Boron-doping introduces conductivity into the otherwise non-conducting diamond,[17-18] giving rise to an electroactive surface whose performance can be superior to that of alternative material such as glassy carbon.[19-20]   Notable advantages of doped diamond include an excellent stability and reproducibility as a result of the chemical inertness, a wide potential working window ranging from -2.0 V up to +3.0 V[18, 21] in aqueous solution due to high over-potential for hydrogen and oxygen evolution and fast reaction kinetics for simple electron transfer processes,[22-23] low background currents and surface inertness that results in high resistance to deactivation.[16, 24-26]   Since the first article on diamond as an electrochemical material was published in 1983 by Iwaki and co-workers,[27] followed by subsequent extensive work by Pleskov and co-workers in 1987,[28] interest in diamond has increased with the discovery that it is possible to produce polycrystalline diamond films with mechanical and electronic properties comparable with natural diamond.[29]   As a result, the excellent combination of intrinsic electrical, thermal, mechanical and optical properties of diamond films results in their having many potential applications.[30] Diamond is now an ideal material of choice for optical coatings, radiation detectors and semiconductor devices working in conditions such as aggressive environments, high temperature, high power, high radiation, and high frequencies.[31-32]

Shang *et al.*[33] recently reported synthesis and electropolymerisation of N-acetyltyramine (PActy) with a negatively-charged sulfobutylether-β-cyclodextrin (SBCD) layer on a 3 mm boron-doped diamond electrode, on which pyrrole was electropolymerised to form a stable and selective film for dopamine detection. At identical concentration (20 μM), 3,4-dihydroxyphenylacetic acid, dopamine, 4-dihydroxyphenylalanine, epinephrine and norpinephrine were all reported to display comparable responses at the unmodified boron-doped diamond electrode, while 0.1 mM concentrations of ascorbic acid and uric acid, respectively, were found to provoke 10-fold higher interference signals compared to that of dopamine alone. In comparison, these modified electrodes demonstrated suppression of the signals from the interferents ranging from ~10-fold for dihydroxyphenylalanine to ~20-fold for uric acid. However, ascorbic acid and 4-dihydroxyphenylalanine still respectively provoked 3-fold and ~70% of the signal response compared to that of dopamine. This observation was attributed to the more porous morphology of the PActy/SBCD films. In contrast, upon electropolymerisation of pyrrole on the Acty/SBCD electrodes, the signal responses of 3,4-dihydroxyphenylacetic acid, ascorbic acid and uric acid were eliminated at the modified electrodes. Dopamine, being the simplest chemical structure, produced the highest response, followed by norpinephrine and epinephrine. The authors proposed the molecular sieving effect (separation based on size) as the reason for this observation. Epinephrine is a secondary amine, hence the authors attributed its bulkier structure to its low response compared to the rest of the matrix. The authors suggested similar reasons for the bulkier ascorbic acid and uric acid. The limit of detection of the boron-doped diamond electrode for dopamine was determined to be 50 nM, while at the SBCD-modified boron-doped diamond electrode, it was lower at 5 nM (with a response time of 1 – 2 s), based on a signal-to-noise ratio of 3 at both boron-doped diamond electrode and SBCD-modified boron-doped diamond electrode. The authors attributed to the very low and stable background due to the boron-doped diamond presence. The authors recommended the modified electrode be applied to dopamine detection in cerebrospinal fluid, after reducing the tip size to sub-micrometer dimensions. In another exciting application of boron-

doped diamond electrodes, Olivia *et al.*[34] have reported eliminating interferences from ascorbic acid in the detection of dopamine using overoxidised polypyrrole-modified boron-doped diamond electrodes. This modification of the electrode was found to have increased the sensitivity of dopamine detection and lowered the limit of detection to 0.1 nM, with a signal-to-noise ratio of 3. This was achieved because the oxidised polypyrrole is a positively charged conducting polymer. Overoxidation of this film results in the increase of carbonyl and carboxylic functionalities that attract cationic dopamine and reject adsorbate anions at physiological pH (7.4). Owing to the inactivity of diamond towards any adsorption processes, the electrode compared favourably with carbon fibre electrodes which deactivate after several measurements. No fouling was observed during a two- month period of *in vitro* dopamine measurements.

In addition, Park *et al.*[35] have reported boron-doped diamond microelectrodes for the *in vitro* chronoamperometric measurement of the catecholamine neurotransmitter, norepinephrine. This new microelectrode, without any protective polymer coating, exhibited a sensitive and stable voltammetric response for norepinephrine released from sympathetic nerves in a laboratory test animal. The background voltammetric current was low (7 nA compared to 20 nA at a carbon fibre electrode), stable (15 min) and independent of the solution pH. The diamond microelectrodes exhibited improved response performance over a conventional carbon fibre in this measurement. Similarly, Venton *et al.*[36] have used electrochemical detection to monitor the actions of cocaine on extracellular dopamine release in the striatum of anesthetised mice. Their study concluded that cocaine enhances dopamine release by mobilising a reserve pool of dopamine-containing synaptic vesicles.

Other alternative methods for introducing electrical conductivity into diamond have been developed. These include dopants such as nitrogen,[37] metal and metal cluster inclusions, sp^2 inclusions in grain boundaries and subsurface hydrogen.[20] Other forms of conductive diamond, such as surface conductive or ultracrystalline diamond have also been reported

in literature.[38-39]   Hian *et al*. have demonstrated that sub-micron grain sized nanocrystalline diamond films, which display conductivity as a result of graphitic inclusions within the grain boundaries, may be preferred over boron-doped diamond films as a choice in electrochemical applications. This is because, compared to boron-doped diamond, nanocrystalline diamond films demonstrate superior advantages, such as wider working potential window, more robust nature of electrode, good and reproducible activity and greater activity towards aqueous systems, compared to conventional diamond electrodes.[19]

3.1.2   A hydrogenated surface

Apart from diamond, another surface that exhibits hydrophobicity is hydrogenated graphitic carbon,[10, 40-41] which is similar to diamond. Compared to polymeric membranes, the effect of directly introducing a hydrogen-terminated layer on carbon electrodes is more likely to yield a low-capacitance film with much less severe coverage problems. The hydrophobic surface of hydrogenated carbon is less susceptible to fouling by hydrophilic large-molecular species.[7] Extensive work has been conducted in hydrogenating carbon surfaces for neurotransmitter detection, much of which have been reported by Swain and co-workers.[2, 42-44] For instance, the group has studied the electrochemistry of anthraquinone-2,6-disulfonate at hydrogenated glassy carbon surfaces.[42] Their findings showed capacitance at the hydrogenated electrode decreased by 50% following hydrogenation. Moreover, the lack of anthraquinone-2,6-disulfonate adsorption at the hydrogenated glassy carbon surface confirmed the surface was non-polar and hydrophobic, leading to electrode longevity in polar solutions. Chen and Swain[2] have investigated the morphology of hydrogenated glassy carbon films and concluded that glassy carbon is characterised by a grainy texture, whereas hydrogenation leads to development of ridge-like formations on the surface. This was attributed to the morphological distortion at edge plane sites of glassy carbon caused by hydrogen

chemisorption. X-ray photoelectron spectroscopy also confirmed the removal of oxygen from glassy carbon after hydrogenation.

Our laboratory had previously reported some preliminary results in using hydrogenated electrodes to resist fouling.[7] The electrodes were hydrogenated using a remote plasma hydrogenation process. In this chapter, we present an alternative methodology involving radio frequency plasma for hydrogenation of yet smaller microelectrodes than previously reported.[2, 42] Results of various characterisation studies on the modified electrodes are also presented. Finally, results of *in vitro* analysis of dopamine in the presence of protein and a known interferent, ascorbic acid are presented.

3.2   Experimental

3.2.1   Reagents

Ultrapure (Milli-Q) water (18.2 MΩ.cm at 25ºC) was used to prepare all solutions. American Chemical Society analytical grade chemicals used in the experiments have been described in Chapter 2.

All analyte solutions and supporting electrolytes were prepared daily and purged with nitrogen for 5 min prior to any analysis. Acetylene and nitrogen were both instrument grade gases from BOC.

3.2.2   Preparation of physically small, hydrogenated carbon electrodes

Initially, physically small carbon electrodes were prepared according to the procedure described in Chapter 2. Electrodes were characterised using cyclic voltammetry

of $Ru(NH_3)_6^{3+}$, and functioning electrodes were subjected to surface characterisation as described below.

3.2.3   Hydrogenation

Physically small carbon electrodes were hydrogenated using a hydrogen deposition setup consisting of a radio frequency plasma-enhanced chemical vapour deposition reactor at the Material Science Laboratory, Commonwealth Scientific and Industrial Research Organisation (Lindfield, NSW 2070, Australia). This method was used to create a stream of hydrogen atoms, which could then interact with the electrode surface, reducing the carbonyl functionalities to C—H bonds that provide a hydrophobic surface. A schematic representation of the setup is shown in Figure 3.1. This setup comprised of a vacuum chamber, in which the specimen to be hydrogenated was placed prior to commencing vacuum. In addition, a pump system to achieve low vacuum, a radio frequency power source and gas delivery components were part of the deposition assembly. The rotary vacuum and a turbo molecular pump worked in conjunction to pump the chamber down to 1 mPa before hydrogenation. The throttle valve was equipped with an internal flap that could open sufficiently to regulate the pressure in the chamber to a specified level. A matching box was used to receive the radio frequency power pulse generated from the radio frequency power supply and apply the required power pulse into the chamber. The sample in the chamber was situated atop a pedestal directly in the path of the oncoming hydrogen gas, which was delivered *via* controlled supply through a mass flow controller (denoted as MFC in Figure 3.1).

The hydrogenation procedure was adapted from that reported by Bendavid *et al*.[45] Upon achieving a base pressure of 1 mPa, plasma treatment of the electrodes was performed using hydrogen at a flow rate of 25 mL/min. The process pressure was set at 6.6 Pa at a radio frequency power (13.56 MHz) of 200 W. Hydrogen gas was pumped into the vacuum chamber for 3 min to provide a hydrogen atmosphere around the electrodes.
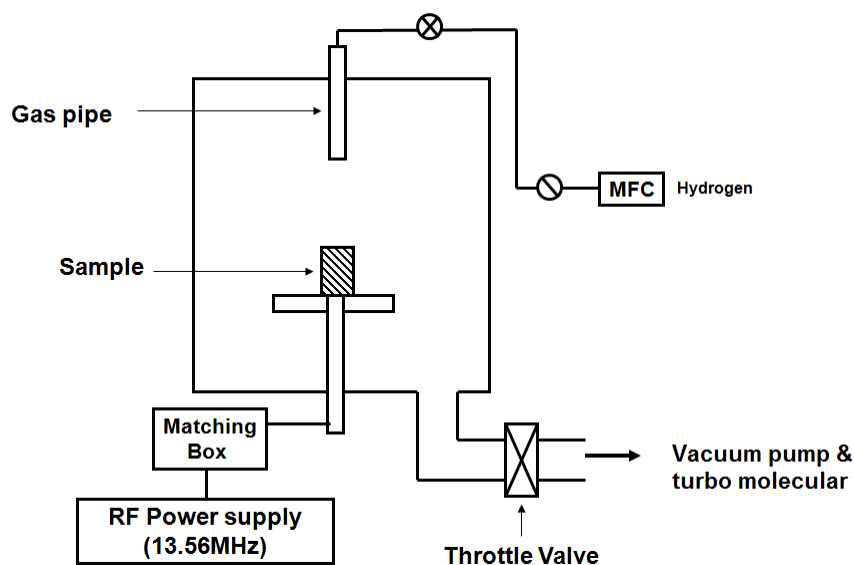
Figure 3.1   Radio frequency plasma setup for hydrogenation (modified from Bendavid *et al.*[45])

3.2.4   Electrochemical detection

To evaluate the success of hydrogenation, chemical characterisation before and after hydrogenation was performed at the hydrogenated carbon electrodes using the following redox markers: (1) 1.0 mM $Ru(NH_3)_6^{3+}$ in 1.0 M KCl as supporting electrolyte; (2) 1.0 mM dopamine in pH 7.4 citrate/phosphate buffer; and (3) 1.0 mM $Fe(CN)_6^{3-}$ in 1.0 M KCl as supporting electrolyte.

3.2.5   Surface morphology study

Changes in the morphology and chemical composition of the electrode surface before and after hydrogenation were studied using several spectroscopic techniques including atomic

force microscopy, Raman spectroscopy and X-ray photoelectron spectroscopy. Detailed instrumentation conditions are specified below.

3.2.6   **Atomic Force Microscopy**

Atomic force microscopy (AFM) was conducted at Department of Physics and Astronomy, Macquarie University. In these experiments, a section of the shank of a hydrogenated electrode was studied using a home-made room temperature confocal sample-scanning fluorescence microscope (100× oil immersion objective lens, Numerical Aperture 1.4) combined with a commercial AFM system (NT-MDT), equipped with a NSG 01 tip (NT-MDT, Holland). Scanning was performed in the semi-contact mode while the electrodes were kept fixed on a stage with two screwable clamps (NT-MDT, Holland). The scanning cantilever was correctly placed to scan the shank area using an OPTEM ZOOM 125 positioning camera (Brook Anco Corporation, Rochester, New York), situated on top of the AFM head and guided using a system of mirrors that provided an image from the top of the cantilever over the sample. Excitation of the nitrogen vacancy complex (N–V) centres was achieved using a 532 nm continuous wave diode pumped solid-state laser (Coherent, Compass). A notch and long pass filter were used in detection to terminate the pump laser beam and to measure the red-shifted fluorescence of the N–V centres.[46]

3.2.7   **Raman Spectroscopy**

Raman spectroscopy was carried out at the Solid State and Elemental Analysis Unit, Mark Wainwright Analytical Centre, University of New South Wales, Australia. These experiments were performed on a Renishaw inVia micro-spectrometer fitted with a 1800l/mm grating and a 50× objective to focus the 514.5 nm line of an Argon ion laser on

the sample. Data were peak fitted without smoothing and a Gaussian baseline correction was applied across the peak fitting range.

3.2.8   X-ray Photoelectron Spectroscopy

X-ray photoelectron spectroscopy (XPS) was carried out using an ESCALAB220i-XL (Thermo Scientific, United Kingdom) at the Solid State and Elemental Analysis Unit, University of New South Wales, Australia. Vacuum conditions were better than 2×10^{-9} mbar, with a non-mono-chromated Al K alpha (energy 1486.6 eV) power source (400 W, 26 mA and 15 kV). Analysis area was approximately 1 mm in cross, photoelectron take off angle: 90 degrees. Pass energy, which refers to electrons of a particular energy permitted to enter the detector, was 100 eV for survey scans or 40 eV for region scans, with step size of 1 eV for survey scans or 0.1 eV for region scans.

3.2.9   Electrochemical measurements

Cyclic voltammetry and chronoamperometry were performed using a potentiostat (eDAQ Pty Ltd., Sydney, Australia) capable of measuring picoamperes of current. This potentiostat was operated using EChem version 2.1.2 software on a PC *via* an E-corder interface (eDAQ Pty Ltd.). A single compartment glass cell that accommodates a Ag|AgCl reference electrode, platinum as counter electrode and either a physically small carbon electrode or a hydrogenated carbon electrode as working electrode was used. All measurements were conducted at room temperature (25ºC). All measurements were carried out within 3 h of fabricating or hydrogenating the electrode.

3.2.10   *In vitro* characterisation of electrodes

In order to mimic the matrix of the extracellular fluid, a solution comprising of 1.0% (v/v) caproic acid (a lipid), 0.1% (w/v) bovine serum albumin and 0.01% (w/v) cytochrome C (both are protein) and 0.002% (w/v) human fibrinopeptide B (a peptide) was prepared.   The procedure described in Section 2.3.10 was followed to evaluate sensitivity and limit of detection for dopamine before and after immersion into the solution.

3.2.11   *In vivo* determination of dopamine

The *in vivo* experimentation procedure used in this study has been described in detail in Section 2.2.5.   Briefly, a bipolar stimulating electrode was implanted in the ventral tegmental area of an anesthetised Sprague Dawley rat and a series of 15 cathodic monophasic current (800 µA) pulses of 0.5 ms duration were delivered to this.   The resulting release of dopamine was recorded using the hydrogenated and bare carbon electrodes that were implanted in the left striatum of the animal.   All currents resulting from the oxidation of dopamine were recorded and current signal feature heights were compared at the start of each experiment and after 60 min.   In conducting these *in vivo* experiments, we have closely adhered to a protocol approved by the Animal Ethics Committee, Macquarie University (Animal Research Authority - 2009/053).

3.2.12   Data analysis

The statistical significance of all correlation coefficients at the 95% confidence level was tested using Student's t-test.   Uncertainties associated with the slope and *y*-intercept of all linear plots were expressed as confidence intervals at the 95% level.   Statistical difference between the mean values of two data sets was tested based on Student's t-test at a 95% level.

3.3   Results and Discussion

3.3.1   Electrochemical measurements

In this chapter, we aim to initially develop and characterise physically small, hydrogenated carbon electrodes that are resistant to fouling. Only physically small carbon electrodes that were found to be functioning, as described in Section 2.3.1, were further hydrogenated and used. In our work, both spectroscopic and electrochemical techniques were employed to characterise the hydrogenated electrodes. Next, the electrodes were subjected to AFM, Raman spectroscopy and XPS to investigate the changes in the morphology of the surface following hydrogenation. This was followed by electrochemical characterisation of the electrodes in several redox systems to determine the electrochemistry of the hydrogenated surface. The electrodes were also subjected to performance characterisation *in vitro* to evaluate their sensitivity and selectivity to dopamine in the presence of interfering ascorbic acid, proteins, peptides and lipids. Finally, the electrodes were applied to *in vivo* detection of dopamine in anesthetised rats. The results obtained in these experiments are described and discussed in detail below.

3.3.2   Atomic force microscopy

AFM of a surface is a useful technique for measuring average surface roughness and morphology.[12, 15] The surface morphology of a bare and a hydrogenated carbon electrode was examined by AFM, and their respective micrograph is depicted in Figure 3.2A and Figure 3.2B. The bare carbon electrode exhibits a non-homogeneous surface with occurrences of islands of grainy texture at some locations along the electrode surface. Based on feature height analysis, the roughness of the carbon film coating on the surface was estimated to be 1 µm. The bare carbon film has island-like or hillock-like amorphous formations of carbon. Similar observation was previously reported by Rezek *et al.*[12] The height of these grainy features is approximately 1.2 µm. On the other hand,
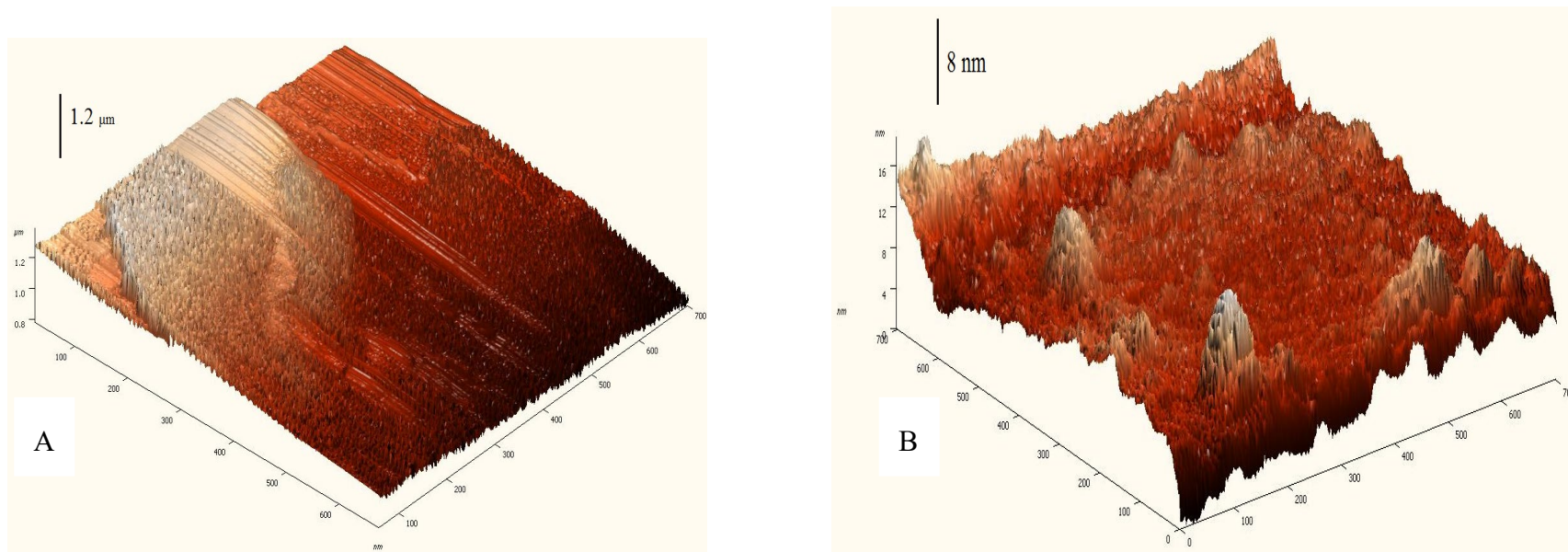
Figure 3.2.   Atomic force micrographs of (A) a bare carbon electrode and (B) a hydrogenated carbon electrode.

as shown in Figure 3.2B, the hydrogenated surface is observed to be rendered to pit-like formations protruding from the surface. These are believed to be a result of carburised Si from substrate and defined as voids.[47] For hydrogenated carbon electrodes at the same resolution, the surface is clearly observed to be less rough by a factor of almost a thousand. The feature heights were estimated to be 8 nm. This is expected as hydrogenation in a plasma environment has been found to yield a reduction in the edge plane sites by atomic hydrogen present in the plasma.[43] It is also in agreement with features reported by Chen *et al.*,[2] who compared feature height of glassy carbon films before and after hydrogenation and concluded that hydrogenation led to reduced feature height, thus smoother films.

3.3.3 Raman spectroscopy

Raman spectroscopy is an effective and non-destructive tool for investigating the detailed bonding structure of carbon films. It is sensitive to the forms of graphite and amorphous carbon microstructures, which produce distinctive Raman bands for the various forms of carbon.[48] The Raman spectrum for a hydrogenated electrode is depicted in Figure 3.3. Two peaks are observed at 1355 cm^{-1} and 1590, cm^{-1} respectively. By comparing with the Raman spectra reported by Filik *et al.*[49] and Goswami *et al.*,[50] the first peak was identified as an A_{1G} or "D" peak attributable to disorder-induced Raman activity of the zone boundary or edge plane phonons at disordered clusters of sp^2 carbon sites. Similarly, the second peak corresponds to an in-plane stretching mode, commonly termed as the E_{2G} or "G" peak,[2, 50] that is attributed to the bond stretching of all pairs of sp^2 atoms in both rings and chains.[49-50] The band area ratio of the D and G peaks was used as a means of evaluating the sp^3 content of carbon films.[49] In our study, this ratio for hydrogenated electrodes was found to be 0.91. A value ranging from 1.3 - 1.5 was previously determined for hydrogenated electrodes.[2, 43, 50] Thus, in comparison, the value of 0.91 obtained in this study confirms the presence of moderate sp^3 content in the film.[50] However, we attribute the lower value in this study than 1.3 - 1.5 to the presence of

isolated regions of sp^2 carbon occurrence on the hydrogenated electrodes, as indicated in Figure 3.2. It is possible that the laser beam in the Raman spectrometer focussed on such regions. Notably, surface hydrogenation is confined to the top most atomic layers at the edge plane sites, while the penetration depth for Raman and the probed area are likely to be far more extensive than the hydrogenated surface coverage, as suggested in the literature.[43]

Furthermore, there might be incomplete hydrogenation of electrode surfaces in our study in the 3 min exposure. The aggressive deposition conditions normally encountered in most plasma systems such as those based on microwave energy, thus contributing to fluxes of energetic hydrogen ions are known to damage tips of microelectrodes, as has been found in earlier studies.[7]
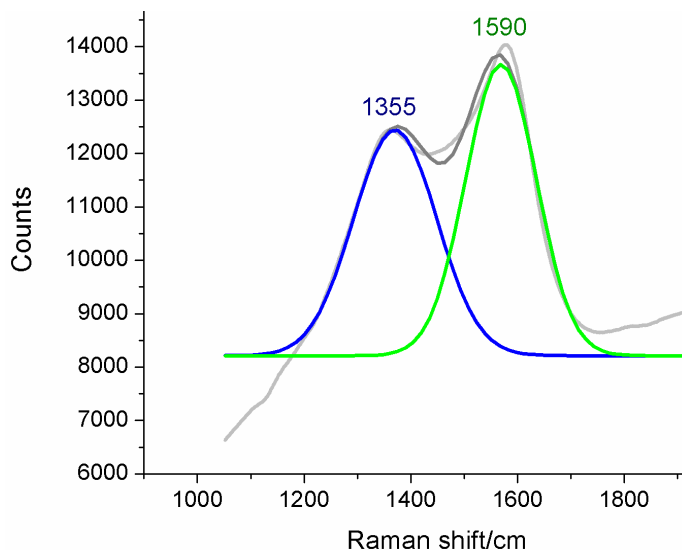
Figure 3.3   Raman shifts for a hydrogenated carbon electrode performed at 514.5 nm excitation.

In this study, even in a relatively low-energy plasma system, the initial exposure to radio frequency plasma for periods exceeding 3 min was found to severely damage the tips.

The current condition of a 3-min deposition time has so far provided an acceptable extent of hydrogenation of the fragile electrode tips.

3.3.4   X-ray Photoelectron Spectroscopy

Next, XPS was performed on the electrodes. XPS is a useful analytical tool for characterisation of industrial materials and molecular structure determination of organic surfaces.[51-52] It permits probing of chemical states of surfaces in greater detail.[51] For carbon film studies, the use of XPS as an analytical tool has become a vital addition for characterisation of carbon films.[45, 53-55] In this experiment, electrodes were subjected to XPS before and after hydrogenation, and the results obtained are shown in Figure 3.4A and Figure 3.4B, respectively. There are two prominent bands at 284 *eV* and 532 *eV* observed both in Figure 3.4A and Figure 3.4B. Bands at similar binding energy have been previously attributed to the presence of carbon (C_{1s})[2, 56] and oxygen (O_{1s}),[2, 57-58] respectively. Therefore, we have accordingly assigned them in this study. In the hydrogenated carbon spectrum (Figure 3.4A), the oxygen peak at approximately 534 *eV* is observed to be smaller than that for carbon at 284 *eV* at the hydrogenated electrode compared to that at the bare carbon electrode (Figure 3.4B). In addition, there are bands at 102 *eV* and 152 *eV* in Figure 3.4B, which are attributed to Si 2*p* and Si 2*s* from the quartz in the capillary.

A comparison of the oxygen/carbon (sp^3) ratio from deconvolution of the peaks in Figure 3.4 can be useful in identifying changes to the amount of oxygen following hydrogenation. Such deconvoluted peaks for bare carbon electrodes and hydrogenated carbon electrodes are presented in Figure 3.5. An O/C ratio of 4.34 was estimated from the results. This is suggestive of an oxygen-rich surface. Following hydrogenation, there is a significant attenuation in the oxygen peak, which provides indirect evidence for the replacement of oxygen by hydrogen following the deposition process. The O/C peak ratio at hydrogenated electrodes was observed to be 0.78. This is considerably higher
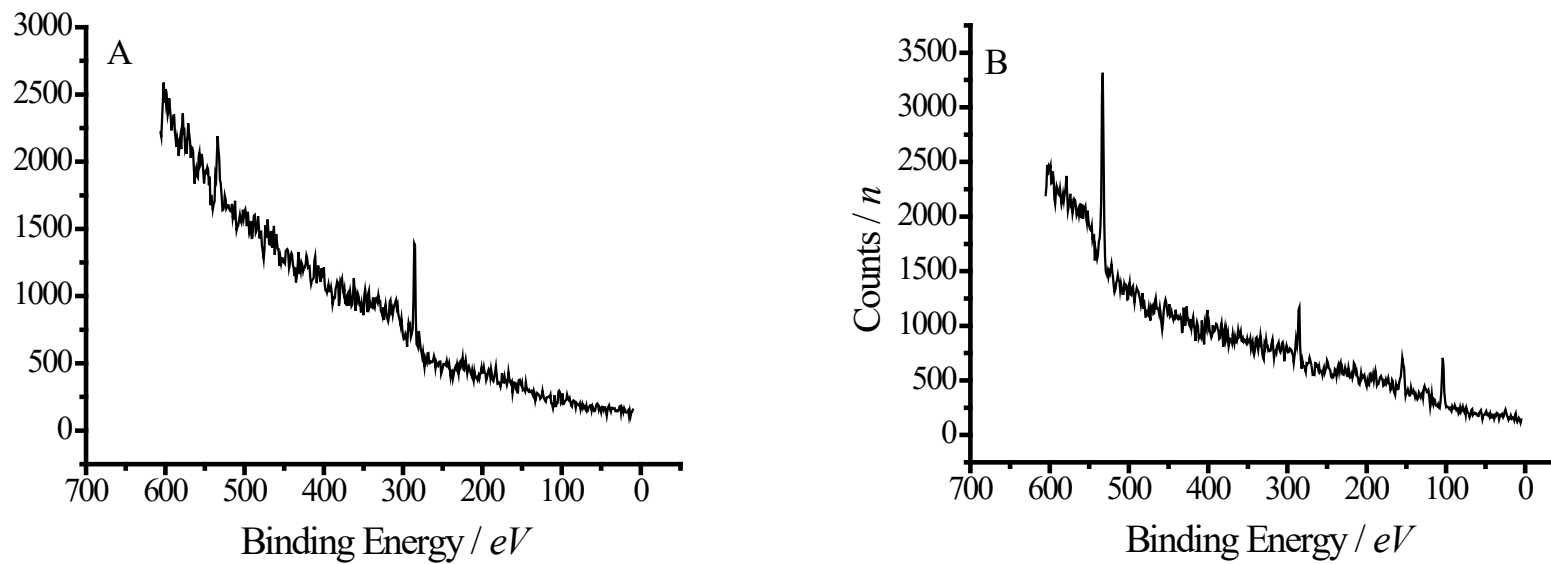
Figure 3.4   XPS spectrum of a hydrogenated carbon electrode (A) and bare carbon electrode (B).
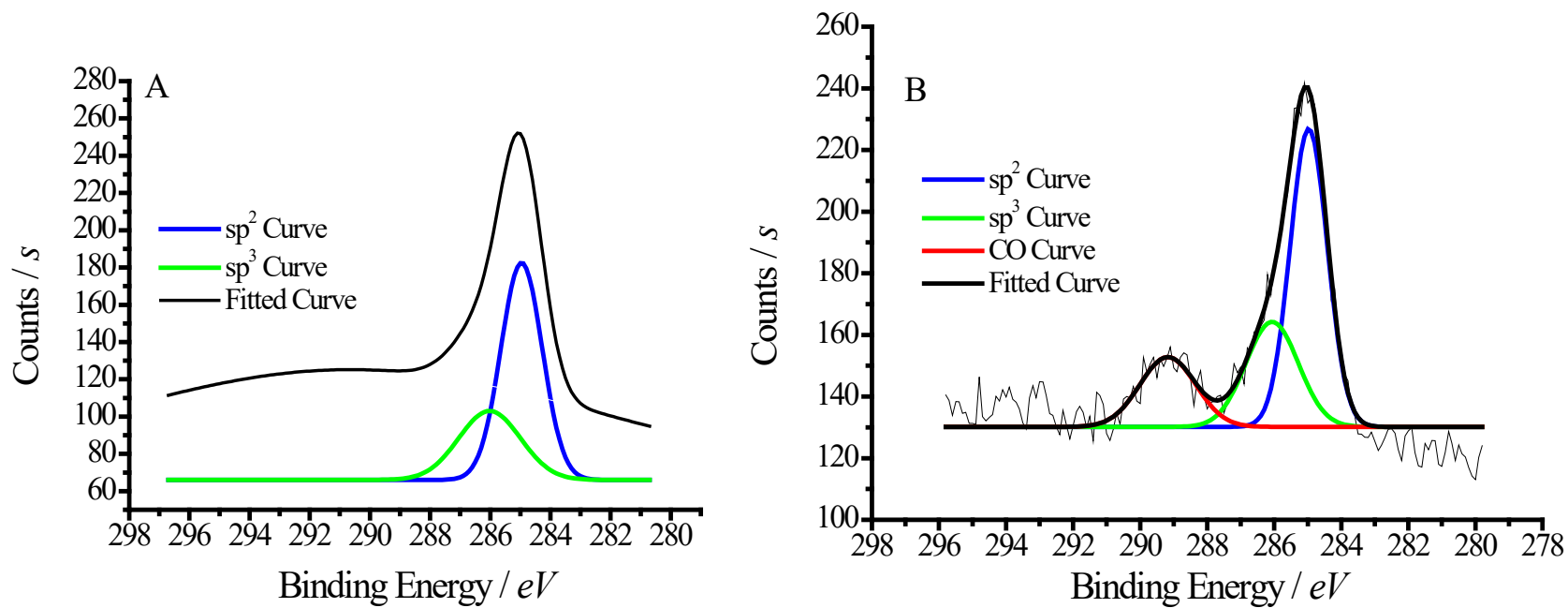
Fig 3.5   Deconvoluted peaks for C_{1s} from XPS spectrum at (A) a bare carbon electrode and (B) hydrogenated carbon electrode (right).

than 0.023 reported previously at hydrogenated carbon electrodes,[2] and quite likely is due to the mild hydrogenation conditions that were adopted in this study to prevent tip damage, as previously discussed in Section 3.3.3. Furthermore, in the deconvoluted C_{1s} spectrum for the bare carbon electrode, three peaks at 285, 286 and 289 *eV* were identified, and these correspond to the C—C bond, the C—O bond and either the C==O or O—C==O bonds.[59] As Yan *et al.*[58] have discussed recently, the shoulder at the higher binding-energy side of the C_{1s} spectrum usually indicates surface carbon-oxygen bonds. In the same article, the authors assumed that C—H bonds are a mixture of sp^2 and sp^3 carbon atoms corresponding to diamond-like hydrogenated carbon and graphitic carbon, respectively. Filik *et al.*[49] have previously performed a three-curve fitting analysis similar to that shown in Figure 3.5A on hydrogenated amorphous carbon films. Based on their peak allocations, a similar labelling approach has been adopted in Figure 3.5. According to the deconvoluted data, the three C_{1s} peaks correspond to full width at half maximum (FWHM) of 1.31 (285), 1.85 (286) and 1.96 (289). The FWHM of 1.31 is in excellent agreement with 1.31, reported previously for graphitic carbon.[58, 60] In addition, a ratio of 2.8 for the sp^2 to sp^3 carbon content for the electrodes was estimated, which is higher than 1.2 found elsewhere previously for diamond-like carbon.[58] This seems acceptable considering these electrodes are hydrogenated for a short duration as discussed in Section 3.3.3., therefore still containing isolated deposits of pyrolytic graphite. It is also noteworthy though that these ratios, established through surface examination techniques such as XPS are not representative of the bulk material but confined to a specific surface only.[49]

For the deconvoluted C_{1s} spectrum for hydrogenated carbon in Figure 3.5B, there are occurrences of the C_{1s} peaks for the fitted curve, the sp^2 carbon as well as sp^3 carbon. However, there is a distinct lack of the C—O peak in the deconvoluted data, for which the reasons are not immediately obvious. The FWHM of the deconvoluted peaks are 1.6 (285 *eV*) and 2.4 (286 *eV*).

The increase of FWHM from 1.3 to 1.6 is in agreement with 1.7 reported previously for diamond-like carbon,[60] and is consistent with the incorporation of a smooth surface devoid of edge plane defects usually achieved following hydrogenation (see Section 2.3.6). While the value of 1.6 falls short of that of diamond-like carbon, it appears to be a consequence of the hydrogenation conditions. The RF plasma is a lower-frequency means of achieving hydrogenation of carbon surfaces and as such, cannot be expected to achieve diamond-like surfaces unless more effective and aggressive hydrogenation is effected at the electrode surface. This is not easily accomplished using physically small electrodes with extremely fragile tips, which would almost invariably shatter if exposed to high-energy beams of energised hydrogen atoms such as those encountered in microwave plasma systems. Ultimately, the FWHM of diamond-like carbon is higher than that for graphite, but lower than that of diamond itself, as a consequence of sp^3 bonds and larger compressive stress.[60] The FWHM values for diamond has previously been reported to be as high as 1.96.[60] The results obtained in this study are therefore consistent with the findings of others.

3.3.5   Voltammetry of hexamine ruthenium(III) chloride

Similar to characterisation of bare physically small carbon electrodes, cyclic voltammetry of 1.0 mM $Ru(NH_3)_6^{3+}$ was conducted at hydrogenated carbon electrodes in 1.0 M KCl as a supporting electrolyte. The electrochemical reactivity of electrodes was assessed by the limiting currents, waveslope and halfwave potential ($E_{\frac{1}{2}}$) values in the redox systems mentioned in Section 3.2.4. The reduction of $Ru(NH_3)_6^{3+}$ is relatively insensitive to the presence of basal and edge planes.[61] Figure 3.6 shows the voltammogram obtained for 1.0 mM $Ru(NH_3)_6^{3+}$ in 1.0 M KCl. As shown, cyclic voltammetry of $Ru(NH_3)_6^{3+}$ at the same electrode shows a 25% decrease in limiting current following hydrogenation. However, there is no discernible change to the sigmoidal shape of the voltammogram, therefore confirming that there is no change to either the graphite packing, introduction of electrode deformities or damage to the surface following plasma treatment. The decrease

in current is attributable to the change in the surface charge following hydrogenation. Before hydrogenation, the reactive edge plane sites at the bare carbon surface would consist of sp^2 carbon attached to oxygen through groups such as carbonyl and quinones.[62] This resulted in a residual negative charge on the surface. Accordingly, a cationic species such as $Ru(NH_3)_6^{3+}$ diffusing to the surface of such electrodes would experience an electrostatic attraction towards the bare carbon electrode surface, leading to increased diffusion towards the electrode. Upon conversion to a hydrogen-terminated surface, negative charge-bearing molecular moieties *e.g.* quinonyl and carbonyl groups are expected to be reduced or removed.

Figure 3.6   Cyclic voltammetry of 1.0 mM $Ru(NH_3)_6^{3+}$ in 1.0 M KCl supporting electrolyte at a bare carbon (dotted) and hydrogenated carbon (solid) electrode. Scan rate: 100 mV/s.

This renders the hydrogenated surface to a lesser-charged surface. DeClements *et al.*[43] have previously suggested that oxygen-bearing functionalities at edge plane sites have the most influence on the reactivity of the carbon surface, with certain functionality types

mediating electron transfer. An extension of this theory would suggest a reduction of oxygen-bearing functionalities by conversion of unsaturated carbon molecules to sp^3 C—H bonds, which would retard the reaction kinetics, leading to a reduced reaction rate determined by rate of electron transfer. In this study, the reduction of the oxygenated functionalities would also affect the surface charge of the carbon, which causes a significant change to the electrostatic dynamics between the redox molecule and the surface. A consequence is the decreased limiting current arising from the reduction of the $Ru(NH_3)_6^{3+}$ compared to that obtained before hydrogenation.

The waveslope data for the reduction of $Ru(NH_3)_6^{3+}$ to $Ru(NH_3)_6^{2+}$ is summarised in Table 3.1. Following hydrogenation, waveslope increased from 77 mV/decade to 110 mV/decade, while the $E_{1/2}$ increased marginally from -187 mV to -177 mV. The reduction of cationic $Ru(NH_3)_6^{3+}$ species is classified as an outer-sphere electron transfer reaction that is relatively insensitive to the surface of the electrode.[62] The only slight shift of the $E_{1/2}$ for reduction of $Ru(NH_3)_6^{3+}$ agrees with this suggestion.

3.3.6   Voltammetry of potassium ferricyanide

The $Fe(CN)_6^{3-}$ redox system is often used to evaluate the extent of surface activation[63] and to probe the effects of surface oxides *via* changes to reaction kinetics.[62, 64] It has previously been shown that the presence of oxides on the electrode surface can accelerate the rate of reactions, and kinetics of the $Fe(CN)_6^{3-} / Fe(CN)_6^{4-}$ redox couple can be used to determine the extent of oxide coverage on the electrode surface.[7] Moreover, reaction kinetics of this couple can also be useful to obtain an estimation of the extent of defect sites on the electrode surface, as increased defects lead to greater exposure of edge planes and thus oxygen functionalities.[65]

Figure 3.7 shows the voltammograms for $Fe(CN)_6^{3-}$ obtained at a carbon and a hydrogenated carbon electrode. The voltammograms at both electrodes clearly show a

39% increase in limiting current after hydrogenation of the carbon electrode surface. This possibly is a partial consequence of $Fe(CN)_6^{3-}$ sensitivity to the monolayer coverage on a carbon surface rather than specific oxygen:carbon ratio,[66] despite significant changes to the nature of the surface following hydrogenation, such as removal of oxygen-bearing moieties.[67-68] The exact mechanism of these interactions is not clear at this stage. As Chen and McCreery[66] have concluded previously, the richness of surface chemistry of solid carbons makes its final properties difficult to predict, evaluate and often reproduce. In addition, the $Fe(CN)_6^{3-}$ system is expected to experience lesser repulsion from the hydrogenated surface than it would for more anionic bare carbon. Therefore, greater diffusion of $Fe(CN)_6^{3-}$ toward the electrode would be expected, leading to increased limiting currents from the reduction of $Fe(CN)_6^{3-}$ to $Fe(CN)_6^{4-}$.
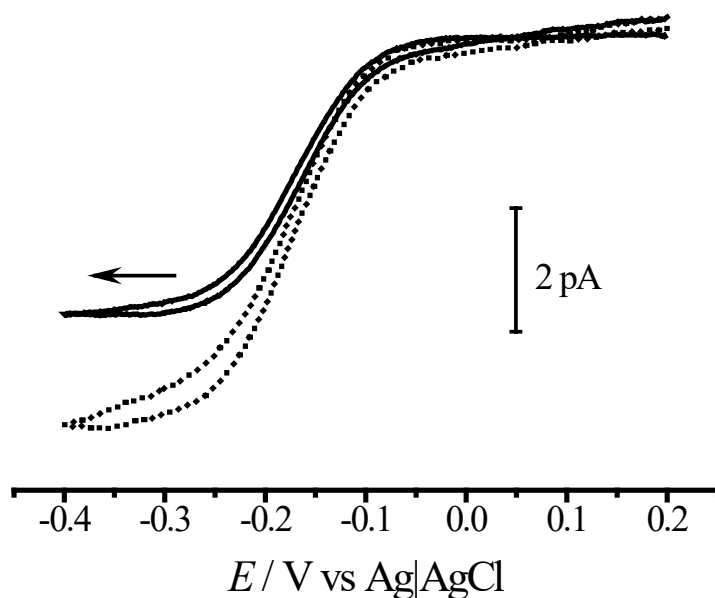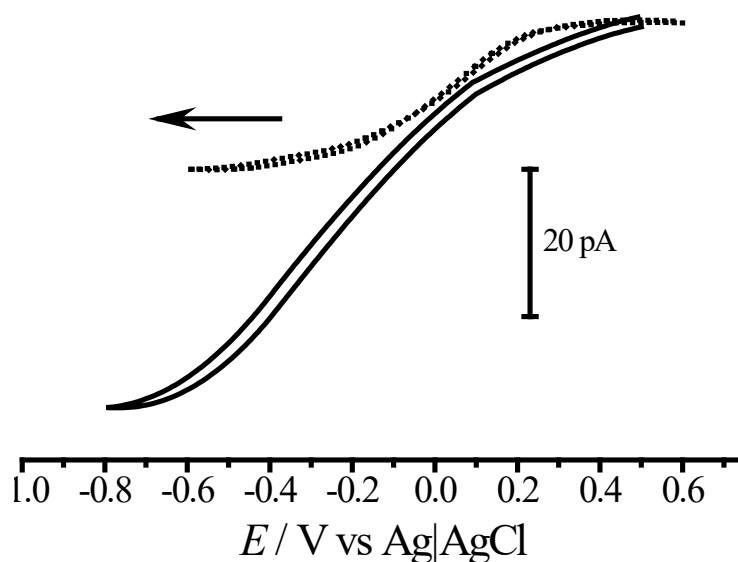

Figure 3.7   Cyclic voltammetry of 1.0 mM $Fe(CN)_6^{3-}$ in 1.0 M KCl supporting electrolyte at bare carbon electrode (dotted line) and hydrogenated carbon electrode (solid line). Scan rate: 100 mV/s.

A small difference between the forward and reverse scan current was observed in the voltammogram. If the re-packing of carbon in the hydrogenated electrode introduces

voids, it leads to areas of non-conductivity and thus capacitance. This is evidenced in a difference in the forward and reverse branches of current following the application of a potential sweep, and its subsequent reversal. Following hydrogenation, the repacking of graphite powder and insertion of a new piece of wire is likely to cause a disruption to the previously   well-ordered and packed graphitic carbon and may also possibly be a cause of the change in the sigmoidal shape that results due to reduction of $Fe(CN)_6^{3-}$ at the surface. For the reduction of $Fe(CN)_6^{3-}$, the $E_{½}$ of the voltammogram shifted negatively from +140 mV to -184 mV following hydrogenation. The waveslope was also observed to decrease from 195 mV/decade to 189 mV/decade, suggesting a quasi-reversible reduction, with the rate controlled by the rate of electron transfer kinetics, rather than diffusion of the species to the electrode surface. We believe the smoother hydrogenated surface containing lesser edge planes caused this change as fewer electron-transfer opportunities existed for the reduction of ferricyanide molecules.[65]

3.3.7   Voltammetry of dopamine

An evaluation of the reaction kinetics of dopamine at physically small electrodes before and after hydrogenation will offer insights on the kinetics of the oxidation of dopamine at the modified electrode surface. This information can be obtained by comparing the cyclic voltammetry of dopamine at electrodes before and after hydrogenation. Characterisation of electrode response to dopamine oxidation will often offer the analyst vital insights into the behaviour of electrodes when they are applied to dopamine oxidation.

The voltammetric signal for oxidation of dopamine is shown in Figure 3.8. Notably, there is an 18% decrease in the limiting current following hydrogenation. This is most likely caused by a reduction in the exposed edge planes at the hydrogenated carbon surface, leading to decreased electrostatic attraction between the electrode surface and cationic dopamine (in pH 7.4 buffer).[69]

100 pA

E / V vs Ag|AgCl
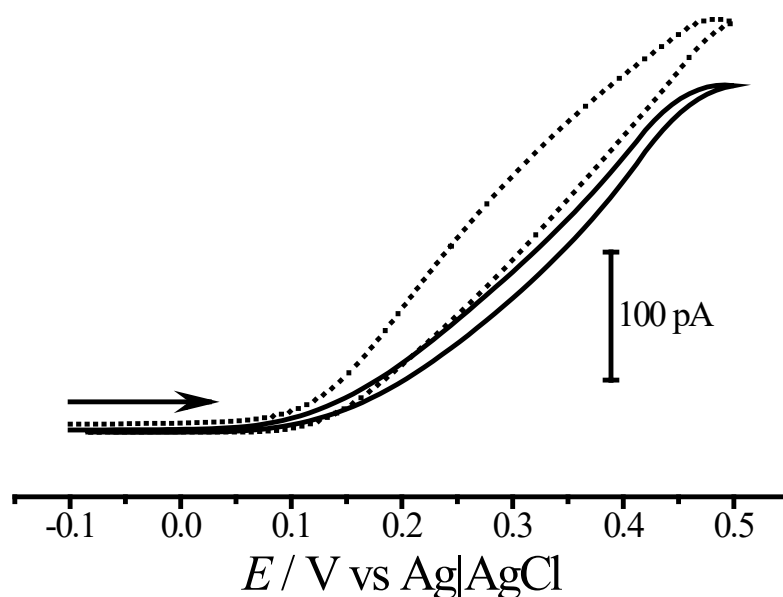
Figure 3.8   Cyclic voltammetry of 1.0 mM dopamine in pH 7.4 citrate/phosphate buffer at bare carbon electrode (dotted line) and hydrogenated carbon electrode (solid line). Scan rate: 100 mV/s.

Figure 3.8 also shows that the oxidation of dopamine at the hydrogenated electrode surface resulted in a negative $E_{½}$ shift slightly from 300 mV to 290 mV, suggesting slower oxidation kinetics at the hydrogenated surface. This observation is in agreement with work reported by Park *et al.*,[70] who have previously found dopamine, as well as other neurotransmitters such as norepinephrine and serotonin, undergo relatively slow electrochemical reaction kinetics at hydrogenated surfaces. This was attributed to the reduced adsorption of the molecules at a non-polar surface, which would otherwise have lowered the activation barrier for electron transfer leading to enhanced rates. This may well apply to the hydrogenated electrodes developed in this study. Furthermore, such sluggish kinetics at the electrode surface following modification would lead to electron-transfer being the rate determining step for the oxidation of dopamine, giving rise to reduced reversibility or quasi-reversibility for the oxidation of dopamine. This is observed to be the case as evidenced by the waveslope data for dopamine oxidation

before and after hydrogenation at the electrode surface, which will be further discussed in Section 3.3.8.

SEM and roughness analysis have previously suggested that higher heterogeneous electron transfer rates are related to rough carbon surfaces with a higher density of edge graphite particles.[71] During the hydrogenation process, carbonyl functionalities present on the reactive edge planes of the carbon surface would have been converted to C—H bonds with reduced surface defects. In the presence of the surface defects *via* the edge planes, the carbonyl functionalities would have facilitated an extended π electron transfer in the redox system, thus permitting more reversible reactions. With removal of the highly-porous edge plane defects after hydrogenation leading to a smoother diamond-like surface, the π electron transfer would have reduced, thus reducing the reversibility of the reaction.

The waveslope for oxidation of dopamine was found to increase from 169 mV/decade at bare carbon electrodes to 192 mV/decade (mean of 7 electrodes) at hydrogenated carbon electrodes. The corresponding $E_{1/2}$ was observed to decrease slightly from 300 mV to 290 mV. The waveslope for dopamine oxidation at the hydrogenated electrode suggests oxidation of dopamine to dopamine-*o*-quinone remains quasi-reversible following hydrogenation. As hydrogenation is a process that results in the smoothening of the edge planes at the carbon surface to a uniform surface devoid of defects,[58] such an observation is consistent with those found previously for similar hydrogenated electrodes.[23]

3.3.8   **Waveslope and halfwave potential**

The need to study the waveslope and $E_{1/2}$ of a reaction has been previously discussed in Chapter 2. A summary of the voltammetric data for the three redox systems at hydrogenated carbon electrodes is presented in Table 3.1.

Redox system	$Ru(NH_3)_6^{3+}$		$Fe(CN)_6^{3-}$		Dopamine	
	$E_{1/2}$ / mV	Waveslope / mV/decade	$E_{1/2}$ / mV	Waveslope / mV/decade	$E_{1/2}$ / mV	Waveslope / mV/decade
Before	-187 ± 7	77 ± 3	109 ± 35	206 ± 25	300 ± 16	169 ± 5
After	-177 ± 23	110 ± 30	-208 ± 69	202 ± 30	290 ± 73	192 ± 23

Table 3.1   Electrochemical parameters[*] of carbon electrodes before and after hydrogenation.

[*]All errors here represent the standard deviation of results obtained from 7 electrodes.

It is observed that the $E_{1/2}$ changes in all three redox systems, without any definite pattern. There are negative shifts in the $E_{1/2}$ for the $Fe(CN)_6^{3-}$ and dopamine systems, respectively, while a positive shift was observed for the $Ru(NH_3)_6^{3+}$ system. The waveslope for each redox reaction at the hydrogenated electrodes shows an increasing trend towards quasi reversibility. For all redox systems, this appears to result from the removal of the reactive edge planes of the carbon film. As previously reported, particularly for $Fe(CN)_6^{3-}$, a loss of edge plane sites leads to slower electron transfer kinetics.[68] Consequently, this would lead to the rate of electron transfer determining the rate of the reaction.

3.3.9   Voltammetry of hydrogenated carbon electrodes in the presence of protein and ascorbic acid

A comparison of the cyclic voltammetry of dopamine at bare carbon and hydrogenated carbon electrodes in the presence of interferents and fouling species can offer insights on electrode performance. In this experiment, 1.0 mM dopamine was prepared in citrate/phosphate buffer solution containing 0.1% (w/v) bovine serum albumin and 100 mM ascorbic acid. The bovine serum albumin mimics a protein-rich environment, while

the 100-fold higher concentration of ascorbic acid represents the higher concentration of the species in the brain compared to that of dopamine.[72-75] Figure 3.9 shows cyclic voltammograms for the oxidation of dopamine at hydrogenated and bare carbon electrodes in the presence of bovine serum albumin and ascorbic acid. As observed, in Figure 3.9A, the cyclic voltammogram of dopamine oxidation at the bare carbon electrode is marked by extremely slow reaction kinetics, as indicated by the ill-defined shape of the voltammogram. In addition, compared to the voltammogram of dopamine alone in pH 7.4 citrate/phosphate buffer at the same electrode in the inset of Figure 3.9A, there are multiple peaks at 0.28 V and 0.39 V, suggesting there is oxidation of at least two species in solution. It is extremely difficult to elucidate any particular peak in this voltammogram. Furthermore, there is an increase in limiting current between -0.1 V to 0.5 V observed at the bare carbon electrode when dopamine oxidation occurs in the presence of ascorbic acid. This is attributed to the re-oxidation of dopamine formed after the product dopamine-*o*-quinone was reduced by ascorbic acid back to dopamine, leading to increased current.[57, 76-77] Due to the similar oxidation potentials of both ascorbic acid and dopamine (between 0.40 – 0.50 V),[78-79] the two shoulders in the voltammogram at the bare carbon electrode in Figure 3.9A arose from the oxidation of both species. In contrast, dopamine oxidation at the hydrogenated electrode resulted in a more well-defined sigmoidal voltammogram, with a clear $E_{1/2}$ at approximately 0.36 V. This agrees with the potential for dopamine oxidation at the hydrogenated electrode surface (Table 3.1). Ascorbic acid in particular has been previously shown to have more positive peak potentials[80] than that for dopamine, hence any positive deviations from that observed for in a mixture of ascorbic acid and bovine serum albumin would have indicated interference from either species. This is clearly not the case at the hydrogenated electrode, where the slight reduction in the $E_{1/2}$ is observed instead. This is quite likely to be a consequence of altered kinetics of dopamine oxidation at the surface, caused by adsorption of hydrophilic protein species from the bovine serum solution on the non-hydrogenated regions on the electrode surface.
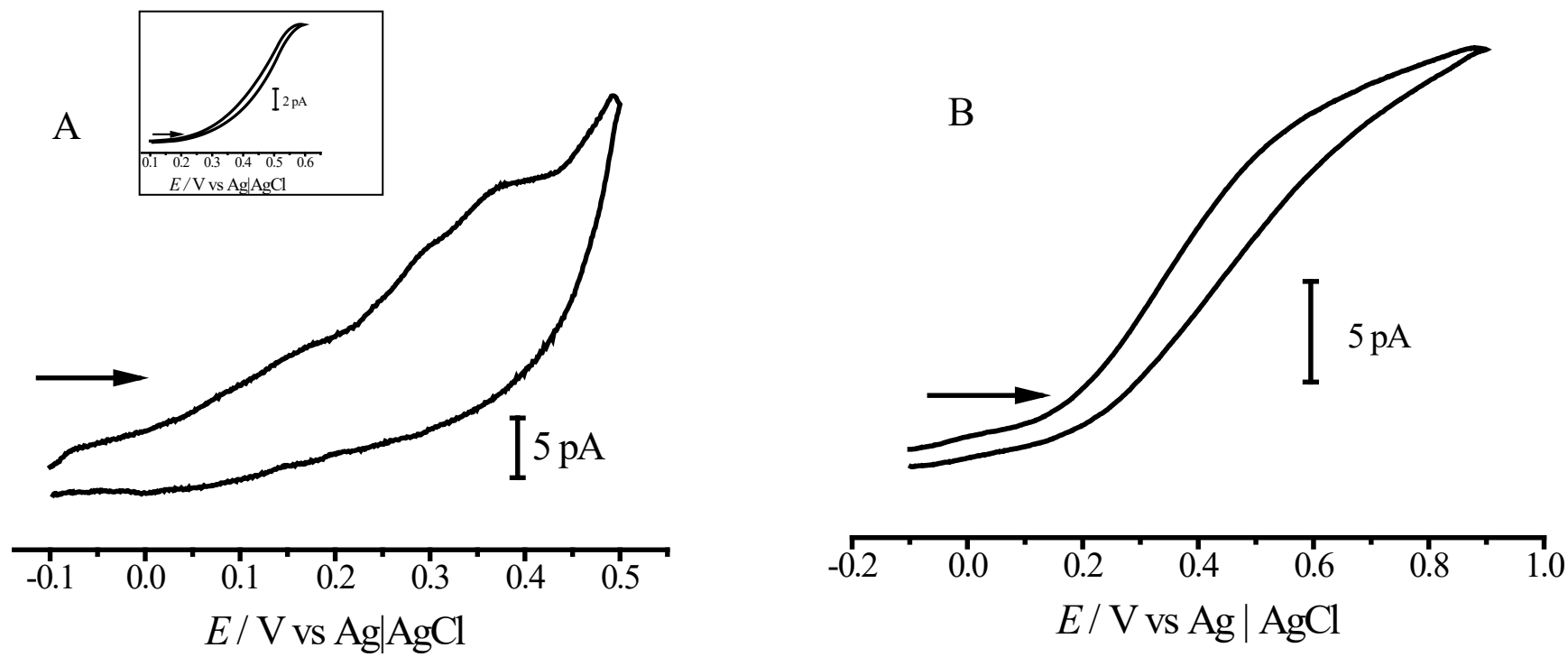
Figure 3.9   Cyclic voltammetry of dopamine oxidation at: bare carbon electrode (A) and hydrogenated carbon electrode (B) in 0.1% (w/v) bovine serum albumin + 100 mM ascorbic acid. Inset: Dopamine oxidation at the same bare carbon electrode in citrate/phosphate buffer. Scan rate: 100 mV/s.

The results depicted in Figure 3.9 suggest hydrogenated electrodes were minimally affected by interference from ascorbic acid. Next, cyclic voltammetry of dopamine was carried at both hydrogenated and bare carbon electrodes to determine the limit of detection and sensitivity to dopamine.

3.3.10   Analytical performance of hydrogenated carbon electrodes

Cyclic voltammetry of dopamine in pH 7.4 citrate/phosphate buffer was performed at hydrogenated carbon electrodes and the current relationship to dopamine concentration was plotted in Figure 3.10. A correlation coefficient of 0.9966 (N = 6), which was found to be statistically significant at the 95% level, was obtained. The linear relationship shown in Figure 3.10 can be expressed as

$$\text{Current / pA} = 0.16 \pm 0.041 \text{ pA/nM} \times [\text{dopamine}] \text{ / nM} + 95.7 \pm 5.14 \text{ pA}$$

In this expression, the uncertainties associated with the slope and the *y*-intercept represent the 95% confidence intervals. For comparison, details for this calibration plot and all other calibration plots are summarised in Table 3.2. Based on the calibration plot, sensitivity was determined as 0.16 pA/nM and limit of detection as 721 pM. In comparison with the sensitivity and limit of detection obtained for bare carbon electrodes (19 pA/nM and 543 pM) in Section 2.3.10, similar limit of detection was achieved, but less sensitivity was observed at hydrogenated electrodes for dopamine compared to bare carbon electrodes. This is attributed to the lower sensitivity to the change in electrostatic interactions between dopamine and the electrode surface before and after hydrogenation. There is enhanced attraction of dopamine towards the bare carbon electrode surface with carbonyl and quinone groups at the surface. Upon hydrogenation, these oxygen-bearing functional groups were converted to sp^3 C—H bonds, leading to a reduction of anionic sites on the hydrogenated electrode surface and, therefore, lesser electrostatic attraction

existed between dopamine and the hydrogenated carbon surfaces, leading to reduced sensitivity for dopamine at these electrodes.
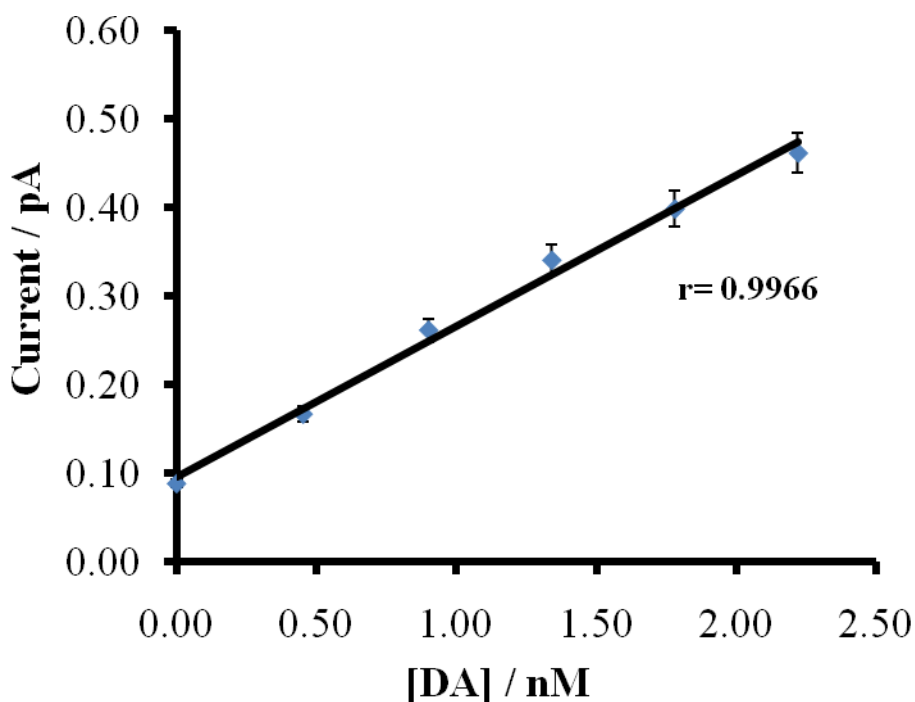
Figure 3.10   Calibration plot of limiting current versus dopamine concentration at hydrogenated carbon electrodes.

Next, hydrogenated carbon electrodes were used to detect dopamine in the presence of 0.1% (w/v) bovine serum albumin protein and 200 μM ascorbic acid. Figure 3.11 shows the linear calibration plot obtained, which can be expressed as

Current / nA = 0.04 ± 0.001 nA/nM × [dopamine] / nM + 0.88 ± 0.054 nA.

Moreover, the sensitivity, and limit of detection were estimated at 0.04 nA/nM and 836 pM, respectively. The limit of detection for dopamine also does not change significantly

when the matrix contains bovine serum albumin and ascorbic acid, although the sensitivity is observed to increase by approximately 200-fold ($N = 6$).

Figure 3.11   Calibration plot of limiting current versus dopamine concentration at hydrogenated electrodes in citrate/phosphate buffer + 0.1% bovine serum albumin + 200 µM ascorbic acid.

This appears to be the result of the conversion to dopamine and re-oxidation to dopamine-*o*-quinone as noted previously. These findings suggest that the electrode sensitivity may be compromised in a matrix containing proteins and interfering ascorbic acid. This limit of detection is lower than that found previously for modified sensors in detecting dopamine such as 0.1 µM for electropolymerised carbazole-coated carbon fibre microelectrodes;[81] and 5 nM for carbon fibre microelectrodes modified by Nafion and single-walled carbon nanotubes.[69]

Meanwhile, the calibration plot for ascorbic acid at hydrogenated carbon electrodes is depicted in Figure 3.12. Notably, the correlation coefficient of 0.9752 for this relationship was lower than that for dopamine (0.9998) at the same hydrogenated electrodes. The relationship between current signal and ascorbic acid concentration can be expressed as

$$\text{Current} / \text{pA} = 0.2 \pm 0.04 \ \text{pA}/\mu\text{M} \times [\text{dopamine}] / \mu\text{M} + 5.00 \pm 0.05 \ \text{pA}$$

From the equation, a limit of detection of 6 µM and and sensitivity of 0.2 pA/µM was obtained at hydrogenated carbon electrodes for ascorbic acid. Evidently, the hydrogenated electrodes exhibited lower sensitivity and higher detection limits for ascorbic acid compared to dopamine in the presence of bovine serum albumin. This demonstrates a degree of selectivity to dopamine over ascorbic acid at hydrogenated carbon electrodes.

The higher limit of detection for ascorbic acid than that for dopamine at the hydrogenated carbon electrodes is likely to be a result of ion-dipole interactions between the ions in solution and the hydrogenated carbon surface. Previously, Tryk *et al.*[82] have demonstrated that, as a result of electrochemical applications, particularly those involving oxidation processes, as in this study, the hydrogenated surface would be oxidised. This can have the effect of producing a surface whose surface starts approaching that of a monolayer of oxygen similar to that formed *via* gentle oxidation without the use of high-energy oxygen atoms. At such a surface, such organic cationic complexes as dopamine were previously demonstrated to be resolved easily from a mixture with ascorbic acid.[83] The reasons for these are not clear, but it has been speculated that ion-dipole and dipole-dipole interactions were involved.[82]
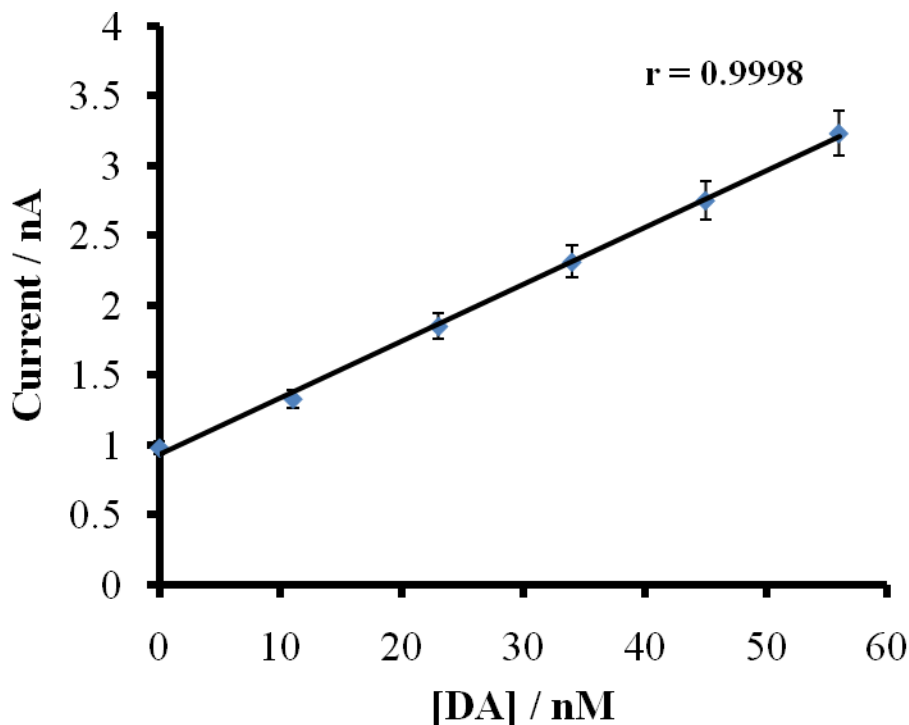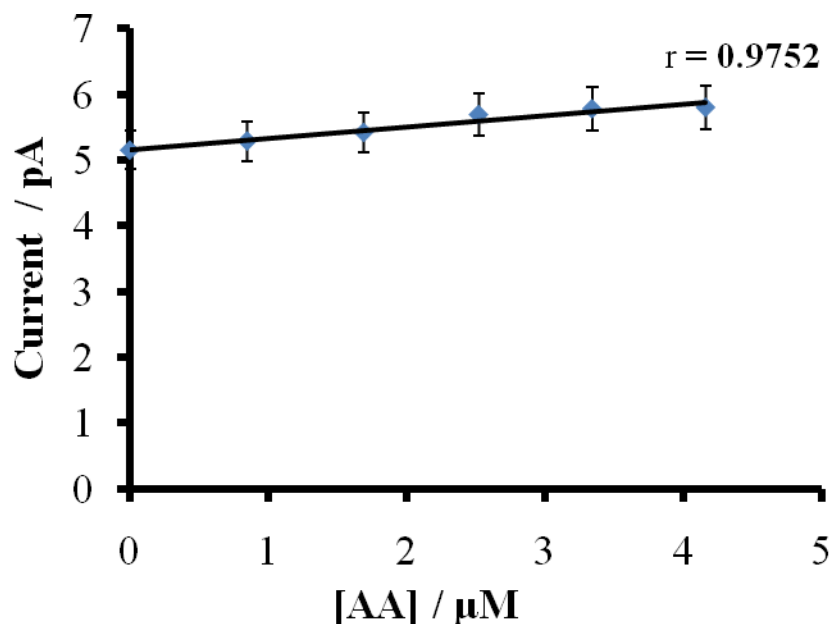
Figure 3.12   Calibration plot of limiting current versus ascorbic acid concentration at hydrogenated electrodes in citrate/phosphate buffer + 0.1% bovine serum albumin.

3.3.11   Electrode performance following *in vitro* exposure

It is useful to determine the extent to which exposure to the brain affects the sensitivity and selectivity of the electrodes to dopamine. Therefore, in this experiment, electrodes were subjected to chronoamperometry to determine the selectivity and selectivity to dopamine. Chronoamperometry was selected over cyclic voltammetry owing to the susceptibility of cyclic voltammetry to charging current effects.

Figure 3.13 illustrates representative calibration obtained at hydrogenated carbon electrodes before (A) and after immersion (B) in the synthetic laboratory solution that consisted of 1.0% (v/v) caproic acid (a lipid), 0.1% (w/v) bovine serum albumin and 0.01% (w/v) cytochrome C (both are protein) and 0.002% (w/v) human fibrinopeptide B (a peptide). Following immersion in the synthetic laboratory solution, little change in the

current relationship to dopamine concentration (0.11 pA/nM) was observed compared to those obtained before immersion (0.16 pA/nM as described in Section 3.3.10). An examination of the calibration plot obtained following immersion in the synthetic laboratory solution yields a reduced correlation coefficient of 0.9874, while the equation for the plot is expressed as

$$\text{Current / pA} = 0.11 \pm 0.017 \text{ pA/nM} \times [\text{dopamine}] / \text{nM} + 2.2 \pm 2.1 \text{ pA}$$
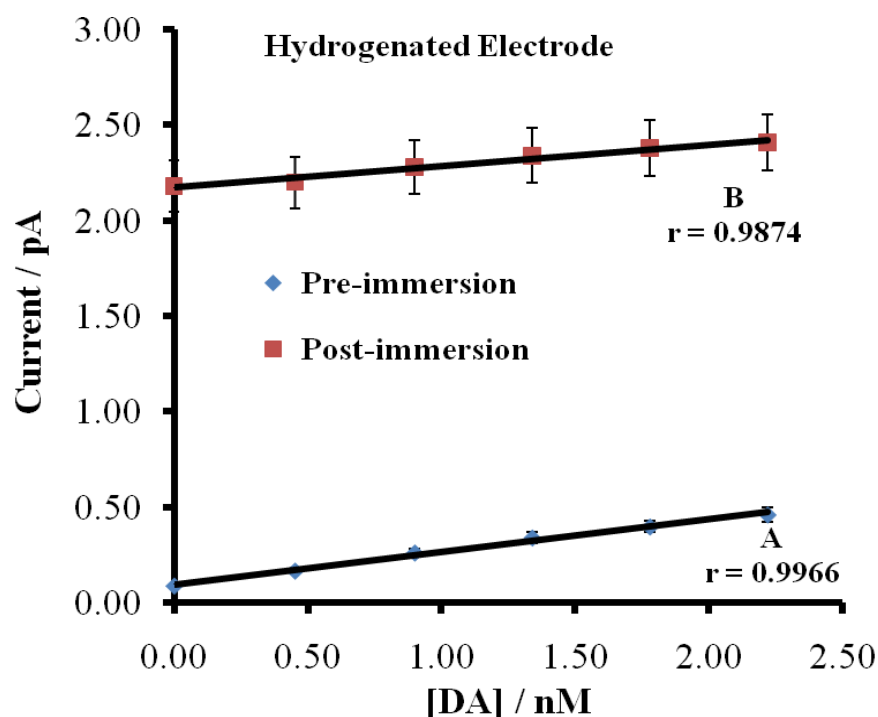
Figure 3.13   Calibration plots of limiting current versus dopamine concentration in a solution of 0.1% (w/v) bovine serum albumin + 1.0% (w/v) caproic acid + 0.002% (w/v) human fibrinopeptide B + 0.01% (w/v) cytochrome C in pH 7.4 citrate/phosphate buffer: before immersion (A) and after immersion (B) at hydrogenated carbon electrodes.

In Figure 3.13B, a 3-order increase in current offset was obtained. This may be due to some extent of adsorption of electroactive species at the electrode surface. Sensitivity was determined to be 0.11 pA/nM while limit of detection was estimated at 720 pM. Compared to the limit of detection and sensitivity of electrodes prior to immersion (721 pM and 0.16 pA/nM respectively), these parameters were not significantly different, suggesting that the response of the electrode surface to dopamine was not overly compromised following exposure to a hydrophilic mixture of high molecular weight proteins, peptides and lipids. It is noteworthy that despite the most vigorous endeavours, it is expected there would be sites on the electrode where carbon-oxygen functionalities may still be prevalent. This is a possibility confirmed from AFM measurements (Section 3.3.2), which shows isolated formations of amorphous carbon still prevailing on hydrogenated electrodes. Based on these findings, it is suggested that hydrogenation might not have resulted in complete passivation of the electrode surface. On these sites of remaining sp^2 carbon, adsorption of high molecular weight species would occur when the same electrode was exposed to the synthetic laboratory solution. The presence of these adsorbates would be expected to behave as an additional layer, which dopamine would have to penetrate before any electro-oxidation could occur. This in turn would cause an impedance, which is possibly the cause of the higher *y*-intercept in the calibration observed in Figure 3.13B.

In comparison to the hydrogenated carbon electrode, the bare carbon electrode displays significant changes in the detection of dopamine following exposure to the synthetic laboratory solution. As previously shown in Section 2.3.12 (Figure 2.23), the bare carbon electrode displayed severe loss of sensitivity and a two-order increase in the limit of detection for dopamine following the immersion in the synthetic laboratory solution. This degraded performance showed the extent of fouling that can be expected at such bare carbon surfaces, as has previously been documented.[84-85] Table 3.2 lists the

measured limit of detection and sensitivity at both hydrogenated and bare carbon electrodes, before and after immersion in the laboratory synthetic solution.

Comparatively, performances of the two electrode types show the hydrogenated electrode has superior fouling-withstanding capabilities. Its performance parameters (limit of detection and sensitivity) for dopamine shows there is virtually no change to the electrode surface despite exposure to a severely fouling environment. Next, to evaluate the performance *in vivo*, the electrodes were applied to *in vivo* dopamine detection in anesthetised rats, as is discussed in the next section.

3.3.12   *In vivo* dopamine detection at hydrogenated carbon electrodes

The rate of fouling can provide a measure of how rapidly the electrode surface undergoes degradation when applied *in vivo*. It also provides a measure of the durability and longevity of surface modifications. To determine the rate of fouling, the dopamine oxidation peak was monitored over 60-min duration while a hydrogenated carbon electrode was implanted in the left striatum of the rat brain. The peak height was measured every 15 min.

Figure 3.14A shows examples of responses obtained after the first series of electrical stimulations at hydrogenated carbon electrodes, similar to Figure 2.24. A cluster of peaks superimposed on a rising current is observed, which corresponds to the release and subsequent oxidation of dopamine at the electrode surface. The corresponding Gaussian-fitted peak is presented in Figure 3.14B. As shown, there is an increase in current at approximately 0.26 V which reaches a maximum at ~ 0.35V and subsequently decays away. The transient increase in current is a result of processes such as release, uptake

Figure	Calibration Plot Type	N	Correlation coefficient	Limit of Detection / pM	Sensitivity / pA/nM
3.10	Dopamine calibration at hydrogenated carbon electrode	8	0.9966	721	0.16
2.19	Dopamine calibration at bare carbon electrode	6	0.9927	543	19
3.11	Dopamine calibration in the presence of 0.1% (w/v) bovine serum albumin + 200 μM ascorbic acid	5	0.9998	836	40
3.12	Ascorbic acid calibration in the presence of 0.1% (w/v) bovine serum albumin	7	0.9752	6,000,000	0.0002
3.13A	Dopamine calibration at hydrogenated electrode prior to incubation in synthetic laboratory solution	8	0.9966	721	0.16
3.13B	Dopamine calibration at hydrogenated electrode after incubation in synthetic laboratory solution	7	0.9874	720	0.11

Table 3.2   Summary of limit of detection and sensitivity data at hydrogenated and bare carbon electrodes.

and diffusion of dopamine, while the decrease in current thereafter is a result of decreasing concentrations of dopamine at the electrode, resulting from processes such as metabolism, uptake and diffusion.[86] The electrical stimulations were repeated every 15 min (data not shown) until 60 min. The results obtained at the end of the experiment are depicted in Figure 3.14C, and the fitted results in Figure 3.14D. A transient decrease in peak current is obtained after 60 min of monitoring.

Figure 3.15 shows a plot of the percentage of dopamine oxidation current remained against a 60-min duration over which hydrogenated carbon electrodes were implanted. In these experiments, we assume negligible fouling at an electrode at the start of the experiment, and denoted as t = 0 min, which corresponds to the application of the first stimulation. The dopamine oxidation peak current was assigned a 100% value at t = 0, and all subsequent dopamine oxidation peak currents were then compared to this value. In general, the percentage of dopamine current remained was observed to decline at all three electrodes over the 60-min duration, with the largest decrease occurring within approximately the first 20 min of implantation. Following this, the percentage of dopamine current was observed to be more constant. There is a possibility of incomplete hydrogenation on the small carbon electrodes, leaving some polar functional groups still exposed on the electrode surface. This may explain the initial decrease in current observed in Figure 3.15. Furthermore, the rate of decay in the dopamine oxidation current at the hydrogenated electrode surface was determined (data not shown), based on the average of the results in Figure 3.15. Accordingly, at the hydrogenated electrodes, this rate was determined to be 0.7635 %/min. In comparison, the corresponding plot at bare carbon electrodes is depicted in Figure 2.25B, which shows a steady rate of diminishing dopamine oxidation peak current.   A comparison of Figure 3.14 to Figure 2.25B shows the effectiveness of the hydrophobic hydrogenated carbon surface against fouling. In addition, the rate of dopamine signal decay at bare carbon electrodes, was found to be 0.9612 %/min. This comparison confirms that the extent of electrode fouling, as evidenced by dopamine oxidation signal decay is greater at the bare carbon electrodes.
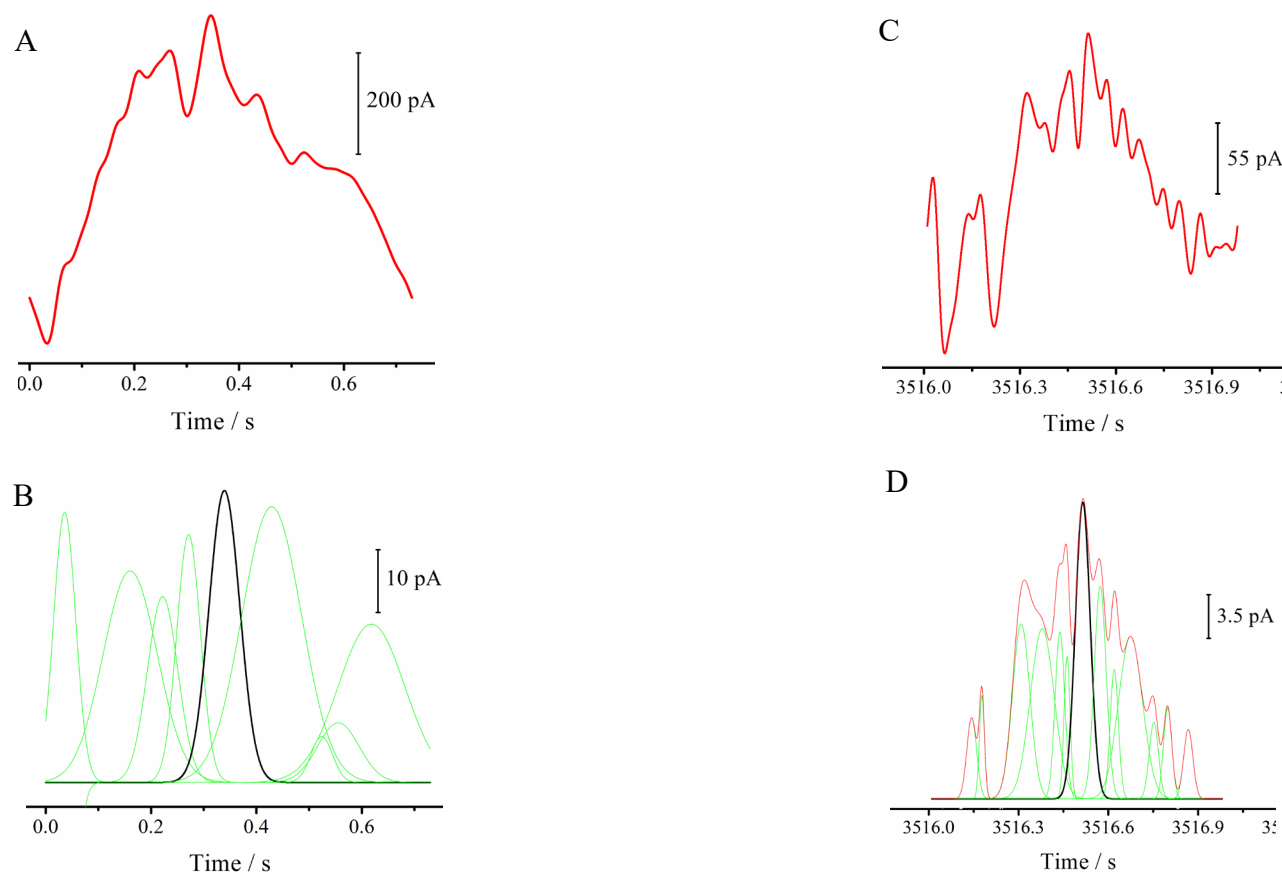
Figure 3.14   Dopamine oxidation signal in the rat striatum at hydrogenated electrodes at the start of the experiment (A) and after 60 min (C). Peaks (B) and (D) denote the fitted current signals at the start and after 60 min of experiment respectively.
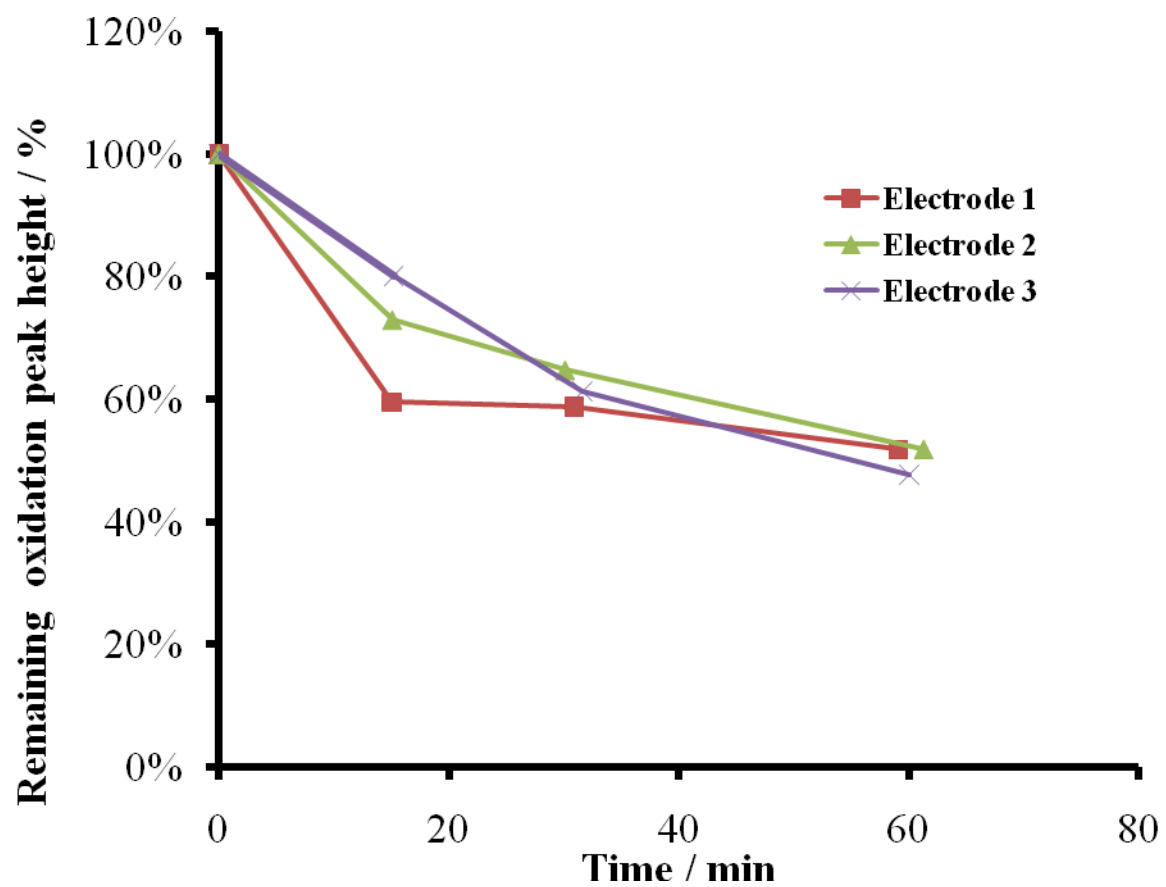
Figure 3.15   Rate of electrode fouling at hydrogenated carbon electrodes.

A comparison between the oxidation peak feature height after 60 min to that at the start as shown in Figure 3.15 reveals a $50 \pm 5\%$ (N = 4) decrease in the oxidation peak signal after 60 min. This extent of current signal deterioration is an improvement compared to $62 \pm 9\%$ (N = 4) at bare carbon electrodes (see Section 2.3.12). Based on Student's t-test, the two means obtained at the start and after 60 min were found to be statistically different from each other. These results support that the bare carbon electrode encounters greater surface degradation following exposure to the extracellular fluid in the striatum while the hydrogenated surface exhibits a higher degree of resistance to fouling. These findings are in good agreement with those of the *in vitro* characterisation of the electrodes in detecting dopamine at the hydrogenated and bare carbon electrodes.   In these characterisation studies, the electrodes demonstrated negligible changes to the limit of detection of and sensitivity to dopamine following exposure to the synthetic laboratory solution.   The results herein suggest that hydrogenation is a successful method of resisting fouling by electroactive species as well as interference from ascorbic acid.

3.4   Concluding remarks

In this study, bare carbon electrodes were subjected to hydrogenation in a low-frequency remote plasma setup to prepare a sp^3 carbon-coated surface. The low-frequency process was preferred owing to the fragility of the electrode tips that are susceptible to physical and chemical damage from otherwise high energy and intensive sources of excited hydrogen atoms such as microwave plasma.

Hydrogenated electrodes were then subjected to chemical and spectral characterisation to verify the presence hydrogenated surface.   Atomic force microscopy confirmed that following hydrogenation, the surface was smoothened from a roughness in the micrometer range to that in nanometers. Finally, XPS studies verified a reduced oxygen

presence on the hydrogenated electrode, to levels comparable with those found previously in the literature.

Electrochemical measurements were performed in three redox systems, the positively-charged $Ru(NH_3)_6^{3+}$, the negatively-charged $Fe(CN)_6^{3-}$, and the positively-charged dopamine in pH 7.4 citrate/phosphate buffer. The voltammetric behaviour of these species at the electrodes before and after hydrogenation pointed to the presence of a surface which had clearly reduced negative polarity and slightly reduced kinetics. These were attributed to the removal of the negatively-charged oxygen moieties formerly present in the edge planes of the carbon film at the bare electrodes. This leads to a smoothening of the surface leading to electrochemical reactions shifting towards quasi reversibility which was observed in all three systems.

The electrodes display lower detection limits and higher sensitivities for dopamine (836 pM and 0.04 nA/nM) over ascorbic acid (6 μM and 0.2 pA/μM) which are required attributes in a sensor for dopamine detection. Furthermore, the hydrogenated electrodes compared favourably with bare carbon electrodes for dopamine detection in a protein-, lipid- and peptide- rich environment. The sensitivity and limit of detection for dopamine at hydrogenated electrodes were observed to change only marginally following exposure to artificial laboratory. Compared to bare carbon electrodes, this indicates that the surface of the carbon electrodes was sufficiently hydrogenated to withstand fouling from high molecular hydrophilic species such as proteins, peptides and lipids.

The *in vivo* results reinforce conclusions drawn from the *in vitro* characterisation of the hydrogenated electrodes. Furthermore, at the hydrogenated electrode, fouling occurs at a rapid rate for the first 20 min of implanting the electrode in the brain. After this initial rapid fouling rate, the electrode surface appears to equilibrate with the environment, and undergoes a considerably slower rate of degradation. These results compare favourably with those of similar monitoring experiments performed at bare carbon electrodes, which

showed consistent fouling of the electrode surface throughout the monitoring period. The signal for dopamine oxidation is observed to degrade to 50% of the original signal at the time of commencement of the experiment when the electrode is implanted into the anesthetised rat brain. This also compares favourably with bare carbon electrodes which demonstrate higher extent of signal decay (62%). The rate of fouling was also observed to be greater at bare carbon electrodes (0.9612 %/min), which is greater than 0.7635 %/min at the hydrogenated electrodes. From these results, it can be concluded that the hydrogenated electrodes can be applied to *in vivo* dopamine detection with acceptable degree of resistance to fouling from high molecular hydrophilic species.

3.5   References

1.   Wang, J., *Analytical Electrochemistry*. Third Edition ed.; John Wiley & Sons: Hoboken, 2006.

2.   Chen, Q.; Swain, G. M., *Langmuir* **1998,** *14* (24), 7017-7026.

3.   Ivandini, T. A.; Sarada, B. V.; Terashima, C.; Rao, T. N.; Tryk, D. A.; Ishiguro, H.; Kubota, Y.; Fujishima, A., *J. Electroanal. Chem.* **2002,** *521* (1-2), 117-126.

4.   Uslu, B.; Topal, B. D.; Ozkan, S. A., *Talanta* **2008,** *74* (5), 1191-1200.

5.   Lee, J. A.; Hwang, S.; Kwak, J.; Park, S. I.; Lee, S. S.; Lee, K.-C., *Sens. Actuators, B* **2008,** *129* (1), 372-379.

6.   Downard, A. J.; Roddick, A. D.; Bond, A. M., *Anal. Chim. Acta* **1995,** *317* (1-3), 303-310.

7.   Alwarappan, S.; Butcher, K. S. A.; Wong, D. K. Y., *Sens. Actuators, B* **2007,** *128* (1), 299-305.

8.   Ferry, Y.; Leech, D., *Electroanalysis* **2005,** *17* (2), 113-119.

9.   Roberts, J. G.; Moody, B. P.; McCarty, G. S.; Sombers, L. A., *Langmuir* **2010,** *26* (11), 9116-9122.

10.   Kaibara, Y.; Sugata, K.; Tachiki, M.; Umezawa, H.; Kawarada, H., *Diamond Relat. Mater.* **2003,** *12* (3-7), 560-564.

11.   Shin, D.; Tryk, D. A.; Fujishima, A.; Merkoçi, A.; Wang, J., *Electroanal.* **2005,** *17* (4), 305-311.

12.   Rezek, B.; Nebel, C. E., *Diamond Relat. Mater.* **2006,** *15* (9), 1374-1377.

13.   Rezek, B.; Nebel, C. E.; Stutzmann, M., *Diamond Relat. Mater.* **2004,** *13* (4-8), 740-745.

14.   Ralchenko, V.; Saveliev, A.; Voronina, S.; Dementjev, A.; Maslakov, K.; Salerno, M.; Podesta, A.; Milani, P., Nanodiamond Seeding for Nucleation and Growth of CVD Diamond Films. In *Synthesis, Properties and Applications of Ultrananocrystalline Diamond*, 2005; pp 109-124.

15.   Fizzotti, F.; Lo Giudice, A.; Manfredotti, C.; Manfredotti, C.; Castellino, M.; Vittone, E., *Diamond Relat. Mater.* **2007,** *16* (4-7), 836-839.

16.   Murilo Sérgio da Silva Julião, Érica C. A. M. Aquiles La S. Neidenêi G. F. Richard G. C. Sílvia H. Pires S., *Electroanal.* **2005,** *17* (3), 269-274.

17.   Scialdone, O.; Galia, A.; Guarisco, C.; Randazzo, S.; Filardo, G., *Electrochim. Acta* **2008,** *53* (5), 2095-2108.

18.   Xiao, L.; Streeter, I.; Wildgoose, G. G.; Compton, R. G., *Sens. Actuators, B* **2008,** *133* (1), 118-127.

19.   Hian, L. C.; Grehan, K. J.; Compton, R. G.; Foord, J. S.; Marken, F., *Diamond Relat. Mater.* **2003,** *12* (3-7), 590-595.

20.   Hian, L. C.; Grehan, Kieron J.; Goeting, Christiaan H.; Compton, Richard G.; Foord, J. S.; Marken, F., *Electroanalysis* **2003,** *15* (3), 169-174.

21.   Soh, K. L.; Kang, W. P.; Davidson, J. L.; Basu, S.; Wong, Y. M.; Cliffel, D. E.; Bonds, A. B.; Swain, G. M., *Diamond Relat. Mater.* **2004,** *13* (11-12), 2009-2015.

22.   Park, J.; Show, Y.; Quaiserova, V.; Galligan, J. J.; Fink, G. D.; Swain, G. M., *J. Electroanal. Chem.* **2005,** *583* (1), 56-68.

23. McNally, M.; Wong, D. K. Y., *Anal. Chem.* **2001,** *73* (20), 4793-4800.

24. Pickles, C. S. J.; Hall, C. E.; Jiang, L.; Perkins, N.; Kleijhorst, R. A. Diamond microelectrodes. 2004-IB2404, 2005012894, 20040727., 2005.

25. Tsunozaki, K.; Einaga, Y.; Rao, T. N.; Fujishima, A., *Chem. Lett.* **2002,** (5), 502-503.

26. Sarada, B. V.; Rao, T. N.; Tryk, D. A.; Fujishima, A., *J. Electrochem. Soc.* **1999,** *146* (4), 1469-1471.

27. Iwaki, M.; Sato, S.; Takahashi, K.; Sakairi, H., *Nucl. Instr. Meth. Phys. Res.* **1983,** *209-210* (Part 2), 1129-1133.

28. Pleskov, Y. V., Synthetic diamond electrodes for electroanalysis and electrolysis. In *Electroanalytical Chemistry Research Developments*, Jiang, P. N., Ed. Nova Science Publishers Inc: Hauppauge, 2007; pp 183-227.

29. Martínez-Huitle, C. A., *Small* **2007,** *3* (9), 1474-1476.

30. Wang, L. J.; Xia, Y.; Fang, Z.; Zhang, W.; Zhang, W.; Shi, W., *J. Mater. Sci. Lett.* **2003,** *22* (20), 1447-1450.

31. Baranauskas, V.; Tosin, M. C.; Peterlevitz, A. C.; Ceragioli, H.; Durrant, S. F., *J. Appl. Phys.* **2000,** *88* (3), 1650.

32. Kromka, A.; Janík, J.; Balon, F.; Kubovic, M.; Cerven, I.; Dubravcová, V., *Thin Solid Films* **2003,** *433* (1-2), 73-77.

33. Shang, F.; Zhou, L.; Mahmoud, K. A.; Hrapovic, S.; Liu, Y.; Moynihan, H. A.; Glennon, J. D.; Luong, J. H. T., *Anal. Chem.* **2009,** *81* (10), 4089-4098.

34. Olivia, H.; Sarada, B. V.; Shin, D.; Rao, T. N.; Fujishima, A., *Analyst* **2002,** *127* (12), 1572-1575.

35. Park, J.; Quaiserova-Mocko, V.; Peckova, K.; Galligan, J. J.; Fink, G. D.; Swain, G. M., *Diamond Relat. Mater.* **2006,** *15* (4-8), 761-772.

36.   Venton, B. J.; Seipel, A. T.; Phillips, P. E. M.; Wetsel, W. C.; Gitler, D.; Greengard, P.; Augustine, G. J.; Wightman, R. M., *J. Neurosci.* **2006,** *26* (12), 3206-3209.

37.   Chen, G., *Talanta* **2007,** *74* (3), 326-332.

38.   Gaudin, O.; Whitfield, M. D.; Foord, J. S.; Jackman, R. B., *Diamond Relat. Mater.* **2001,** *10* (3-7), 610-614.

39.   Hiramatsu, M.; Lau, C. H.; Bennett, A.; Foord, J. S., *Thin Solid Films* **2002,** *407* (1-2), 18-25.

40.   Hupert, M.; Muck, A.; Wang, J.; Stotter, J.; Cvackova, Z.; Haymond, S.; Show, Y.; Swain, G. M., *Diamond Relat. Mater. 12* (10-11), 1940-1949.

41.   Horinek, D.; Serr, A.; Geisler, M.; Pirzer, T.; Slotta, U.; Lud, S. Q.; Garrido, J. A.; Scheibel, T.; Hugel, T.; Netz, R. R., *Proc. Natl. Acad. Sci. U. S. A.* **2008,** *105* (8), 2842-2847.

42.   Xu, J.; Chen, Q.; Swain, G. M., *Anal. Chem.* **1998,** *70* (15), 3146-3154.

43.   DeClements, R.; Swain, G. M.; Dallas, T.; Holtz, M. W.; Herrick, R. D.; Stickney, J. L., *Langmuir* **1996,** *12* (26), 6578-6586.

44.   Zhao, H.; Bian, X.; Galligan, J. J.; Swain, G. M., *Diamond Relat. Mater. 19* (2-3), 182-185.

45.   Bendavid, A.; Martin, P. J.; Randeniya, L.; Amin, M. S., *Diamond Relat. Mater.* **2009,** *18* (1), 66-71.

46.   Bradac, C.; Gaebel, T.; Naidoo, N.; Rabeau, J. R.; Barnard, A. S., *Nano Letters* **2009,** *9* (10), 3555-3564.

47.   Barrat, S.; Guise, A.; Aouni, A.; Diani, M.; Bauer-Grosse, E., *Diamond Relat. Mater. 17* (4-5), 428-434.

48.   Bormett, R. W.; Asher, S. A.; Witowski, R. E.; Partlow, W. D.; Lizewski, R.; Pettit, F., *J. Appl. Phys.* **1995,** *77* (11), 5916.

49. Filik, J.; May, P. W.; Pearce, S. R. J.; Wild, R. K.; Hallam, K. R., *Diamond Relat. Mater.* **2003,** *12* (3-7), 974-978.

50. Goswami, R.; Jana, T.; Ray, S., *J. Phys. D: Appl. Phys.* **2008,** *41* (15), 155413.

51. Swift, A. J., *Microchimica Acta* **1995,** *120* (1), 149-158.

52. Sabbatini, L.; Zambonin, P. G., *J. Electron. Spectrosc. Relat. Phenom.* **1996,** *81* (3), 285-301.

53. Manfredotti, C.; Fizzotti, F.; Lo Giudice, A.; Manfredotti, C.; Castellino, M.; Bonino, P.; Vittone, E., *Diamond Relat. Mater.* **2008,** *17* (7-10), 1154-1158.

54. Popov, C.; Kulisch, W.; Bliznakov, S.; Mednikarov, B.; Spasov, G.; Pirov, J.; Jelinek, M.; Kocourek, T.; Zemek, J., *Appl Phys A-Mater* **2007,** *89* (1), 209-212.

55. Donner, S.; Li, H.-W.; Yeung, E. S.; Porter, M. D., *Anal. Chem.* **2006,** *78* (8), 2816-2822.

56. Selvaraju, T.; Ramaraj, R., *J. Electroanal. Chem.* **2005,** *585* (2), 290-300.

57. Xiao, Y.; Guo, C.; Li, C. M.; Li, Y.; Zhang, J.; Xue, R.; Zhang, S., *Anal. Biochem.* **2007,** *371* (2), 229-237.

58. Yan, X. B.; Xu, T.; Yang, S. R.; Liu, H. W.; Xue, Q. J., *J. Phys. D: Appl. Phys.* **2004,** *37* (17), 2416-2424.

59. Technology, N. I. o. S. a., NIST X-ray Photoelectron Spectroscopy Database Gaithersburg, 2003; Vol. Version 3.5.

60. Li, G.; Xia, L. F.; Ma, X. X.; Sun, Y., *Acta Metallurgica Sinica(English letters)* **1999,** *12* (4), 551-556.

61. Chen, P.; Fryling, M. A.; McCreery, R. L., *Anal. Chem.* **1995,** *67* (18), 3115-3122.

62. Ji, X.; Banks, C. E.; Crossley, A.; Compton, R. G., *ChemPhysChem* **2006,** *7* (6), 1337-1344.

63. Fagan, D. T.; Hu, I. F.; Kuwana, T., *Anal. Chem.* **1985,** *57* (14), 2759-2763.

64. Holloway, A.; Wildgoose, G.; Compton, R.; Shao, L.; Green, M., *J. Solid State Electrochem.* **2008,** *12* (10), 1337-1348.

65. Cline, K. K.; McDermott, M. T.; McCreery, R. L., *J. Phys. Chem.* **1994,** *98* (20), 5314-5319.

66. Chen, P.; McCreery, R. L., *Anal. Chem.* **1996,** *68* (22), 3958-3965.

67. McDermott, C. A.; Kneten, K. R.; McCreery, R. L., *J. Electrochem. Soc.* **1993,** *140* (9), 2593-2599.

68. Rice, R. J.; Pontikos, N. M.; McCreery, R. L., *J. Am. Chem. Soc.* **1990,** *112* (12), 4617-4622.

69. Jeong, H.; Jeon, S., *Sensors* **2008,** *8* (11), 6924-6935.

70. Park, J.; Quaiserova-Mocko, V.; Patel, B. A.; Novotny, M.; Liu, A.; Bian, X.; Galligan, J. J.; Swain, G. M., *Analyst* **2008,** *133* (1), 17-24.

71. Fanjul-Bolado, P.; Hernandez-Santos, D.; Lamas-Ardisana, P. J.; Martin-Pernia, A.; Costa-Garcia, A., *Electrochim. Acta* **2008,** *53* (10), 3635-3642.

72. Xu, G.-R.; Xu, M.-L.; Zhang, J.-M.; Kim, S.; Bae, Z.-U., *Bioelectrochemistry* **2008,** *72* (1), 87-93.

73. Sun, W.; Yang, M.; Jiao, K., *Anal. Bioanal. Chem.* **2007,** *389*, 1283-1291.

74. Miele, M.; Fillenz, M., *J. Neurosci. Methods* **1996,** *70* (1), 15-19.

75. Brazell, M. P.; Marsden, C. A., *Brain Res.* **1982,** *249* (1), 167-172.

76. Venton, B. J.; Troyer, K. P.; Wightman, R. M., *Anal. Chem.* **2002,** *74* (3), 539-546.

77. Ali, S. R.; Parajuli, R. R.; Ma, Y.; Balogun, Y.; He, H., *J. Phys. Chem. B* **2007,** *111* (42), 12275-12281.

78. Schenk, J. O.; Miller, E.; Rice, M. E.; Adams, R. N., *Brain Res.* **1983,** *277* (1), 1-8.

79.   Ambrosi, A.; Morrin, A.; Smyth, M. R.; Killard, A. J., *Anal. Chim. Acta* **2008,** *609* (1), 37-43.

80.   Robinson, D. L.; Venton, B. J.; Heien, M. L. A. V.; Wightman, R. M., *Clinical Chemistry (Washington, DC, United States)* **2003,** *49* (10), 1763-1773.

81.   Ates, M.; Sarac, A.; Turhan, C.; Ayaz, N., *Fibers Polym.* **2009,** *10* (1), 46-52.

82.   Tryk, D. A.; Tachibana, H.; Inoue, H.; Fujishima, A., *Diamond Relat. Mater.* **2007,** *16* (4-7), 881-887.

83.   Popa, E.; Notsu, H.; Miwa, T.; Tryk, D. A.; Fujishima, A., *Electrochem. Solid-State Lett.* **1999,** *2* (1), 49-51.

84.   Fujishima, A.; Rao, T. N.; Popa, E.; Sarada, B. V.; Yagi, I.; Tryk, D. A., *J. Electroanal. Chem.* **1999,** *473*, 179-185.

85.   Hashemi, P.; Dankoski, E. C.; Petrovic, J.; Keithley, R. B.; Wightman, R. M., *Anal. Chem.* **2009,** *81* (22), 9462-9471.

86.   Michael, D. J.; Wightman, R. M., *J. Pharm. Biomed. Anal.* **1999,** *19* (1-2), 33-46.

CHAPTER 4

ASSEMBLY OF A PLASMA-ASSISTED CHEMICAL VAPOUR DEPOSITION SYSTEM FOR FILM GROWTH AND HYDROGENATION

This chapter describes the development and assembly of a diamond chemical vapour deposition system. Diamond is of interest to electrochemists exploring the physical environment using electrochemistry and micro-voltammetric sensors. As described in Chapter 2, bare electrode material such as carbon tends to be susceptible to fouling by large molecular-weight hydrophilic species. Therefore, as described in Sections 3.1.1 and 3.1.2, an electrode surface modified by a hydrophobic layer such as diamond, or diamond-like hydrogenated carbon may repel such species more effectively than bare carbon electrode surfaces and allow for measurements *in vivo*.

In this chapter, the deposition system was fabricated to enable deposition of diamond films onto pre-seeded silica substrates. In addition, with manipulation of gas input, chamber pressure, excitation power and exposure time (to the activated hydrogen atoms), such a deposition apparatus can also be utilised for hydrogenation of bare carbon electrode surfaces.

The scope of this study was to:

1) hydrogen-terminate a previously deposited layer of pyrolysed carbon; and,

2) deposit a diamond layer onto pre-seeded quartz substrates.

This would then pave the way for incorporation of a similar film onto electrodes for *in vivo* dopamine detection. This chapter describes the assembly and use of such a deposition system. It begins with an overview of the literature, including the importance of diamond film growth and applications. Literature for hydrogenated electrodes utilised for *in vivo* applications has already been discussed in Chapter 3 and will not be examined here. The methodology adopted in developing these films is outlined, followed by hydrogenation of carbon surfaces. The results of characterisation studies to assess the quality of diamond film growth are also discussed.

4.1 Diamond deposition

The combination of intrinsic electrical, thermal, mechanical and optical properties of diamond films leads to a range of potential applications.[1] Diamond is an ideal material choice for optical coatings, radiation detectors and semiconductor devices working under extreme conditions such as aggressive environments, high temperature, high power, high radiation, and high frequencies.[2-3]

The diamond deposition process begins with the seeding process. [4] Seeding of substrates, typically using diamond grains prior to deposition increases nucleation of the growing film.[2] Nucleation involves the agglomeration of diamond into clusters. It is during the nucleation stage that the density of the diamond particles, alignment of the crystallites,[5] and ultimately the properties, morphology and homogeneity of the resulting diamond films are determined.[6] The growth and coating formation occurs as a result of creative manipulation of substrate conditioning, deposition parameters such as pressure, gas ratio, flow-excitation medium, substrate exposure time and post-deposition treatment. The different deposition parameters and values ultimately influence the quality, uniformity and characteristics of the final film.[7] These are discussed in detail in the following.

4.1.1   **Surface pre-treatment**

Spontaneous nucleation of diamond on a substrate has a low occurrence-probability. For instance, the nucleation density of diamond on silicon is typically of the order of 10^4 nuclei/cm^2. Considerably higher nucleation centre density must be achieved on the silicon substrate to produce thin, continuous films or conformal diamond coatings. This necessitates deliberate diamond seeding on the substrate before or during diamond deposition.[4] Providing nucleation sites prior to deposition is effective in depositing diamond onto the substrate. This is due to the diamond nuclei that form in the gas phase being unstable until they reach a certain critical size. Moreover, nucleation on untreated surfaces is slow and leads to a very slow growth rate of the film.[8] It has been well known that diamond nucleates well on itself and cubic boron nitride; scratching of nondiamond surfaces with diamond abrasive materials enhances the diamond nucleation, and, diamond deposition without surface pre-treatments such as scratching, oiling, or diamond-like carbon deposition does occur, but at a reduced nucleation rate. Without the surface   pre-treatment, deposition of thin, continuous diamond films is not possible.[9] It has previously been reported that following treatment, nucleation density of 10^8 - 10^{10} /cm^2 is observed, leading to grains of 0.1 - 1.0 μm in size forming on the substrate. These subsequently evolved into columnar crystallites with their size gradually increasing with film thickness.[4]

Thus, in order to improve low nucleation, a variety of surface pre-treatment methods may be applied to the substrate. These include abrading the surface by either mechanical or ultrasonic abrasion with diamond or hard powders, seeding with diamond grits, ion implantation[5] or application of a negative bias[10] to the substrate. The grains and scratches provoked by grains of diamond on the substrate surface act as nucleation centres.[2] Hirmke *et al.*[11] have demonstrated that imperfections in the form of rough surface structures of monocrystalline seeds up to 5 μm grain size do not impede the development of flat smooth surfaces, desired for single crystalline growth. In contrast, diamonds grown on the seeds with a grain size larger than the threshold 5 μm displayed

poor qualities such as undefined morphology, with twining planes and shapes.[12] Depending on the substrate material, the nucleation time may be very long and the nuclei density may also be very low.[2] Diamond nucleation critically determines the properties, morphology, and homogeneity of the resulting films (such as density of diamond particles and alignment of the crystallites), and chemical vapour deposition diamond principally depends on surface pre-treatment, substrate materials and deposition parameters.[6] Seeding of substrates, typically using diamond grains prior to chemical vapour deposition increases nucleation of the growing film.[2]

Among surface pre-treatment methods, the mechanical polishing with diamond paste and ultrasonic pre-treatment of the surface in diamond powder suspensions[13] are widely used for nucleation enhancement. Of these, ultrasonic pre-treatment using diamond slurry is most commonly used because of the ease of its application to substrates with all sorts of complex geometry and shape. Furthermore, a better quality of replicas with homogenous film morphology may be achieved by depositing a nanocrystalline diamond layer on the film/substrate interface by seeding.[4-5] Recent work in the literature has followed this approach, with studies being reported on seeded diamond growth onto tungsten[14] and porous silicon[15] for instance. In a study to compare the effects of diamond polishing and ultrasonication as surface perturbation methods, Ascarelli and Fontana report higher nucleation density of diamond in scratched "lines" created by polishing than in areas where no lines were scratched. Increasing the paste grit resulted in reduced nucleation density, while for samples cleaned by ultrasonicating, there was an absence of line-pattern nucleation. The size of the diamond grit was found to be directly proportional to the nucleation density.[13] Hirmke *et al.* have utilised hot filament chemical vapour deposition to investigate the influence of seed particles on crystal growth, and suggested that imperfections in form of rough surface structures of monocrystalline seeds up to 5 μm grain size do not impede the development of flat smooth surfaces. Monocrystalline diamond particles of 5 μm grain size were also found to be suitable for seeding.[11]

Recent work by Naguib *et al.*[16] reported synthesising extremely smooth (6 nm root mean square roughness over 4 μm^2) ultra-nanocrystalline diamond films of 100 nm thickness using microwave plasma chemical vapour deposition with the aid of a 10 nm tungsten interlayer between the silicon substrate and the diamond film. The metal interlayer served to enhance the initial nucleation density, which led to reduced surface roughness and reduced the time required to produce a coalesced and continuous high-quality film. No reason for this enhancing property of tungsten was provided, and similar experiments involving other metals such as titanium, chromium and molybdenum were reported to yield lesser enhancement of ultra-nanocrystalline diamond nucleation. Similar work by Danen *et al.*[17] has explored the possibility of utilising ultra-dispersed nanodiamond particles that were buried under a sol-gel titanium oxide layer, spin-coated on ultra-dispersed nanodiamond seeded silicon substrates. Immersed in conventional H_2/CH_4 microwave plasma in a CVD setup, dissolution of the ultra-dispersed nanodiamond grain was observed to occur, which was believed to have resulted in the generation of nucleation sites *via* carbon transport from the ultra-dispersed nanodiamond seeds into and through the titanium oxide layer. This step was attributed to be the source of new diamond nuclei which ultimately resulted in higher nucleation density, compared to depositions where no ultra-dispersed nanodiamond seeds were buried.

4.1.2   Gas phase deposition of diamond

Over the last two decades, diamond chemical vapour deposition (CVD) science and technology has developed dramatically. This is due in large part to the highly promising and unusual electronic, optical, thermal and mechanical properties,[18] and radiation hardness of diamond[19] and CVD films.[20] These in turn enable diverse applications including hard coatings, tools, optical and electronic components,[21] thermal management, corrosion protection[22] and radiation detection.[19-20]

Within the large number of CVD techniques such as plasma assisted CVD at microwave, radio frequency, hot filament CVD, electron, laser-assisted CVD, ion beam, and halogen-carbon thermal CVD techniques have demonstrated success in diamond growth.[23] Of these, microwave plasma-assisted CVD is one of the most common methods for synthesis of nanodiamond.[8, 17, 24] The role of the plasma here is two-fold. It provides high-energy electrons that collide with neutral gas molecules, often breaking chemical bonds, exciting and activating the working gas. Plasma ions are also accelerated to a substrate, and subsequent bombarding of these can significantly influence film growth, its composition, microstructure and stress. In some deposition processes, the plasma electrons or ions are utilised, in others, the electrons and ions can work simultaneously. Most importantly, chemical reactions can be initiated at near room temperature in a plasma without elevating substrate temperature.[25] This is certainly an important consideration when the substrate is fragile, such as in this work, with micrometre-range capillary tips.

Diamond deposition through microwave plasma-assisted CVD uses a mixture of a carbon precursor (e.g. methane) with either hydrogen, nitrogen or argon. Depending on the process conditions, different 0-D nanodiamond forms can be predominantly observed, either as isolated particles in the gas phase or nuclei and clusters on the substrate surface. Furthermore, the process can lead to the formation of 3-D structures, nanocrystalline diamond films in pure form or as a composite of nanocrystals embedded in an amorphous carbon matrix.[26] Figure 4.1 shows images of 0-D nanodiamond clusters and 3-D nanocrystalline diamond films.
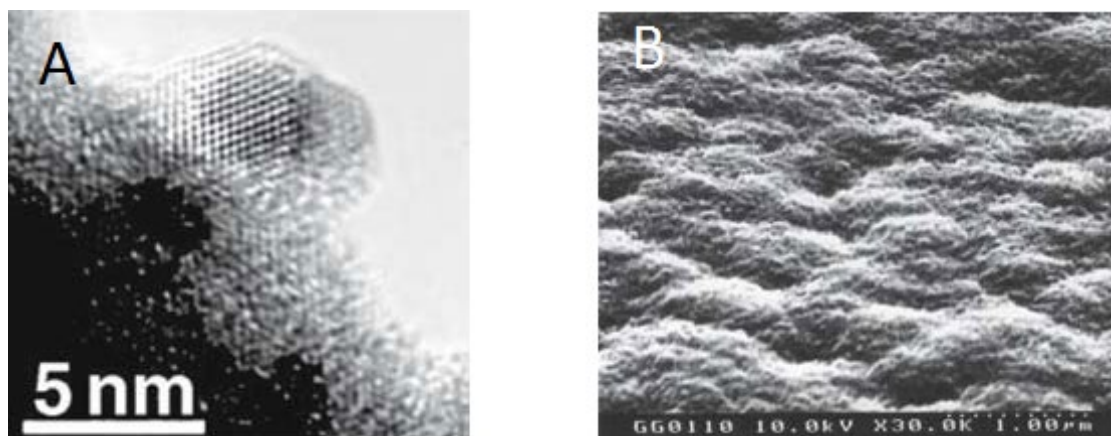
Figure 4.1   A 0-D nanodiamond cluster (A) and 3-D nanocrystalline diamond film (B). Figure obtained from Popov.[26]

4.1.3   The use of microwave plasma chemical vapour deposition

Microwave plasma-assisted CVD has been extensively documented in the literature as a means of depositing diamond films for a variety of purposes. Recently, Jian *et al.* have reported deposition of p-type freestanding diamond films from a 2% mixture of CH_4 in H_2 at 5 kPa and substrate temperature of 750°C. Following deposition, the silicon substrates were chemically etched to obtain p-type freestanding diamond at the nucleation side (surface roughness below 5 μm). These were then subjected to hydrogen plasma at 750°C for different time intervals to investigate the resulting p-type behavior of the undoped, p-type freestanding diamond nucleation surfaces by the Hall Effect measurement. Subsequent deposition of n-type zinc oxide films to form a heterojunction was also undertaken.[21] Wang *et al.*[1] report deposition of selective [100] oriented diamond films on Si [100] substrates with patternings achieved by microwave plasma-assisted CVD. Achatz *et al.* have characterised nanocrystalline diamond deposited via conventional hydrogen-rich (99%) CH_4/H_2 gas phase using hot filament CVD and ultra-nanocrystalline diamond films grown from an argon-based (1.4%) $Ar/N_2/CH_4$ gas phase via microwave plasma-assisted CVD to study the microstructure of

the films using AFM in the tapping mode, X-ray diffraction, Raman spectroscopy and photothermal deflection spectroscopy (PDS). Ultra-nanocrystalline diamond was described as having a cauliflower-type appearance with obvious smaller grain size (6 nm) than that for nanocrystalline diamond (150 nm). Based on Raman spectroscopy and XPS, ultra-nanocrystalline was found to consist of randomly oriented grains where the surface roughness was independent of thickness, and no columnar growth structure could be found. Ultra-nanocrystalline diamond was also found to have higher n-type conductivity, owing largely to the presence of nitrogen in between the grain boundaries.[27]

In the CVD process, constituents of the vapour phase react chemically near or onto a substrate surface to form a solid product.[28] This technology has found widespread application,[29-33] and has become commonly utilised to create thin films and coatings,[28] such as hydrogenated silicon;[34] boron, carbon and nitrogen coatings;[35] nickel coatings;[36] and nanocrystalline and ultra-nanocrystalline diamond[27] among others.

One of the main features of CVD is its versatility for synthesising both simple and complex compounds with relative ease and at generally low temperatures. Both the chemical composition and the chemical structure of the resulting coating can be selected by controlling the reaction chemistry and the deposition conditions. Fundamental principles of CVD include an interdisciplinary range of gas phase reaction chemistry, thermodynamics, kinetics, transport mechanisms, film growth phenomena and reactor engineering.[28]

Basic chemical reactions in a CVD system include thermal decomposition, oxidation, reduction, hydrolysis, nitride and carbide formation, synthesis, disproportionation and chemical transport. In more complex situations, a sequence of several reaction types may occur simultaneously to create a particular end-product. Thus, specific deposition variables, such as temperature, pressure, input-gas type and concentrations and flow rates, the geometry of the reactor, the power supplied to it and operating principle in turn

determine the deposition rate and the properties of the deposited film.[28]   A suitable reactor system must allow transport of the reactant and any diluent gases to the reaction site, which is often a substrate upon which deposition is sought. In addition, the reactor must be able to provide the necessary activation energy to the reactants by way of heat, radiation or plasma, and be able to maintain a specific system pressure and temperature. It must allow the chemical processes necessary for film deposition to precede, and at the same time remove any by-product gases or vapours that may affect the deposition process.   These functions must be implemented with adequate control, maximal effectiveness and safety.[28]   Any design of a reactor thus must keep these considerations paramount.

4.1.4 Types of carbon and their Raman spectra

Various forms of carbon can be deposited using manipulation of the pressure and temperature of the deposition environment.[9, 15, 37-38]   These include amorphous[39] and diamond-like carbon, polycrystalline diamond films and single-crystal diamond.[40] Depending on the size of the crystallites, polycrystalline diamond can be further classified into microcrystalline (for micrometre-dimensioned crystallites) and nanocrystalline diamond (for nanometer-sizes grain size), respectively.[41-42]   Raman spectroscopy is a suitable technique to characterise these different forms of carbon due to its sensitivity to change of translational symmetry.[43]

Amorphous carbon can exist in the hydrogenated or non-hydrogenated forms,[44-45] and therefore can comprise of both sp^2- and sp^3-bonded carbon. Such films are generally deposited by a variety of deposition techniques.   These include the low-frequency inductively and capacitively coupled plasma-assisted CVD,[46-47] microwave plasma-assisted CVD,[48-49] the electron cyclotron resonance-radio plasma technique, magnetron sputtering and the remote plasma-assisted CVD technique.[50-51]   In CVD, the

substrate onto which the film is to be grown can often be kept remote from bombardment of energetic particles, so the level of substrate damage is low.[52]

One of the main features of the Raman spectrum of this form of carbon is the fingerprint asymmetric, broad "G" peak centred between 1530 - 1580 cm^{-1}. This arises from the stretching of all pairs of sp^2 atoms in both rings and chains present as graphite.[4, 53-55] A second "D" peak at ~1340 cm^{-1} arises as a result of the breathing modes of the sp^2 atoms in rings.[54-55] Figure 4.2 depicts the typical Raman spectra of amorphous carbon, obtained from Jiaqi *et al.*,[44] annealed at different temperature levels (inserted therein).

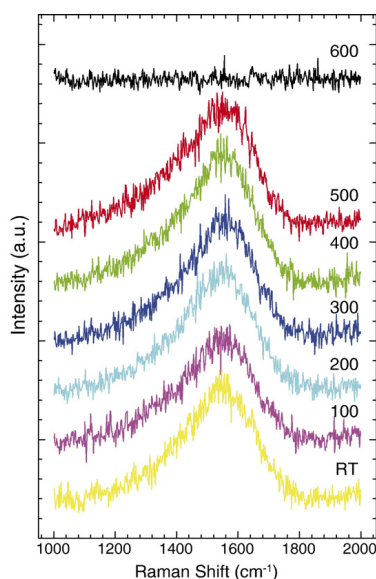Figure 4.2   The in-situ Raman spectra of amorphous carbon films cooled at different temperature levels (ºC) by a liquid nitrogen pump. Obtained from Jiaqi *et al.*[44]

Compared to amorphous carbon, polycrystalline diamond is a patchwork of minuscule diamond crystals, often with graphite crystals.[56] The diamond crystals have been reported to be randomly-oriented, with characteristic sizes ranging from 5 - several

hundred micrometers for polycrystalline diamond,[57-58] and 3 - 50 nm grain sizes for nanocrystalline diamond films.[16, 59] The deposition process for microcrystalline diamond films is proposed to proceed *via* the formation and migration of the hydrocarbon gas in the vicinity of the surface, abstraction of hydrogen from the molecule, dehydrogenation of the absorbed complex, followed by the recombination of the hydrogen atoms. While some degree of nondiamond may be incorporated during this nucleation process, atomic hydrogen in the deposition chamber prevents the nondiamond carbon impurity on the surface, often by etching the graphitic state, thus favouring the growth of diamond.[60] The subsequent Raman spectrum thus shows a prominent narrow band for diamond at 1332 cm^{-1}, without any significant sp^2 graphitic carbon-related peaks at 1580 cm^{-1}. The 1332 cm^{-1} peak is the signature peak of diamond.[12, 21] A representative Raman spectrum of microcrystalline diamond, adapted from Uppireddi *et al.*[61] is shown in Figure 4.3
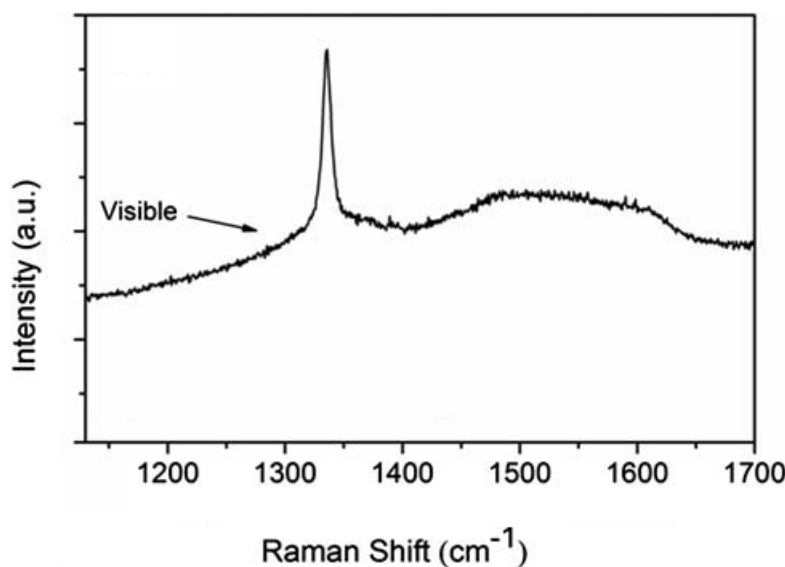
Figure 4.3   The Raman spectrum of a microcrystalline film showing the diamond peak at 1332 cm^{-1}. Obtained from Uppireddi *et al.*[61]

In contrast, nanodiamond films are an intermediate between microcrystalline diamond and amorphous diamond-like carbon.[62] They possess smaller grain size in the nanometer range, due to which, nanodiamond films also possess greater surface to volume ratio.[63] Moreover, with decreased grain size to the nanometre scale, there is increasing π-bonded carbon at the grain boundaries (rather than specific carbon phases) in the nanocrystalline films, which often results in a scattering intensity in the 1400 - 1600 cm^{-1} range.[64] Figure 4.4, adapted from Larijani *et al*.[65] shows the Raman spectrum for a nanodiamond film. Noteworthy in the diagram is the narrow diamond at 1332 cm^{-1}, over a large scattered peak between 1275 cm^{-1} to 1400 cm^{-1}.
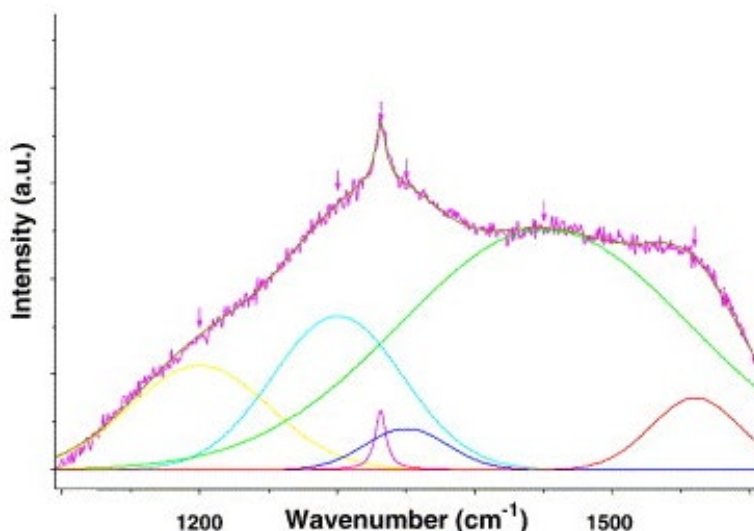
Figure 4.4　　　The Raman spectrum of a nanodiamond film showing the diamond peak at 1332 cm^{-1}. Obtained from Larijani *et al*.[65]

Compared to films of diamond, the deposition of single diamond crystals of high purity has reportedly been successful using both high-pressure-high-temperature conditions with increasing methane concentration. Plasma CVD[11] as well as with low-pressure-high temperature[66] have been used as a means to enhance growth of the crystal. The addition of 1% - 5% addition of N_2 has also been reported to have created more growth sites

during deposition, leading to 3-fold increase in growth rate as well as promoting [100] face growth.[66-67]   The resulting single diamond crystals are up to > 40 μm size.[68]   The Raman spectra of such crystals typically depicts a single sharp diamond peak at 1332 cm^{-1}, as shown in Figure 4.5 (adapted from Yan *et al.*[67]).
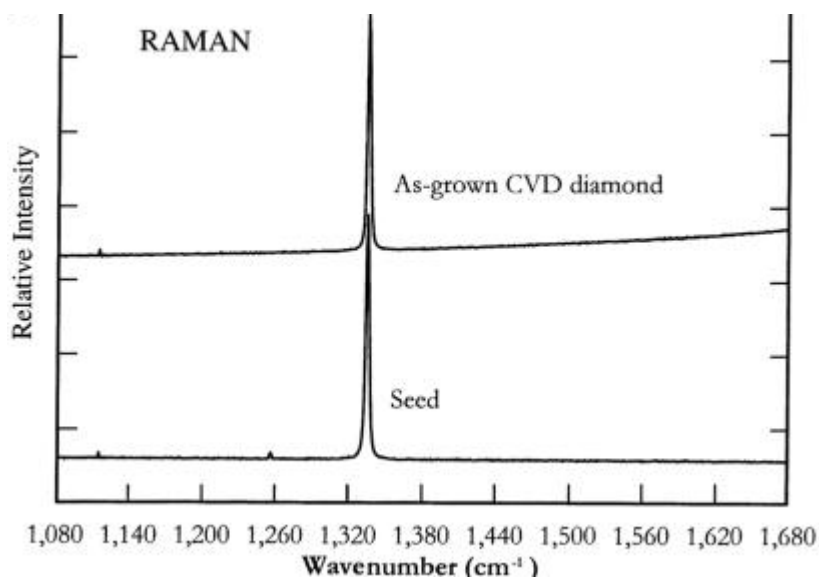
Figure 4.5   The Raman spectrum of a single diamond crystal film showing the
                 diamond peak at 1332 cm^{-1}. Adapted from Yan *et al.*[67]

In this study, the CVD system was utilised to achieve hydrogenation of the surfaces of physically small (< 3 μm radius) graphitic carbon electrode tips.   Results of surface characterisation of these electrodes are discussed.   In addition, we aimed to deposit various types of diamond films through microwave plasma-assisted CVD from CH_4 and H_2 as precursor gases.   Results for characterisation of these films are presented and discussed as well.

4.2 Experimental

4.2.1   Reagents

Ultrapure (Milli-Q) water (18.1 MΩ.cm at 25°C) was used to prepare all solutions. ACS analytical grade absolute methanol, absolute ethanol and anhydrous acetone were sourced from Univar. Ultra high purity nitrogen, methane and hydrogen gases were purchased from BOC Gases, Australia. Alumina powder (1 μm agglomerate-free) was obtained from Leco Corporation, Michigan, USA. Graphitic carbon powder was obtained from Sigma, Australia. The epoxy for sealing fabricated electrodes was Bond VLI (Kua Sen Enterprises Company Limited, China). Diamond for seeding was obtained from De-Beers Industrial Diamond). All chemicals were used without further purification.

4.2.2   Assembly of a microwave plasma-assisted chemical vapour deposition system

The hydrogen-deposition system relied on excitation and activation of neutral gaseous hydrogen molecules, which then initiated reactions of the gas onto the solid carbon surface of physically small electrodes. The excitation was achieved by bombarding the gaseous hydrogen with high-energy electrons generated from a thermionic cathode. This is an efficient method of utilising plasma to facilitate such reactions without having to raise the substrate temperature otherwise needed to achieve the same reaction through classical chemical pathways, and often also at the cost of consequent substrate degradation.[25, 69]

The main components of the deposition system comprised a gas delivery system, main deposition chamber, a rotary vacuum pump, pressure readout devices, and a gas exhaust system. Each of these is described in detail in the following sections.

4.2.3   The vacuum system

The vacuum system was modified from the setup as designed and assembled by Butcher.[52] It centred around a custom-made quartz tube of length 695 mm and outer diameter 25 mm inside which the deposition and hydrogenation was carried out, as shown in Figure 4.6. The right end of the tube connected to a Pirani 10 vacuum gauge (Edwards), capable of measuring between 0.002 - 0.100 mbar pressure, and a MKS Instruments 650 Series Pressure Controller. The pressure controller was used to set and maintain the required pressure inside the quartz tube, while the Pirani gauge monitored pressure ranging less than 1.33 mbar. The length of the tube passed through the centre of the microwave cavity which is where the plasma cloud was situated during experiments.

On the right-end of the microwave cavity was the magnetron which delivered 2.45 GHz wavelength microwave energy. On the left-end of the quartz tube was a quartz viewport that permitted both sample loading, as well as optical characterisation of the plasma.
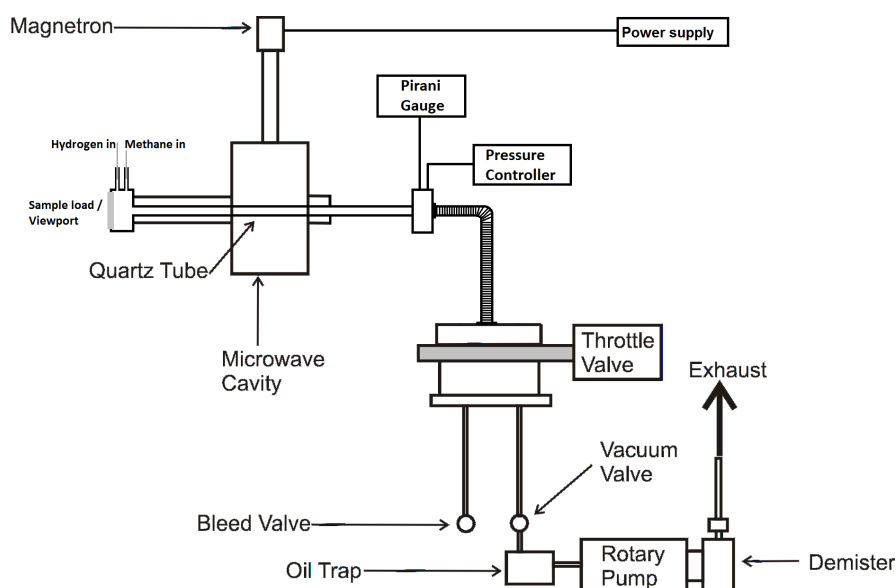
Figure 4.6   Schematic of the deposition system

The quartz tube connected to the rotary pump *via* a motorised throttle valve with a sealing flapper (MKS Instruments). The throttle valve was connected to the pressure controller through which the required vacuum level could be programmed and maintained. A bleed valve was connected to release the vacuum when the system was not in use. The rotary pump employed was a dual stage Edwards model E2M12 pump capable of displacing 14.2 m^3/cm^3 (and achieving an ultimate pressure of 1.33 x 10^{-4} mbar), and was used to rough-pump the chamber. The pump was also connected to the chamber with an Edwards inlet catch pot (Model Number ITC20) foreline trap. This was packed with activated alumina to arrest any backstreaming of rotary pump oil during vacuum conditions. The output from the rotary pump was passed through an Edwards EMF10 oil mist filter before being vented to a roof exhaust system.

4.2.4   Gas delivery into system

In deposition from a gaseous phase, accurate, reproducible and reliable supply of gas is critical in determining the attributes of the deposited film, such as thickness and composition.[70] It is therefore imperative that the gas delivery components are impermeable to atmospheric influences, can deliver the gas at a range of flow rates, and more important, that this flow rate is easily measurable.

In the hydrogenation setup, ultra high purity hydrogen gas was channelled via a ball valve to a previously calibrated (within 6 months) Tylan mass flow controller (FC-280) capable of delivering up to 2 L/min of gas. The mass flow controller was connected to a locally constructed mass flow meter (Macquarie Engineering & Technology Services) which permitted calibration of the controller as well as a digital readout. From the mass flow controller, the gas was passed through another ball valve and then into the vacuum system. The incorporation of dual valve control of gas flow was for safety reasons, which allowed for instant termination of gas supply if required.

4.2.5   The microwave system

A modified microwave system comprising the plasma source, power supply, channelling waveguide and microwave cavity from previous work of Butcher[52] were assembled. The Sanyo Model 2M214 magnetron, previously extracted from a domestic microwave oven had an excitation capacity of approximately 2.45 GHz. Modification of the magnetron involved a dedicated high-power (3000 V) supply unit for the heated cathode which permitted regulation of the applied potential to the magnetron itself. Prior calorimetric measurements have shown the microwave system was capable of delivering a maximum of 611 W.[52]

The magnetron, waveguide, microwave cavity and quartz tube were enclosed in a locally-constructed radiation cage (Macquarie Engineering Technology Services) to prevent radiation leakage. In addition, for safety reasons, an electronic radiation detector was employed to monitor microwave leakage, while the CVD system was in operation.

4.3 Application of deposition system to hydrogenation and diamond deposition

4.3.1   Hydrogenation of physically small bare carbon electrodes

This section describes the efforts to commence hydrogenation of previously-fabricated bare carbon electrodes. The method for the fabrication has been described in Chapter 2, and was similar to that reported by Alwarappan *et al.*[50] These electrodes were electrochemically characterised and subjected to XPS before and after hydrogenation in the deposition system.

Following initial characterisation, the prefabricated electrodes were prepared for hydrogenation. This preparation involved removal of any material present on the

electrode, such as the sealing epoxy and the metal wire, which would introduce impurities to the vacuum chamber. Thus the conducting wire was physically extracted from the opposite end of the pulled tip and then any remaining traces of epoxy were removed. The electrode was then rinsed with ultra high purity acetone to remove any traces of contamination that would have contaminated the high purity vacuum environment in which hydrogen deposition occurs. For this reason, electrodes prior to hydrogenation were handled using nitrile powder-free gloves.

The electrodes were loaded into the vacuum chamber by a custom-made quartz loading device (Custom Blown Glassware Pty Ltd, Sydney, Australia) as shown in Figure 4.7. It comprised of a quartz rod (diameter 7 mm) with a quartz boat (8 mm × 20 mm) attached at the end to house the substrate. The tube was sufficiently long enough to permit the boat to reach into the plasma.
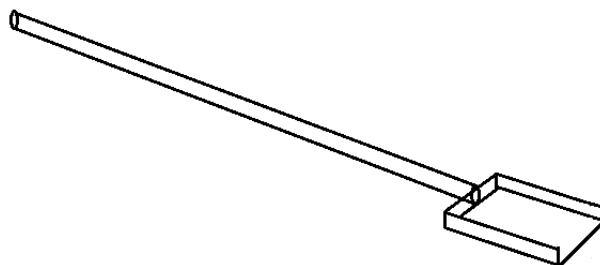

Figure 4.7   Custom-built quartz loading device utilised to house samples during deposition

The loading device was also rinsed with acetone to avoid any contamination. Following this, it was carefully loaded into the plasma chamber, away from the active plasma cloud. This is because it has previously been reported that locating the sample in direct contact

or path of the plasma can be detrimental to the electrode surface tip (of the type utilised in this study), following exposure to charged particles from the plasma.[50]

Upon loading the sample 15 cm downstream of the plasma, the rotary pump was turned on and the system pulled to vacuum (approximately down to 0.5 ± 0.1 mbar), as indicated by a MKS 650 Series Pressure Controller (MKS Instruments), with readout obtained from an Inficon pressure transducer (Type CM100 – G100A), with a measurement range up to 133 mbar. This was run for 18 hours without stopping the pump. Allowing a vacuum to be established for an extended period such as this removes any impurities introduced inside the chamber during sample loading. Following this, a steady flow of hydrogen was activated at 40 mL/min for 10 minutes and the pressure was allowed to increase to 66 ± 0.13 mbar as set on the pressure controller. This pressure was maintained for the next part of the procedure.

Next, the power to the magnetron was turned on to enable microwave generation, by means of a locally constructed magnetron power supply (Macquarie Engineering Technology Services), capable of delivering between 0 – 220 V. Plasma was struck at a voltage setting of approximately 165 V and maintained in a flow of hydrogen at 100 mL/min for 5 minutes. During this period, the pressure and gas flow rate were regularly monitored as they have a direct bearing on the conditions inside the microwave cavity (plasma) and the chamber (vacuum). These settings were obtained from previous trials with carbon-coated capillaries inside the quartz tube to determine optimum parameters for hydrogenation.

After subjecting the electrodes to plasma treatment, the power supply was reduced to zero, which switched the plasma off. The electrodes were then cooled for 20 min in a stream of hydrogen at 100 mL/min. This method of cooling in a hydrogen environment has previously been reported in the literature,[49, 71] with documented evidence of increased

hydrogen content in silane layers when cooling is effected in the presence of atomic hydrogen.[72]

Following the cooling process, the system was maintained under vacuum (66 ± 0.13 mbar for 1.5 hours) to completely cool the samples, after which they were removed. After removal from the chemical vapour deposition system, the electrodes were repacked with graphitic carbon powder (to replace any loss from ejecting the conducting wire prior to hydrogenation), and a new silver-coated wire reinserted before resealing with epoxy. These electrodes were then re-characterised in the same redox systems as previously, to determine changes in the electrochemical behaviour of the systems at the now modified electrodes.

4.3.2   Diamond deposition

4.3.2.1   Gas delivery

Ultra high purity gases (methane and hydrogen) were fed through dedicated gas inputs into the vacuum line. Gas flow was manipulated and measured using a locally-constructed mass flow controller (Macquarie Engineering and Technology Services). Hydrogen gas was regulated via a Tylan (FC-280) mass flow controller capable of delivering up to 2 L/min, while methane was passed through a Tylan (FC-2900) mass flow controller capable of delivering up to 100 mL/min of methane gas flow.

4.3.2.2   Substrate seeding

Diamond was grown on seeded quartz substrates. Substrates were prepared as described previously[59] by cutting a (1 cm × 1 cm) quartz sample into 5 mm × 5 mm squares using a diamond scriber and cleaned with acetone. This was followed by seeding of the

substrates using a 50:50 (v/v) mixture of diamond powder with 1 μm agglomerate-free alpha alumina powder (4 g) and mixed in 15 mL absolute methanol. The larger sized alumina particles bombard and abrade the quartz substrate, creating sub-micron sized damage sites and defects in which diamond particles can then embed. This seeding process by ultrasonic treatment in a suspension of diamond powder is an effective means which does not suffer from the limitations of incomplete nucleation.[4] Seeding involved placing the substrates inside this mixture and subjecting it to ultrasonication for 30 min. Following this, the substrates were removed and subjected to further ultrasonic treatment in 20 mL solutions of absolute methanol, followed by absolute ethanol and later, Milli-Q water. Next, the substrates were dried under nitrogen gas and stored in a dessicator.

4.3.2.3　　　Deposition process

Prior to deposition, the system was pumped down to the lowest possible pressure, typically at 0.044 - 0.070 mbar, using the Pirani gauge. The system was continuously pumped down to vacuum for a minimum of 24 h prior to actual deposition. The purpose of this is to enable removal of any impurities that would have entered the vacuum system during the loading of samples. Following 24 h of pumping, the pressure was set to a predetermined value and gas flow initiated. Substrates were loaded onto the sample holder, which was degreased prior using acetone and wiped clean with tissue prior to loading the substrate inside the vacuum tube.

4.3.2.4　　　Deposition parameters

Growth experiments focused on the change in pressure and the concentration of methane with respect to hydrogen. Concentration here refers to the relative percentage (v/v) of the gases. In all cases, the plasma was struck at 40 mbar, and then increased to the respective pressure as required for the deposition experiment. Three parameters were varied for

deposition: deposition pressure, deposition time and percentage methane flow (relative to hydrogen flow). Table 4.2 lists the conditions utilised in the film growth experiments.

Deposition	Voltage / V	[CH$_4$] / %	Pressure / mbar	Time / min
1	160	3.0	66	30
2	180 - 194	1.5	66	30
3	170	3.0	40	30
4	170	1.5	66	300
5	183	3.0	40	1

Table 4.2   Deposition parameters for individual experiments

Power was varied to the magnetron as needed to sustain stable plasma. This is denoted by the variable voltage setting in each set of conditions.

4.4 Characterisation studies

4.4.1   Raman spectroscopy

Raman spectroscopy was performed on a Renishaw inVia micro-spectrometer fitted with a 1800l/mm grating and a 50× objective to focus the 514.5nm line of an Argon ion laser onto the sample. Data was peak fitted without smoothing, using Gaussian fitting to deconvolute peaks and quantify peak feature characteristics.

4.4.2   Scanning electron microscopy

Scanning electron microscopy (SEM) was performed using a JEOL - JSM 6480-LA Variable pressure scanning electron microscope. A subset of only those samples which gave rise to peaks in the Raman spectrum attributed to diamond previously was examined using SEM.

4.4.3   Optical emission spectroscopy of plasma

Optical emission spectroscopy was used to analyse the plasma during the deposition stage. The measurement was taken during the first 30 minutes of deposition using an Ocean Optics USB 2000 spectrometer capable of 14 grating sizes. For the ultraviolet visible range, a grating of 2 was used.

4.5 Results and discussion

4.5.1 X-Ray Photoelectron Spectroscopy at hydrogenated

carbon electrodes

The XPS study of a surface can yield useful information about atomic composition at the surface. In Figure 4.8A, the fitted XPS spectra of a hydrogenated carbon electrode (N = 4) is presented, with two prominent bands of interest: the carbon (sp^3) peak, prevalent at 284 eV, and the oxygen peak occurring at 532 eV. As depicted, the fitted peaks for oxygen and carbon (sp^3) yield an oxygen/carbon (O/C) ratio (based on peak heights) of 1.7. In comparison, Figure 4.8B presents the XPS results for a bare carbon electrode   (N = 4). Data from fitting of the peaks shows that peak height ratio between oxygen and carbon being 4.7 for the bare carbon electrode. This is a considerably higher
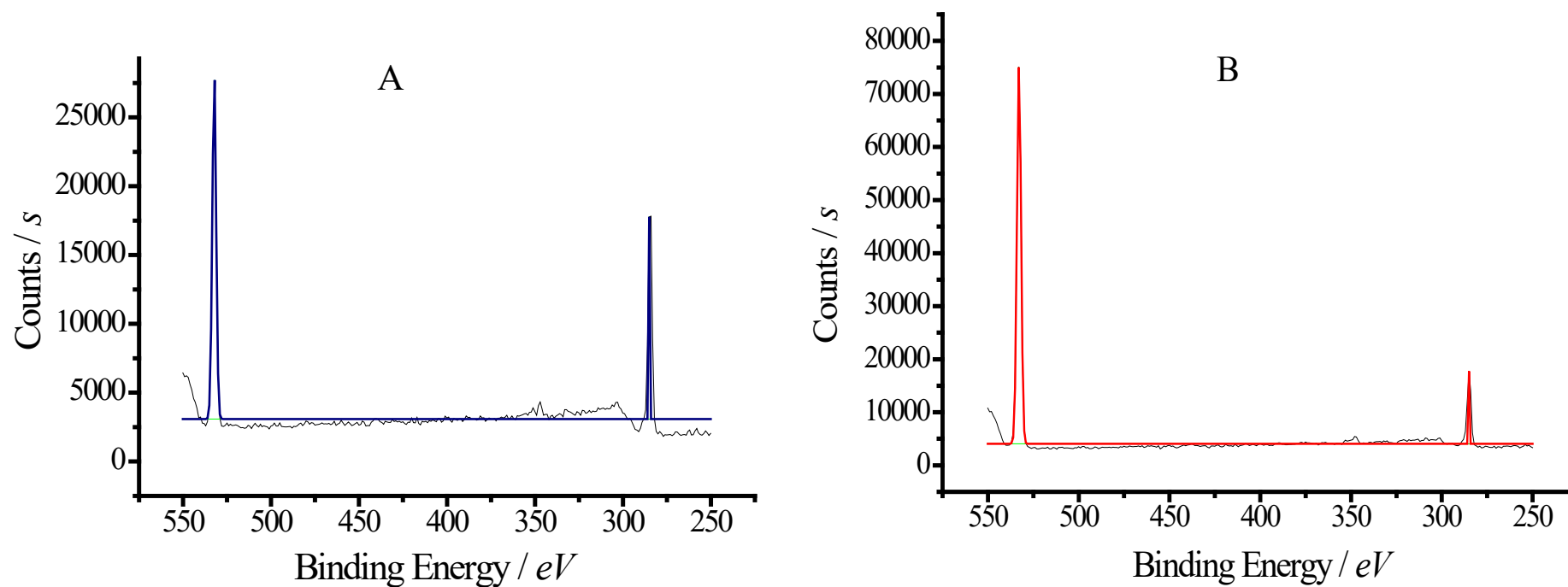
Figure 4.8   XPS spectra of a hydrogenated carbon electrode (A) and bare carbon electrode (B).

value than that at hydrogenated carbon electrodes. Following hydrogenation in the CVD reactor, the surface of bare carbon would be expected to undergo alteration in smoothness as well as atomic composition. Plasma enhanced CVD is a process where atomic hydrogen attacks any exposed defect sites at the carbon film surface, and in the process, replaces the oxygenated functional groups with hydrogen. We propose that this is the reason for the reduction of the O/C ratio of 4.7 obtained at bare carbon electrodes to 1.7 following hydrogenation. The O/C value for bare carbon electrodes denotes a high proportion of oxygen to carbon, and is possibly associated with graphitic carbon coverage on the electrode surface. Such a surface has an appreciable amount of oxygenated sites.[73] Previously, it has been shown that carbon electrodes fabricated through pyrolysis of acetylene such as those in this study are more akin to highly oriented pyrolytic graphite.[74] As a result, a high O/C ratio of 4.7 is consistent with the expectation for such electrodes. Moreover, the hydrogenation process is supposed to be progressing inward from the surface defect sites, causing the planar sp^2 aromatic rings to distort into cyclohexane-like sp^3-hybridised alicyclic rings.[48] Mehandru *et al*.[75] have previously performed modelling using large cluster models to show that a single hydrogen atom will chemisorb on both edge and basal planes, but strongly on the former. The sequential addition of the hydrogen atoms to the tetrahedral shape-coordinated ring structures was also described as being distorted by this incorporation of hydrogen. Based on these findings, any oxygen present at either site will be replaced with hydrogen as the unsaturated carbon bonds are converted to saturated sp^3 type. The results from Figure 4.8 are consistent with these findings. The line shapes of the C_{1s} peaks provide information about the chemical bonding environment, and fitting these peaks to suitable functions allows this information to be extracted.[76] In Figure 4.9, the deconvoluted peaks from carbon atoms at both bare carbon and hydrogenated electrode surfaces are presented. The sp^3 carbon at 285 *eV* at the hydrogenated carbon electrode in Figure 4.9A has a FWHM of 1.6 cm^{-1}. In comparison, for the bare carbon electrode in Figure 4.9B, a value of 1.4 cm^{-1} was obtained. This value is slightly higher than what has been normally found for pure graphitic surfaces
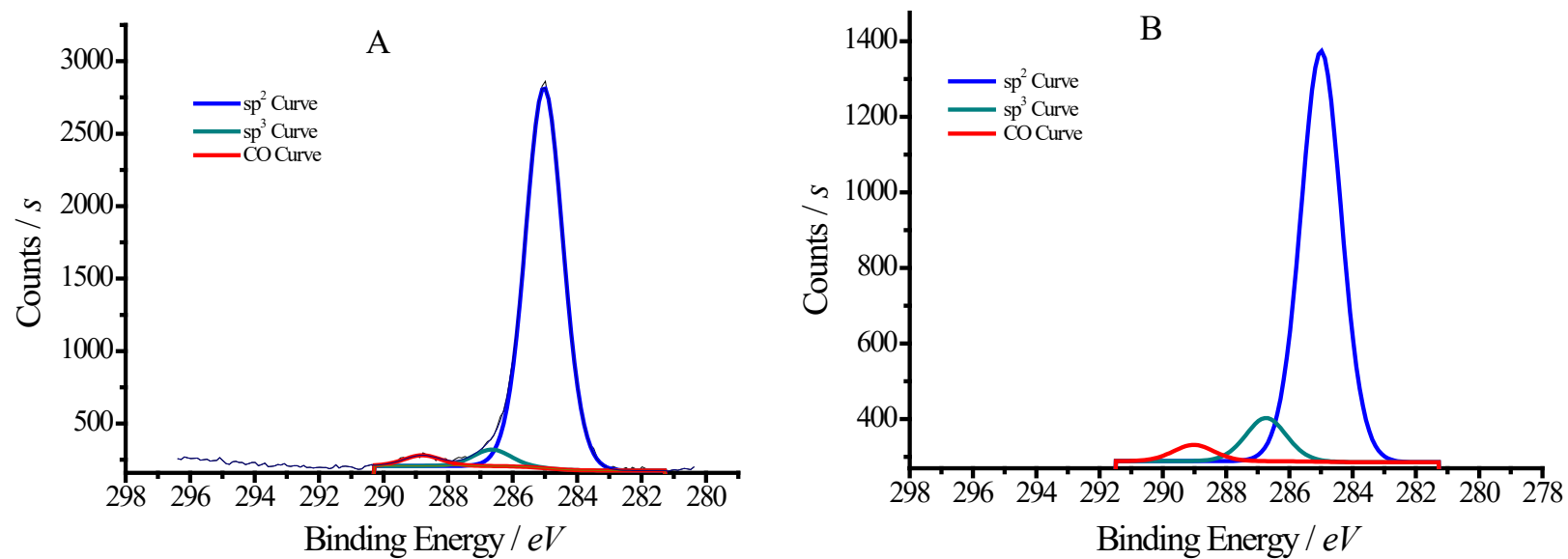
Figure 4.9   Deconvoluted peaks from the C_{1s} bands from the XPS spectrum of a hydrogenated carbon electrode (A) and bare carbon electrode (B).

(1.3),[77-78] suggesting there may be a higher degree of smoothness to these bare carbon surfaces than is normally found at graphitic films. This inference is in agreement with the findings of McNally, earlier.[74] On the other hand, the value for hydrogenated carbon (1.6 cm^{-1}) is higher than that for bare carbon electrodes which is consistent with the effects of removal of the edge plane defects on the basal bare carbon surface that would impart a greater degree of smoothness on the hydrogenated film.

4.5.2   Optical emission spectrum of the plasma

An emission spectrum of the plasma was obtained during a 5 h deposition experiment with 3% methane and is shown with labels in Figure 4.10. A pronounced peak at 656 nm is evident, which is attributed to the α-Balmer series for hydrogen. In addition, sharp peaks at approximately 434 nm and 486 nm corresponding to H$_\gamma$ and H$_\beta$ respectively.[79] In addition, there are prominent bands for the hydrogen Balmer series as well as for CH$^+$. These are from the energised products of the plasma, arising from the source hydrogen and methane gases inside the chamber. The oxygen vacancies are quite possibly atmospheric oxygen that may be infiltrating into micro-sized chinks in the connectors and attachments in the system. Overall, the spectrum confirms that the plasma is essentially dominated by energised atoms of hydrogen and carbon-related radicals.

4.5.3   Deposition experiments

In this study, we aimed to deposit polycrystalline diamond on seeded silica substrates via chemical vapour deposition using a range of pressure settings, deposition durations and methane concentrations. The resulting films were subjected to Raman spectroscopy to determine the nature of carbon bonding in the bulk sample. Finally, the deposited samples were subjected to scanning electron microscopy to examine the film morphology. The results of these characterisations are discussed in the following.

(i) Quartz UV Cutoff
(ii) CH^+ (424 nm)
(iii) Hydrogen Balmer-β (486.1 nm)
(iv) Oxygen vacancies (480 nm)
(v) C_2 Swan Band
(vi) Balmer series for atomic H
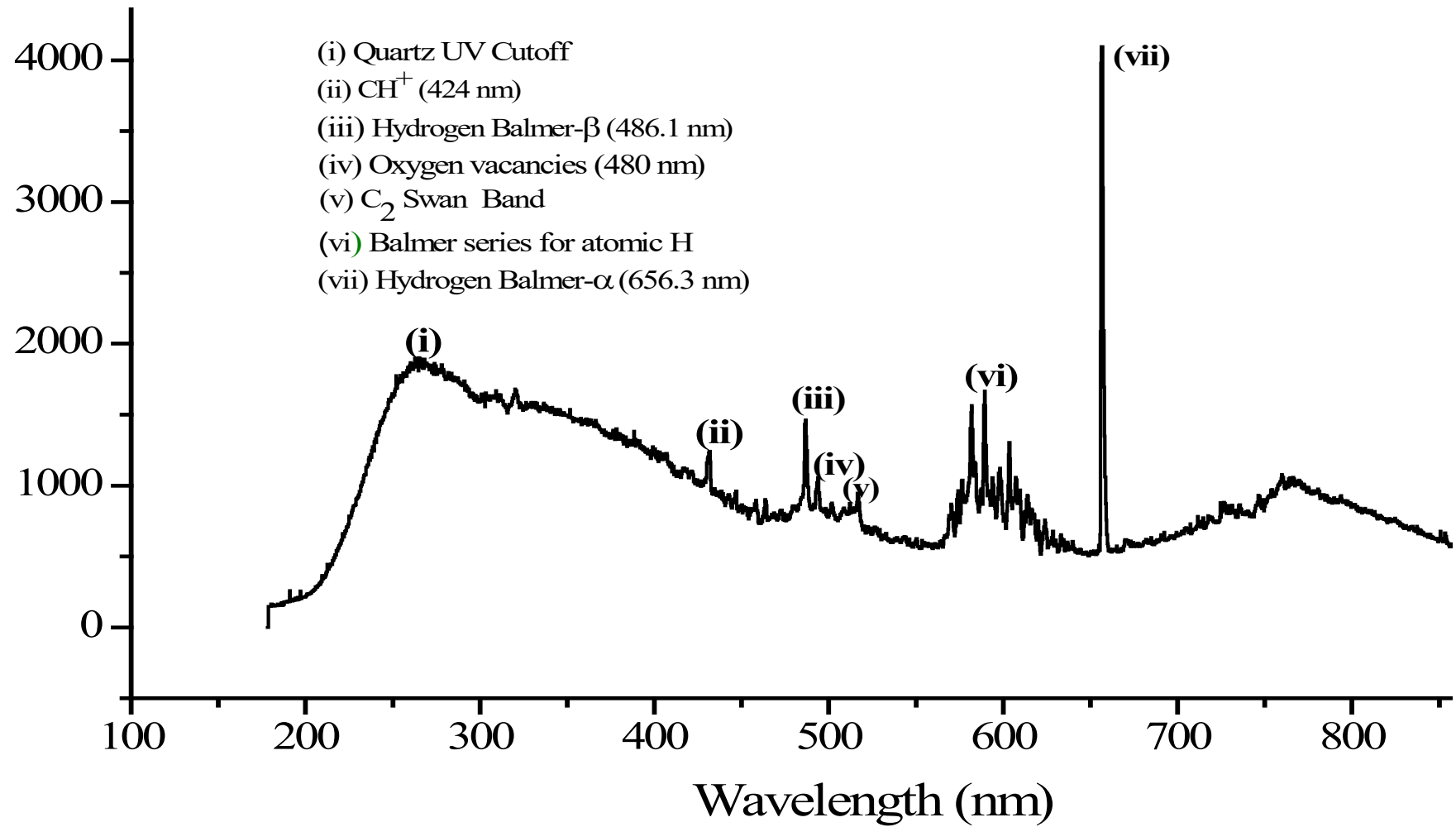(vii) Hydrogen Balmer-α (656.3 nm)

Figure 4.10   Optical Emission Spectrum of the microwave plasma used to deposit films at 30 minutes in the deposition.

A variety of carbon forms, with discrete morphologies and grain sizes were deposited. To aid in the interpretation of the results in the following sections, Table 4.3 lists the qualitative and quantitative information pertaining to the films discussed, including terminologies applied.

Formation	Observed Raman spectrum peaks	Peak FWHM	References
Amorphous	~1360 cm^{-1} ~1560 cm^{-1}	~100 cm^{-1} ~50 cm^{-1}	Ferrari and Robertson[54] Achatz *et al.*[27]
Cauliflower / ballas	~1340 - 1360 cm^{-1} ~1560 cm^{-1}	~100 cm^{-1} ~50 - 100 cm^{-1}	Haubner and Lux[80]
Microcrystalline diamond	~1333 cm^{-1} ~1550 cm^{-1}	~6 cm^{-1} ~200 cm^{-1}	Wang *et al.*[1] Okada *et al.*[81]
Nanocrystalline diamond	1330 - 1334 cm^{-1} ~1350 cm^{-1} ~1550 cm^{-1}	~50 cm^{-1} ~50 cm^{-1} ~110 cm^{-1}	Forbes *et al.*[82] Hiramatsu *et al.*[83] Soga *et al.*[41]

Table 4.3　　　Raman Peak information for diamond films in previous studies.

The data obtained from samples was compared with that listed in Table 4.3, and interpreted accordingly.　The Raman spectra of samples were used to evaluate the presence of diamond, and the nature of carbon bonding prevalent in the bulk sample. Where present, the FWHM of the diamond peak in the Raman spectrum of a sample was compared with the literature to identify the possible type of diamond responsible for the peak.　Furthermore, SEM images of the samples were examined to obtain more information on the morphology of the samples.

4.5.3.1   Deposition of amorphous carbon

In the first two experiments, methane concentration (3.0%) and deposition time (30 min) were kept constant, while the deposition pressure was kept at 66 mbar and 40 mbar for Experiments 1 and 2 respectively. The resulting Raman spectrum for each experiment is presented in Figure 4.11. Peaks were fitted using the Gaussian function and the fitted peak data is also presented. As shown in Figure 4.11A for Experiment 1, there are prominent D and G bands at 1343 cm^{-1} and 1566 cm^{-1} respectively. These are due to the sp^2 carbon content of the bulk sample. No discernible diamond peak can be visible in the spectrum, where the characteristic 1332 cm^{-1} region is dominated by the D band. However, Haubner and Lux have previously obtained similar spectral data for coarse ballas diamond samples, and have stated the possibility that the diamond peak is too weak to show up on Raman spectra.[80] This has also been discussed by Okada *et al.*,[81] who reported that the diamond peak obtained in a Raman spectrum using 514.5 nm excitation (similar to those in this study) is particularly hard to discern from those arising due to sp^2 carbon, as a result of the resonance Raman effect. Thus, it is important to note that an absence of the diamond peak at 1332 cm^{-1} does not necessarily indicate a lack of diamond. Moreover, weak diamond peaks have also been attributed to a consequence of large strain, arising from small grain sizes and numerous grain boundaries in nanodiamond aggregates.[84] Furthermore, as the amount of CH_4 present in the deposition affects the amount of amorphous sp^2 carbon bonding in the sample, the resulting D peak often overlaps with that of diamond.[85] Thus, for Experiment 1, we exercise caution in the interpretation of results, and therefore reserve ruling out nanodiamond presence in the sample. The material grown in Experiment 1 is amorphous, and based on previous work, likely to contain both sp^2- and sp^3-bonded carbon.[44-45, 55]

An examination of the Raman spectrum of Experiment 2 also features prominent D and G peaks at 1350 cm^{-1} and 1546 cm^{-1} respectively. There is an absence of the diamond peak, which we attribute to the possibilities aforementioned for Experiment 1. A slight bump at ~1145 cm^{-1} is observed in Figure 4.11B, which has previously been related to the
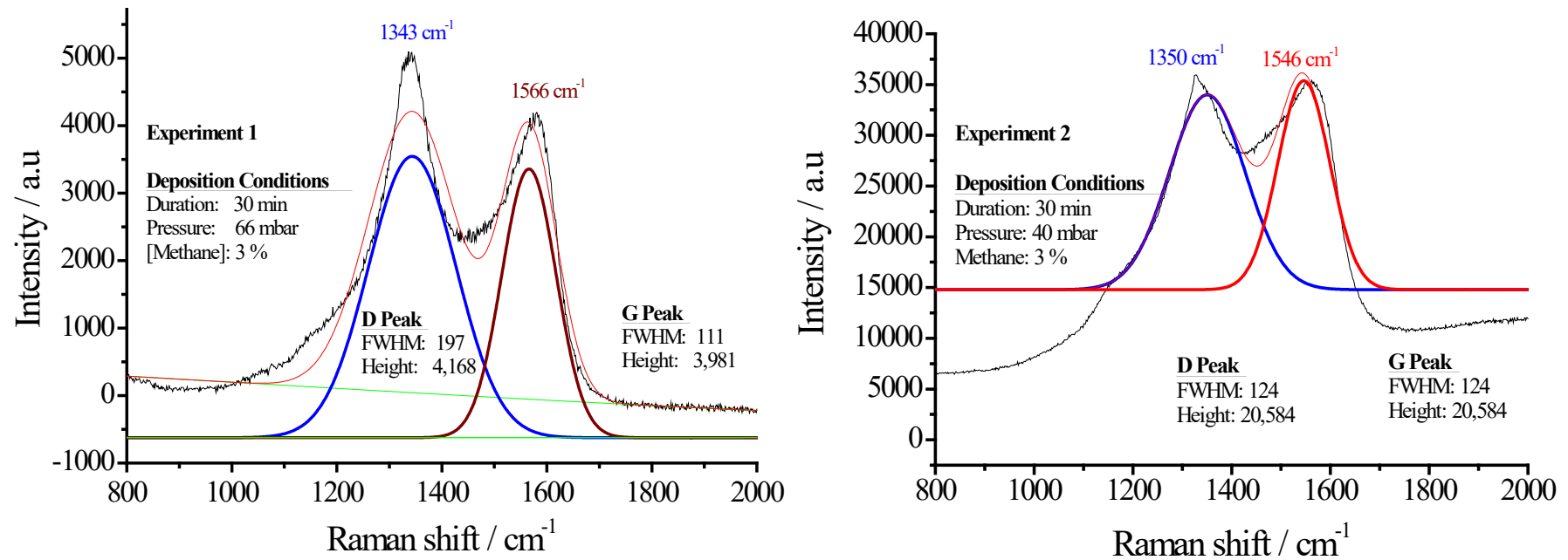
Figure 4.11   Raman spectrum of amorphous carbon containing original and fitted data and deposition conditions at Experiments 1 and 2 showing the graphite bands.

presence of nanocrystalline diamond, or disordered sp3 carbon phase.[4, 85] This suggests the sample may constitute nanocrystalline diamond, but is otherwise dominated by sp^2-bonded amorphous carbon.

SEM images of the samples obtained in Experiments 1 and 2 are presented in Figure 4.12A and Figure 4.12B, respectively. In Figure 4.12A, discrete, round cluster-like deposits are observed. Moreover, a lower-resolution scan of the sample (data not shown) revealed that the sample comprised of agglomerate clusters dispersed over the substrate. The sample also consisted of non-continuous films and individual clusters. This suggests that the deposited sample may predominantly be composed of amorphous carbon, deposited sporadically throughout the substrate. In the background, smaller grain-like particles are observed to be scattered around the clusters, possibly composed of amorphous carbon, interlaced with smaller grains of nanodiamond.

In Figure 4.12B, the sample has cauliflower-like formations (containing unknown spherical deposits) on the structures, similar to that in Figure 4.12A. Dua *et al*.[7] have suggested that in order to form nucleated clusters, species must have high kinetic energies. With lower pressure, there are fewer collisions between species in the chamber, which naturally means there is less kinetic energy loss among species. Retaining high kinetic energy imparts high surface mobility onto the species, which then promotes aggregation of the precursors (seeded diamond in this study), thereby increasing nucleation and growth on the substrate. Our results in Experiment 2, with a greater continuity in the film at a lower pressure than in Experiment 1, are therefore in agreement with these theories.

4.5.3.2   **Microcrystalline diamond deposition**

In the third experiment, the concentration of methane was lowered to 1.5%, while the pressure and deposition time were maintained at 66 mbar and 30 min respectively. The Raman spectrum of the sample obtained is presented in Figure 4.13. As depicted in
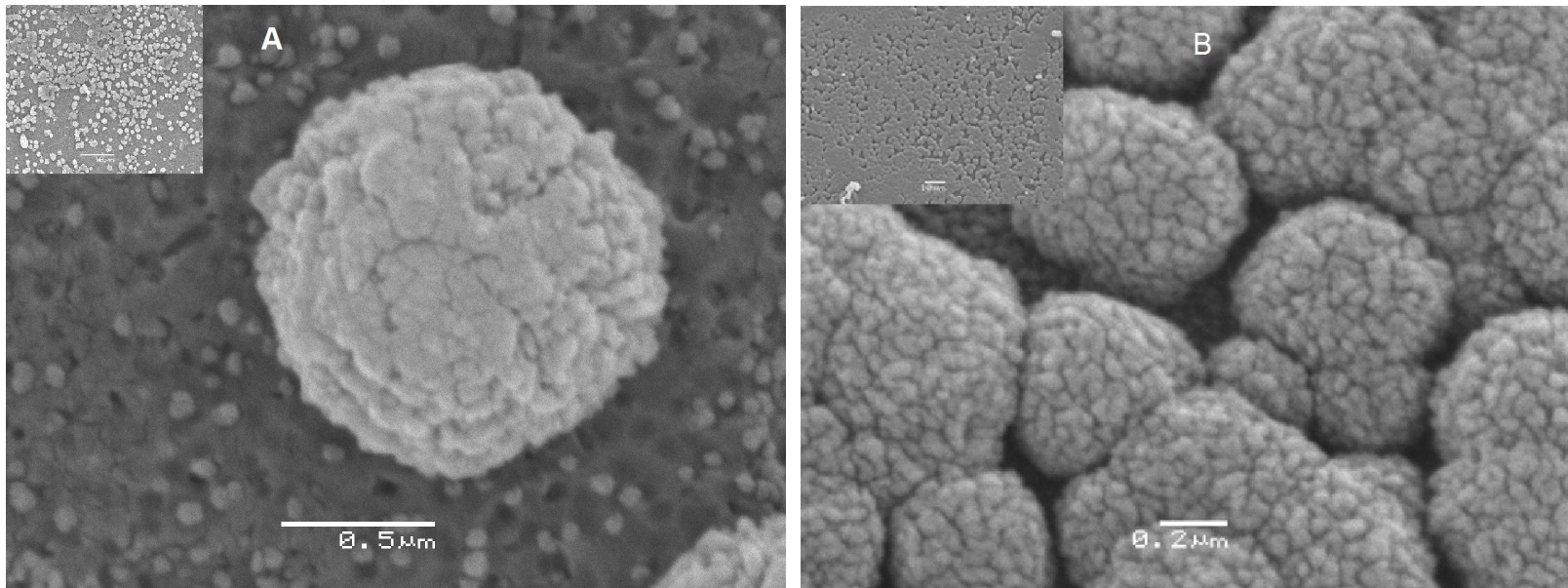
Figure 4.12   Scanning electron microscopic image of amorphous carbon in Experiment 1 (A) and Experiment 2 (B).   INSET: Lower magnification image of same sample.

Figure 4.13, there is a peak at 1333 cm^{-1}, which we attribute to diamond.[14, 86]   In addition, a broad G peak is observed in the spectrum, suggesting sp^2 carbon content in the film.   Other researchers have determined the FWHM for diamond peaks and have concluded that the asymmetry and width of the diamond peak increase as the particle size decreases.[65, 87] A comparative survey of the literature on studies of FWHM reveals those on natural, single-crystal diamond (6 cm^{-1}),[1] and polycrystalline diamond films deposited on [100] silica (7 cm^{-1}).[9] Our diamond films show a higher peak thicknesses (15 cm^{-1}) compared to these previously-reported values, possibly due to smaller particle sizes in our sample than those found previously. A comparison of the crystallite sizes reported by Wang *et al.*[1] (~10 μm) with those obtained in this deposition experiment (~1 μm), discussed in the following section) confirms this.

SEM was then employed to examine the morphology of the deposited film.   The resulting micrograph is shown in Figure 4.14. The crystals therein show a defined morphology with smooth, flat [100] and [111] faces. Moreover, the cubic crystals are ~1 μm in size, and are observed to disperse throughout the sample without agglomerating into a continuous film.   The information depicted in the inset of Figure 4.14 is representative of the entire sample, where discrete cubo-octaedric crystals were obtained. The discrete crystalline diamond is attributed to the relatively short deposition time (30 min), which permits formation of single crystals. It is noteworthy that similar crystals have been previously reported by Hirmke *et al.*, who seeded 1 – 20 μm diamond particles diluted in ethanol and applied to tungsten substrates in a hot filament chemical vapour deposition reactor with tungsten filaments.[11] The study also used extremely low methane contents (0.3%) in the feed gas along with high substrate temperatures which allowed single diamond nuclei of a sufficiently large (up to 80 μm) size to grow. We note similar observations in Experiment 3, with those of Hirmke *et al.*, where the cubo-octaedric crystals obtained were a result of a lower feed rate for methane (1.5%, compared to 3% for Experiments 1 and 2). Moreover, Haubner and Lux have noted that the transition between faceted diamond crystals (as in Experiment 2) and ballas diamond begins when
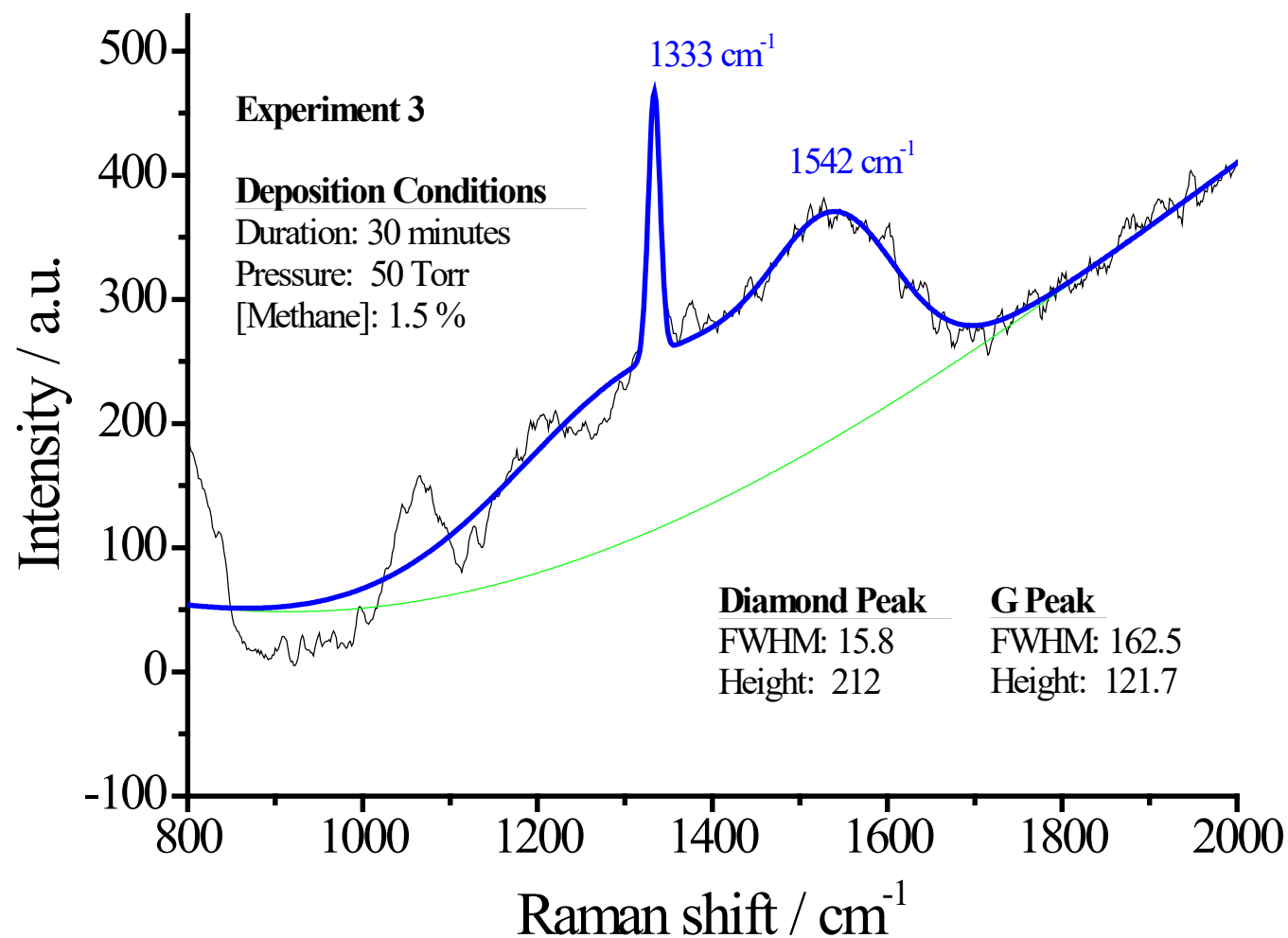
Figure 4.13   Raman spectrum of Experiment 3 containing original and fitted data as well as deposition conditions.

the proportion of CH_4 to H_2 exceeds 1.5%.[80] With the CH_4 concentration in Experiment 2 yielding faceted crystals, our results are in agreement with this observation.
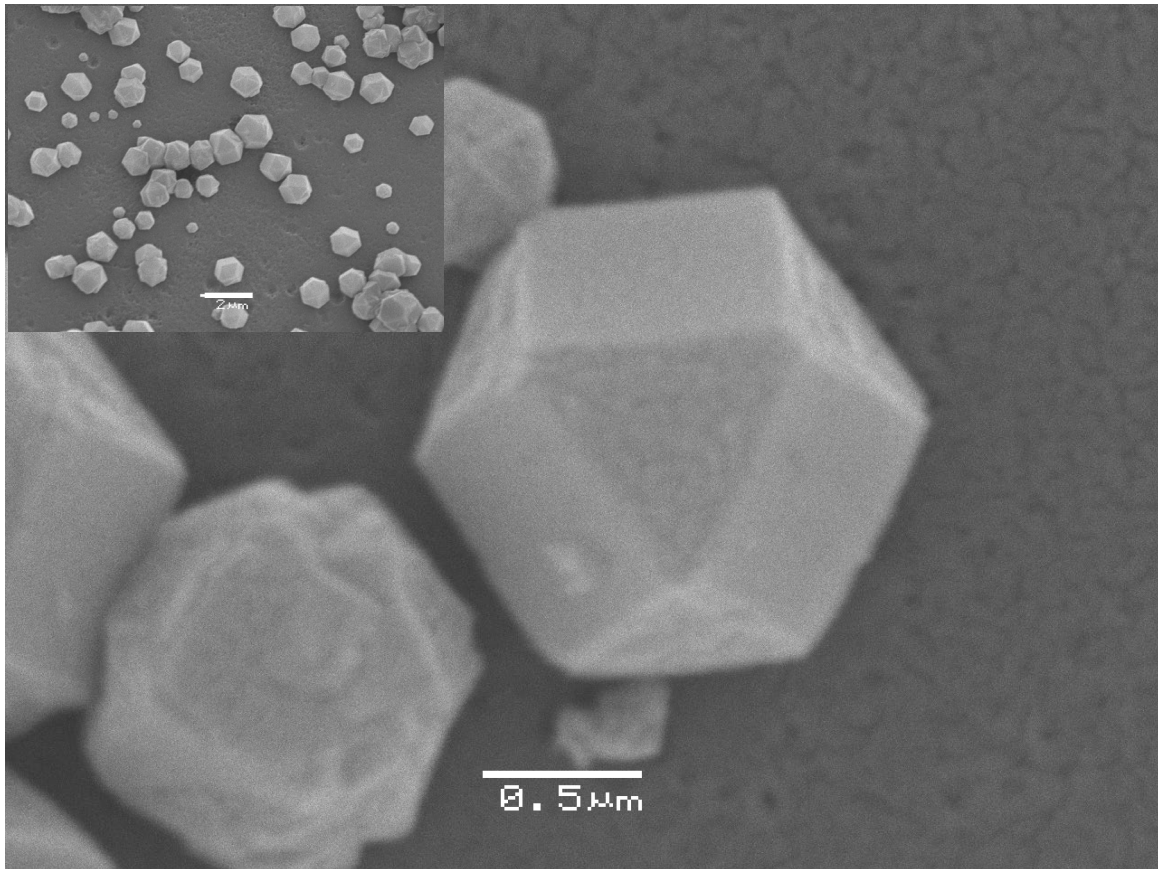
Figure 4.14   Scanning electron microscopic image of microcrystalline diamond.
                 INSET: Lower magnification image of the same film.

According to Chein *et al.*,[88] in a plasma deposition system comprising of CH_4 as a source gas, the concentration of methane in the gas mixture influences the growth rate, the surface morphology and the quality of the diamond film. A higher component of CH_4 was mentioned by the authors as a possible cause of increased deposition rate, as well as a higher proportion of graphitic components in the deposit. The authors also noted a

concentration of 6% methane concentration in hydrogen as leading to especially good crystallinity and surface morphology for a diamond homoepitaxial process.

4.5.3.3   Nanocrystalline diamond deposition

In the next two experiments, all parameters were varied, with methane concentration maintained at 1.5% and 3%, deposition time kept at 300 min and 1 min, and deposition pressure controlled at 66 mbar and 40 mbar for Experiments 4 and 5, respectively. The Raman spectra obtained for these experiments are presented in Figure 4.15. In Figure 4.15A, the sharp diamond and graphite (G) peaks are evident at 1332 cm^{-1} and 1564 cm^{-1} respectively. In addition, a small peak at 1145 cm^{-1} confirms nanocrystalline diamond presence as well. The FWHM for the graphite peak was unobtainable, but that for diamond was found to be ~50 cm^{-1}.

In Figure 4.15B, there is a sharp peak obtained at 1331 cm^{-1}, that can be attributed to the presence of diamond in the sample. In addition there is another broad peak at 1512 cm^{-1}, which is a result of sp^2 carbon, while a small peak at approximately 1145 cm^{-1} confirms the presence of nanocrystalline diamond.[4] In addition, there is extensive luminescence from the sample, as evidenced by its sloping baseline and mentioned as a common occurrence with diamond samples.[54, 65] Moreover, the D peak is seen to have an FWHM of 17.8, which most closely resembles that of nanodiamond.[65]

Figure 4.16A depicts the scanning electron micrograph of the sample in Experiment 5, which shows there is a layer of nucleated cauliflower-like structures aggregating into ~ 2 µm in size clusters. The clusters are also observed to be coalescing into more continuous films which is depicted in the inset of Figure 4.16A. Moreover, the individual crystals of diamond as shown on the substrate are ~100 nm, which is in the size-range of nanodiamond.
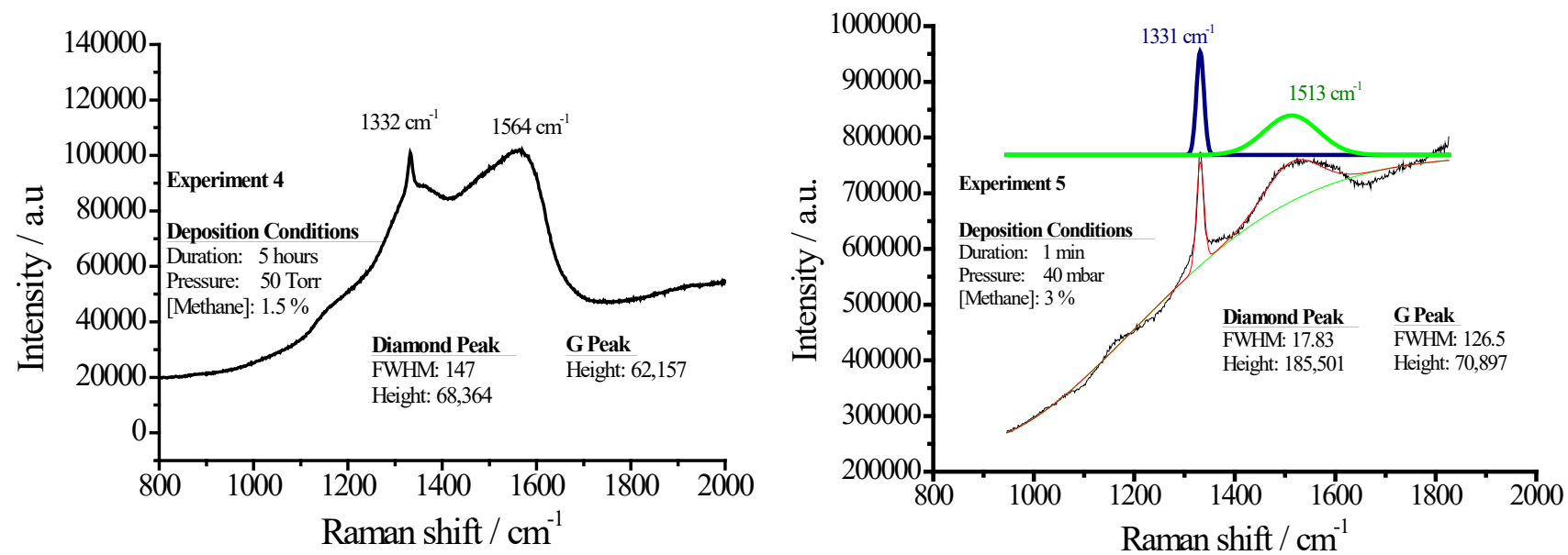
Figure 4.15   Raman spectrum of nanocrystalline diamond containing original and fitted data and deposition conditions.
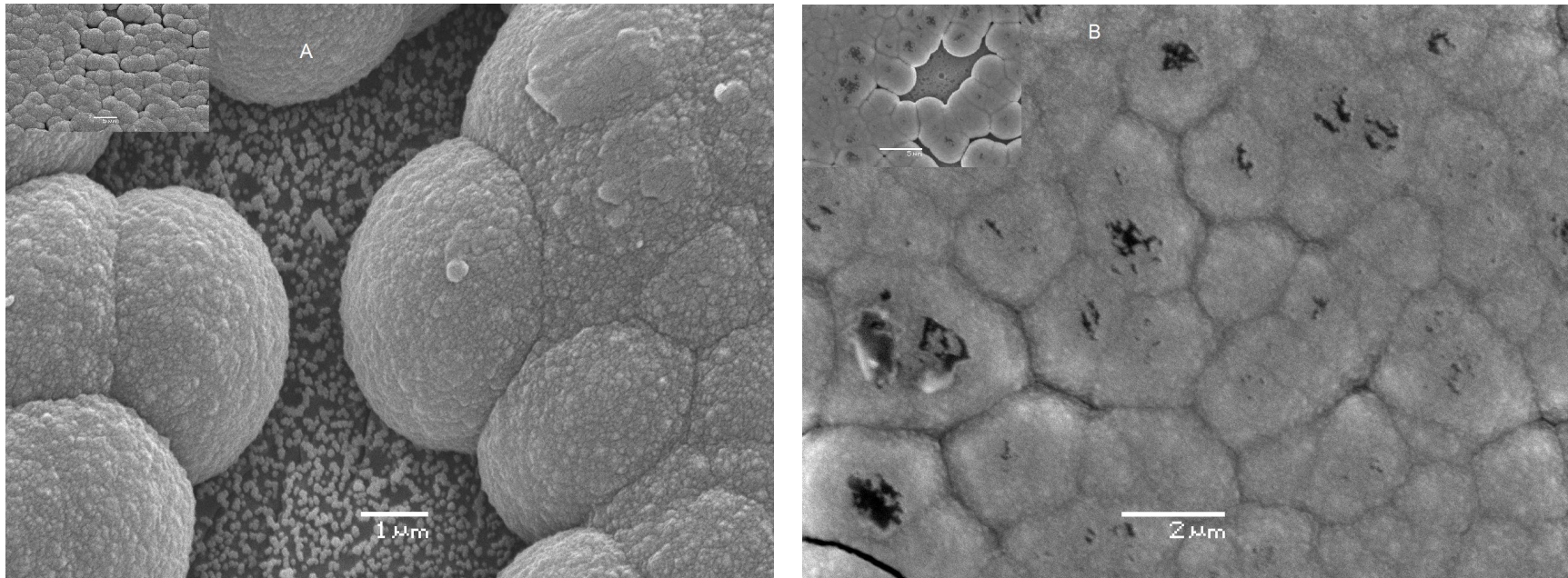
Figure 4.16   Scanning electron microscopic image of nanocrystalline diamond film in Experiment 4 (A) and Experiment 5 (B).

INSET: Lower magnification image of the same film.

Similarly, in Figure 4.16B, large sized clusters in the micrometer range are observed. Clusters in Figure 4.16B are almost twice the size of those in Figure 4.16A. In addition, the clusters are coalesced into continuous film, as is observed in Figure 4.16B (inset). Since film continuity is prevalent in the sample depicted in Figure 4.16B despite the relatively short deposition time, it is likely that under the prevailing conditions in our CVD system, deposition time may not an overly critical factor. The consolidation of what appears to be nucleation clusters is compact, with minimal gaps. Deposition of the film under these conditions suggests the optimum film of large grains and nucleation clusters, compacted into an almost continuous film may not require as harsh and extreme conditions as has been reported for films of similar morphologies elsewhere. Ralchenko *et al.*[4] have utilised microwave plasma CVD to deposit films using 4% CH_4 in H_2, with deposition pressure of 105 mbar and substrate temperature of 740º C. Their findings showed a higher incidence of nanocrystalline diamond than that in Experiment 5, although no detail was presented showing the film imagery.

4.5.4   Comments on diamond deposition in this study

Among the five deposition experiments undertaken, three samples (from Experiments 3 - 5) demonstrate definite evidence of polycrystalline diamond presence. As has been stated by Haubner and Lux,[80] the main parameter for diamond growth is the atomic hydrogen concentration. This is observed in Experiments 1 and 2, which had the highest CH_4 concentrations (3%) in the chamber during deposition. The resulting films demonstrated prominent D and G peaks, suggesting predominantly high sp^2 carbon content. Experiment 5 also had 3% CH_4 concentration, and the Raman spectrum of the resulting sample has a G peak present. The occurrence of G peaks was noted in all the Raman spectra, implying that a mix of diamond and sp^2 bonded carbon exists in all samples.

In nanocrystalline films, up to 10% of the carbon has been suggested to exist π-bonded in 2 to 4 atom-wide grain boundaries, that as a result of the π-bonding, are regions of conductivity.[64] This has also been confirmed by findings of others,[63, 89] such as Gan *et al.*, who have attributed conductivity at the inter-grain material in ultra nanocrystalline diamond to significant electron-hopping between traps located on or between the grain boundaries.[63] Therefore, situation of sp^2-bonded carbon at nanodiamond film grain boundaries can impart electrical conductivity in the films, making them an attractive option for electrochemical applications.

Depositions with lower pressure (40 mbar) produced more continuous films with larger nucleation densities, which have been attributed to etching of the graphite as it competes with the formation of diamond.[5, 90] In addition, based on the kinetic theory of gases, with lower pressure of the chamber, the mean free path of the gases therein increases, which means lower collisions and loss of kinetic energy from the species. The highly-energised species aggregate at the precursors leading to increased nucleation and substrate growth.

Based on FWHM measurements, the nature of the films are consistent with the literature. The nature of peaks in the respective Raman spectrum for each deposited sample is consistent with those in the literature. These findings thus confirm that the study produced amorphous carbon and polycrystalline diamond, with both microcrystalline and nanocrystalline grain sizes.

4.6 Concluding remarks

The assembly of a chemical vapour deposition system for this study set out to achieve two objectives. First, it was to be able to hydrogenate bare carbon surfaces. The second was to deposit diamond films onto seeded substrates. Optimisation of the pressure, duration of plasma exposure conditions and flow rate of precursor gases in the quartz

tube can be manipulated with successful results for hydrogenation. The hydrogenation of physically small bare carbon electrodes was verified by XPS, which confirmed that there was a decrease in the O/C ratio. Furthermore, the decoupled peak information from the C_{1s} band in the XPS spectra for electrodes before and after hydrogenation confirms the conversion of the surface from graphitic to diamond-like. These are consistent with the findings of others.

A variety of diamond films were successfully deposited, and their diamond content was verified using a mixture of Raman spectroscopy and SEM. There was evidence of diamond presence in four samples. All samples demonstrated presence of sp^2-bonded carbon. The nucleation clusters of diamond were of varying sizes in response to the process parameters applied. The presence of sp^2-bonded carbon between diamond grain boundaries might possibly impart electric conductivity in the films. With careful manipulation of these parameters, namely pressure, duration, and methane concentration, diamond films of defined morphology consistent with the literature have been fabricated. Further exploratory work can focus on successfully seeding pulled quartz capillaries which can then be extended to diamond deposition onto these capillaries for fabrication of diamond-coated electrodes.

4.7 References

1.   Wang, L. J.; Xia, Y.; Fang, Z.; Zhang, W.; Zhang, W.; Shi, W., *J. Mater. Sci. Lett.* **2003,** *22* (20), 1447-1450.

2.   Baranauskas, V.; Tosin, M. C.; Peterlevitz, A. C.; Ceragioli, H.; Durrant, S. F., *J. Appl. Phys.* **2000,** *88* (3), 1650.

3.   Kromka, A.; Janík, J.; Balon, F.; Kubovic, M.; Cerven, I.; Dubravcová, V., *Thin Solid Films* **2003,** *433* (1-2), 73-77.

4.   Ralchenko, V.; Saveliev, A.; Voronina, S.; Dementjev, A.; Maslakov, K.; Salerno, M.; Podesta, A.; Milani, P., Nanodiamond Seeding for Nucleation and Growth of CVD Diamond Films. In *Synthesis, Properties and Applications of Ultrananocrystalline Diamond*, 2005; pp 109-124.

5.   Dua, A. K.; Roy, M.; Nuwad, J.; George, V. C.; Sawant, S. N., *Appl. Surf. Sci.* **2004,** *229* (1-4), 254-262.

6.   Wang, S. G.; Zhang, Q.; Yoon, S. F.; Ahn, J.; Wang, Q.; Yang, D. J.; Huang, Q. F.; Rusli; Tang, W. Z.; Lu, F. X., *Diamond Relat. Mater.* **2002,** *11* (9), 1683-1689.

7.   Dua, A. K.; George, V. C.; Friedrich, M.; Zahn, D. R. T., *Diamond Relat. Mater.* **2004,** *13* (1), 74-84.

8.   Guerin, D.; Ismat Shah, S., *J. Mater. Sci. Lett.* **1997,** *16* (6), 476-478.

9.   Rudder, R. A.; Hudson, G. C.; Posthill, J. B.; Thomas, R. E.; Markunas, R. J., *Appl. Phys. Lett.* **1991,** *59* (7), 791.

10.   Wittorf, D.; Jäger, W.; Dieker, C.; Flöter, A.; Güttler, H., *Diamond Relat. Mater.* **2000,** *9* (9-10), 1696-1702.

11.   Hirmke, J.; Schwarz, S.; Rottmair, C.; Rosiwal, S. M.; Singer, R. F., *Diamond Relat. Mater.* **2006,** *15* (4-8), 536-541.

12.   Liu, X.; Jia, X.; Guo, X.; Zhang, Z.; Ma, H.-a., *Cryst. Growth Des.* **2010,** *10* (7), 2895-2900.

13.   Ascarelli, P.; Fontana, S., *Appl. Surf. Sci.* **1993,** *64* (4), 307-311.

14.   Suzuki, A.; Ivandini, T. A.; Yoshimi, K.; Fujishima, A.; Oyama, G.; Nakazato, T.; Hattori, N.; Kitazawa, S.; Einaga, Y., *Anal. Chem.* **2007,** *79* (22), 8608-8615.

15.   Ferreira, N. G.; Azevedo, A. F.; Beloto, A. F.; Amaral, M.; Almeida, F. A.; Oliveira, F. J.; Silva, R. F., *Diamond Relat. Mater.* **2005,** *14* (3-7), 441-445.

16.   Naguib, N. N.; Elam, J. W.; Birrell, J.; Wang, J.; Grierson, D. S.; Kabius, B.; Hiller, J. M.; Sumant, A. V.; Carpick, R. W.; Auciello, O.; Carlisle, J. A., *Chem. Phys. Lett.* **2006,** *430* (4-6), 345-350.

17. Daenen, M.; Zhang, L.; Erni, R.; Williams, O. A.; Hardy, A.; Van Bael, M. K.; Wagner, P.; Haenen, K.; Nesládek, M.; Van Tendeloo, G., *Adv. Mater.* **2009,** *21* (6), 670-673.

18. Martínez-Huitle, C. A., *Small* **2007,** *3* (9), 1474-1476.

19. Zhang, M.-l., *Journal of Shanghai University (English Edition)* **2006,** *10* (6), 561-562.

20. Oleinik, I. I.; Pettifor, D. G.; Sutton, A. P.; Butler, J. E., *Diamond Relat. Mater.* **2000,** *9* (3-6), 241-245.

21. Jian, H.; Jianmin, L.; Linjun, W.; Run, X.; Weimin, S.; Yiben, X., *Plasma Sci. Technol.* **2009,** *11* (3), 302-306.

22. Actis, P.; Denoyelle, A.; Boukherroub, R.; Szunerits, S., *Electrochem. Commun.* **2008,** *10* (3), 402-406.

23. Liu, H.; Dandy, D. S., *Diamond Chemical Vapor Deposition: Nucleation and Early Growth Stages*. Noyes Publications Park Ridge, NJ, 1995.

24. Hian, L. C.; Grehan, Kieron J.; Goeting, Christiaan H.; Compton, Richard G.; Foord, J. S.; Marken, F., *Electroanal.* **2003,** *15* (3), 169-174.

25. Musil, J., *Vacuum* **1986,** *36* (1-3), 161-169.

26. Popov, C., Nanostructured Carbon Materials. In *Functional Properties of Nanostructured Materials*, 2006; pp 387-398.

27. Achatz, P.; Garrido, J. A.; Williams, O. A.; Bruno, P.; Gruen , D. M.; Kromka, A.; Steinmüller, D.; Stutzmann, M., *Phys. Status Solidi A* **2007,** *204* (9), 2874-2880.

28. Kern, W.; Schuegraf, K., K., *Deposition Technologies and Applications: Introduction and Overview*. Noyes Publications: Park Ridge, 1988; p 413.

29. Hikavyy, A.; Clauws, P.; Deferme, W.; Bogdan, G.; Haenen, K.; Nesladek, M., *Diamond Relat. Mater.* **2006,** *15* (4-8), 682-686.

30. Gaudin, O.; Whitfield, M. D.; Foord, J. S.; Jackman, R. B., *Diamond Relat. Mater.* **2001,** *10* (3-7), 610-614.

31. Leech, P. W.; Perova, T.; Moore, R. A.; Reeves, G. K.; Holland, A. S.; Ridgway, M., *Diamond Relat. Mater.* **2006,** *15* (9), 1266-1270.

32. Sarada, B. V.; Rao, T. N.; Tryk, D. A.; Fujishima, A., *J. Electrochem. Soc.* **1999,** *146* (4), 1469-1471.

33. Soh, K. L.; Kang, W. P.; Davidson, J. L.; Basu, S.; Wong, Y. M.; Cliffel, D. E.; Bonds, A. B.; Swain, G. M., *Diamond Relat. Mater.* **2004,** *13* (11-12), 2009-2015.

34. Nakashita, T.; Osaka, Y.; Hirose, M.; Imura, T.; Hiraki, A., *Jpn. J. Appl. Phys.* **1983,** *22* (12), 1766-1770.

35. Ahn, H.; Alberts, L.; Wöhle, J.; Rie, K. T., *Surf. Coat. Technol.* **2001,** *142-144*, 894-898.

36. Vizireanu, S. I.; Mitu, B.; Dinescu, G., *Surf. Coat. Technol.* **2005,** *200* (1-4), 1132-1136.

37. Popov, C.; Kulisch, W.; Bliznakov, S.; Mednikarov, B.; Spasov, G.; Pirov, J.; Jelinek, M.; Kocourek, T.; Zemek, J., *Appl Phys A-Mater* **2007,** *89* (1), 209-212.

38. Sh, M.; Ternyak, O.; Akhvlediani, R.; Lafosse, A.; Bertin, M.; Azria, R.; Hoffman, A., *physica status solidi (a)* **2007,** *204* (9), 2909-2914.

39. Sozin, Y. I.; Katsay, M. Y., Amorphous Diamond, Its Production, Identification and Some Properties. In *Innovative Superhard Materials and Sustainable Coatings for Advanced Manufacturing*, Lee, J.; Novikov, N.; Turkevich, V., Eds. Springer Netherlands: 2005; Vol. 200, pp 319-326.

40. Martineau, P. M.; et al., *J. Phys. Condens. Matter* **2009,** *21* (36), 364205.

41. Soga, T.; Sharda, T.; Jimbo, T., *Phys. Solid State* **2004,** *46* (4), 720-725.

42. Vojs, M.; Veselý, M.; Redhammer, R.; Janík, J.; Kadlecíková, M.; Danis, T.; Marton, M.; Michalka, M.; Sutta, P., *Diamond Relat. Mater. 14* (3-7), 613-616.

43. Wu, Q.; Yu, L.; Ma, Y.; Liao, Y.; Fang, R.; Zhang, L.; Chen, X.; Wang, K., *J. App. Phys.* **2003,** *93* (1), 94-100.

44. Jiaqi, Z.; Jiecai, H.; Songhe, M.; Jia, L.; Chunzhu, J.; Shuping, L.; Yuebing, Z.; Bengkang, T., *Diamond Relat. Mater.* **2007,** *16* (3), 558-561.

45. Jackson, S. T.; Nuzzo, R. G., *Appl. Surf. Sci.* **1995,** *90* (2), 195-203.

46. Sun, Z.; Xu, S.; Ostrikov, K. N., *Diamond Relat. Mater.* **2002,** *11* (1), 92-97.

47. Azuma, K.; Shirai, H.; Kouchi, T., *Thin Solid Films* **1997,** *296* (1-2), 72-75.

48. Xu, J.; Chen, Q.; Swain, G. M., *Anal. Chem.* **1998,** *70* (15), 3146-3154.

49. Foord, J. S.; Lau, C. H.; Hiramatsu, M.; Jackman, R. B.; Nebel, C. E.; Bergonzo, P., *Diamond Relat. Mater.* **2002,** *11* (3-6), 856-860.

50. Alwarappan, S.; Butcher, K. S. A.; Wong, D. K. Y., *Sens. Actuators, B* **2007,** *128* (1), 299-305.

51. Goswami, R.; Jana, T.; Ray, S., *J. Phys. D: Appl. Phys.* **2008,** *41* (15), 155413.

52. Butcher, K. S. A. Aluminium Nitride Insulating Thin Films Grown on Damage Susceptible Semiconductors. Macquarie University, Sydney, 1997.

53. Remes, Z.; Kromka, A.; Potmesil, J.; Vanecek, M., *physica status solidi (a)* **2008,** *205* (9), 2158-2162.

54. Ferrari, A. C.; Robertson, J., *Phys. Rev. B* **2001,** *64* (7), 075414.

55. Yan, P.; Yang, S.-z.; Li, B.; Ren, Y.; Chen, X., *Mater. Chem. Phys.* **1996,** *45* (2), 167-170.

56. Yarnell, A.; Washington, C., The many facets of man-made diamond. *Chemical & Engineering News* February 2, 2004, 2004, pp 26-31.

57. Lisi, N.; Giorgi, R.; Dikonimos, T.; Salernitano, E.; Gagliardi, S.; Giorgi, L.; Contini, V.; Morales, P., *Diamond Relat. Mater.* **2010,** *19* (11), 1382-1386.

58. Obraztsov, A. N.; Pavlovsky, I. Y.; Izumi, T.; Okushi, H.; Watanabe, H., *Appl. Phys. A.* **1997,** *65* (4), 505-509.

59. Rabeau, J. R.; John, P.; Wilson, J. I. B.; Fan, Y., *J. Appl. Phys.* **2004,** *96* (11), 6724-6732.

60. Tiwari, R. N.; Chang, L., *J. Appl. Phys.* **2010,** *107* (10), 103305-7.

61. Uppireddi, K.; Resto, O.; Weiner, B.; Morell, G., *Nanoscale Res. Lett.* **2008,** *3* (2), 65-70.

62. Pleskov, Y. V., Synthetic diamond electrodes for electroanalysis and electrolysis. In *Electroanalytical Chemistry Research Developments*, Jiang, P. N., Ed. Nova Science Publishers Inc: Hauppauge, 2007; pp 183-227.

63. Gan, L.; Bolker, A.; Saguy, C.; Kalish, R.; Tan, D. L.; Tay, B. K.; Gruen, D.; Bruno, P., *Diamond Relat. Mater.* **2009,** *18* (9), 1118-1122.

64. Gruen, D. M., *Annu. Rev. Mater. Sci.* **1999,** *29* (1), 211-259.

65. Larijani, M. M.; Navinrooz, A.; Le Normand, F., *Thin Solid Films* **2006,** *501* (1-2), 206-210.

66. Meng, Y.-f.; Yan, C.-s.; Lai, J.; Krasnicki, S.; Shu, H.; Yu, T.; Liang, Q.; Mao, H.-k.; Hemley, R. J., *Proc. Natl. Acad. Sci. U. S. A.*

67. Yan, C.-s.; Vohra, Y. K.; Mao, H.-k.; Hemley, R. J., *Proc. Natl. Acad. Sci. U. S. A.* **2002,** *99* (20), 12523–12525.

68. Xiao-Bing, L.; Xiao-Peng, J.; Hong-An, M.; Wei, H.; Xin-Kai, G.; Hong-Sheng, J., *Chin. Phys. Lett.* **2009,** *26* (3), 38102-38104.

69. Nguyen, V. S., *Plasma-Assisted Chemical Vapor Deposition*. Noyes Publications: Park Ridge, 1988; p 413.

70. Cho, S.; Lee, Y.; Choi, D.; Kim, T., *J. Electroceram.* **2006,** *17* (2), 811-816.

71. Rezek, B.; Nebel, C. E., *Diamond Relat. Mater.* **2006,** *15* (9), 1374-1377.

72. Feenstra, K. F.; Alkemade, P. F. A.; Algra, E.; Schropp, R. E. I.; Weg, W. F. v. d., *Prog. Photovoltaics Res. Appl.* **1999,** *7* (5), 341-351.

73.   Ji, X.; Banks, C. E.; Crossley, A.; Compton, R. G., *ChemPhysChem* **2006,** *7* (6), 1337-1344.

74.   McNally, M.; Wong, D. K. Y., *Anal. Chem.* **2001,** *73* (20), 4793-4800.

75.   Mehandru, S. P.; Anderson, A. B.; Angus, J. C., *J. Phys. Chem.* **2002,** *96* (26), 10978-10982.

76.   Filik, J.; May, P. W.; Pearce, S. R. J.; Wild, R. K.; Hallam, K. R., *Diamond Relat. Mater.* **2003,** *12* (3-7), 974-978.

77.   Yan, X. B.; Xu, T.; Yang, S. R.; Liu, H. W.; Xue, Q. J., *J. Phys. D: Appl. Phys.* **2004,** *37* (17), 2416-2424.

78.   Li, G.; Xia, L. F.; Ma, X. X.; Sun, Y., *Acta Metallurgica Sinica(English letters)* **1999,** *12* (4), 551-556.

79.   Darwiche, S.; et al., *J. Phys. D: Appl. Phys.* **2007,** *40* (4), 1030.

80.   Haubner, R.; Lux, B., *Int. J. Refract. Met. Hard Mater* **2002,** *20* (2), 93-100.

81.   Okada, K.; Kanda, H.; Komatsu, S.; Matsumoto, S., *J. Appl. Phys.* **2000,** *88* (3), 1674-1678.

82.   Forbes, I. S.; Rabeau, J. R.; Wilson, J. I. B.; John, P., *Mater. Sc. Tech.* **2003,** *19* (5), 1.

83.   Hiramatsu, M.; Lau, C. H.; Bennett, A.; Foord, J. S., *Thin Solid Films* **2002,** *407* (1-2), 18-25.

84.   Shiryaev, A. A.; Iakoubovskii, K.; Grambole, D.; Dubrovinskaia, N., *J. Phys. Condens. Matter* **2006,** *18*, 493-501.

85.   Sun, Z.; Shi, J. R.; Tay, B. K.; Lau, S. P., *Diamond Relat. Mater.* **2000,** *9* (12), 1979-1983.

86.   Compton, R. G.; Foord, John S.; Marken, F., *Electroanal.* **2003,** *15* (17), 1349-1363.

87.   Bergman, L.; McClure, M. T.; Glass, J. T.; Nemanich, R. J., *J. Appl. Phys.* **1994,** *76* (5), 3020-3027.

88.   Chein, T.-H.; Wei, J.; Tzeng, Y., *Diamond Relat. Mater.* **1999,** *8* (8-9), 1686-1696.

89.   Cleri, F.; Keblinski, P.; Colombo, L.; Wolf, D.; Phillpot, S. R., *Europhys. Lett.* **1999,** *46* (5), 671-677

90.   Kim, D. G.; Lee, H. C.; Lee, J. Y., *J. Mater. Sci.* **1993,** *28* (24), 6704-6708.

CHAPTER 5

CONCLUDING REMARKS

5.1 Thesis summary and conclusion

The research in this thesis was motivated by the need for detecting dopamine *in vivo* in the presence of ascorbic acid and without substantial transient loss of the signal and in the presence of ascorbic acid. Dopamine is an ubiquitous neurotransmitter in the mammalian central nervous system that modulates many aspects of brain circuitry. It also plays a crucial role in the functioning of the central nervous, cardiovascular, renal and hormonal systems. Irregularities in dopamine transmission or loss of dopaminergic neurons have been attributed to illnesses and conditions including Parkinson's disease and schizophrenia. Thus, it is of interest to measure dopamine in the extracellular fluid in animals in order to monitor neurotransmission processes and correlate neurochemistry with behaviour. Very often, the detection of dopamine *in vivo* using conventional carbon electrodes with a hydrophilic surface is fraught with challenges. High molecular weight and electroactive proteins, peptides and lipids adsorb on the bare carbon surface, preventing dopamine from accessing the electrode surface, and its subsequent oxidation. This phenomenon is referred to as fouling. In addition, oxidation of ascorbic acid takes place at a similar oxidation potential to that of dopamine at bare carbon electrodes, and its oxidation signal often interferes with dopamine response.

To overcome these challenges, this study explored modification of the surfaces of physically small bare carbon electrodes of approximately 2 μm radius and 4 μm axial length. These electrodes were subjected to two surface modification methods to evaluate their resistance to fouling. The first modification, outlined in Chapter 2, involved

electrodeposition of a layer of *p*-phenylacetate on bare carbon electrodes. Electrode performance was evaluated using voltammetry of four redox markers: hexamine ruthenium(III) chloride, dopamine, potassium ferricyanide and anthraquinone-2,6-disulfonate. Characterisation in these redox systems confirmed the existence of an anionic film monolayer, which exhibited slower reaction kinetics at the modified surface in all the redox systems. Furthermore, based on the voltammetric characterisation, the bare carbon electrode surface was also demonstrated to comprise of predominantly basal planes.

In vitro characterisation of the *p*-phenylacetate film-coated electrodes showed the electrodes displayed 35% suppression in the ascorbic acid oxidation signal. This was attributed to electrostatic interactions between the anionic ascorbic acid (pKa = 4.2) and similarly-anionic *p*-phenylacetate film coating on the modified electrodes. The film coating was also observed to be stable over a period of 40 days, with 11% decrease in dopamine oxidation current. This compared with 90% reduction observed at bare carbon electrodes. The sensitivity and limit of detection of film-coated electrodes were determined to be 16 pA/nM and 541 pM, respectively. This compared favourably with a sensitivity and limit of detection of 19 pA/nM and 543 pM obtained at bare carbon electrodes, respectively. At the film-coated electrodes, in the presence of 200 µM ascorbic acid and 0.1% (w/v) bovine serum albumin, the limit of detection was found to increase to 6 nM, while sensitivity increased to 0.10 nA/nM. This is a consequence of the fouling environment around the electrode as well as the re-reduction of dopamine-*o*-quinone to dopamine, which artificially increases the dopamine response by increasing limiting currents. In contrast, the limit of detection of the film-coated electrodes to ascorbic acid in the presence of 0.1% (w/v) bovine serum albumin was estimated to be 1.4 µM while sensitivity was 0.1 nA/µM. The results confirm that the electrode sensitivity and limit of detection are favourable towards dopamine over ascorbic acid.

In *in vitro* experiments, the electrodes were subjected to incubation in a synthetic laboratory solution comprising 1.0% (v/v) caproic acid (a lipid), 0.1% (w/v) bovine serum albumin and 0.01% (w/v) cytochrome C (both are protein) and 0.002% (w/v) human fibrinopeptide B (a peptide). The performance of the film-coated electrodes was found to be affected slightly with sensitivity increasing from 16 pA/nM to 50 pA/nM. Similarly, limit of detection was observed to decrease only slightly from 541 pM to 385 pM. In comparison, calibration plots to determine the same parameters at bare carbon electrodes following incubation yielded statistically-insignificant results. This was attributed to extreme surface degradation at the electrodes. The conclusions from *in vitro* experiments indicated that the film-coated electrodes tend to display relative stability in limit of detection and sensitivity towards dopamine.

To evaluate the real-life performance of the electrodes, both film-coated and bare carbon electrodes were applied to *in vivo* dopamine detection in the left striatum of anesthetised rats. To evoke dopamine, the ventral tegmental area of the rat brain was electrically stimulated. The dopamine oxidation signal was compared at the start of the experiment and after 60 mins as an indicator of electrode fouling. At the film-coated electrodes, 50% decay in oxidation peak current was found, which compared favourably to 62% at bare carbon electrodes. At film-coated electrodes, ~25 - 40% reduction in oxidation peak current was observed to occur in the first 40 min, after which the rate of fouling was observed to diminish, leading to less than 50% decrease in the oxidation peak current. This suggests the longevity of the film may be until 40 mins following implantation.

The second modification was the hydrogenation of the bare carbon electrode surface, as outlined in Chapter 3. Bare carbon electrodes were hydrogenated using radio frequency plasma hydrogenation and characterised before and after the modification. Results from AFM, Raman spectroscopy and XPS confirmed the presence of a smooth carbon surface with greater presence of sp^3-bonded carbon compared to bare carbon electrodes.

Moreover, the proportion of oxygen to carbon was observed to be lesser at the hydrogenated carbon surface than that at bare carbon.

Voltammetric studies in hexamine ruthenium(III) chloride, dopamine and potassium ferricyanide at the hydrogenated electrodes suggested a change from an anionic surface at bare carbon electrodes to a lesser-charged surface at the hydrogenated electrodes. In addition, all three redox systems displayed quasi-reversibility at the electrodes following hydrogenation which was attributed to the removal of reactive edge planes by hydrogenation.

Cyclic voltammetry of dopamine in the presence of 0.1% (w/v) bovine serum albumin and 100 mM ascorbic acid was carried out at hydrogenated and bare carbon electrodes. The results revealed the presence of multiple peaks in the voltammogram for oxidation of dopamine at the bare carbon electrode. Furthermore, the ill-defined shape of the voltammogram revealed slow electrode kinetics for dopamine oxidation at the bare carbon electrode. On the other hand, dopamine oxidation at the hydrogenated electrode resulted in a well-defined sigmoidal voltammogram with a halfwave potential of 0.36 V, which is consistent with that for dopamine oxidation.

To evaluate the performance, the limit of detection and sensitivity of the electrode was determined. These parameters were found to be 721 pM and 0.16 pA/nM, respectively. The limit of detection is comparable to that at a bare carbon electrode, but the sensitivity for dopamine was found to be greater at bare carbon surface. This appeared to be a consequence of the anionic carbonyl and quinonyl groups at the bare carbon surface which electrostatically attract dopamine to the surface. With the conversion of such a surface to one bearing mainly sp^3 C—H bonds after hydrogenation, there was less electrostatic attraction between dopamine and the hydrogenated surface, thus causing reduced sensitivity to dopamine. The limit of detection did not change significantly for the hydrogenated electrode when applied to dopamine detection in the presence of 0.1%

(w/v) bovine serum albumin and 200 μM ascorbic acid. However, the sensitivity was observed to increase approximately 200-fold. This is possibly a consequence of the re-reduction of dopamine-*o*-quinone to dopamine, followed by its oxidation, leading to artificially-high limiting current for dopamine. This results in an increase in the amount of dopamine at the electrode, which leads to increased oxidation of the species, thereby increasing the limiting current. In comparison to dopamine, ascorbic acid detection at the hydrogenated electrodes in the presence of 0.1% (w/v) bovine serum albumin was observed to have a limit of detection of 6 μM and sensitivity of 0.171 pA/μM, indicating a higher limit of detection and lower sensitivity to ascorbic acid at hydrogenated carbon electrodes, compared to that for dopamine.

Hydrogenated carbon electrodes demonstrated little variation and performance following exposure to a synthetic laboratory solution. The limit of detection remained the same (from 721 to 720 pM), while the sensitivity reduced slightly from 0.16 pA/nM to 0.11 pA/nM. These findings at the hydrogenated carbon electrodes compare favourably to those at bare carbon electrodes. Similar findings were observed for both sets of electrodes during *in vivo* dopamine detection. After 60 min of *in vivo* dopamine monitoring, hydrogenated carbon electrodes displayed a 50% reduction in oxidation signal height, which compares favourably to 62% at bare carbon electrodes. In addition, at hydrogenated carbon electrodes, the rate of fouling was observed to be most severe (40% reduction) within the first 20 min after commencing monitoring. During the remaining 40 min, the signal decay was only 10%. It is likely that the steeper reduction in current in the first 20 min or so was due to a gradual build-up of materials adsorbing on the electrode, thus leading to decreased dopamine current. After this interval, possible equilibration of the material built-up on on the electrode could have been achieved, thus a slower rate of electrode fouling was observed after 20 min of implanting the electrode. In contrast, the bare carbon electrode was observed to be steadily fouled throughout the experiment. The results from the *in vivo* monitoring of the dopamine signal affirm that

hydrogenation of the bare carbon electrode surface is an effective strategy in withstanding fouling.

5.2   Performance comparison between electrodes

Table 5.1 provides the limit of detection and sensitivity obtained for dopamine at *p*-phenylacetate   film-coated, hydrogenated and bare carbon electrodes. The limit of detection for all electrode types is similar in magnitude, while the *p*-phenylacetate film-coated and bare carbon electrodes display higher sensitivities for dopamine compared to hydrogenated carbon electrodes. This is likely to be a consequence of the presence of anionic groups and regions on both electrode surfaces, which causes electrostatic attraction between the cationic dopamine (in pH 7.4 citrate/phosphate buffer) and the respective anionic surfaces. In comparison, the hydrogenated carbon electrode surface, which is dominated by sp^3 C—H bonds, is expected to be largely neutral to any charged species, thus the low sensitivity to dopamine. Moreover, all three electrode types have lower limit of detection than the nM range that has been found previously for carbon-based electrodes.[1-2]

	Limit of Detection / pM	Sensitivity / pA/nM
p-phenylacetate film-coated carbon electrode	541	16
Hydrogenated carbon electrode	721	0.16
Bare carbon electrode	543	19

Table 5.1   Comparison of limit of detection and sensitivity at *p*-phenylacetate film-coated, hydrogenated and bare carbon electrodes.

5.3   Rate of fouling at physically small electrodes

Apart from monitoring the decay in the dopamine oxidation signal over a specified period, we have also examined the rate of signal decay at both *p*-phenylacetate film-coated and hydrogenated carbon electrodes. As expected, the results indicated that the rate of fouling was most severe at unmodified, bare carbon electrodes, where there was a steady decrease in oxidation current throughout the experiment. In comparison to bare carbon electrodes, both film-coated electrodes and hydrogenated electrodes varied in the rate of fouling. At film-coated electrodes, the electrode suffered 25% - 40% fouling in the first 40 min, followed by a more severe rate of fouling thereafter. This suggests that the film-coating on the electrode surface resisted fouling for 40 min, after which its performance was considerably reduced. In comparison, hydrogenated electrodes suffered 40% reduction in current signal height in the first 30 min, after which electrode fouling was observed to be reduced to 10%. This rate of current decay suggested that it takes the hydrogenated electrodes ~30 min to equilibrate with the *in vivo* environment, following which the electrode does withstand fouling to an extent. It can thus be concluded that the hydrogenated electrode surface achieves faster stability than the *p*-phenylacetate film-coated electrode. Moreover, at the conclusion of the experiment, the variability in the remaining current height is greatest at film-coated electrodes. This suggests that these electrodes have variability in their performance, possibly a consequence of film-coating variability.

Overall, the results demonstrated that the rate of fouling at modified electrodes was lesser than those at bare carbon electrodes. Furthermore, at the conclusion of the experiment after 60 min, the film-coated electrodes were observed to be undergoing steady fouling at a faster rate than at the commencement of the monitoring whereas the rate of decay had slowed at hydrogenated electrodes. Thus, the comparative rate of fouling performance of the modified electrodes demonstrated that the hydrogenated electrodes had a stable surface and greater precision compared to film-coated electrodes. It can therefore be

concluded that the hydrogenated electrodes have more superior performance *in vivo* compared to film-coated electrodes.

5.4   Fouling resistance of electrodes *in vivo*

A comparison of the decay in oxidation signal height obtained from *in vivo* dopamine detection at the three electrode types in this study is presented in Table 5.2. As shown, there was an equivalent decay in dopamine oxidation peaks at both *p*-phenylacetate film-coated carbon electrodes and hydrogenated carbon electrodes.   Both types of electrode modification resulted in similar levels of resistance to electrode fouling when applied to dopamine detection *in vivo.* It was observed that there was a slightly higher standard deviation in the results among the film-coated electrode electrodes. However, this is possibly a result of the variability in the film-coated electrode surface, and a phenomenon noted previously for similar covalent films.

Electrode type	Decay in signal after 60 min / %	Decay in dopamine oxidation signal / %/min
p-phenylacetate film-coated carbon electrode	50 ± 11	0.9361 ± 0.2859
Hydrogenated carbon electrode	50 ± 5	0.7635 ± 0.0909
Bare carbon electrode	62 ± 9	0.9612 ± 0.0793

Table 5.2   Decay in dopamine oxidation signal feature height at all *p*-phenylacetate film-coated, hydrogenated and bare carbon electrodes.

Among all three electrode types in Table 5.2, bare carbon electrodes were observed to suffer the highest degree of electrode fouling. This confirmed that both film-coated electrodes and hydrogenated electrodes are effective in resisting fouling to a greater extent than unmodified bare carbon electrodes. Moreover, as depicted in Table 5.2, the greatest rate of dopamine oxidation signal decay was observed at the bare carbon electrodes, followed by *p*-phenylacetate film-coated electrodes. The hydrogenated electrodes demonstrated the slowest rate of oxidation peak decay. Based on this data, the hydrogenated electrodes displayed the greatest superiority in withstanding electrode fouling, followed by film-coated electrodes.

5.5   A deposition system for diamond film synthesis

In Chapter 4, the assembly of a CVD system was reported, which succeeded in achieving two objectives. It enabled CVD of diamond films on nucleated substrates. In addition, the deposition system was also capable of hydrogenation of bare carbon surfaces. The study showed that optimisation of the pressure, duration of plasma exposure conditions and flow rate of precursor gases in the silica tube can result in successful hydrogenation and diamond deposition. Hydrogenation on physically small bare carbon electrodes was verified by XPS, which confirmed that there was a decrease in the O/C ratio. Furthermore, the decoupled peak information from the C_{1s} band in the XPS spectra for electrodes before and after hydrogenation confirms the conversion of the surface from graphitic to diamond-like. These are consistent with the findings of others.[3-4]

Diamond deposition using the assembled system was successfully undertaken, and the resultant films were characterised to confirm diamond presence using a mixture of Raman spectroscopy and SEM. Among five samples studied, all demonstrated evidence of amorphous carbon and polycrystalline diamond presence. Moreover, the nucleation clusters of diamond were of varying sizes in response to the process parameters applied. With careful manipulation of these parameters, namely pressure, duration, and methane

concentration, diamond films of defined morphology consistent with the literature have been fabricated. Further exploratory work can focus on successfully seeding pulled quartz capillaries which can then be extended to diamond deposition onto these capillaries for fabrication of diamond-coated electrodes.

5.6   Future directions

This study has demonstrated that both *p*-phenylacetate film-modified and hydrogenated carbon electrodes exhibit a degree of resistance to fouling *in vivo*. While these two strategies were effective in achieving better performance than bare carbon electrodes, the hydrogenated surface clearly exhibited better performance over the film-coated electrodes, which showed evidence of film compromise and lack of longevity.

The stability of the hydrogenated surface can be related to its diamond-like sp^3 carbon content, which is hydrophobic and stable over time. Such passive surfaces are easily accomplished by introducing molecular hydrogen on the sp^2-rich graphitic form of carbon in carefully-controlled plasma systems. In this study, a two-step approach was followed, in which physically small carbon electrodes were initially fabricated, and then hydrogenated in a separate step. Future work on fabricating such electrodes can be performed *in situ* using the CVD setup as reported in Chapter 4. This method eliminates an extra step, which is likely to increase the fabrication success rate.

The deposition system is also envisaged to be applicable to deposition of diamond from a carbon-based precursor and hydrogen gases. Owing to time constraint, this was not pursued far enough in the present work. With suitably-seeded quartz capillaries as substrate material, nanodiamond films may be deposited in the assembly, using an appropriate timeframe to achieve film growth without significantly disrupting the fine tips of pulled quartz capillaries. The diamond-coated capillaries could then be utilised as diamond electrodes. As the diamond films prepared in this study exhibited variable sp^2

carbon content, possibly at the diamond grain boundaries, it is likely that these films would display electrochemical conductivity *via* the sp²-bonded carbon. This would make them suitable as probes. Moreover, with the superior properties of diamond such as wider working potential window, favourable electron transfer kinetics, surface inertness resulting in high resistance to deactivation as well as low background current, these diamond electrodes are expected to exhibit advancements over the already improved properties of the hydrogenated electrodes in this study. The potential utilisation of such electrodes as analytical probes for *in vivo* dopamine detection is exciting, and may bear promising outcomes.

In this study, the fabrication success rate of hydrogenated electrodes was estimated to be 50%. It would be feasible to continue detailed experimentation into improving this rate using radio frequency plasma as an excitation source. The success rate is affected by damage induced by directly exposing the fragile tips of the electrodes to the radio frequency radiation, which causes tip shattering. Therefore, exploring an alternative site within the vacuum chamber for electrode placement has merits in the quest for reducing tip damage, without compromising on the effectiveness of the hydrogenation process. Moreover, as noted in Chapter 3, evidence from AFM measurements and subsequent characterisation of electrode performance suggests full hydrogenation of the electrode surface was not achieved. An alternative positioning of the electrodes during the hydrogenation process will also open up possibilities of longer hydrogenation time, which may have a bearing on the effectiveness of the hydrogenation process, while delivering an enhanced success rate among the electrodes.

As an alternative to hydrogenation based on radio frequency- and microwave plasma excitation methods, a chemical method to convert aldehydes, ketones, alcohols and carboxylic acids into their corresponding alkanes was recently reported.[5-6] This approach is applicable to a carbon surface containing molecular moieties such as quinonyl and

carboxyl functional groups.[7] During hydrogenation of bare carbon films, these moieties are reduced to methyl functional groups. This procedure for reducing these groups chemically can use either diethylsilane or *n*-butylsilane as the reducing agent in the presence of the Lewis acid catalyst, tris(pentafluorophenyl) borane.[6] The mechanisms for reduction of a carboxylic acid via the method are shown in Figure 5.1.
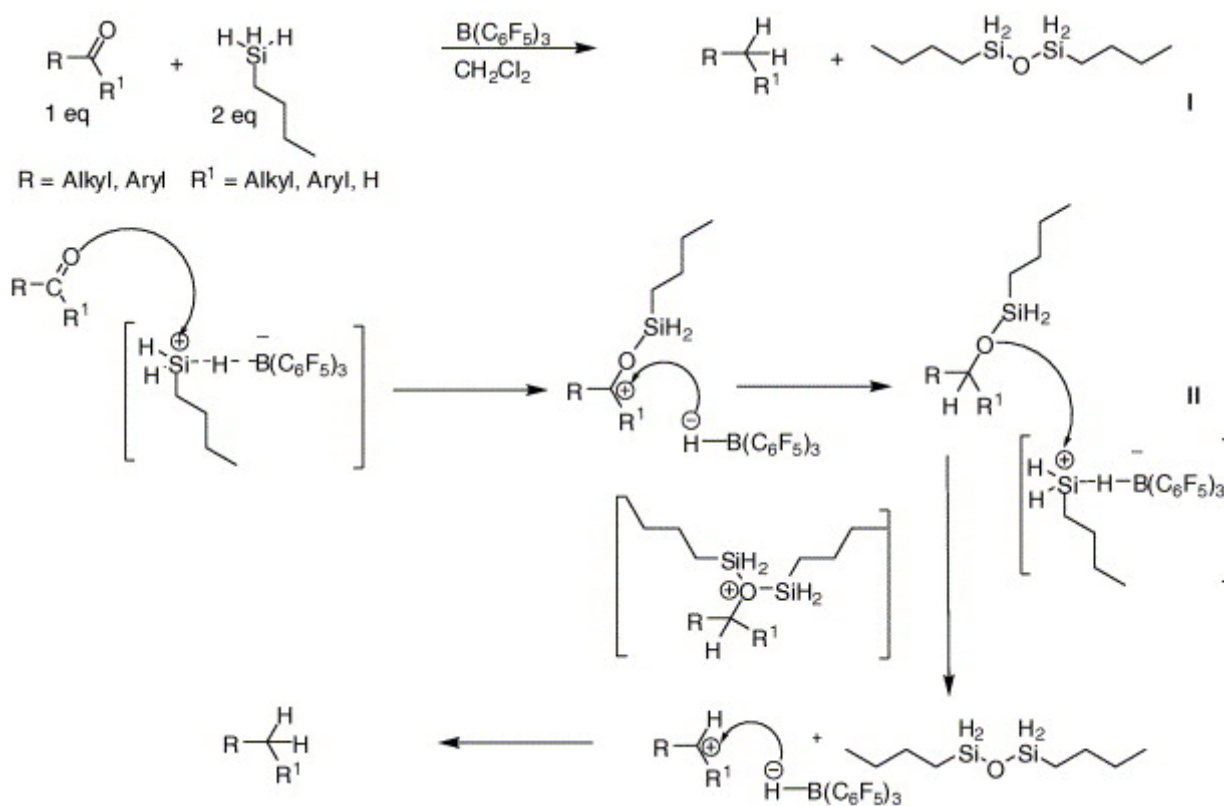

Figure 5.1   Reduction of a ketone functional group by single-step reduction with diethyl silane (I), and multi-step reduction with *n*-butylsilane (II). Adapted from Nimmagadda and McRae.[5]

As indicated in Figure 1, the mechanism can proceed *via* a single step with diethyl silane (Scheme I), or in a multi-step reaction with *n*-butylsilane, catalysed by tris(pentafluorophenyl) borane (Scheme II). The method holds considerable promise as a non-energy based reaction, which can facilitate surface modification without substantial physical tip damage. An electrode surface containing quinonyl and carboxylic groups, such as that of physically small carbon electrodes in this study could be a viable substrate for modification by this approach.

Graphene is an alternative material that can provide an electroactive layer for electrodes. The species consists of an atom-thick sheets of carbon, organised in a honeycomb structure.[8] It exhibits unusual electrical conductivity, high specific surface area and high mechanical, thermal and chemical stabilities.[9] Its unique electrical properties arise from the confinement of electrons in two dimensions, making graphene an attractive option as potential nanoscale building blocks for applications such as field-effect transistors, gas sensors and electromechanical resonators.[10] Dopamine detection with graphene modifications on glassy carbon electrodes, such as Cu_2O/graphene nanocomposites prepared through a polyol process using ethylene glycol as the solvent and reducing agent has been reported with success.[11] Limit of detection at this electrode, determined *in vitro* was 10 nM for dopamine alone, and 0.2 µM (with a signal-to-noise ratio of 3) in the presence of 500 µM uric acid. Elsewhere, a composite of *β*-cyclodextrin and graphene sheets on glassy carbon electrodes was found to exhibit more reversible reaction kinetics for dopamine, using cyclic voltammetry than at bare graphene sheets.[12] A limit of detection of 5 nM for dopamine was obtained at the modified electrode. Furthermore, a recent study by Alwarappan *et al.*[13] has immobilised graphene nanosheets on a glassy carbon electrode. This electrode was then applied to repeated cyclic voltammetry (50 scans) of 500 µM cytochrome C (a protein) in pH 7.4 phosphate buffer saline solution. After 50 scans, the electrode only exhibited 7.5% decrease in the observed signal. Based on this result, the authors concluded that graphene, without requiring any acid or electrochemical pretreatment, demonstrates a degree of resistance to fouling from protein.

Notably, all graphene applications to dopamine detection are hitherto limited to the use of macroelectrodes.[9-12, 14] Therefore, it may be feasible to apply graphene-modified physically small electrodes to selectively detect dopamine in the presence of ascorbic acid. Moreover, any such study may find merits in exploring the attachment of graphene to the bare carbon electrode surface such that subsequent conversion of the atom-thick carbon sheet to a hydrophobic, sp^3-bonded film may impart fouling-resistant capabilities as well.

Finally, the use of multi-walled carbon nanotubes and single-walled carbon nanotubes has been reported in the literature previously for the detection of dopamine.[2, 15] Notably, these nanotubes have extensive occurrences of exposed edge planes, which are responsible for rapid electron-transfer reactions at their surfaces.[16-17] Previous work has also focussed on the antifouling properties of carbon nanotubes.[18-19] For instance, Swamy and Venton[19] have reported the successful detection of dopamine in the presence of serotonin using cyclic voltammetry performed at Nafion-dispersed single-walled carbon nanotubes on carbon fibre electrodes. The study reported that oxidation of serotonin produces hydroxylated products and dimers that subsequently foul bare carbon electrode surfaces. The electrodes were applied to fast-scan cyclic voltammetry of dopamine, with 1 µM injections of serotonin for 3 s, every 15 min. After 25 injections, the nanotube-modified electrode demonstrated only 10% reduction in sensitivity whereas a bare carbon fibre electrode lost approximately 40% sensitivity. The stable response of the modified electrodes, compared to that at bare carbon fibre electrodes, demonstrated the anti-fouling properties of the carbon nanotubes on the electrode. The study also noted the presence of Nafion alone on the carbon fibre surface did not elicit any improvement in current response, nor did the signal-to-noise ratio change, thus attributing the superior performance of the modified electrodes to carbon nanotubes only. As reported by the authors, the exact mechanism by which carbon nanotubes exhibit resistance to fouling was still not known. However, they proposed that oxidative products of serotonin adsorbed on the nanotubes-modified carbon electrode, and instead of inhibiting, they

promote electron transfer during further serotonin oxidation. More recently, in studying the antifouling properties of carbon nanotubes, Alwarappan *et al.*[20] performed dopamine detection at activated single-walled carbon nanotubes by applying an anodising potential of +1.6 V for 600 s, followed by a cathodisation potential at -1.2 V for 300 s. The study found that, following activation and 25 repeats of cyclic voltammetry at 100 mV/s, dopamine oxidation current decreased by 42% at single-walled carbon nanotubes, compared to 3% decrease at activated carbon nanotubes. The authors attributed the enhanced performance of the activated carbon nanotubes to greater sp^3 character in the carbon atoms, which was suggested to cause lesser delocalisation of π-electrons throughout the surface. The bare carbon surface in our study has demonstrated predominantly basal planes, which was identified as a possible reason for quasi-reversibility in reactions at the electrode surface. We envisage that immobilisation of carbon nanotubes on the surface of bare carbon electrodes of the type in this study will considerably enhance reaction reversibility at the electrode surface through augmentation of edge planes, while offering a greater degree of antifouling capabilities. Moreover, the activation procedure of Alwarappan *et al.*[20] may be an appropriate modification to evaluate fouling-resistance *in vivo* at such electrodes. However, it is essential to monitor the coverage of carbon nanotubes on a carbon electrode such that it remains structurally small for detection of dopamine *in vivo*.

5.7   References

1.   Ates, M.; Sarac, A.; Turhan, C.; Ayaz, N., *Fibers Polym.* **2009,** *10* (1), 46-52.

2.   Jeong, H.; Jeon, S., *Sensors* **2008,** *8* (11), 6924-6935.

3.   Bormett, R. W.; Asher, S. A.; Witowski, R. E.; Partlow, W. D.; Lizewski, R.; Pettit, F., *J. Appl. Phys.* **1995,** *77* (11), 5916.

4.   Li, G.; Xia, L. F.; Ma, X. X.; Sun, Y., *Acta Metallurgica Sinica(English letters)* **1999,** *12* (4), 551-556.

5.   Nimmagadda, R. D.; McRae, C., *Tetrahedron Lett.* **2006,** *47* (32), 5755-5758.

6.   Nimmagadda, R. D.; McRae, C., *Tetrahedron Lett.* **2006,** *47* (21), 3505-3508.

7.   Holloway, A.; Wildgoose, G.; Compton, R.; Shao, L.; Green, M., *J. Solid State Electrochem.* **2008,** *12* (10), 1337-1348.

8.   Xu, L. Q.; Yang, W. J.; Neoh, K.-G.; Kang, E.-T.; Fu, G. D., *Macromolecules* **2010,** *43* (20), 8336-8339.

9.   Han, D.; Han, T.; Shan, C.; Ivaska, A.; Niu, L., *Electroanal.* **2010,** *22* (17-18), 2001-2008.

10.   Kim, Y.-R.; Bong, S.; Kang, Y.-J.; Yang, Y.; Mahajan, R. K.; Kim, J. S.; Kim, H., *Biosens. Bioelectron.* **2010,** *25* (10), 2366-2369.

11.   Zhang, F.; Li, Y.; Gu, Y.-e.; Wang, Z.; Wang, C., *Microchim. Acta* **2011**, 1-7.

12.   Tan, L.; Zhou, K.-G.; Zhang, Y.-H.; Wang, H.-X.; Wang, X.-D.; Guo, Y.-F.; Zhang, H.-L., *Electrochem. Commun.* **2010,** *12* (4), 557-560.

13.   Alwarappan, S.; Joshi, R. K.; Ram, M. K.; Kumar, A., *Appl. Phys. Lett.* **2010,** *96* (26), 263702-3.

14.   Hou, S.; Kasner, M. L.; Su, S.; Patel, K.; Cuellari, R., *J. Phys. Chem. C.* **2010,** *114* (35), 14915-14921.

15.   Hočevar, S. B.; Wang, J.; Prakash, D. R.; Musameh, M.; Ogorevc, B., *Electroanal.* **2005,** *17* (5-6), 417-422.

16.   Jang, I. Y.; Ogata, H.; Park, K. C.; Lee, S. H.; Park, J. S.; Jung, Y. C.; Kim, Y. J.; Kim, Y. A.; Endo, M., *J. Phys. Chem. Lett.* **2010,** *1* (14), 2099-2103.

17.   Biddinger, E. J.; Ozkan, U. S., *J. Phys. Chem. C.* **2010,** *114* (36), 15306-15314.

18.   Wang, J.; Deo, R. P.; Musameh, M., *Electroanal.* **2003,** *15* (23-24), 1830-1834.

19.   Swamy, B. E. K.; Venton, B. J., *Analyst* **2007,** *132* (9), 876-884.

20.   Alwarappan, S.; Prabhulkar, S.; Durygin, A.; Li, C., *J. Nanosci. Nanotechnol.* **2009,** *9*, 2991-2996.

APPENDICES

Appendix 1   Publications and Presentations Arising from Work Presented in this Thesis

Appendix 2   Journal Article

Britz, D.; Chandra, S.; Strutwolf, J.; Wong, D. K. Y., *Electrochimica Acta* **2010,** *55* (3), 1272-1277.

A copy of the above journal article is included in the following pages.

Appendix 3   Book Chapter

Chandra, S.; Wong, D. K. Y., Electrochemical detection of neurotransmitters at structurally small electrodes. In *Nanostructured Materials for Electrochemical Biosensors*, Umasankar, Y.; Kumar, S. A.; Chen, S.-M., Eds. Nova Science Publishers: New York, 2009; pp 317-337.

Appendix 4   Conference Presentations

Chandra, S.; McMullan, S.; Martin, P. J.; Bendavi, A.; Wong, D. K. Y., Detecting dopamine at structurally small carbon electrodes. In *The 11th International Chemistry Conference and Exhibition in Africa (11 ICCA)*, Egypt, **2010**; p 23.

Chandra, S.; Miller, A.; Martin, P. J.; Bendavid, A.; Wong, D. K. Y., Dopamine detection *in vivo* at fouling-resistant hydrogenated electrodes. In *18th RACI Research and Development Topics Meeting*, Hobart, Tasmania, **2010**; p 40.

Chandra, S.; McMullan, S.; Martin, P. J.; Bendavid, A.; Wong, D. K. Y., Detection of dopamine *in vivo* using hydrogenated microelectrodes. In *The 61st Annual Meeting of the International Society of Electrochemistry*, International Society of Electrochemistry: Nice, France, **2010**; p 143.

Wong, D. K. Y.; Chandra, S.; Alwarappan, S.; McMullan, S.; Martin, P. J.; Bendavi, A., Physically Small Hydrogenated Carbon Electrodes for Biosensing (Invited Speaker). In *Pittcon Conference & Expo 2010*, Orlando, Florida, **2010**; p 110.

Chandra, S.; McMullan, S.; Wong, D. K. Y., Detection of dopamine at *p*-phenylacetate film-modified physically small electrodes *in vivo* In *Royal Australian Chemical Institute's 13th National Convention in conjunction with the 12th IUPAC International Congress of Pesticide Chemistry*, RACI, IUPAC: Melbourne Convention & Exhibition Centre Melbourne, Australia, **2010**; p 56.

Chandra, S.; Martin, P. J.; Bendavid, A.; Wong, D. K. Y., In vitro detection of dopamine at *p*-phenylacetate-coated carbon electrodes. In *17th RACI Research and Development Topics Meeting*, Griffith University, Gold Coast, Queensland, **2009**; p 16.

Chandra, S.; Wong, D. K. Y., In Vitro Detection of Dopamine at Phenylacetate film-Coated Physically Small Carbon Electrodes In *16th RACI Research and evelopment Topics Meeting* Sydney, Australia, **2008**; p 35.

The final pages of this thesis have been removed as they contain published material. Please refer to the following citation for details of the article contained in these pages.

Britz, D.,Chandra, S., Strutwolf, J., & Wong, D. K. Y. (2010). Diffusion-limited chronoamperometry at conical-tip microelectrodes. *Electrochimica Acta*, 55(3), 1272-1277.